ML-TR-64-162

OXIDATION OF TUNGSTEN AND OTHER REFRACTORY METALS

(Proceedings of Joint AIME/Air Force Materials Laboratory Symposium)

PAUL L. FAUST, PROJECT MONITOR

TECHNICAL DOCUMENTARY REPORT No. ML-TDR-64-162

APRIL 1965

AIR FORCE MATERIALS LABORATORY
RESEARCH AND TECHNOLOGY DIVISION
AIR FORCE SYSTEMS COMMAND
WRIGHT-PATTERSON AIR FORCE BASE, OHIO

ML-TR-64-162

OXIDATION OF TUNGSTEN AND OTHER REFRACTORY METALS

(Proceedings of Joint AIME/Air Force Materials Laboratory Symposium)

PAUL L. FAUST, PROJECT MONITOR

FOREWORD

The Institute of Metals Division (IMD) of the American Institute of Mining, Metallurgical, and Petroleum Engineers (AIME) and the AF Materials Laboratory, Research and Technology Division, Air Force Systems Command, Wright-Patterson Air Force Base, Ohio, conducted a symposium on the Oxidation of Tungsten and Other Refractory Metals during the 1962 Fall Meeting of the Metallurgical Society of the AIME. The symposium, consisting of two sessions, was held 31 October 1962 at the Statler-Hilton Hotel, New York City. Dr. E. A. Gulbransen, Westinghouse Electric Corporation, was the overall Chairman and Mr. Paul L. Faust of the Physical Metallurgy Branch, AF Materials Laboratory, was the Symposium Project Manager for the Air Force. The symposium together with this report covering its proceedings was initiated under Project No. 7312, "Metal Surface Protection and Deterioration," Task No. 731202, "Metal Surface Deterioration." The manuscript was released by the author 1 February 1965 for publication as an RTD technical report.

Nine papers were presented, eight of which are included in this report. The paper given by Dr. R. F. Walker, National Bureau of Standards, on the subject "Techniques for Studying Solid-Gas Reactions Above 1600°C" was not available for publication.

Mr. Faust and personnel of the AF Materials Laboratory extend their thanks to the speakers for their excellent presentations and the members of the Corrosion Resistant Materials Committee of the IMD for their assistance in arranging the symposium. They particularly wish to express their gratitude to Dr. Gulbransen for his assistance in promoting the need for this meeting.

Publication of this technical documentary report does not constitute Air Force approval of the report's findings or conclusions. It is published only for the exchange and stimulation of ideas.

This technical report has been reviewed and is approved.

O. O. SRP, Acting Chief
Physical Metallurgy Branch
Metals and Ceramics Division
Air Force Materials Laboratory

ABSTRACT

This report consists of eight papers presented at a symposium conducted by the AIME and the AF Materials Laboratory, Research and Technology Division, Wright-Patterson Air Force Base, Ohio, on the Oxidation of Tungsten and Other Refractory Metals. The symposium, consisting of two sessions, was held 31 October 1962 in New York City. Topics discussed included progress in research and in experimental methods in the investigation of the kinetics and mechanisms of oxidation of tungsten, tantalum, and columbium.

INTRODUCTORY REMARKS

Paul L. Faust

Since World War II metallurgical research at the AF Materials Laboratory has been largely a history of development of corrosion resistant alloys. Although the intent of much of the effort expended has been to produce materials of superior mechanical properties at elevated temperatures, the realities of environment have demanded compromises. In spite of the compromises a good measure of success has been realized with the so-called superalloys, and oxidation resistant compositions with excellent mechanical properties have been achieved at temperatures approaching the melting point of the base metal. With the refractory metals such compromises have not been so successful. Those additives which benefit the oxidation resistance of the matrix metal have a disastrous effect on mechanical properties. Compromises have been made, of course. D-38, for instance, a columbium-titanium-zirconium alloy has neither good oxidation resistance nor impressive mechanical properties at elevated temperatures. It does accept a silicide coating rather well, however, and should find application where ductility and the short term oxidation resistance afforded by siliciding are more important than strength. But no refractory metal alloy has demonstrated properties at a high fraction of matrix melting point which even approach the excellent combination of mechanical and chemical properties of the superalloys at 1600° to 2000°F. Alloy design becomes a dilemma, particularly in the cases of tantalum and tungsten where density considerations preclude use at temperatures much below 3000°F. The heavy additions of aluminum, zirconium, chromium or other reactive metals indicated for oxidation protection so depress the melting point that the alloy is mechanically worthless.

Despite the obvious difficulties involved in their use, mechanical properties, particularly high strength-to-weight ratios at extreme temperatures, indicate a rather broad use of the refractory metals and their alloys in Air Force systems and ultimately in commercial applications. Use of a columbium in place of a nickel-based alloy for jet engine turbine blades for instance would permit an increase in turbine inlet temperature of about 400°F. Improvements in maximum thrust and fuel consumption realized thus would far outweigh the disadvantages of increased engine weight.

Incorporation of molybdenum and columbium alloys into re-entry vehicles for frontal and near frontal structures will permit the development of glide re-entry vehicles with a minimum of expendable structure.

If any such applications are to be used, however, catastrophic oxidation must be avoided. Until recently, except for silicide type coatings, there has been no process for the protection of refractory metals, and the silicides leave a great deal to be desired.

Current coatings for molybdenum permit perhaps 30 minutes of operation at temperatures above 2000°F. Silicides for columbium and tantalum have been even less successful. And then there is tungsten. Silicide coatings of tungsten fail at about 3300°F, the approximate lower limit of utility of tungsten on a strength-to-weight basis. There are new protective processes being developed for the refractory metals; but thus far they have not materialized.

We see then that the refractory metals and their alloys have mechanical properties which render them irreplaceable at extreme temperatures combined with oxidation rates which render them useless for most applications of interest to the Air Force.

Because the problems are so acute and the solutions so desirable, it was decided several years ago to undertake detailed studies of the kinetics and mechanisms of refractory metal oxidation. The intention has been to provide insights into probable methods of protection and to establish actual oxidation

rates for these metals over a wide range of temperatures and pressures of oxygen and other oxidizing vapors.

Many investigations have contributed to the body of data on refractory metal oxidation independently of Air Force support. It is certainly true, however, that the burden of establishing a coherent picture has fallen to researchers under AF Materials Laboratory sponsorship. The papers which follow represent a measure of how far the effort has progressed and how far it has to go.

METHODS FOR STUDYING HIGH TEMPERATURE OXIDATION REACTIONS

Rudolph Speiser*
G. R. St.Pierre*

INTRODUCTION

The refractory metals react with the components of the atmosphere: O_2, N_2, CO_2, and H_2O vapor; and with the products of fuel combustion to form oxides, nitrides, and carbides. The chemical equilibrium between the metals and the reactants determine what compounds and phases can be formed while the rate at which these reactions occur is determined by the details of the kinetics of reaction. The conditions under which the reactions are usually experimentally observed are such as to make them quite irreversible resulting in complex heterogeneous systems.

The reaction starts initially at the metal-gas interface and as the reaction proceeds one or more layers of compounds may be interposed between the gaseous environment and the metal substrate. The products of reaction may be solid, liquid, or gaseous. The nature and character of the films formed on the metal surface determine the rate of transfer of reactants and products between the metal substrate and the gaseous environment.

To determine and comprehend the mechanism of reaction, the pertinent chemical equilibria and the reaction kinetics must be studied. In this review, we are concerned principally with the techniques used to study the oxidation of the refractory metals Mo, W, Nb, and Ta. Techniques used to determine the metal-oxygen phase equilibria, the rates of oxidation, the defect structure of the oxides, and the volatile products of oxidation are discussed.

METAL-OXYGEN EQUILIBRIA

For the most part, the oxidation of the refractory metals has been studied at pressures of oxygen in considerable excess of the decomposition pressure of the least stable oxide, i.e., the highest oxide (the metal ion in its highest valence state). Thus, the chemical potential of oxygen varies from values in excess of that required to form the metal oxide with the metal ion in its maximum valence state, at the oxide-gas interface, to zero corresponding to the pure metal substrate. Hence, multilayered oxide scales are formed upon the metal surface making it difficult to ascertain the mechanism of oxidation due to the complexity of the system being studied. It is desirable to control and maintain the partial pressure of oxygen so that the several oxides of a metal can be separately formed and investigated. However, this goal requires a technique where pressures of oxygen in the range of 10^{-12} atmospheres or less are accurately defined, maintained, and controlled. Direct oxidation with O_2 gas at these pressures is nearly impossible to achieve experimentally; the most sophisticated vacuum pumping systems can barely attain this pressure, the slightest leak or gaseous desorption from the interior surface of the reaction vessel would raise the pressure several orders of magnitude.

Partial pressures of O_2 in this range can be obtained in certain instances by use of gas-metal equilibria (References 1, 2, and 3) of the type,

$$xM + yH_2O = M_xO_y + yH_2 \qquad (1)$$

*Department of Metallurgy, The Ohio State University, Columbus, Ohio.

and,

$$xM + yCO_2 = M_xO_y + yCO \qquad (2)$$

In this method the composition of mixtures of H_2O-H_2 or CO_2-CO is adjusted over the metal at a given temperature so that the equilibrium composition is obtained.

The equilibrium decomposition pressures of the oxides of the refractory metals are tabulated in Table 1 for the refractory metal oxides. It can be seen that MoO_3 and WO_3 are easily reducible whereas Nb_2O_5 and Ta_2O_5 are reduced only with difficulty even at elevated temperatures with H_2O-H_2 and CO_2-CO mixtures. Moreover, except at temperatures in excess of 2000°K, very high ratios of H_2-H_2O and CO-CO_2 are required to obtain the equilibria represented by Equations 1 and 2 in the case of Nb and Ta. The suboxides of these elements require even higher ratios. Thus, the phase equilibria for the Mo-O and W-O can be conveniently determined by equilibrating H_2O-H_2 and CO_2-CO mixtures with these metals and their oxides, whereas equilibration of these gaseous mixtures with Nb and Ta would be very difficult to carry out experimentally. Furthermore, perusal of the data in Table 1 shows, that in the case of W, the ratios, H_2-H_2O and CO-CO_2, are near unity over a temperature range of 1000°K and likewise in the case of Mo over a somewhat shorter range. However, these ratios differ greatly from unity in the case of Nb and Ta. This means that the equilibrating gas mixtures over Mo and W behave like buffered systems; small leaks or back diffusion of air into the apparatus, cause little change in the P_{H_2}-P_{H_2O} or CO-CO_2 ratios*. Unfortunately, the opposite is true in the case of Nb and Ta.

In summary, the gas-metal equilibration according to Equations 1 and 2 can be successfully applied to Mo and W to determine the Mo-O and W-O phase equilibria and the thermodynamics, but only in a limited fashion to the Nb-O system. Several investigators have applied this technique to tungsten (References 4, 5, and 6), molybdenum (References 12 and 13), and niobium (Reference 62).

*This statement can be easily demonstrated:

$$\Delta(P_{H_2}/P_{H_2O}) = \frac{P_{H_2O}\,\Delta P_{H_2} - P_{H_2}\,\Delta P_{H_2O}}{P_{H_2O}^2} \approx \frac{(P_{H_2O} + P_{H_2})\,\Delta P}{P_{H_2O}^2}$$

since

$$\Delta P_{H_2O} = -\Delta P_{H_2} = \Delta P.$$

If $P_{H_2O} = P_{H_2}$, then

$$\Delta(P_{H_2}/P_{H_2O}) \approx \frac{2\Delta P}{P_{H_2O}} \approx 0, \text{ if } P_{H_2O} >> \Delta P.$$

If $P_{H_2} >> P_{H_2O}$, then

$$\Delta(P_{H_2}/P_{H_2O}) \approx \frac{P_{H_2}}{(P_{H_2O})^2}\,\Delta P >> 0, \text{ if } P_{H_2O} \approx \Delta P.$$

Description of Gas-Metal Equilibration Technique (Reference 4)

In the case of W, the specific equilibria involved are

$$0.5WO_2(s) + H_2(g) = 0.5W(s) + H_2O(g) \quad (3)$$

$$0.5WO_2(s) + CO(g) = 0.5W(s) + CO_2(g) \quad (4)$$

$$\frac{1}{18}W_{18}O_{49}(s) + CO(g) = \frac{18}{13}WO_2(s) + CO_2(g) \quad (5)$$

$$\frac{9}{32}W_{20}O_{58}(s) + CO(g) = \frac{10}{32}W_{18}O_{49}(s) + CO_2(g) \quad (6)$$

$$10WO_3(s) + CO(g) = \frac{1}{2}W_{20}O_{58}(s) + CO_2(g) \quad (7)$$

These equilibria can be combined with the equilibrium reactions,

$$2H_2 + O_2 = 2H_2O \quad (8)$$

and,

$$2CO + O_2 = 2CO_2 \quad (9)$$

to compute the standard free energies of formation of the several oxides of tungsten.

Equilibration experiments are performed by determining the H_2O-H_2 or CO_2-CO ratio in equilibrium with a particular pair of oxide phases. Figure 1 is a schematic representation of the furnace and microbalance arrangement employed. In each case a strip of tungsten or prepared single oxide compact is suspended in the furnace. A controlled mixture of A-H_2-H_2O or CO-CO_2 is passed over the specimen. The oxidizing ratio (CO_2-CO or H_2O-H_2) is adjusted to establish conditions of specimen weight gain and then readjusted for conditions of specimen weight loss. By alternating from weight loss to weight gain it is possible to adjust to a gas ratio for which the specimen weight does not change after prolonged holding. This procedure clearly establishes equilibrium conditions and is in no way dependent on kinetic considerations because the equilibrium gas composition is approached from both sides of equilibrium. X-ray diffraction examination is used to verify the phases present.

Apparatus

A furnace capable of operation in the temperature range desired with a temperature control of ±1°C. For weight change observations several balances of different sensitivities and capacities: 0.1mg to 10^{-3}mg sensitivities.

The CO-CO_2 gas mixtures should be prepared from commercial gases of high purity and then further purified by conventional gas trains. The composition of the gas mixture can be adjusted and determined by the use of calibrated flow meters, orsat analyses, and gravimetric analysis.

The A-H_2-H_2O are prepared from A and H_2 of high purity. The A and H_2 are additionally purified by standard procedures, metered and mixed, and passed through a water saturator held at a carefully controlled temperature. The ratio of P_{H_2O}-P_{H_2} is varied by adjusting the relative amounts of A and H_2 at a constant saturator temperature in accordance with the Equation:

$$\frac{P_{H_2O}}{P_{H_2}} = \left(\frac{P_{H_2O}}{P_T - P_{H_2O}}\right)\left(1 + \frac{\dot{n}_A}{\dot{n}_{H_2}}\right) \quad (10)$$

The P_{H_2O} is established by the saturator temperature. P_T is the total pressure and $\dot{n}_A/\dot{n}_{H_2}$ is the ratio of the molar flow rates of A and H_2.

Discussion

Care must always be taken when applying this technique at high temperatures and high partial pressures of H_2O; under these conditions, Mo and W oxides form volatile complexes with water. At high P_{CO}/P_{CO_2} ratios tungsten will tend to form carbides (Reference 10). In the correct range of temperatures and composition these difficulties can be avoided. Thermal segregation of H_2 and H_2O can take place if there is a steep temperature gradient; preheating

of the equilibrating gas will minimize this effect (References 3 and 7). Mixing a heavy gas such as A with the H_2 will also reduce un-mixing to negligible error (References 7, 8, and 9). Instead of varying the composition of the equilibrating gas mixture at constant temperature, one can maintain the composition constant and vary the temperature. A number of variants of this method have been applied. For example, Griffis (Reference 5) used a closed dynamic system in which the equilibrating gaseous mixture (H_2 - H_2O) was circulated by a gas solenoid pump. Argon was not used as a diluent and as a consequence a troublesome thermal segregation problem had to be solved.

Data obtained by the apparatus described in this paper are shown in Figures 2 and 3, while Figure 4 summarizes the W-O phase equilibrium at one atmosphere total pressure deduced from these data.

Calorimetric Method of Determining Thermodynamic Data

This method can be applied to the four refractory metal oxides, MoO_3, MoO_2 (Reference 14), WO_3, WO_2 (Reference 15), Nb_2O_5 (Reference 17), and Ta_2O_5 (References 16 and 17). The results of combustion calorimetry (Reference 18), low-temperature heat capacity measurements (Reference 18), and high-temperature heat content measurements can be combined with entropy data to give the free energy of formation of these oxides as a function of the temperature. The partial pressure of O_2 in equilibrium with these oxides can then be computed from free energies of formation. This method is quite accurate for determining the free energies of formation of the oxides of highest valence, and less accurate for the lower oxides because of the difficulties of their preparation. The intermediate oxides of W and Mo have not been successfully investigated by this method, nor does it seem likely that the more stable lower oxides of Nb and Ta can be profitably studied by this procedure.

The enthalpies and free energies of formation of WO_3 and WO_2 determined by the gas equilibration method (Reference 4) and the calorimetric (Reference 18) method are in excellent agreement and the data obtained by St. Pierre et al. (Reference 4), for the intermediate oxides $W_{18}O_{49}$ and $W_{20}O_{58}$ are consistent with these data also.

Galvanic Cells

The galvanic cell is one of the most precise methods of determining thermodynamic quantities related to chemical equilibria. Kiukkola and Wagner (Reference 19) developed a high-temperature galvanic cell utilizing a solid electrolyte (ZrO_2 - 15 percent CaO) and solid electrodes applicable to oxygen concentration cells. It was shown that the conduction was nearly 100 percent ionic and independent of the oxygen pressure and satisfactory results have been obtained with this electrolyte in the temperature range 750° to 1200°C. A cell for measuring the oxygen potential corresponding to various CO_2/CO ratios is shown in Figure 5. Typical data are shown in Figure 6. The vertical coordinate gives the P_{O_2} as determined from electromotive force measurements and the horizontal coordinate the P_{O_2} as computed from the CO_2/CO ratio at 1000°C. The agreement is excellent for this rather difficult measurement.

Three types of oxygen concentration cells used in this laboratory are shown in Figure 7. Once again the equilibria pertaining to the Mo-O and W-O systems can be easily determined by this procedure. Gerasimov, Vasileva, Chusova, Geiderich, and Timojereva (Reference 20) have determined the $\Delta F°$'s for the reactions

$$W(s) + O_2(g) = WO_2(s) \qquad (11)$$

and

$$\frac{36}{13} WO_2(s) + O_2(g) = \frac{2}{13} W_{18}O_{45}(s) \qquad (12)$$

by the galvanic cell method. These data are in very good agreement with the data obtained by St. Pierre et al. The application of this method to niobium and tantalum oxides is more difficult due to the greater stability of

these oxides — side reactions with the solid electrolyte occur more readily with the more stable oxides. Foster in this laboratory, however, has successfully investigated the cell

$$\begin{array}{c|c|c} Cr & ZrO_2 & TaO_2 \\ Cr_2O_3 & CaO & Ta_2O_5 \end{array}$$

Since the oxides of niobium are less stable, it is probable that these oxides would be more amenable to study by this method than the oxides of tantalum.

Solubility Limits

Solubility limits can be determined by standard X-ray lattice parameter and metallographic methods.

Vapor Pressure Method — Knudsen Effusion (Reference 21)

The equilibrium between the refractory metal oxides and their vapors have been investigated by several vapor pressure techniques. Effusion techniques can be applied with success in the pressure range of 10^{-6} to 10^{-9} atmospheres. In this method, the vapor flows from a space, where it is in equilibrium at some given temperature with a condensed phase, through an orifice into a high vacuum ($P < 10^{-6}$ Torr). If the pressure is low enough, so that the ratio of the mean free path in the vapor to the diameter of the orifice is greater than 10, the vapor pressure is given by the relation (Reference 22),

$$p = \frac{m}{K}\sqrt{\frac{2\pi RT}{M}} \qquad (13)$$

where m is the mass effusing per unit time per unit area, M is the molecular weight of the vapor, and K is Clausing's (Reference 23) correction factor, which corrects the effusion rate for the finite thickness of the orifice. Recently, Hirth and Winterbottom have shown, that vapor molecules impinging upon the inner surface of the Knudsen cell lid are adsorbed, diffuse along the surface through the orifice to the external surface of the lid to form an annular ring surrounding the orifice — desorption from this annular ring leads to apparent rates of effusion which are higher than the equilibrium rate. Increasing the thickness of the orifice decreases the magnitude of this effect but increases the size of the Clausing correction. The thickness of the orifice should be optimized so that the errors due to these two opposing effects is minimized. If the vaporizing coefficient differs appreciably from unity, the apparent pressure should be measured as a function of orifice area and then extrapolated to zero area to yield the equilibrium pressure.

The rate of vaporization may be measured in a number of ways (Reference 21): (1) total weight change of the Knudsen cell for a measured time interval; (2) continuously weighing while the cell is suspended from a balance beam or a quartz spiral spring; and (3) measuring a fraction of the vapor deposited upon a target.

However, unambiguous vapor pressure data cannot be obtained if more than one molecular species is present in the vapor phase; the precise composition of the vapor phase must be ascertained. In general, the vapor in equilibrium with refractory oxides at elevated temperatures is a complex mixture. The most reliable analyses of the vapors effusing from a Knudsen cell have been obtained with the mass spectrograph. Pioneering research of this kind was carried out in the determination of the thermodynamics of gaseous carbon molecules in equilibrium with graphite by Chupka and Inghram (Reference 25). Berkowitz, Chupka, and Inghram (Reference 26) ascertained the equilibrium of powdered MoO_3 and WO_3 with their respective vapors by mass spectrographic analysis of the vapor effusing from a Knudsen cell. These authors showed that the principal gaseous species in the vapor phase were the polymeric molecules $(MoO_3)_n$ and $(WO_3)_n$, where $n = 3, 4,$ and 5. Combining the analysis of the vapor composition reported by Berkowitz et al., with their own rate of Knudsen effusion measurements, Blackburn, Hoch, and Johnston (Reference 27) calculated the thermodynamic functions for several oxide-vapor equilibria.

Blackburn (Reference 27) compared his results with those of Berkowitz (Reference 26), Ueno (Reference 28) (Knudsen effusion and quartz balance respectively) and Ariya (Reference 29) (transportation method) in Tables 2 and 3. The agreement between the data obtained by these several methods is poor.

Inghram, Chupka, and their collaborators (Reference 30) and others (see review by Inghram and Devwart, Reference 30), using the mass spectrometer in the study of the thermodynamics of chemical reactions at elevated temperatures, have generally employed magnetic focusing mass spectrometers. Professor David White, Department of Chemistry, The Ohio State University, has developed the use of a Bendix Time-of-Flight Mass Spectrometer in conjunction with a Knudsen effusion cell to study the equilibrium between condensed phases and their vapors (Reference 31). The Metallurgy Department, The Ohio State University, has also purchased a Bendix Time-of-Flight Mass Spectrometer with a Knudsen effusion cell attachment. This instrument (using procedures and modifications developed by Professor White and his collaborators) is being used to study the volatile complexes of the refractory metal oxides with water vapor. A brief description of the principles of operation of this instrument follows.

Time-of-Flight Mass Spectrometer (Reference 32)

A schematic diagram of the Time-of-Flight Mass Spectrometer (TOF-MS) is shown in Figure 8. Not shown is the furnace containing the Knudsen effusion cell which is directly coupled to the TOF-MS. Neutral molecules from the Knudsen cell effuse into the ion-source region where ions are formed by bombardment of the neutral particles by a pulsed (10,000 pulses per second) beam of electrons of controlled energy. Between electron pulses, the first grid in the ion gun is pulsed to -270 volts for a time sufficient to allow the ion bunch to pass through this grid into the final grid, where the ions are accelerated by a 2800-volt potential. After passing through this grid, the ion bunch moves 100 centimeters down a field free "drift path" tube to an ion detector. The geometry and potentials of the apparatus are designed to yield a time of flight which is proportional to $\sqrt{2m/e}$, where m is the mass of the ion and e is the ion's charge. Mass separation results only from mass dependent velocities, ions with the lowest mass-to-charge ratio having the shortest time of flight. The ion detector is a magnetic electron multiplier. The output of the ion signal collector is displayed on an oscilloscope synchronized with and triggered by signals from the mass spectrometer. The accuracy of the TOF-MS is greatly improved by the incorporation of an analog output system so that the data can be recorded as well as simultaneously displayed on the oscilloscope.

The furnace containing the Knudsen cell is shown in Figure 9. The Knudsen cell can be either heated by electron bombardment or by radiation. The temperature is measured through an observation port by an optical pyrometer sighted directly upon the orifice of the Knudsen cell or by thermocouples directly attached to the base of the cell. Provision is also being made to pass water vapor directly into the Knudsen cell so that the molecular weight of volatile refractory-metal-oxide-H_2O complexes can be ascertained. An example of the resolution attainable with the TOF-MS is shown in the determination of the vapor pressure of neodymium (Reference 33, Figure 10). The mass spectrum of the isotopes of neodymium are shown and the experimental abundances are compared with those published in the literature.

Gravimetric Methods for Determination of the Homogeneity Range in Refractory Metal Oxides

Rigorously, all solid or liquid oxides exhibit some degree of nonstoichiometry at finite oxygen pressures and temperatures above absolute zero; whether or not a homogeneity range is exhibited depends upon the sensitivity of the measurements. The metal-oxygen system, consisting of one condensed phase and a vapor phase in equilibrium, is bivariant according to the Gibbs phase rule. In this case the total vapor

pressure as well as the partial pressures of the species in the vapor phase change with the composition of the condensed phase at constant temperature. When two condensed phases and the vapor phase are in equilibrium, the system is invariant and the total pressure, as well as the partial pressures of the several molecular species in the vapor phase, is independent of the composition of the condensed phase. Gulbransen and his coworkers (Reference 36) have attempted to determine the composition limits for the tungsten phases WO_2, $W_{18}O_{49}$, and WO_3 by measuring the vapor pressure over these oxides by the Knudsen effusion method. The Knudsen cells loaded with powdered oxide samples were suspended from a quartz spring balance. The whole assembly was enclosed in a high vacuum chamber and the Knudsen cell was heated by radiation emitted by a susceptor heated by induction. Weight changes were determined by measuring the contraction of the quartz spring. They found that above 1200°C the vapor pressure over the heterogeneous system was independent of the composition and a function of the composition over the homogeneous system. This behavior conforms to the phase rule.

Kofstad and Anderson (Reference 37) and Kofstad (Reference 38) have determined the relative defect structure of α-Nb_2O_5 in the temperature range 750° to 1200°C by equilibration with oxygen in the pressure range of 1 to 0.001 atm and at much lower oxygen pressures corresponding to equilibration with mixtures of CO and CO_2. The relative deviation from stoichiometry (oxygen deficiency) was measured gravimetrically. The oxide specimen was suspended from a quartz spring and the change in weight upon equilibration with O_2 or CO-CO_2 mixtures was determined from the change in extension of the quartz spring. Brauer (Reference 39) estimates that the oxygen deficiency lies within the composition limits, $NbO_{2.50}$-$NbO_{2.40}$, in the temperature range 1350° to 1400°C.

Similar studies by Kofstad (Reference 40) on Ta_2O_5 reveal a formula for this oxide corresponding to Ta_2O_{5-x} (x = 0.005 to 0.006) in the temperature range 1200° to 1400°C. The narrower homogeneity limits for Ta_2O_5 compared to Nb_2O_5 is not surprising since Ta_2O_5 is much more stable than Nb_2O_5.

Gas Entrainment

In this method*, a carrier gas flowing over the condensed phase, is saturated with vapor so that gas plus vapor is in equilibrium with the condensed phase at a given temperature; the vapor is then condensed out of an accurately measured volume of the flowing gas mixture, and finally, the condensate is precisely weighed. (See Figure 11.) The flow rate of the carrier gas must be carefully controlled; Lepore and Waser (Reference 34) have shown that the flow rate must be adjusted so that the apparent vapor density (see Figure 12) is independent of the rate of flow of the carrier gas, because only in this case, is the carrier gas vapor saturated; at lower rates, the rate of diffusion of the vapor is greater than the flow rate of the carrier gas so that the apparent vapor density is higher than the density corresponding to the vapor saturated gas; at higher rates, the flow rate is higher than the rate of evaporation from the solid or liquid surface; consequently the carrier gas can never be saturated with vapor.

The partial pressure of a given molecular species, i, in the vapor can be calculated from the ideal gas equation,

$$P_i = \frac{W_i}{M_i} \cdot \frac{R}{V} T \qquad (14)$$

where W_i is the weight of species i entrained, M_i is the molecular weight and V is the volume of carrier gas. Obviously the amount and molecular weight of every specie present in the vapor must be ascertained. Ackermann and his coworkers (Reference 35) have used the entrainment method to measure the vapor density in equilibrium with molybdenum trioxide and

*Also referred to as the transpiration or transporation method.

tungsten trioxide. These investigators assumed that the composition of the vapor in their experiments corresponded to the trimer, tetramer, and pentamer trioxide species reported by Berkowitz, Chupka and Inghram (Reference 26) in their mass spectroscopic investigations of MoO_3 and WO_3. Ackermann, et al. (Reference 35) compared the results of their research with those of other investigators in Table 4. The data in Table 4 are in poor agreement; however, there is satisfactory agreement between the data of Berkowitz et al., and Ackermann et al.

KINETICS OF OXIDATION

The experimental procedures generally employed in the investigations of the kinetics of oxidation are well known and voluminously described in the literature (see for example Kubaschewski and Hopkins, Reference 41). Certainly an extensive description of experimental methods related to this topic is not warranted in this review — only a brief discussion of several topics of interest to the authors is given.

Gravimetric Method

In this method, the change in weight of the specimen is measured as a function of time at constant temperature. Several pieces of apparatus (References 4, 36, and 37), described in previous sections of this paper, have been used to gravimetrically measure rates of oxidation. The vacuum microbalance devised by Gulbransen (Reference 42) is especially worthy of mention because of its high sensitivity (0.5 μ gm) and its rapid response.

In our laboratory there is a program under way to measure the rate of oxidation of tungsten to WO_2; compacts of WO_2 to $W_{18}O_{49}$; $W_{18}O_{49}$ to WO_3; and finally, to oxidize tungsten in an atmosphere that leads to the formation of a multilayer oxide scale. The aims of this program are being fulfilled with the apparatus depicted in Figure 1, utilizing the proper oxidizing mixtures of CO-CO_2 or H_2-H_2O. The pure suboxides of tungsten are prepared by equilibrating the oxide with the requisite CO-CO_2 or H_2-H_2O mixtures.

The same apparatus and technique can be successfully employed to study the rate and mechanism of oxidation of molybdenum; niobium, possibly, if the required high ratio of H_2-H_2O can be controlled with sufficient accuracy; and tantalum, probably not at all.

Gravimetric Method: High Pressures (Reference 43)

Apparatus and procedures for rate measurements at hyperatmospheric pressures, over a considerable range of temperatures, is described by Ong and Fassel, Jr., in another paper in this symposium*.

Gravimetric Method: Volatilization of Oxides

Numerous investigators have measured and noted the volatility of molybdenum (References 44, 45, 46, 47, and 53) and tungsten (References 48 through 52) oxides at elevated temperatures. The enhanced rate of volatilization of the oxides of tungsten in the presence of water vapor has been measured by several investigators (References 49, 50, 54, and 55). In this laboratory (Reference 56), the apparatus schematically represented in Figure 1 also has been used to measure the rate of volatilization of the several oxides of tungsten in the presence of water vapor. Compacts of the different oxides of tungsten were suspended from the balance arm in a flowing gaseous mixture composed of H_2-H_2O-Ar. The H_2-H_2O ratio was adjusted to correspond to the equilibrium oxygen partial pressure of the suboxide under study. Argon was used as a diluent—thus the partial pressure of H_2O could be varied without altering the oxygen chemical potential. The data obtained by this procedure for the various

*See "High Pressure Oxidation of Refractory Metals—Experimental Methods and Interpretation."

oxides of tungsten is presented elsewhere in this symposium — all of the oxides of tungsten seem to form stable gaseous hydrates at elevated temperatures. It can be seen that the volatility rate of each oxide increases with an increase in the partial pressure of H_2O. These data are discussed further in another paper in this symposium (G. R. St.Pierre and R. Speiser, "Reaction of Gaseous Systems with Tungsten at Elevated Temperatures").

Diffusion

The solubility of oxygen in molybdenum and tungsten is quite low, apparently unmeasurable, although sufficient internal oxidation can occur (at grain boundaries) to cause embrittlement. On the other hand, the solubility of oxygen in columbium and tantalum is high enough to be measurable (References 57 through 60). Klopp, Maykuth, Sims, and Jaffee (Reference 59) determined the rate of solution of oxygen in niobium by measuring knoop hardness across specimens exposed to oxygen at elevated temperatures. Assuming a linear relationship between oxygen concentration and hardness, diffusion coefficients were calculated from Fick's second law of diffusion. Klopp et al. (Reference 59) expressed the temperature dependence of the diffusity of oxygen in niobium by the relation,

$$D = 4.07 \times 10^{-3} e^{-\frac{24,900}{RT}}$$

where D is the diffusion rate in cm^2 per second. This result is in fair agreement with data of Ang (Reference 58) who estimated his diffusivities from internal friction measurements and obtained a value of 27,600 cal per gram for the activation energy.

Kofstad, Kalvenes, Anderson, and Lunde (Reference 61) determined the rate of diffusion of Nb^{95} in sintered Nb_2O_5. Plane surfaces of the sintered Nb_2O_5 compacts were coated with a thin layer of Nb_2O_5 containing the radioisotope Nb^{95}; several specimens were also made up as sandwiches with the radioactive layer in the middle. The diffusion anneal was of three days duration in a furnace supplied with a continuous current of oxygen. The samples were then sectioned and the activity in each section determined. A Geiger Muller counter was used to determine the β-activity and a scintillation counter to determine this α-activity. It was found that Nb diffusion occurred principally by grain boundary migration, lattice diffusion being extremely slow by comparison. This result is not surprising, since Nb_2O_5 is an oxygen deficient lattice (Reference 37) oxygen ion migration being the most probable mechanism of ion transport through the oxide lattice.

ACKNOWLEDGMENT

The research by the authors reported in this paper was sponsored by the United States Air Force under Contract AF 33(616)-8005.

REFERENCES

1. P. H. Emmett and J. F. Schultz. J. Am. Chem. Soc, 55, 1376. (1933).

2. L. S. Darken and R. W. Gurry. J. Am. Chem. Soc, 67, 1398. (1945).

3. J. Chipman and M. G. Fontana. J. Am. Chem. Soc, 56, 2011. (1934); Trans. Am. Soc. Met. 24, 313. (1936).

4. G. R. St.Pierre, W. T. Ebihara, M. J. Pool, and R. Speiser. Trans. Am. Soc. Met. 224, 259. (1962).

5. R. C. Griffis, J. Electrochem. 106, 418. (1959).

6. L. A. Vasil'eva, L. Ya. Gerasimov, and Yu. P. Siamanov. J. Phys. Chem. (U.S.S.R.) 331, 682 (1957).

7. J. Chipman, J. F. Elliot, and B. L. Averbach. "The Physical Chemistry of Metallic Soluting and Intermetallic Compounds," Nat. Physical Lab., Symposium No. 9. Vol. I. 1B. (1959).

8. M. N. Dastur and J. Chipman, J. Am. Chem. Soc, 56, 2011. (1934); Trans. Am. Soc. Met. 24, 313. (1936).

9. T. P. Floridas and J. Chipman, Trans. Faraday Soc. 49, 171. (1953).

10. G. W. Orton, Doctoral Dissertation, Metallurgical Eng. Dept., Ohio State University (1961).

11. Chaudron, Ann. Chim. 16, 221 (1921).

12. Tonosaki, Bull. Inst. Phys. Chem Res. Tokyo, 19, 126 (1940).

13. N. A. Gokcen. J. Metals. 5, 1019. (1953).

14. A. D. Mah. J. Am. Chem. Soc. 61, 1572. (1957).

15. A. D. Mah, J. Am. Chem. Soc. 81, 1582 (1959).

16. J. P. Coughlin, U. S. Bur. Mines Bull. No. 542.

17. R. L. Orr, J. Am. Chem. Soc. 75, 2808. (1953).

18. E. G. King, W. W. Weller, and A. U. Christensen. R. I. Bur. Mines. 5664. (1960).

19. K. Kiukkola and C. Wagner. J. Electrochem. Soc. 104, 379. (1957).

20. J. L. Gerasimov, L. A. Vasil'eva, T. P. Chusova, V. A. Geiderich, and M. Timojereva. Doklady Akad. Nauk. U.S.S.R., 134, No. 6, 1350. (1960).

21. R. Speiser and J. W. Spretnak. "Vacuum Metallurgy." Electrochem. Soc. (1955).

22. M. Knudsen. Ann. Physik, 28, 75. (1909).

23. P. Clausing. Ann Physik, 12, 961. (1932). (See S. Dushman, Vacuum Technique, 99 (1949). John Wiley & Sons, Inc., New York, for a tabulation of Clausing's correction values.)

24. J. P. Hirth and W. L. Winterbottom. J. Chem. Physics, 37, 784. (1962).

25. W. A. Chupka and M. G. Inghram. J. Chem. Phys. 21, 371, 1313. (1953); ibid. 22, 1742. (1954); Memories de la Société Royale des Sciences de Liège Quatrieme Série. Tome XV, 373. (1954).

26. J. Berkowitz, M. G. Inghram, and W. A. Chupka. J. Chem. Physics. 26, 842. (1957); ibid. 27, 85. (1957).

27. P. E. Blackburn, M. Hoch and H. L. Johnston. J. Phys. Chem. 62, 769. (1958).

28. K. Ueno. J. Chem. Soc. Japan, 62, 990. (1941).

29. S. M. Ariya, S. A. Shchukarev and V. B. Glushkova. Zhur. Obshchei Khim. 23, 2063. (1953).

30. M. G. Inghram and J. Drowart. "Mass Spectrometry Applied to High Temperature Chemistry." Proceedings of an International Symposium on High Temperature Technology. The McGraw-Hill Book Co., Inc. New York (1960). pp. 219-240.

31. D. White, A. Sommer, P. N. Walsh, and H. W. Goldstein. "The Application of the Time-of-Flight Mass Spectrometer to the Study of Inorganic Materials at Elevated Temperatures." to be published.

32. W. C. Wiley and I. H. McLaren. Rev. Sci. Instr. 26, 1150. (1955); W. C. Wiley. Science. 124, 217. (1956); D. B. Harrington. "Time-of-Flight Mass Spectrometry." Encyclopedia of Spectroscopy. Ed. C. F. Clark. Rheinhold Pub. Corp. (1960). pp. 628-647.

33. D. White, P. N. Walsh, H. W. Goldstein and D. F. Dever. J. Physical Chem. 65, 1404. (1961).

34. J. V. Lepore and J. R. Waser. "A Discussion of the Transpiration Method for Determining Vapor Pressure." MDDC-1188. U. S. Atomic Energy Commission.

35. R. J. Ackermann, R. J. Thorn, C. Alexander, and M. Tetenbaum. J. Physical Chem. 64, 350. (1960).

36. P. E. Blackburn, K. F. Andrew, E. A. Gulbransen, and F. A. Brassart. WADC Technical Report 59-575, Part II. Wright Air Development Center, Wright-Patterson Air Force Base, Ohio. June 1961.

37. P. Kofstad and P. B. Anderson. Tech. Note No. 1. Contract No. AF 61(052)-460. Central Institute for Industrial Research, Oslo, Norway. October 1961.

38. P. Kofstad. Tech. Note No. 4 (Revised). Contract No. AF61(052)-460. Central Institute for Industrial Research, Oslo, Norway, January 1962.

39. G. Brauer. Z. Anorg. Allg. Chem., 248, 1. (1941); Naturwiss. 28, 30. (1940).

40. P. Kofstad. J. Electrochem. Soc. 109, 776. (1962).

41. O. Kubaschewski and B. E. Hopkins. Oxidation of Metals and Alloys. 2nd Ed. Butterworth, London. (1962).

42. E. A. Gulbransen. Rev. Sci. Instr. 15, 201. (1944); Trans. Electrochem. Soc. 81, 327-339. (1942); "Vacuum Microbalance: High-Temperature Reactions." Advances in Catalysis. Vol. V. Academic Press Inc., New York, N. Y. 1953. pp. 130-137.

43. W. McKewan and W. M. Fassel. Trans. AIME. 197, 1127. (1953); R. C. Peterson, W. M. Fassel, and M. E. Wadsworth. Trans. AIME. 200, 1038. (1954).

44. M. Simnad and A. Spilners. Trans. AIME. 203, 1011. (1955).

45. E. S. Jones, Capt. J. F. Mosher, R. Speiser, and J. W. Spretnak. Corrosion. 14, 20. (1958).

46. J. W. Hickman and E. A. Gulbransen. Met. Tech. 14, TP 2144. (1947).

47. E. A. Gulbransen and W. S. Wysong. Met. Tech. 14, TP 2226. (1947).

48. E. A. Gulbransen and W. S. Wysong. Trans. AIME. 175, 611. (1948).

49. W. W. Webb, J. T. Norton, and C. J. Wagner. Electrochem. Soc. 103, 107. (1956).

50. T. Millner and J. Nengebauer. Nature. 163, 601. (1949).

51. V. I. Arkharov and Y. D. Kazmanov. Fizike Metallov I Metallove Denies. 2, 361. (1956). (Brutcher Translation No. 4104).

52. K. F. Andrew, A. Merlin, and E. A. Gulbransen. WADC Technical Report 59-575, Part I. Wright Air Development Center, Wright-Patterson Air Force Base, Ohio. February 1960.

53. E. A. Bartlett and D. N. Williams. Trans. AIME. 212, 280. (1958).

54. G. R. B. Elliot. U. of Calif. Radiation Lab. Report No. URCL-1831. (1952).

55. O. Glemser and H. G. Volz. Naturiwissench. 43, 33. (1956).

56. J. E. Battles, W. T. Ebihara, W. P. Meuli, M. J. Pool, R. Speiser, J. W. Spretnak, and G. R. St.Pierre. ARL-TR-62-324. Aeronautical Research Laboratories, Wright-Patterson Air Force Base, Ohio. (1962) Contract AF33-(616)-5721.

57. A. W. Seybolt, Trans. AIME. 200. 774. (1954).

58. C. Y. Ang, Acta Met. 1, 123. (1953).

59. W. D. Klopp, C. T. Sims, and R. I. Jaffee. Trans. Am. Soc. Metals. 51, 282. (1959); W. D. Klopp, D. J. Maykuth, C. T. Sims, and R. I. Jaffee. Battelle Memorial Inst. Report No. 1317. (1959).

60. P. Kofstad. Tech. Note No. 2. Grant AF-EOAR-61-42. Central Institute for Industrial Research, Oslo, Norway. November 1961; ibid. Tech. Note No. 3. October 1961.

61. P. Kofstad, O. Kalvenes, P. B. Anderson, and G. Lunde. Tech. Note No. 3. Contract AF61(052)-460. Central Institute for Industrial Research, Oslo, Norway. October 1961.

62. P. Süe. Compte Rendu. 208, 1088. (1939).

TABLE 1

OXYGEN PRESSURE IN EQUILIBRIUM WITH OXIDES

	Easily Reducible				Reducible with Difficulty			
	MoO_3		WO_3		Nb_2O_5		Ta_2O_5	
Temp, °K	1000	2000	1000	2000	1000	2000	1000	2000
P_{O_2}	10^{-17}	10^{-6}	10^{-21}	10^{-6}	10^{-31}	10^{-11}	10^{-34}	10^{-13}
P_{H_2}/P_{H_2O}	0.036	0.48	1.6	0.49	10^5	114	5×10^6	580
P_{CO}/P_{CO_2}	0.026	0.44	1	4.8	10^5	500	4×10^6	2550

TABLE 2

HEAT AND ENTROPY OF VAPORIZATION OF MoO_3*

Author	Temp., °K	ΔH_T kcal / mole of $(MoO_3)_3$	ΔS_T e.u.	ΔF_{900} kcal / mole of $(MoO_3)_3$
Ueno**	928	63.7	46.5	22.9
Ariya**	964	68.1	56.9	18.8
Berkowitz	850	80.0	65.6	21.0
Blackburn	900	79.7	67.8	18.7

*Blackburn, Hoch, and Johnston (Reference 27).

**The values for ΔF_{900} from Ariya (Reference 29) and Ueno (Reference 28) are corrected to $(MoO_3)_3(g)$.

TABLE 3

HEAT AND ENTROPY OF VAPORIZATION OF WO_3

Author	Temp., °K	ΔH_T kcal / mole of $(Wo_3)_3$	ΔS_T e.u.	ΔF_{1000} kcal / mole of $(WO_3)_3$
Ueno*	1368	112.6	57.3	34.2
Berkowitz	1368	130	69.5	34.9
Blackburn	1500	108.0	54.1	33.9

*Ueno's data are corrected to $(WO_3)_3(g)$.

TABLE 4

HEATS AND ENTROPIES OF SUBLIMATION AND VAPORIZATION OF MOLYBDENUM TRIOXIDE

Investigators	Temp., °K	ΔH°_T (kcal mole^{-1} of vapor)	ΔS° (e.u. mole^{-1} of vapor)
Ueno	908-948	62.5	42.8
Ariya	941-987	67.0	53.3
Zelikman et al*	1178-1373**	35.6	24.9
Berkowitz et al	810-1000	85.4	71.7
Blackburn et al	808-958	78.8	66.6
Ackermann et al	980-1060	87.8	73.0

*From boiling point and transpiration methods of liquid molybdenum trioxide. From A. N. Zelikman, N. N. Gorovitz, and T. E. Prcsenkova. J. Inorg. Chem. U. S. S. R 1, 332. (1956).

**Measurements made above the melting point.

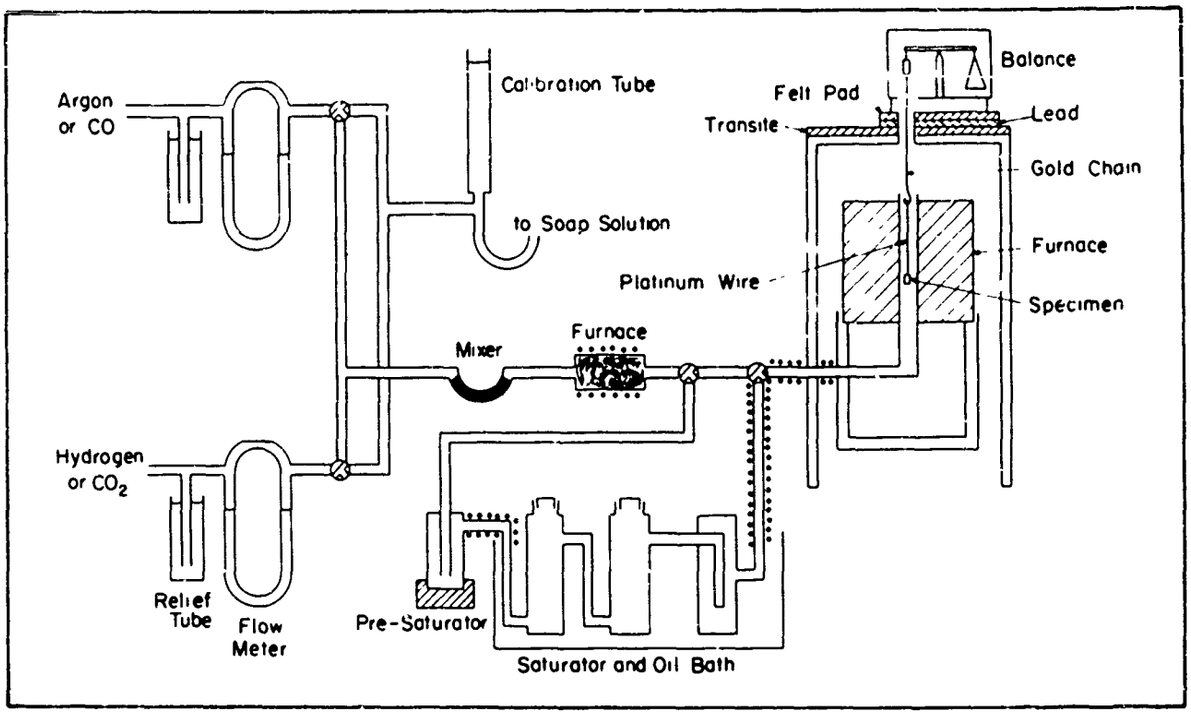

Figure 1. Schematic Representation of Apparatus Used for $CO-CO_2$ and H_2-H_2O Equilibration

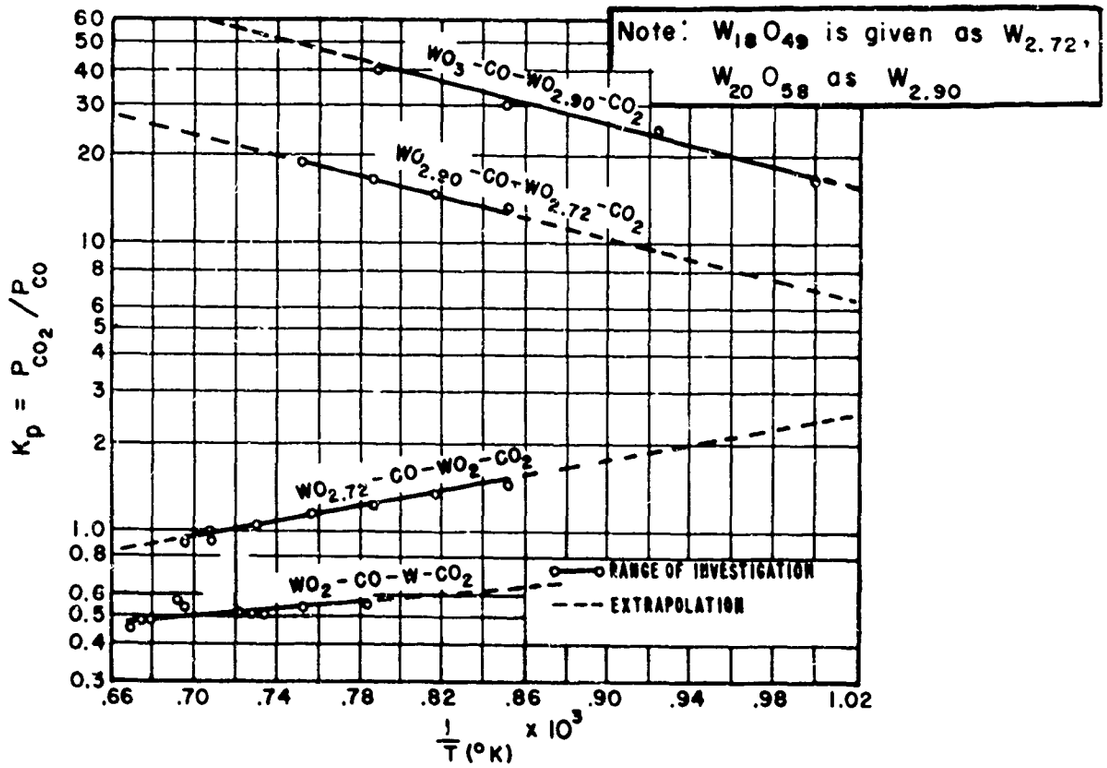

Figure 2. CO_2-CO Ratios for Tungsten Oxide Equilibria

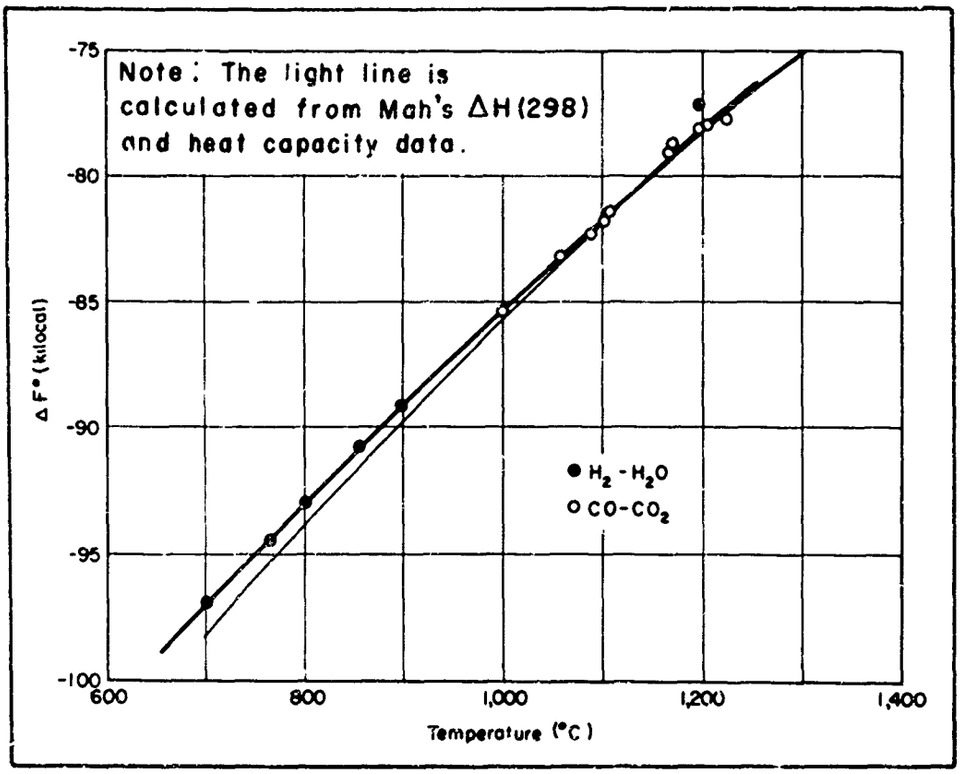

Figure 3. ΔF° for the Reaction: $W + O_2 = WO_2$.

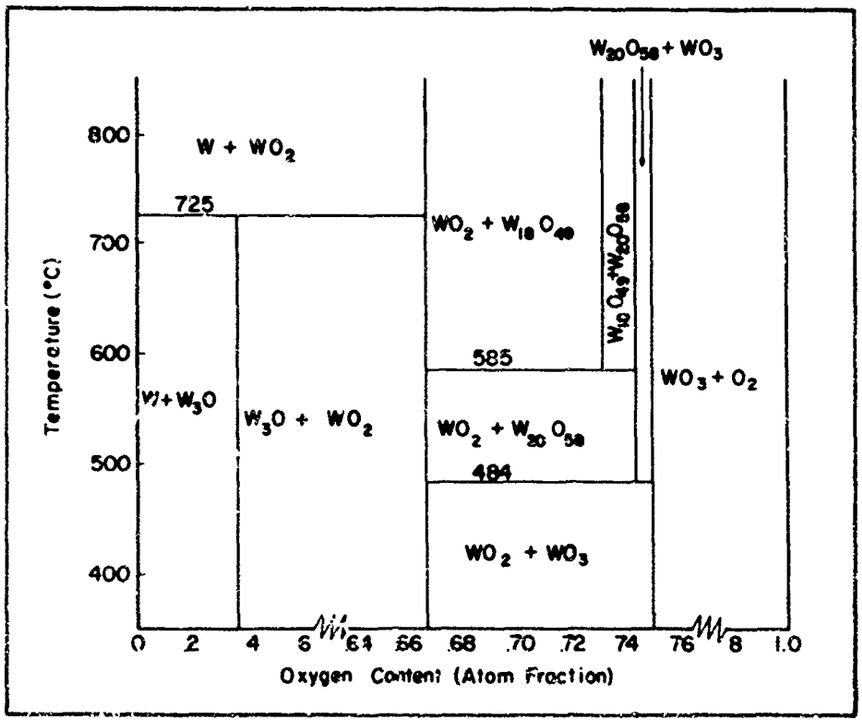

Figure 4. The Tungsten-Oxygen Phase Equilibria at One Atmosphere Total Pressure

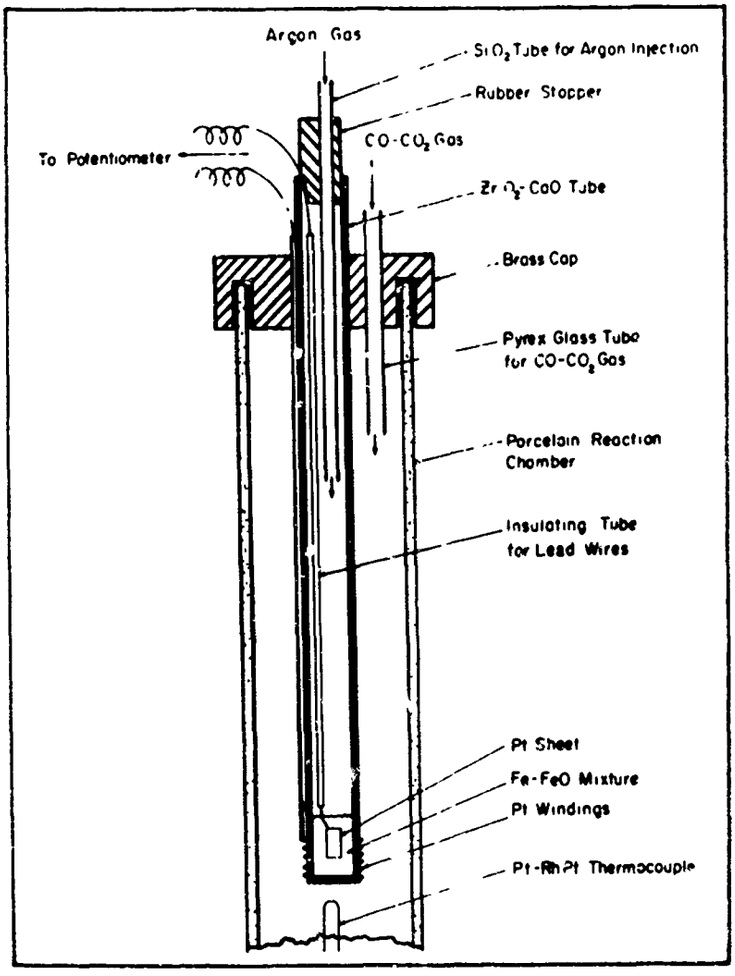

Figure 5. Schematic Diagram of the Oxygen Gauge Used to Determine CO-$C_{\frac{1}{2}}$ Ratios

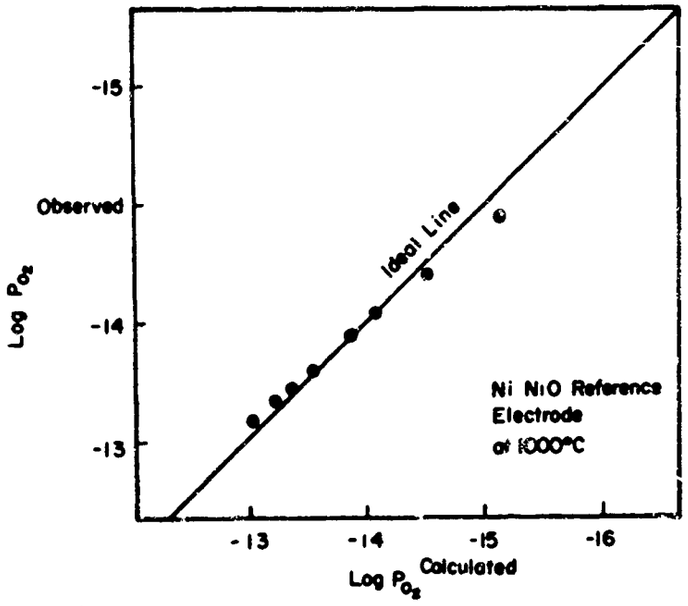

Figure 6. Relationship Between the Observed and Calculated Oxygen Pressures at 1000° C

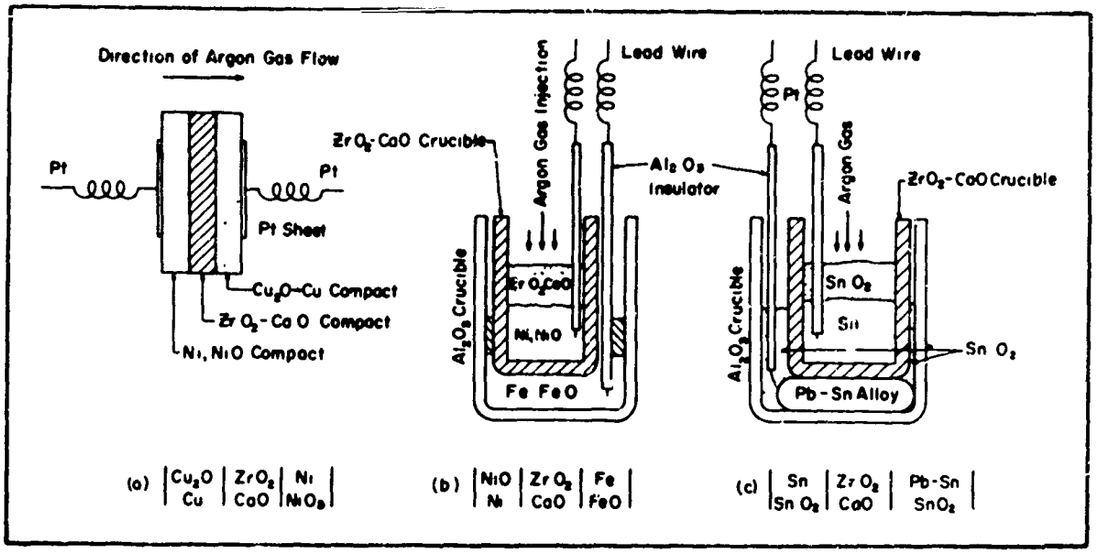

Figure 7. Three Types of Oxygen Concentration Cells

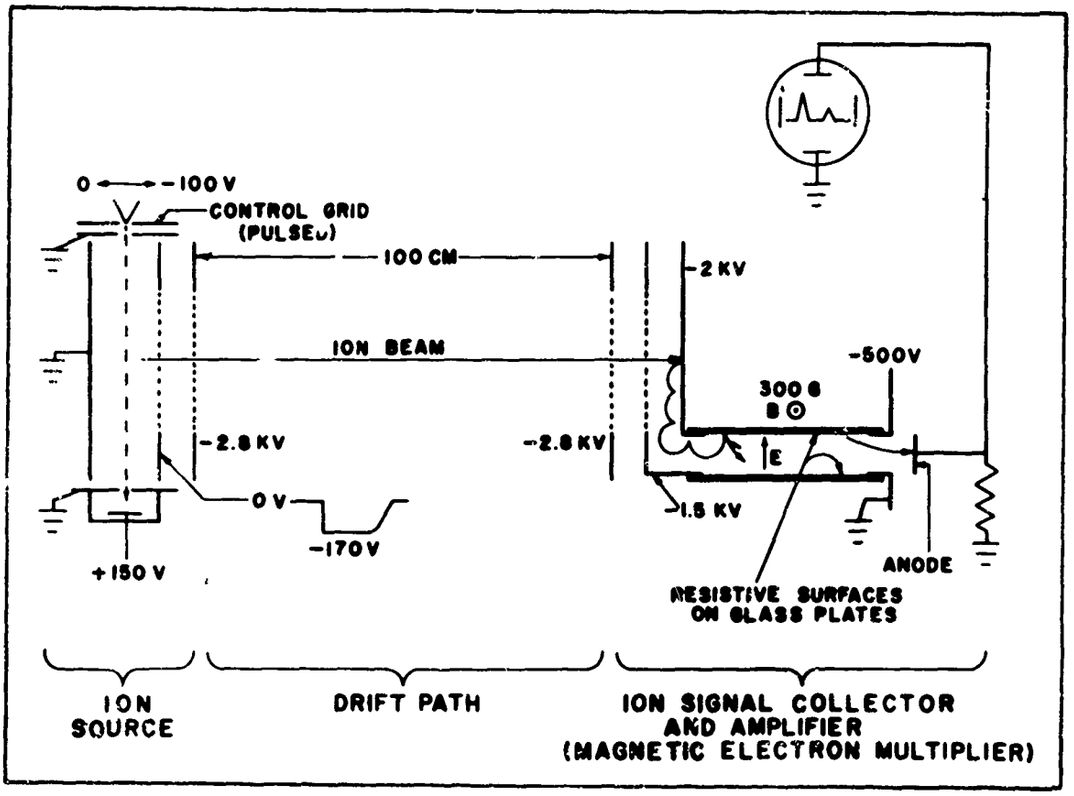

Figure 8. Schematic Diagram of Bendix Time-of-Flight Mass Spectrometer

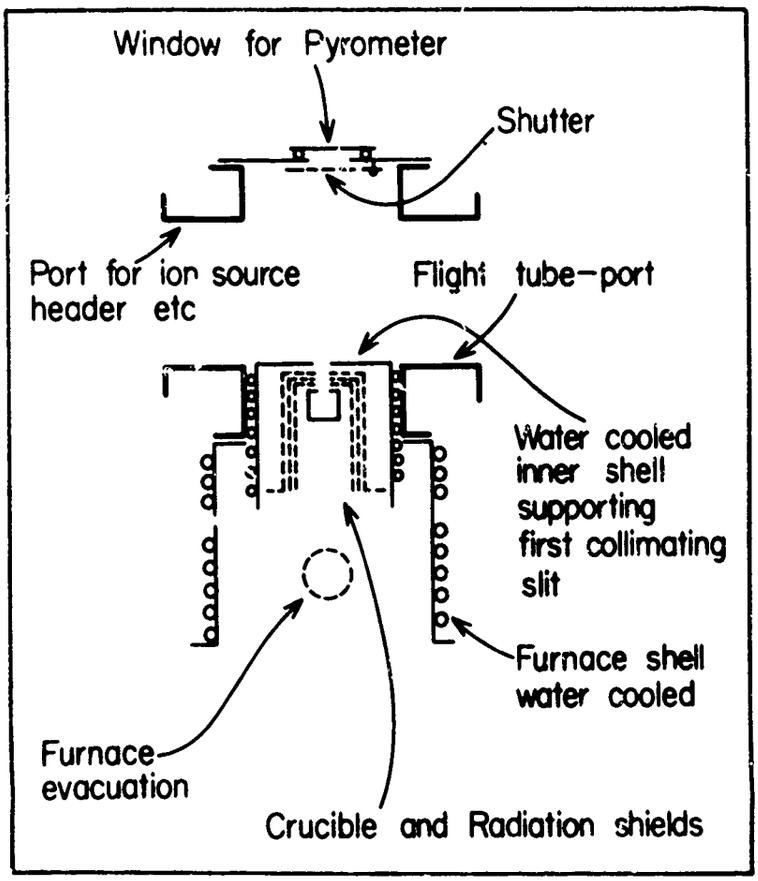

Figure 9. Furnace Containing Knudsen Cell for Use With Time-of-Flight Mass Spectrometer (Schematic)

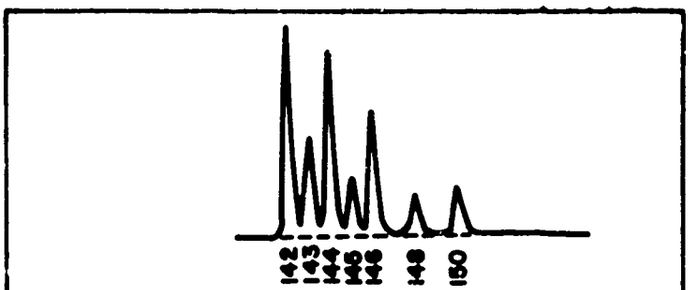

PERCENT

MASS	LITERATURE	EXPERIMENTAL
142	26.9	27.2
143	12.2	13.0
144	23.9	24.1
145	8.3	7.7
146	17.3	16.5
148	5.8	5.4
150	5.7	6.1

Figure 10. Mass Spectrum of the Isotopes of Neodymium

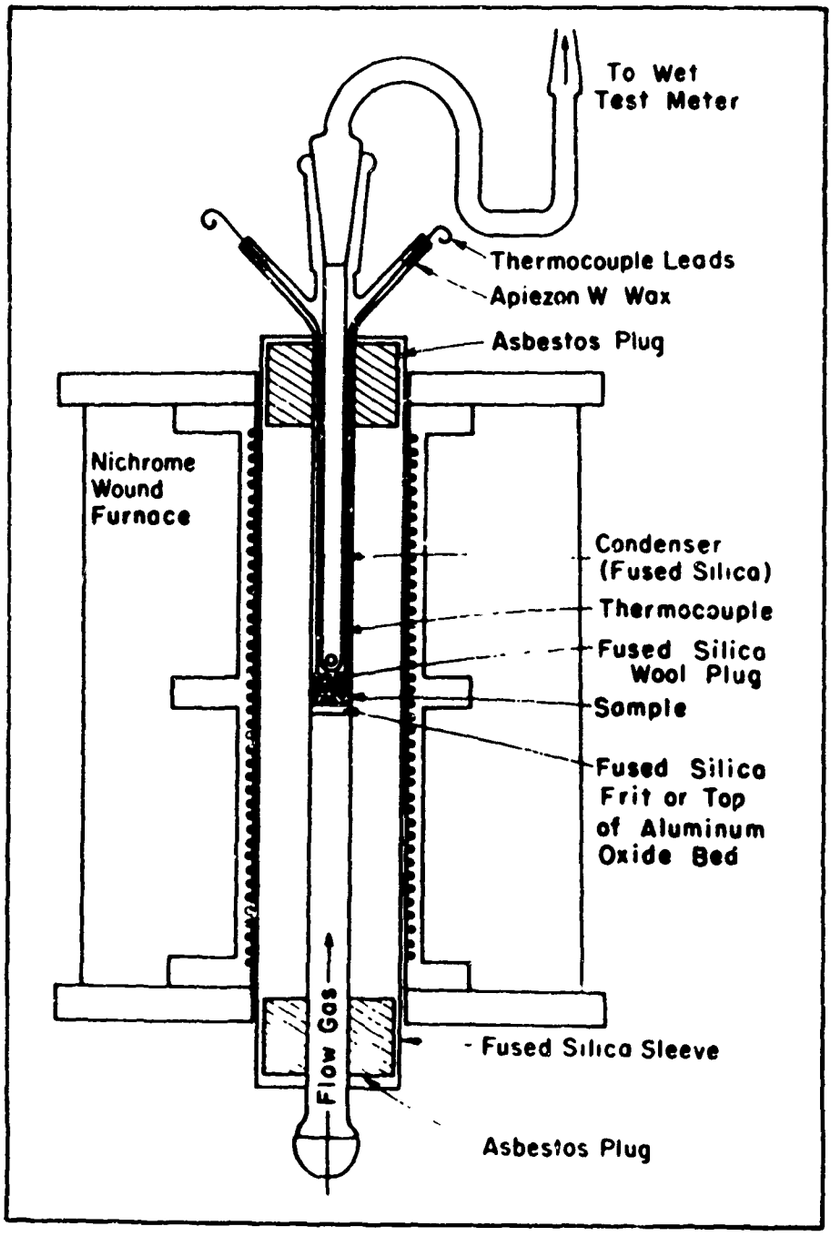

Figure 11. Schematic Sketch of Apparatus Used to Transpire Gaseous Molybdenum

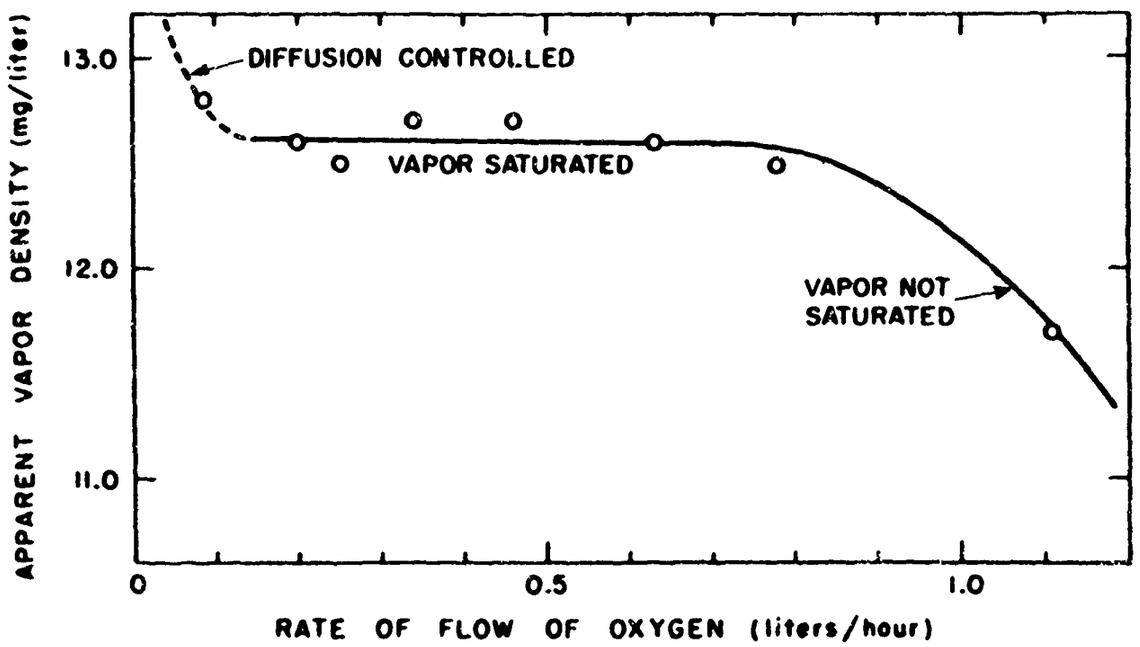

Figure 12. Variation of the Amount of Molybdenum Trioxide With Flow Rate at 1000° K

HIGH PRESSURE OXIDATION OF REFRACTORY METALS — EXPERIMENTAL METHODS AND INTERPRETATION

W. M. Fassel, Jr. *
J. N. Ong*
A. M. Saul*

INTRODUCTION

Early in 1948, as part of a study on incendiary magnesium alloys (Reference 1), it was found that the ignition temperature varied with the oxygen overpressure in a complex manner. The correlation between the change in ignition temperature and oxidation rate with alloying (Reference 2) suggested that the oxidation processes influenced the temperature at which active combustion could occur. Numerous unsuccessful attempts were made to explain the observed variations using existing oxidation theory as a basis (Reference 3).

At that time, it should be noted, no quantitative data was available on the oxidation rate of any metal at pressures above one atmosphere (Le Chatelier reported that a black oxide was formed on silver at 300°C with 15 atm oxygen pressure (Reference 4)).

The principal theoretical analysis of the pressure effect on the oxidation rate of metals was that of Wagner and co-workers. In their treatment, which had been experimentally confirmed only for pressures below one atmosphere, they suggested that the oxidation rate would vary as some fractional power (1/7 for Cu, 1/6 for Ni) of the oxygen pressure at the gas/oxide interface. This treatment (References 5 and 6) has been reviewed in detail in a number of recent publications (Reference 7).

The surprising lack of data on the oxidation rate of metals at hyperatmospheric pressures coupled with the inability of any known oxidation theory to explain the observed variation of the ignition temperature of magnesium versus pressure and the limited theoretical work at pressure, suggested that this area could fruitfully be explored.

DEVELOPMENT OF EXPERIMENTAL METHODS

Late in 1949, work was started on the development of equipment suitable for the continuous quantitative measurement of oxidation rates at high oxygen pressures. As an initial goal, pressures to 600 psia oxygen at 1000°C were to be achieved with the equipment.

Gravimetric methods were preferred because of their inherent simplicity and the directness of the method. Volumetric methods were not considered suitable because of the difficulty in maintaining a leak-free system at high pressures and in accurately measuring the volume of gas consumed by any reasonable technique at 40 atmospheres pressure.

A number of possible gravimetric methods were considered. For quantitative measurements at hyperatmospheric pressures, the quartz spring balance first used by Leontis and Rhines (Reference 2) for oxidation rate studies has many advantages. None of the more elaborate techniques considered then or tried over the past 10 years has proved better and more trouble free than the simple quartz spring microbalance.

The initial equipment designed to use this technique at pressures to 40 atmospheres is shown in Figure 1 (Reference 8).

*Aeronutronic Division, Philco Corporation.

The nichrome V-wound furnace was enclosed in a steel pressure vessel equipped with a variety of flanges for assembly, access to samples, observation windows, and power leads.

While this unit was successfully used on copper to 600 psia 0_2 at 900°C, a number of difficulties inherent to the design were encountered. One of the most troublesome of these was the spurious oscillation of the quartz spring balance. This became progressively worse with increased pressure and temperature. Experimentally, it was found that this problem could be substantially reduced by decreasing the diameter of the upper furnace section (N of Figure 1, original I.D. 4 inches) as well as the diameter of the furnace tube. Locating the quartz spring farther from the hot zone also tended to reduce the magnitude of the oscillations. In addition to the above problem, the massive nature of the unit made repairs difficult and time-consuming.

Based on the above observations, the furnace was completely redisigned. The general arrangement of the pressure shell, weighing components, and furnace element are shown in Figure 2. The sectional arrangement of the furnace allows easy replacement of any of the component parts. The most frequent failures are the heating elements and thermocouples. The heating unit consists of a 1-inch I.D. Alundum core (Norton No. 11756) 23 inches long. The core is wound with three separate windings individually controlled. The temperature of the center winding is automatically controlled by a Leeds and Northrup Speedomax control system which adjusts the power input from a 15-amp powerstat. The upper and lower guard rings, N, are controlled manually by similar powerstats.

The guard ring heating elements, N, overlap the end sections of M by about 1-1/4 inches. The overlapped section is backed off 3/16 inch from the controlled section by short sectors of a similar Alundum core. This arrangement has been found to give a very uniform temperature over a 4-inch length in the tube. Four thermocouples, T, are used. The upper and lower thermocouples in winding, M, are used to adjust the power input to the guard rings, N. One of the center thermocouples controls the winding temperature and the other is used exclusively to measure the sample temperature. This couple is shielded by a parabolic Alundum shield so that it effectively "looks" only at the sample, as shown in Figure 3.

Temperature checks using very fine thermocouple wire welded directly to the metal samples show the true sample temperature to be within ±1°C of the measured sample temperature at 700°C. The thermocouple leads, S, through the furnace shell are modified No. 18 spark plugs. The center electrode was removed and replaced with the appropriate metal or alloy to prevent junction error.

Thermal insulation becomes a very serious difficulty at higher pressures (above 300 psi). This is apparently due to the increased thermal conductivity of the oxygen. At pressures above 600 psi, water cooling must be used on the exterior shell.

Originally, teflon gaskets were used. Two failures occurred. While the reason is not known, teflon apparently decomposes rapidly to gaseous products at 80° to 100°C in oxygen at 500 to 600 psi. It should, therefore, be used with extreme caution under these conditions. Garlock "900" gaskets (compressed asbestos) have been successfully substituted in all regions where the temperature is above 35°C.

Figure 4 is a detailed drawing of the winch mechanism and window block.

This basic design has been used successfully over the past ten years for a variety of quantitative rate measurements at hyperatmospheric pressures (References 9 through 16).

In 1958, the design was modified slightly for McKewan to investigate the reduction of Fe_2O_3 at high hydrogen pressures (Reference 17). This unit was made entirely of stainless steel to minimize corrosion by water vapor formed from the reaction. In

this modification, all power and thermocouple leads were transferred to the top of the furnace shell to simplify repairs.

Recently, a number of modifications have been developed to extend the range and versatility of this basic unit. The operating conditions for the various types shown in Figures 5, 6, 7, and 8 are summarized in Table 1.

THE PRESSURE EFFECT

The variety of environmental conditions to which metals are being subjected, ranging from oxidizing to reducing combustion product gas mixtures and from high pressure combustion chambers to high altitude flight paths at temperatures from ambient to metal melting points, has placed emphasis on the necessity for experimental work to determine the effect of gas pressure on the reaction rate of metals. In general, the effect of gas pressure on metal-gas reactions should be considered from several viewpoints: (1) thermodynamics and kinetics, (2) the type of reactor used to conduct experiments, and (3) the influence of pressure on product phase stability.

Thermodynamics and Kinetic Considerations

Consider a simple chemical reaction in which a metal, (Me), reacts with oxygen, (O_2), to form one oxide product

$$a \cdot Me + \frac{b}{2} O_2 \rightarrow Me_a O_b \qquad (1)$$

A general rate equation may be written in the form

$$\text{Rate} = \frac{d(m/A)}{dt} = k_f f([Me], [O_2]) - k_r f([Me_a O_b]) \qquad (2)$$

The definition of m is normally in terms of reactant oxygen consumption (gm). A is the area over which the reaction occurs (cm^2); t is the time (sec); k_f and k_r are the forward and reverse reaction rate constants; and $f([Me], [O_2])$, and $f([Me_a O_b])$ are functions of reactant and product concentrations respectively. The particular form of the above functions will depend on whether the kinetic mechanism is elementary, complex, or chain (Reference 18).

At conditions not equivalent to equilibrium one term in Equation 2 will normally predominate.

When $\Delta F<0$, the rate of decomposition of the products is generally negligible and the rate may be written

$$\frac{d(m/A)}{dt} = k_f f([Me], [O_2]) \qquad (3)$$

When the mechanism is first order complex chain (Reference 19), Equation 3 may be expressed as a function of oxygen concentration or pressure only

$$\frac{d(m/A)}{dt} = k_f f([O_2]) = k_f f'(P_{O_2}) \qquad (4)$$

When $\Delta F>0$, $k_r f([Me_a O_b]) > k_f f([Me], [O_2])$ and the consumption of reactant may proceed only when the reaction products are continually removed from the reaction interface.

Removal of the gaseous product species is generally accomplished by diffusion through a gas boundary layer lying between the bulk gas region and the reaction interface. It is assumed that no mixing occurs in this layer and, therefore, a steady state concentration gradient can be established. The rate of transport by diffusion across a boundary layer of thickness, x, is given by (References 20 and 21)

$$\text{Rate} = \frac{d(m/A)}{dt} = \frac{MDP}{aRTx} \ln\left(\frac{P-P_b}{P-P^e}\right) \qquad (5)$$

where M is the molecular weight of the diffusing product species, D is its diffusion coefficient (cm^2/sec), a is the stoichiometric coefficient of the metal, R is the gas constant (cm^3 atm/mol°K), T is the temperature at

the reaction interface, (°K), x is the thickness of the boundary layer of gas (cm), P is the bulk gas pressure (atm), P_b is the partial pressure of the diffusing species in the bulk gas (atm) and P^o is the partial pressure of the diffusing species at the reaction interface. If the rate of chemical reaction at the interface is rapid relative to the rate of diffusion through the boundary layer, then P^o represents the equilibrium partial pressure of the product species at the reaction interface.

It is apparent that this type of reaction will be sensitive to the nature of the flow of gases around the specimen. Thus, under dynamic flow conditions, the bulk gas is characterized by an essentially constant temperature and composition due to turbulence — the greater the turbulence, the thinner the boundary region. Boundary layer thickness can be computed, in general, from fluid dynamic considerations (References 20 and 22). In an open flow system, the bulk gas remains relatively unsaturated with respect to the gaseous product species; that is, P_b remains quite small compared to P. If P^o_b is also quite small compared to P, then Equation 5 simplifies to

$$\frac{d(m/A)}{dt} = \frac{MDP^o}{aRTx} \qquad (6)$$

In a closed flow system, the bulk gas continues to recirculate and saturate with respect to the gaseous product species. P_b thus approaches P^o and the rate of consumption of reactant approaches zero. If the bulk gas temperature is lower than the temperature at the reaction interface, P_b may actually exceed P^o if the thermodynamic stability of the gaseous product species increases with decreasing temperature. As an example, consider the reaction of graphite at 2100°K with hydrogen at 16.7 atmospheres to produce methane (Reference 23). The equilibrium partial pressure of methane at the reaction interface is 9.0×10^{-2} atmosphere, which also is the upper limit for P_b at 2100°K. At a bulk gas temperature of 1000°K, for example, equilibrium partial pressure of methane is 2.8×10^{-1} atmosphere. Thus, P_b can exceed P^o, and a steady state condition is possible in which carbon or graphite redeposits on the original hot surface. The situation is additionally complicated in that graphite displays preferential crystallographic sites for reaction. Thus, the hot surface available for redeposition may be different than the surface available for reaction with hydrogen. Another example of a system exhibiting this type of behavior is the Pt-O system (References 24 and 25).

Pressure experiments, in some circumstances, may permit differentiation between rate Equations 4 and 5 or 6, since in the latter case, the effect of pressure on the rate may be in direct proportion to the effect of reactant pressure on product pressure as determined by the equilibrium expression for Equation 1 (References 24 and 25), whereas in the former case, this will depend upon the nature of the intermediate species and the type of rate controlling process.

Type of Process

For phase boundary and diffusion controlled processes, Equation 4 takes the following forms

$$\text{Rate} = \frac{d(m/A)}{dt} = k_s C_s \quad \text{(phase boundary)} \qquad (7)$$

$$\text{Rate} = \frac{d(m/A)}{dt} = \left(\frac{D_{ox}\,\Delta C_{ox}\,\rho_{ox}\,MO_b/MeO_b}{2}\right)^{1/2} \frac{1}{t^{1/2}} \quad \text{(diffusion)} \qquad (8)$$

$$\text{Rate} = \frac{d(m/A)}{dt} = \left(\frac{D_i}{\pi}\right)^{1/2} \frac{C_i}{t^{1/2}} \quad \text{(interstitial diffusion)} \qquad (9)$$

where k_s is the specific reaction rate constant, (sec^{-1}), C_s(g/cm^2) is the intermediate surface species concentration, D_{ox} is the diffusion coefficient of species diffusion through the oxide (cm^2/sec), ΔC_{ox} is the concentration difference of intermediate species existing across the oxide phase (g/cm^3), ρ_{ox} is the oxide density, M_{O_b/Me_aO_b} is the molecular weight ratio of the subscripted quantities, and D_i and C_i are the corresponding quantities for interstitial diffusion of oxygen in the metal. The pressure dependence on concentration in each case will depend on the nature of the intermediate species controlling the rate of reaction.

Pressure Dependence on Concentration

The pressure and temperature dependence on the intermediate species concentration is normally obtained by assuming that equilibrium chemisorption precedes the rate determining step. For phase boundary reactions, the intermediate species is chemisorbed oxygen and the expression takes the form (Reference 26)

$$C_s = C_s^{\circ}\left(\frac{K_s P_{O_2}^{1/2}}{1 + K_s P_{O_2}^{1/2}}\right) \qquad (10)$$

where $K_s = \exp(\Delta S_s/R)\exp-(\Delta H_s/RT)$ is the equilibrium constant for the reaction: $1/2\ O_2$ + Site $\rightleftharpoons$ Site···O. ΔS_s and ΔH_s are respectively the entropy and enthalpy of adsorption, C_s° is a conversion factor (gm/cm^2), and ideality is assumed.

In Equation 8, transport of oxygen or metal across the oxide is by means of an anion or a cation vacancy gradient. Since the vacancy concentration at either the oxide-gas or oxide-metal interface is usually negligible in the above two cases, the value of ΔC is effectively that of either the concentration of anion vacancies at the oxide-metal interface or the concentration of cation vacancies at the oxide-gas interface.

When vacancy formation is preceded by oxygen chemisorption on the surface, the following expressions for pressure dependency result (Reference 16)

a. Anion vacancy or unionized cation vacancy.

$$\Delta C_{V_O} \text{ or } \Delta C_{V_M} = \Delta C_s\left(\frac{K_s K_1 P^{1/2}}{1 + K_s K_1 P^{1/2}}\right) \qquad (11)$$

b. Singly ionized cation vacancy

$$\Delta C_{V_M}' = \Delta C'\left(\frac{K_s K_1' P^{1/2}}{1 + K_s K_1' P^{1/2}}\right)^{1/2} \qquad (12)$$

c. Doubly ionized cation vacancy

$$\Delta C_{V_M}'' = \Delta C''\left(\frac{1/4\, K_s K_1'' P^{1/2}}{1 + K_s K_1'' P^{1/2}}\right)^{1/3} \qquad (13)$$

ΔC°, $\Delta C'$ and $\Delta C''$ are conversion factors (gm/cm^3) and K_1, K_1' and K_1'' are the respective equilibrium constants for the reactions:

a. Site···O $\overset{K_1}{\rightleftharpoons}$ V_{Me} + MeO or Site···O $\overset{K_1}{\rightleftharpoons}$ O

b. Site···O $\overset{K_1'}{\rightleftharpoons}$ V_{Me}' + ⊕ + MeO and

c. Site···O $\overset{K_1''}{\rightleftharpoons}$ V_{Me}'' + 2⊕ + MeO

Equations 10 through 13 are characterized by the fact that the intermediate species concentration governing the rate of reaction is pressure insensitive at high pressures and low temperatures and pressure sensitive

at low pressures and high temperatures as indicated in Figure 9. When these transitions occur, the reaction rate constant and the concentration terms in Equations 7, 8, and 9 may often be differentiated and enthalpies of adsorption and vacancy formation may be differentiated from the enthalpy of activation. Pressure dependencies of the type represented by Equation 10 have been shown to be exhibited by tantalum (References 10, 27, 28, and 29), columbium (References 30, 31, 32, and 33), and tungsten (References 6 and 19); that of Equation 11 by cobalt (Reference 15) and tungsten (Reference 19); and that of Equation 12 by nickel (Reference 16). Pressure dependencies for oxides different from the type MeO may be determined by standard methods (Reference 34).

Effect of Pressure on Reaction Class

Composite effects will arise if more than one reaction occurs, either simultaneously or consecutively. Use of the pressure variable under these circumstances will permit separation of these processes if their pressure dependencies are different at constant temperature (References 19, 27, 33, and 35).

Influence of Reactor on Oxidation Experiments

Equations 4 and 5 should be used under the assumption that an unlimited supply of both metal and reacting gas comprises the system. Under experimental conditions the metal coupon used is generally small; however, area corrections to account for specimen depletion during reaction are generally made so that data is normalized on an extended area basis.

In a closed reactor (volume constant), for $\Delta F>O$ reactions when the pressure of reactant, P, is large, the expression for the amount of solid reacted with time takes the form

$$\Delta m/A = \frac{P^{o}MV}{aRTA}\left(1 - \exp - \frac{DA}{Vx}t\right) \qquad (14)$$

This reaches a limiting value of $\frac{P^{o}MV}{aRTA}$ and has an initial slope of $\frac{P^{o}MD}{aRTx}$ from which the value D/x may be calculated (Fig. 10).

For $\Delta F>O$ reactions, if the pressure dependency is given by Equation 10 for example; the pressure of the reactor would be determined by the pumping speed, S, (cm^3atm/sec) according to (Reference 36)

$$\frac{dp}{dt} = -\frac{S}{V}p = -\frac{p}{V}\left[\frac{b}{a}\frac{k_s}{N}C_o^{o}\left(\frac{K_s P^{1/2}}{1+K_s P^{1/2}}\right)\frac{AR_g}{P}\right] \qquad (15)$$

using Equation 7, with the stoichiometric coefficients a and b, the molecular weight of oxygen, M, the temperature of the gas, T_g, and the reactor volume, V.

This yields for the reactor pressure the expression

$$(P_o - P) + \frac{2}{K_s}\left(P_o^{1/2} - P^{1/2}\right) = \frac{S}{V}t \qquad (16)$$

where P_o is the original pressure of the reactor.

The variation of pressure with time is shown in Figure 11 together with weight gain plots of pressure insensitive ($K_s >> 1$) and pressure sensitive ($K_s << 1$) phase boundary reactions. It is seen that for equivalent reaction times pressure sensitive reactions deviate from linearity, whereas pressure sensitive reactions remain linear virtually to exhaustion of oxygen.

Effect of Pressure on Phase Stability

The effect of pressure on the phase stability of products of reaction is well known. It appears worthwhile, however, to point out that the form of rate equations will depend

on the number and order of product phases formed. Copper may be used as an illustrative example. By referring to the P-T diagram for Cu-O, Figure 12, it will be seen that in region I the reaction of Cu with O will involve only evaporation of copper from the surface with possible subsequent reaction to form CuO(V) (Reference 37). In region II, the growth rate of Cu_2O is parabolic with a pressure dependence of either Equation 12 (Reference 12) or Equation 13 (Reference 5).

In region III, the overall rate is parabolic with CuO forming from Cu_2O. The overall pressure dependence will be different since although the formation rate of CuO is probably pressure dependent according to Equations 11 or 12, the Cu_2O formation rate is now pressure insensitive since the defect concentration at the Cu_2O-CuO interface will remain essentially constant. For purposes of discussion, the effects of nucleation and growth of the CuO from the Cu_2O phase have been neglected. Similar considerations apply for other metals although most others are considerably less stable, i.e., $\Delta F << O$ and lowering pressure may not be expected to change the number of product phases as readily.

In summary, the type of rate equations encountered for various metal gas reactions are presented in Table 2. The values of the rate constants and pressure dependencies for those metals which have been worked out are given in the Appendix.

Example:

The oxidation of molybdenum and tungsten offers interesting examples wherein all of the foregoing considerations should be taken into account for a complete analysis.

At temperatures below the melting point and at moderate pressures, both metals oxidize according to the consecutive reactions

$$Me + O_2 \rightarrow MeO_2 \quad (\Delta F < 0) \qquad (17)$$

$$MeO_2 + \tfrac{1}{2} O_2 \rightarrow MeO_{3(s)} \quad (\Delta F < 0) \qquad (18)$$

$$MeO_{3(s)} \rightarrow \frac{1}{n} (MeO_3)n\ (vap) \quad (\Delta H > 0) \qquad (19)$$

Reaction (17) is diffusion controlled, reaction (18) is phase boundary controlled and reaction (19) is gas boundary layer diffusion controlled, whose rates are given by Equations 8, 7, and 6 respectively. (See Table 2.) Reactions (17) and (18) exhibit pressure-insensitive to pressure-sensitive transitions in rate behavior in the case of W and probably in the case of Mo (Reference 38) according to Equations 10 and 9 (Reference 19).

For reaction (19) the rate of evaporation is proportional to the partial pressure P° of $(WO_3)n_{vap}$, according to Equation 6 and virtually insensitive to the oxygen overpressure, P, as given in Equation 5 and is related to the enthalpy of evaporation, ΔH_{vap} (Reference 39), by the Clausius-Clapeyron equation. The temperatures at which this process becomes appreciable at atmospheric pressure, for example, are from 950°C to 1100°C in the case of W and above about 850°C in the case of Mo. It is then that any weight measurement will become flow sensitive either in a flow reactor or by convective flow in a closed system. The volatility rate of trioxide does not necessarily affect the overall metal reaction rate but failure to account for the flow sensitivity of trioxide volatilization has given rise to conflicting observations on the reaction rates of these two metals (References 22, 40, and 41).

APPENDIX

Rate Constant Values For Tungsten

Phase - Boundary Process ($WO_2 + \frac{1}{2} O_2 \rightarrow WO_3$)

$3.6 \times 10^3 \left(\frac{sec}{hr}\right) 1000 \left(\frac{mg}{gm}\right) \nu_3 C_s^o$	$= 7 \times 10^{10}$ mg/cm^2 hr
ΔH^*	= 45.9 kcal / mole
$\exp (S_s / R)^*$	$= 2.2 \times 10^{-5}$
ΔH_s^*	= − 21.7 kcal / mole

Diffusion Process ($W + O_2 \rightarrow WO_2$)

$3.6 \times 10^3 \left(\frac{sec}{hr}\right) 10^6 \left(\frac{mg^2}{gm^2}\right) D_{ox} \rho_{ox} M_{O_2} / WO_2 \Delta C_{ox}^o$	$= 7.5 \times 10^{15}$ mg^2/cm^4 hr
ΔH_d^*	= 68 kcal / mole
$\exp (\Delta S_{ox} / R)^{**}$	$= 1.133 \times 10^{-6}$
ΔH_{ox}^{**}	= −27.6 kcal / mole

Rate Constants For Columbium

Oxygen - Diffusion Process ($Cb + \frac{y}{2} O_2 \rightarrow CbOy$)

$D_o^{1/2} C_i r$	$= 2.85 \times 10^{-3}$ gm/cm^2 sec$^{1/2}$
ΔH_{id}^*	= 29.4 kcal/mole

Phase - Boundary Process 2 ($CbOy + \left(\frac{5-2y}{4}\right) O_2 \rightarrow Cb_2O_5$

$3.6 \times 10^3 \left(\frac{sec}{hr}\right) 10^3 \left(\frac{mg}{gm}\right) \nu_{s2} C_{s2}^o$	$= 6.67 \times 10^{17}$ mg/cm^2 hr
ΔH_{s2}^*	= 56.92 kcal / mole
$\exp (\Delta S_{s2} / R)^*$	$= 5.7 \times 10^{-14}$
ΔH_{s2}^*	= -44.66 kcal / mole

*Use Equation 10.

**Use Equation 11.

Phase-Boundary Process 1 $\left(CbO_z + \left(\frac{5-2z}{4}\right) O_2 \rightarrow Cb_2O_5 \right)$

$3.6 \times 10^3 \left(\frac{sec}{hr}\right) 10^3 \left(\frac{mg}{gm}\right) \nu_{s1} C^o_{s1}$	$= 9.65 \times 10^{14}$ mg/cm^2 hr
ΔH^*_{s1}	= 59.52 kcal/mole
$\exp (\Delta S_{s1}/R)^*$	$= 4.55 \times 10^{-12}$
ΔH^*_{s1}	= -50.112 kcal/mole

Rate Constant Values For Tantalum

Oxygen-Diffusion Process $\left(Ta + \frac{y}{2} O \rightarrow TaOy \right)$

$D_o^{1/2} C_i r$	$= 4.93 \times 10^{-3}$ gm/cm^2 sec$^{1/2}$
ΔH^*_{id}	= 23.1 kcal/mole

Phase-Boundary Process 2 $\left(TaOy + \left(\frac{5-2y}{4}\right) O_2 \rightarrow Ta_2O_5 \right)$

$3.6 \times 10^3 \left(\frac{sec}{hr}\right) 10^3 \left(\frac{mg}{gm}\right) \nu_{s2} C^o_{s2}$	$= 8.41 \times 10^{18}$ mg/cm^2 hr
ΔH^*_{s2}	= 70.73 kcal/mole
$\exp (\Delta S_{s2}/R)^*$	$= 1.19 \times 10^{-16}$
ΔH^*_{s2}	= -64.0 kcal/mole

Phase-Boundary Process 1** $\left(TaO_z + \left(\frac{5-2z}{4}\right) O_2 \rightarrow Ta_2O_5 \right)$

$3.6 \times 10^3 \left(\frac{sec}{hr}\right) 10^3 \left(\frac{mg}{gm}\right) \cdot \nu_{s1} C^o_{s1} \exp(\Delta S_{s1}/R)$	$= 1.22 \times 10^5$ mg/cm^2 hr
$\Delta H_{s1} + \Delta H^*_{s1}$	= 18.3 kcal/mole

*Use Equation 10.

**Rate constants not fully separable because of the lack of pressure-insensitive data for this process.

Rate Constant Values For Cobalt

Diffusion Process $\left(Co + \frac{1}{2} O_2 \rightarrow CoO\right)$

$3.6 \times 10^3 \left(\frac{sec}{hr}\right) 10^6 \left(\frac{mg^2}{gm^2}\right) D_{ox} \rho_{ox} M_{O/CoO} \Delta C^o = 3.85 \times 10^9 \ (mg^2/cm^4 \ hr)$

$\Delta H_d^{\ddagger} = 59.6 \ (kcal/mole)$

$\exp (\Delta S_{ox}/R)^* = 6.11 \times 10^{-4}$

$\Delta H_{ox}^* = -17.9 \ (kcal/mole)$

Rate Constant Values For Nickel

Diffusion Process $\left(Ni + \frac{1}{2} O_2 \rightarrow NiO\right)$

$3.6 \times 10^3 \left(\frac{sec}{hr}\right) 10^6 \left(\frac{mg^2}{gm^2}\right) D_{ox} \rho_{ox} M_{O/NiO} \Delta C^o \exp (\Delta S_{ox}/R)^{**}$

$= 4.9 \times 10^{-1} \ (mg^2/cm^4 \ hr)$

$\Delta H_d^{\ddagger} + \Delta H_{ox}^{**} = 50.5 \ (kcal/mole)$

*Use Equation 11.
**Use Equation 12.

REFERENCES

1. W. M. Fassel, Jr., L. B. Gulbransen, J. R. Lewis, and J. H. Hamilton, Transactions of AIME. V. 191, 1951, p. 522, J. of Metals, July 1951, p. 522.

2. T. E. Leontis and F. N. Rhines, Transactions of AIME, V. 166, 1946, p. 265, Metals Technology, June, 1946.

3. H. Eyring and B. J. Zwolinski, "The Critical Temperature for Combustion of Metals and Their Alloys," Record of Chemical Progress, Wayne University, July-October, 1947.

4. H. LeChatelier, Ztsch. Physik Chem., V. 1, 1887, p. 516.

5. C. Wagner and K. Grunewald, Ztsch. Physik Chem., B40, 1938, p. 455.

6. C. Wagner, Ztsch. Physik Chem., B21, 1933, p. 25, B32, 1936, p. 447.

7. O. Kubaschewski and B. E. Hopkins, Oxidation of Metals and Alloys, Academic Press, Inc., New York. Second Edition, 1962, pp. 82-96.

8. W. M. McKewan and W. M. Fassel, Jr., Transactions of AIME, 195 197, pp. 1127-1130, J. of Metals, September 1953.

9. W. M. Fassel, Jr., R. C. Peterson, D. W. Bridges, and J. P. Baur, "High-Pressure Oxidation Rate of Metals," Pacific Northwest Metals and Minerals Conference AIME, 1954, Portland, Oregon.

10. R. C. Peterson, W. M. Fassel, Jr., and M. E. Wadsworth, "High-Pressure Oxidation of Metals: Tantalum in Oxygen." Transactions of AIME, V. 200. pp. 1038-1044. J. of Metals. V. 6.

11. J. P. Baur, D. W. Bridges, and W. M. Fassel, Jr., "High-Pressure Oxidation of Metals: Oxidation of Metals Under Condition of Linear Temperature Increase." J. Electrochemical Society, V. 102, August, 1955, pp. 490-496.

12. J. P. Baur, D. W. Bridges, and W. M. Fassel, Jr., "Oxidation of Oxygen Free High Conductivity Copper to Cu_2O," J. Electrochemical Society, V. 103, May, 1956, pp. 273-281.

13. J. P. Bauer, D. W. Bridges, and W. M. Fassel, Jr., "High-Pressure Oxidation of Metal: Tungsten in Oxygen," J. Electrochemical Soc., V. 103, June 1956, pp. 326-330.

14. D. W. Bridges, J. P. Baur, Gretta S. Baur, and W. M. Fassel, Jr., "Oxidation of Copper to Cu_2O and CuO," J. Electrochemical Soc., V. 103, September 1956, p. 475-478.

15. D. W. Bridges, J. P. Baur, and W. M. Fassel, Jr., "Effect of Pressure on the Oxidation Rate of Cobalt," J. Electrochemical Soc., V. 103, No. 11, November 1956, p. 614-618.

16. J. P. Baur, R. W. Bartlett, J. N. Ong, Jr., and W. M. Fassel, Jr., "High-Pressure Oxidation of Metals; Nickel in Oxygen," to be published J. Electrochem. Soc.

17. W. M. McKewan, "Reduction Kinetics of Magnetite in Hydrogen at High Pressures," Transaction of AIME, V. 224, April 1962, pp. 387-393.

18. K. J. Laidler, Chemical Kinetics, Chapter 7, The McGraw-Hill Book Co., New York, 1950.

19. J. N. Ong, Jr., "Oxidation of Refractory Metals as a Function of Pressure, Temperature, and Time: Tungsten in Oxygen," J. Electrochem. Soc., V. 109, 1962, p. 284.

20. S. J. Yosim, R. L. McKisson, A. M. Saul, and D. E. McKenzie, "Some Corrosion Considerations of High-Temperature Gas-Cooled Reactions," Progress in Nuclear Energy, Series IV, V. 2, 1960, p. 301.

21. T. K. Sherwood, Absorption and Extraction, The McGraw-Hill Book Co., New York, 1937, p. 7.

22. J. L. Modisette and D. R. Schryer, An Investigation of the Role of Gaseous Diffusion in the Oxidation of a Metal Forming a Volatile Oxide, NASA TN D-222, March 1960.

23. Unpublished data, performed for Advanced Research Projects Agency, Contract NOw 61-0905-c, Task D. ARPA Order No. 22-62, Aeronutronic, September 1962.

24. G. C. Fryburg and Helen M. Murphy, TN, Trans. Met. Soc. AIME, V. 212, 1958, p. 660.

25. G. S. Fryburg and Helen M. Petrus, "Kinetics of the Oxidation of Platinum," J. Electrochem. Soc., V. 108, 1961, p. 496.

26. S. Glasstone, K. J. Laidler, and H. Eyring, The Theory of Rate Processes, Chapter 7, The McGraw-Hill Book Co., New York, 1941.

27. J. N. Ong, Jr., "Oxidation of Refractory Metals as a Function of Pressure, Temperature and Time: Tantalum in Oxygen," Transactions of AIME, V. 224, 1962, p. 991.

28. M. G. Cowgill and J. Stringer, "Effect of Oxygen Pressure on the High-Temperature Oxidation of Tantalum," J. Less Common Met. V. 3, 1960, p. 233.

29. P. Kofstad, "Oxidation of Tantalum in the Temperature Range 500° to 700°C," J. Inst. Metals, V. 90, 1961-1962, p. 253.

30. D. W. Bridges and W. M. Fassel, Jr., "High-Pressure Oxidation of Niobium," J. Electrochem. Soc., V. 103, 1956, p. 326.

31. T. Hurlen, "Oxidation of Niobium," J. Inst. Metals, V. 89, 1960-1961, p. 273.

32. P. Kofstad and H. Kjollesdal, "Oxidation of Niobium in the Temperature Range 500 to 1200°C, Transactions Met. Soc. AIME, V. 221, 1961, p. 285.

33. J. N. Ong, Jr. and W. M. Fassel, Jr., "Kinetics of Oxidation of Columbium and Other Refractory Metals," Corrosion, Vol 18, P382C, 1962.

34. F. A. Kroger and H. J. Vink, "Relations Between the Concentrations of Imperfections in Crystalline Solids," Solid State Physics, V. 3, F. Seitz and D. Turnbull, Editors, Academic Press Inc., New York, 1956.

35. J. N. Ong Jr. and W. M. Fassel, Jr., "Effects of Alloying Elements on the Oxidation of Refractory Metals," AIME Refractory Metals Symposium, April 12-13, 1962, Chicago.

36. S. Dushman, Scientific Foundations of Vacuum Technique, John Wiley and Sons, Inc., New York, 1958, p. 121.

37. M. S. Sodna and Y. P. Varshni, Indian J. Phys., V. 27, 1953, p. 520.

38. R. C. Peterson and W. M. Fassel, Jr., "High-Pressure Oxidation of Metals - Molybdenum in Oxygen," TR No. 6, September 1954, Army Ordnance Contract DA 04-495-ORD-237, University of Utah.

39. E. A. Gulbransen and K. F. Andrew, "Kinetics of Oxidation of Pure Tungsten from 500° to 1300°C," J. Electrochem. Soc. V. 107, 1960, p. 619.

40. C. R. Wilks, "Effects of Temperature, Pressure, and Mass Flow on Oxidation of Molybdenum," SAMPE Eastern Division Meeting, Cambridge, Massachusetts, 3 May 1960.

41. E. S. Bartlett and D. N. Williams, "The Oxidation Rate of Molybdenum in Air," Transactions of AIME, V. 212, 1950, p. 280.

42. G. R. Wallwork and A. E. Jenkins, "Oxidation of Titanium, Zirconium, and Hafnium," J. Electrochem. Soc., V. 106, 1959, p. 10.

43. M. W. Mallett and B. G. Koehl, "Kinetics of the Tantalum-Hydrogen Reaction," J. Electrochem. Soc., V. 109, 1962, p. 968.

44. R. Speiser and G. R. St. Pierre, "Research on the Oxidation Behavior of Tungsten," Ohio State University Research Foundation, Columbus, Ohio, Report 831-9, WADD Contract No. AF 33(616)-5721, October 1960.

45. W. Feitknecht, Z. Electrochemie, V. 35, 1929, p. 142.

46. G. Valensi, Int. Cong. on Surface Reactions, 1948, p. 156.

47. W. W. Webb, J. T. Norton, and C. Wagner, "Oxidation of Tungsten," J. Electrochem. Soc., V. 103, p. 107.

48. J. Loriers, Acad. Sci. Paris, V. 231, 1950, p. 522.

TABLE 1

HIGH PRESSURE FURNACE DESIGNS FOR SOLID GAS REACTION RATE MEASUREMENTS

Model	Figure	Shell Material	Heater and Type	Temp. Range ^{o}C	Pressure Range psia	Atmosphere
II	2	Steel	Kanthal A-1 3 Zone Control	400-1200	0.1-1000	O_2, N_2, Air
III	5	304 Stainless	Kanthal A-1 3 Zone Control	400-1100	0.1-600	O_2, N_2, Air, H_2
III	5	Steel	Kanthal A-1 Pt-40%Rh	400-1200 800-1500	0.1-600 0.1-600	O_2, N_2, Air O_2, N_2, Air
IV	6	Steel	Silicon Carbide Tube	700-1600	0.1-600	O_2, N_2, Air
V	7	304 Stainless	R. F. Induction	1000-2700	0.1-600	O_2, N_2, Air, H_2 HCl, H_2O, CO, Hf
VI	8	Steel and Stainless	Split Graphite Resistor and ZrC_2 Muffle	1000-2000	0.1-100	O_2, N_2, Air with Argon Backing Gas

TABLE 2. SUMMARY OF RATE EQUATIONS ENCOUNTERED IN OXIDATION OF METALS SHOWING TIME AND PRESSURE DEPENDENCY

CHEMISTRY	REACTION CLASS	RATE CONTROLLING PROCESSES	RATE EQUATIONS (GAS CONSUMPTION BASIS)	EXAMPLES	REFERENCES	PRESSURE DEPENDENCY	REMARKS
$Me + \frac{x}{2} O_2 \rightarrow MeO_x$	Simple	Interstitial diffusion	$\frac{d\lvert m_{O_2}/A\rvert}{dt} = \left(\frac{D_i}{w}\right)^{\frac{1}{2}} \frac{C_i}{t^{\frac{1}{2}}}$	$Ti + 1.75\ O_2 \rightarrow TiO_{1.35}$	41 42	Not known	Subsequent reaction to TiO_2
				$Ta + \frac{x}{2} N_2 \rightarrow TaN_x$	43	Not known	
$aMe + \frac{b}{2} O_2 \rightarrow Me_aO_b$	Simple	Oxide diffusion	$\frac{d\lvert m_{O_2}/A\rvert}{dt} = \left(\frac{D_i C_i \rho_{M_{O_2}} / M_{Me_aO_b}}{2}\right)^{\frac{1}{2}} \frac{1}{t^{\frac{1}{2}}}$	$Co + \frac{1}{2} O_2 \rightarrow CoO$	15	Eq 11	
				$Ti + \frac{1}{2} O_2 \rightarrow TiO$	16 5	Eq 12 or $P^{\frac{1}{6}}$	P seems to increase not definitely established
				$2Cu + \frac{1}{2} O_2 \rightarrow CoOCu_2O$	12 5	Eq 12 or $P^{\frac{1}{8}}$	No pressure insensitivity of region II Fig 12.
				$W + O_2 \rightarrow WO_2$	44	Eq 11	
$aMe + \frac{b}{2} O_2 \rightarrow Me_aO_b$	Simple	Phase boundary	$\frac{d\lvert m_{O_2}/A\rvert}{dt} = k_a C_a$	$WO_2 + \frac{1}{2} O_2 \rightarrow WO_3$	19 13	Eq 10	
				$2Ta + \frac{5}{2} O_2 \rightarrow Ta_2O_5$	10 27	Eq 10	Two modifications of Ta_2O_5 form at different rates.
				$2Cb + \frac{5}{2} O_2 \rightarrow Cb_2O_5$	30 32 33	Eq 10	" " " Cb_2O_5 " " " "
$Me + \frac{b}{2} O_2 \rightarrow Me_aO_b(vap)$	Simple	Gas boundary layer diffusion	$^{wl}\frac{d\lvert m_{Me}/A\rvert}{dt} = \frac{MPP^o}{\sqrt{2\pi MRT}} \ln\left\lvert\frac{P+P^o}{P-\frac{b}{a}P^o}\right\rvert$	$Pt + O_2 \rightarrow PtO_{2(vap)}$	24 25	P	*Solid consumption basis. $\Delta P > 0$, $T > 450^oC$
$Me_aO_b(s) \quad Me_aO_b(vap)$			$^{wl}\frac{d\lvert m_{Me_aO_b}/A\rvert}{dt} = -\frac{MPP^o}{\sqrt{2\pi MRT}}$	$WO_{3(s)} \rightarrow \frac{1}{n}(WO_3)_{n(vap)}$	27	Oxygen pressure insensitive	**Weight loss basis. $\Delta H_{vap} > 0$.
$Me + \frac{b}{2} O_2 \rightarrow Me_aO_b$	Consecutive	Oxide diffusion	$\frac{d\lvert m_{O_2}/A\rvert}{dt} = \left(\frac{D_i C_i \rho_{M_{O_2}} / M_{Me_aO_b}}{2}\right)^{\frac{1}{2}} M_{Me_aO_b} \cdot \frac{1}{t^{\frac{1}{2}}} +$	$2Cu + \frac{1}{2} O_2 \rightarrow Cu_2O$	8 45	P insens	CuO formation rate also dependent on nucleation and growth from Cu_2O (Ref. 12)
$Me_aO_b + \frac{c-b}{2} O_2 \rightarrow Me_aO_c$		Oxide diffusion	$\left(1 - \frac{1}{M_{O_c}/O_b}\right) \left(\frac{D_i C_i \rho_{M_{O_2}} / M_{Me_aO_c}}{2}\right)^{\frac{1}{2}} M_{Me_aO_c} \frac{1}{t^{\frac{1}{2}}}$	$Cu_2O + \frac{1}{2} O_2 \rightarrow 2CuO$	44	P insens	of region III Fig 12.
$Me + \frac{b}{2} O_2 \rightarrow Me_aO_b$	Consecutive	Oxide diffusion	$\frac{d\lvert m_{O_2}/A\rvert}{dt} = \left(\frac{D_i C_i \rho_{M_{O_2}} / M_{Me_aO_b}}{2}\right)^{\frac{1}{2}} \frac{1}{t^{\frac{1}{2}}} - \frac{1}{M_{O_c}/O_b} k_a C_a$	$W + O_2 \rightarrow WO_2$	19 13 27	Eq 11	Similar equations for Mo. When WO_3 volatility appreciable weight gain rate is flow sensitive.
$Me_aO_b + \frac{c-b}{2} O_2 \rightarrow Me_aO_c$		Phase boundary	valid over $\int_0^{t_m} \frac{d\lvert m_{O_2}/A\rvert}{dt}$, where $t_m = \frac{D_i C_i \rho_{M_{O_2}} / M_{Me_aO_b}}{2\left(k_a C_a M_{O_2}/O_c\right)^2}$ and $\frac{d\lvert m_{O_2}/A\rvert}{dt} = k_a C_a$	$WO_2 + \frac{1}{2} O_2 \rightarrow WO_3$	47 48	Eq 10	
same oxide in (6) above volatilizes by $Me_aO_{c(s)} \rightarrow Me_aO_{c(vap)}$	Consecutive	Gas boundary layer diffusion	$^{wl}-\frac{d\lvert m_{Me_aO_c}/A\rvert}{dt} = \frac{MPP^o}{\sqrt{2\pi MRT}}$	$WO_{3(s)} \rightarrow \frac{1}{n}(WO_3)_n$		Oxygen pressure insensitive	*For weight change rate when $\frac{d\lvert m_{O_2}/A\rvert}{dt} > M_{O_c}/M_{Me_aO_c} \frac{d\lvert m_{Me_aO_c}/A\rvert}{dt}$ add volatility rate to (6) above. (Flow sensitive) For weight change rate when $\frac{d\lvert m_{O_2}/A\rvert}{dt} < M_{O_c}/M_{Me_aO_c} \frac{d\lvert m_{Me_aO_c}/A\rvert}{dt}$ use $-\frac{1}{M_{O_c}/M_{Me_a}} \cdot \frac{d\lvert m_{O_2}/A\rvert}{dt}$ in lieu of $\frac{d\lvert m_{O_2}/A\rvert}{dt}$ in (5) above. (Flow insensitive)
$Me + \frac{x}{2} O_2 \rightarrow Me_aO_b$	Simultaneous	Phase boundary	$\frac{d\lvert m_{O_2}/A_I\rvert}{dt} = \lvert k_a C_a\rvert_I$	$2Cb + \frac{5}{2} O_2 \rightarrow Cb_2O_{5(I)}$	(Cb) 33 (Ta) 27	Eq 10	Similar behavior by Ta. Two modifications of Cb_2O_5 (or Ta_2O_5) arise from transformed and untransformed surface phase at different rates. Reaction areas A_I and A_{II} temperature and time dependent due to nucleation, precipitation and growth phenomena. Overall rate is the sum of the individual rates.
$Me + \frac{c}{2} O_2 \rightarrow Me_aO_c$		Phase boundary	$\frac{d\lvert m_{O_2}/A_{II}\rvert}{dt} = \lvert k_a C_a\rvert_{II}$	$2Cb + \frac{5}{2} O_2 \rightarrow Cb_2O_{5(II)}$		Eq 10	
$Me + \frac{x}{2} O_2 \rightarrow MeO_x$		Interstitial diffusion	$\frac{d\lvert m_{O_2}/A\rvert}{dt} = \left(\frac{D_i}{w}\right)^{\frac{1}{2}} \frac{C_i}{t^{\frac{1}{2}}}$	$Cb + \frac{x}{2} O_2 \rightarrow CbO_x$		Not known	

I—Lower section of furnace shell
J—Alundum shield
K—Grain Alundum
L—Furnace insulation
M—Thermocouple and power leads
N—Upper section of furnace
O—Spring balance
P—Suspension chain
Q—Stainless steel drum
R—Packing gland
S—Packing gland
T—Access opening
U—Pt-20 pct Rh suspension wire
V—Access opening
W—Microscope
X—Cathetometer
Y—Observation window
Z—Sample

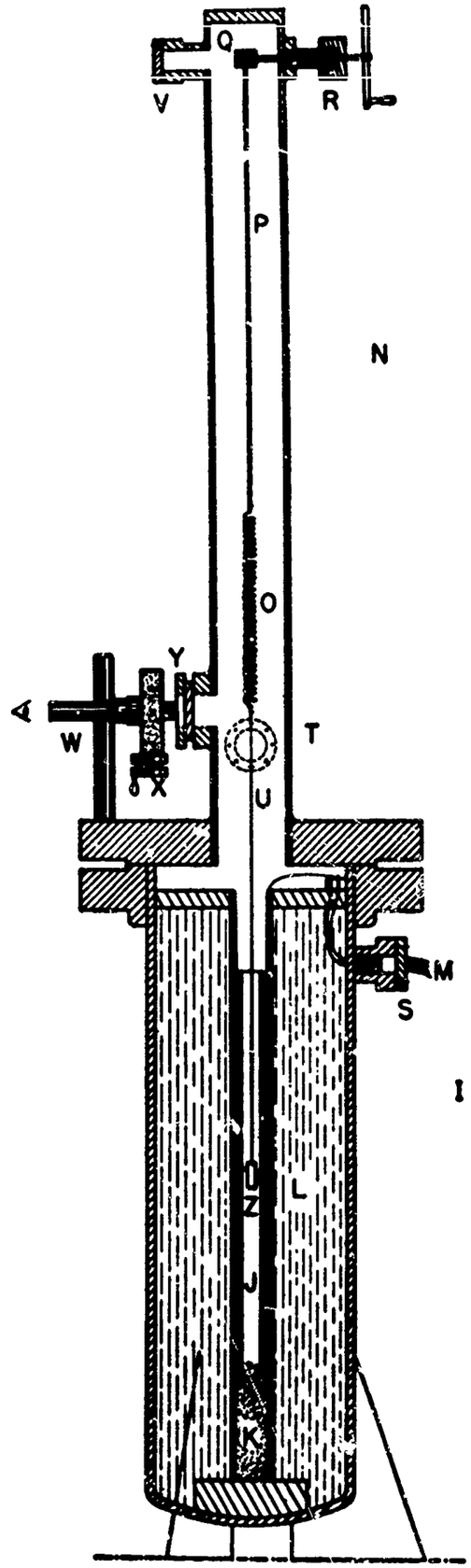

Figure 1. High Pressure Oxidation Furnace

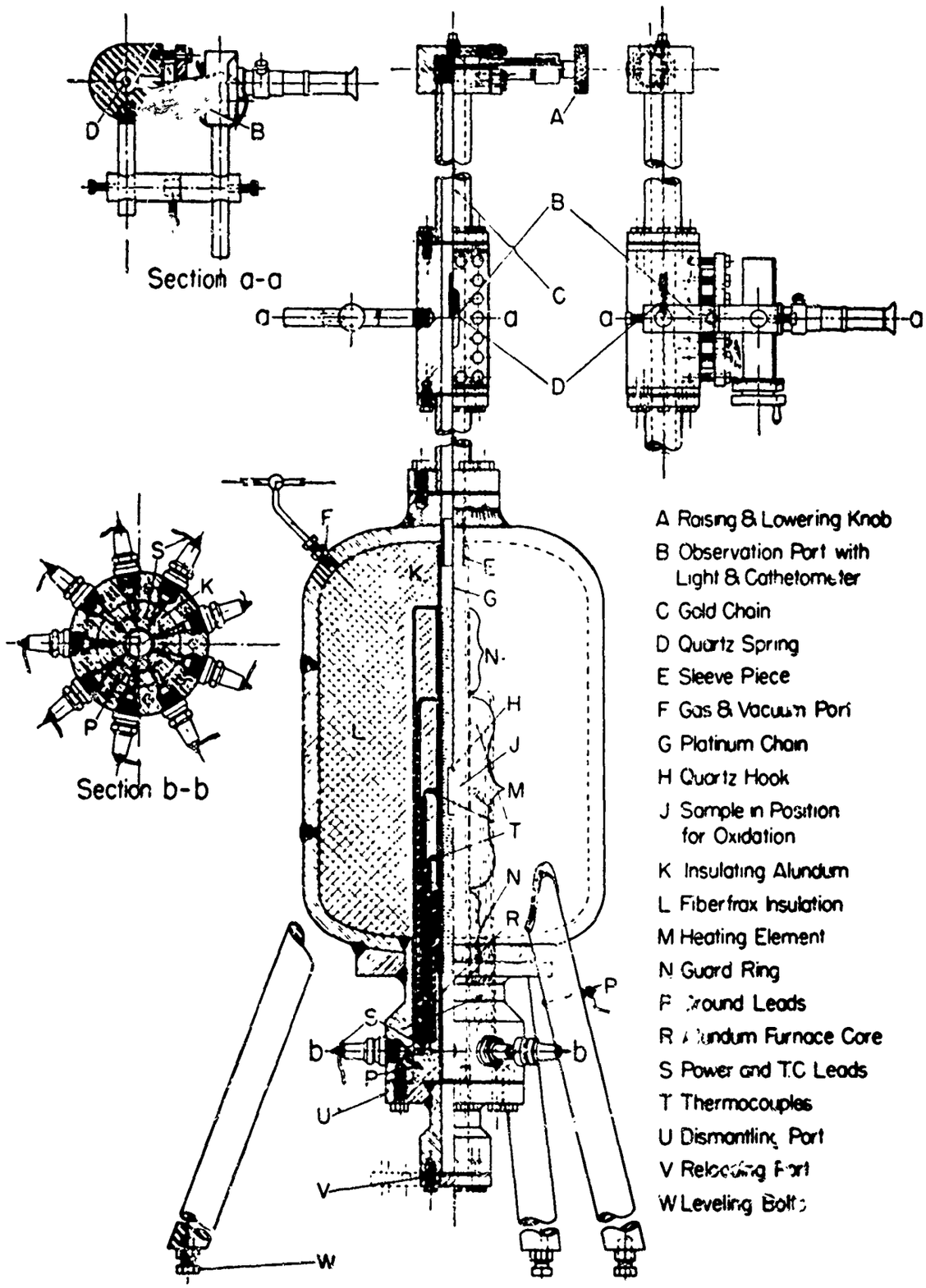

Figure 2. Kanthal A-1 High Pressure Oxidation Furnace (Mk II)

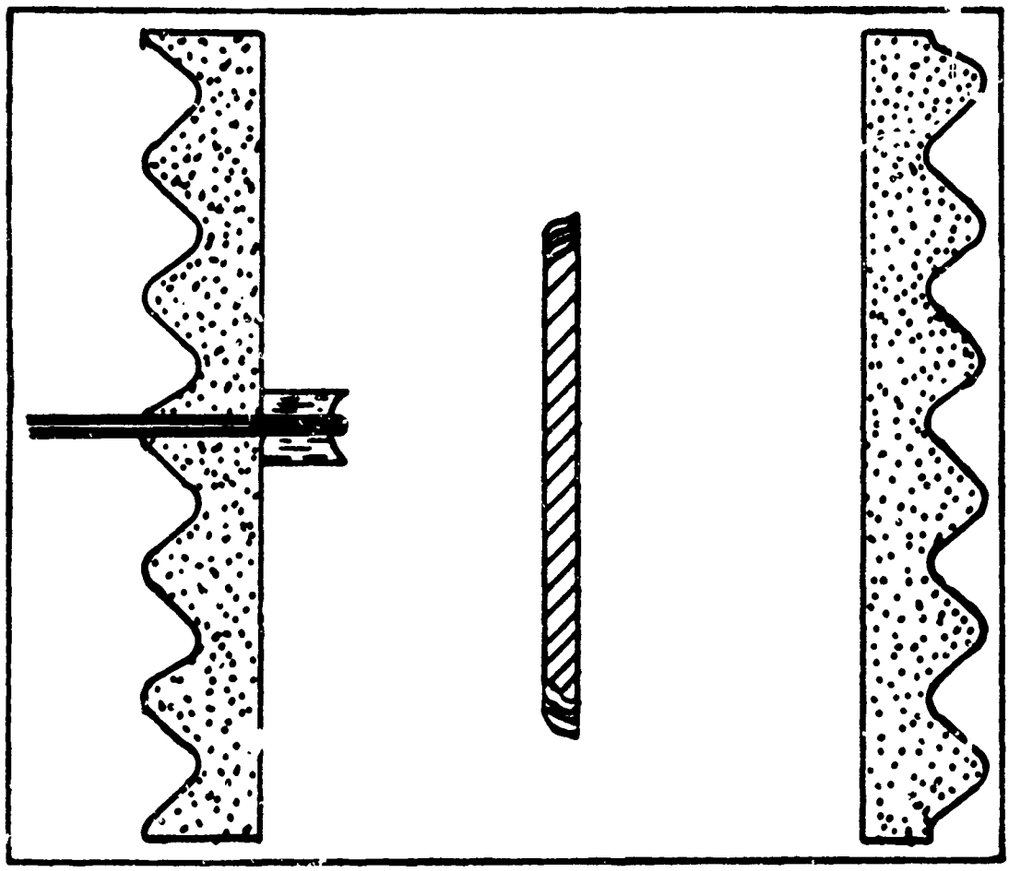

Figure 3. Schematic Arrangement of Sample Thermocouple and Shield

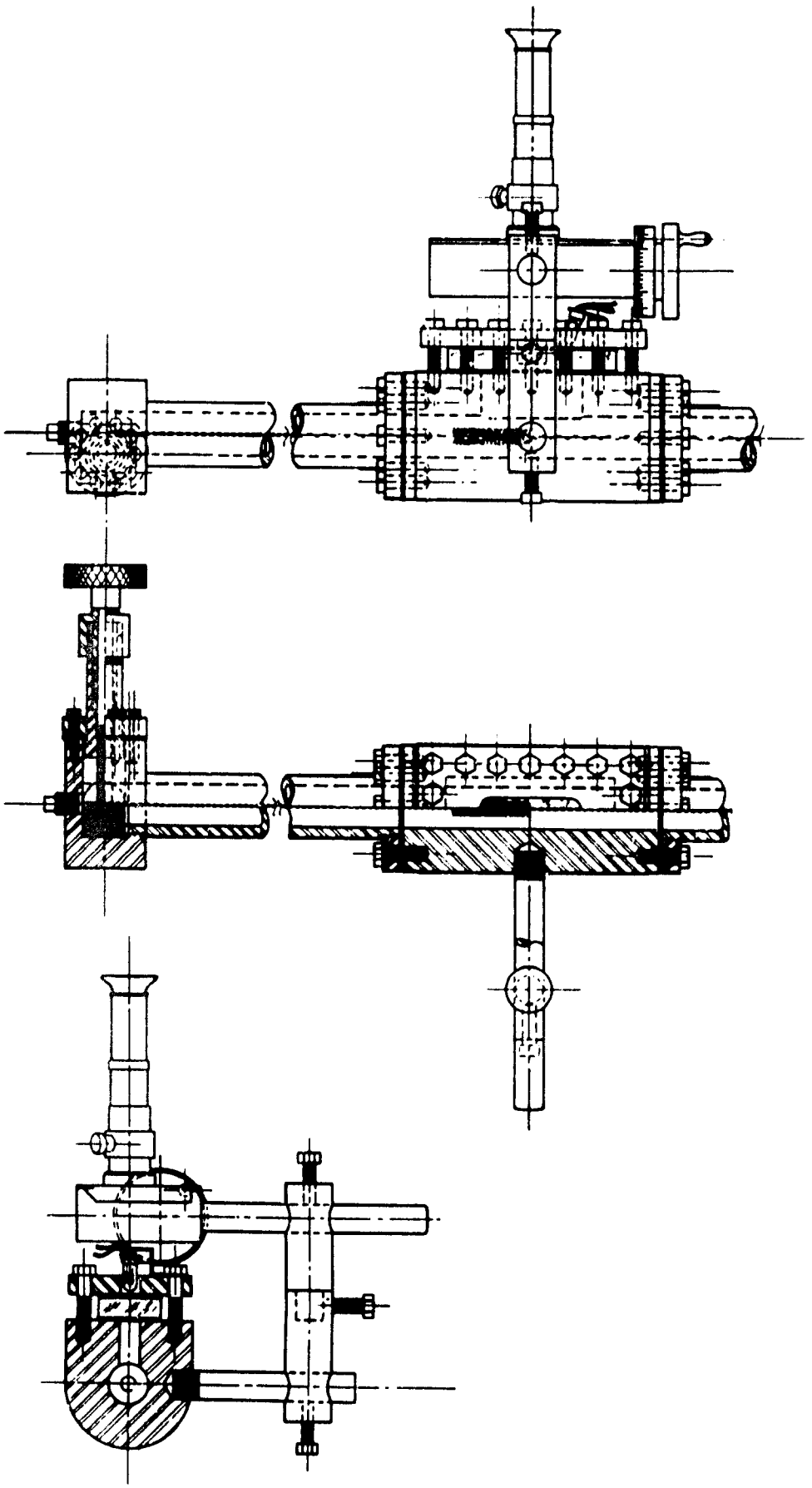

Figure 4. Winch and Window Block Assembly

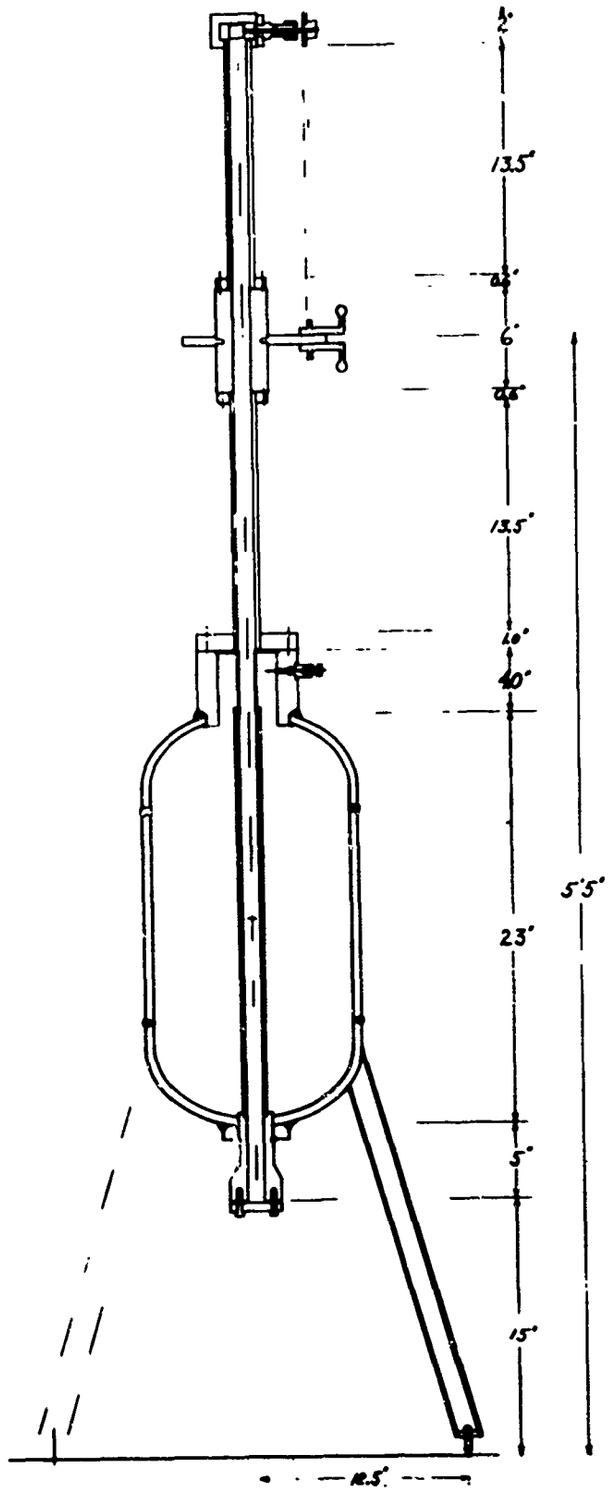

Figure 5. Kanthal A-1 Furnace Showing Transposition of Thermocouples

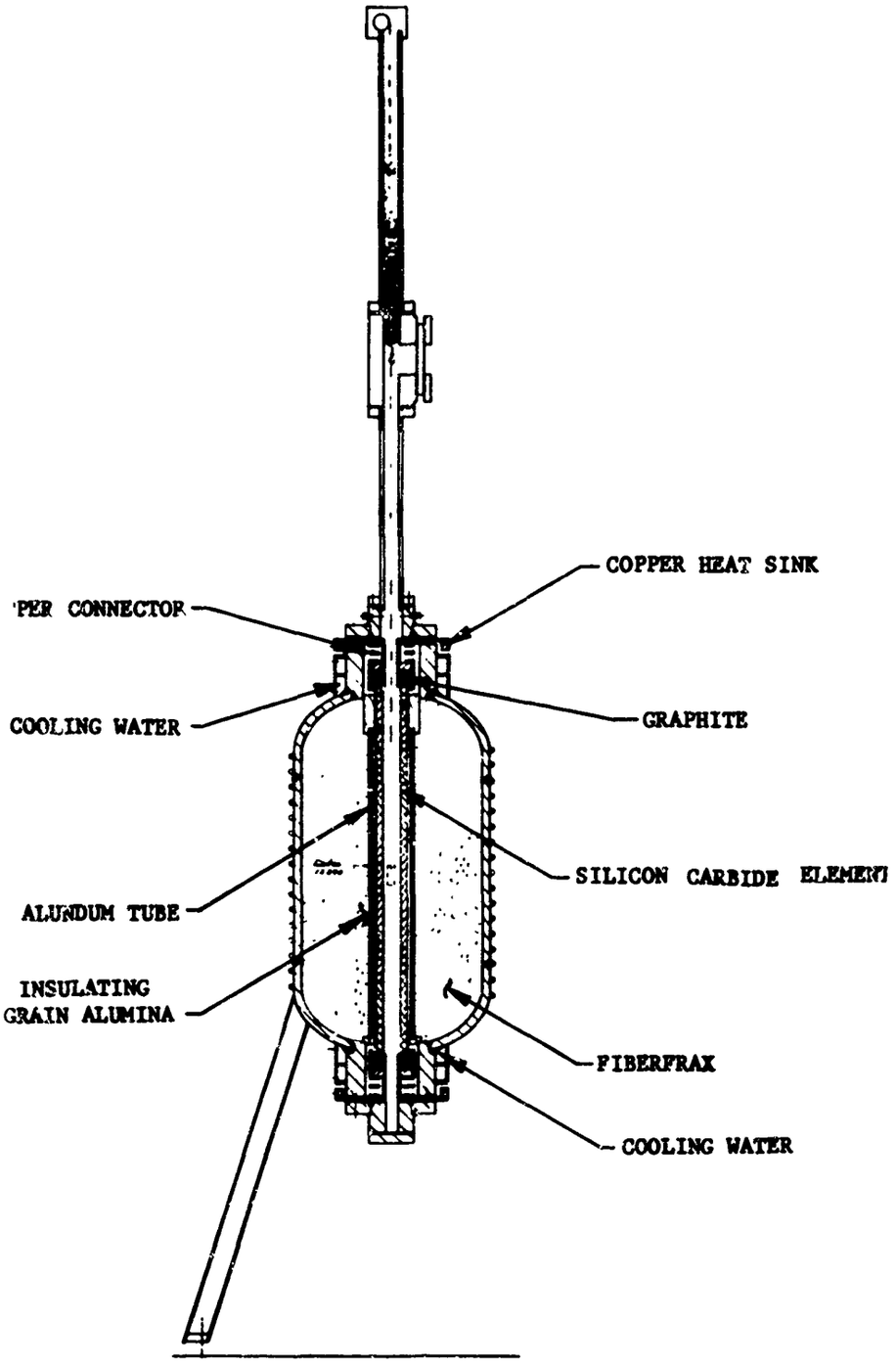

Figure 6. Silicon Carbide Tube Furnace

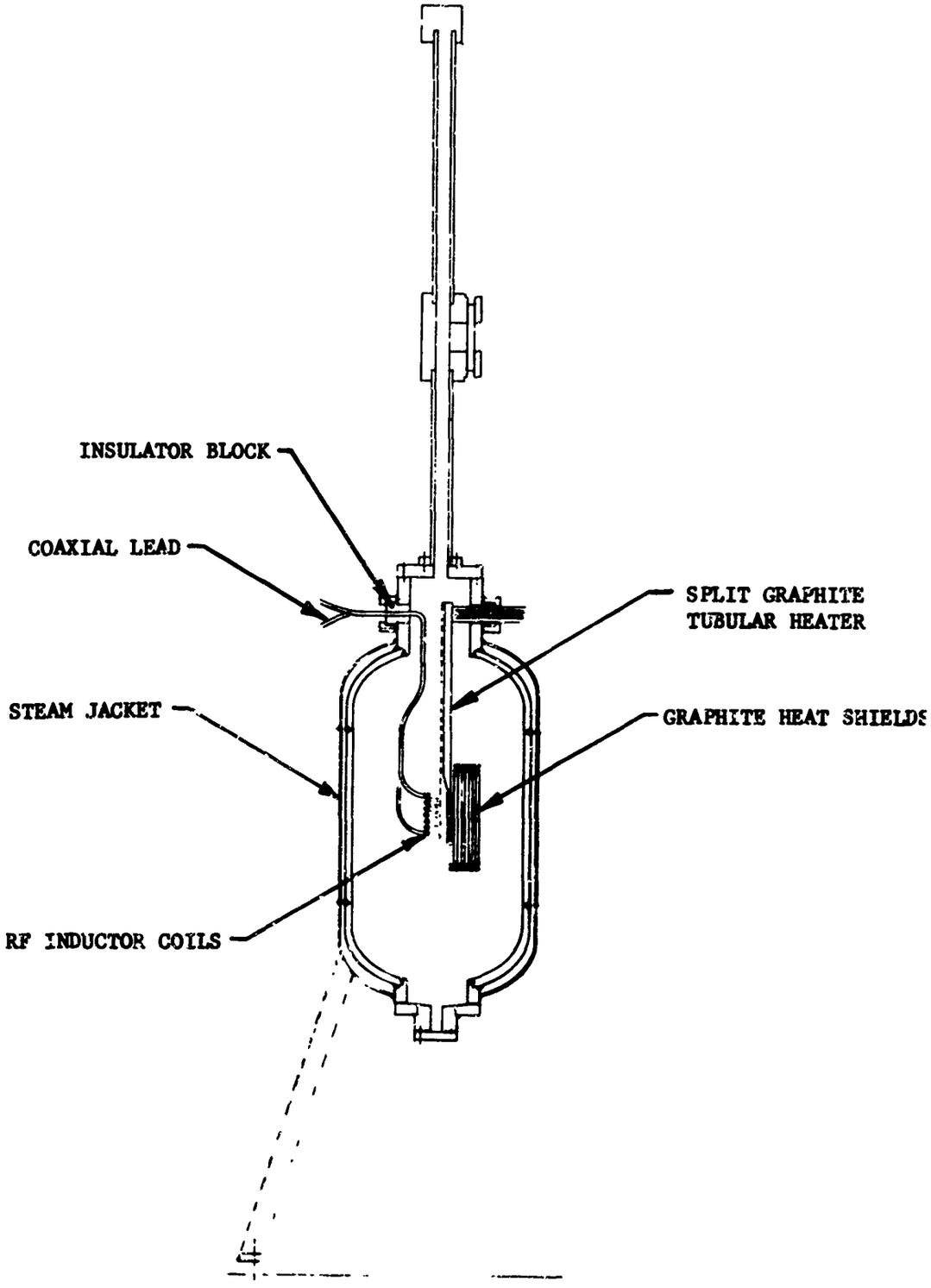

Figure 7. RF Induction or Split Graphite Furnace

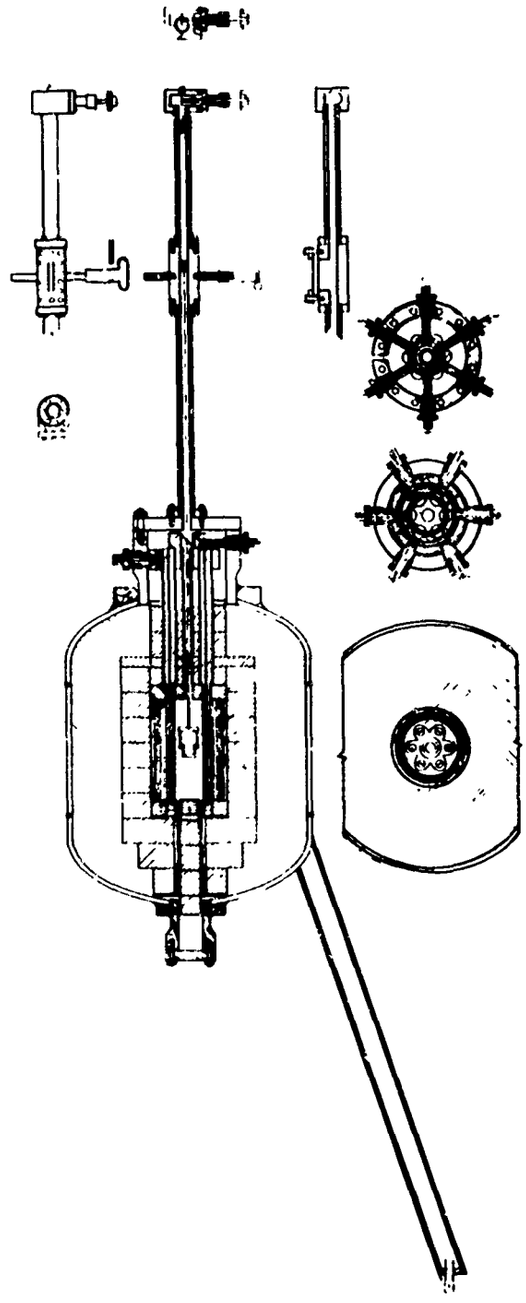

Figure 8. Split Graphite Resistor Furnace (Shown Without Muffle)

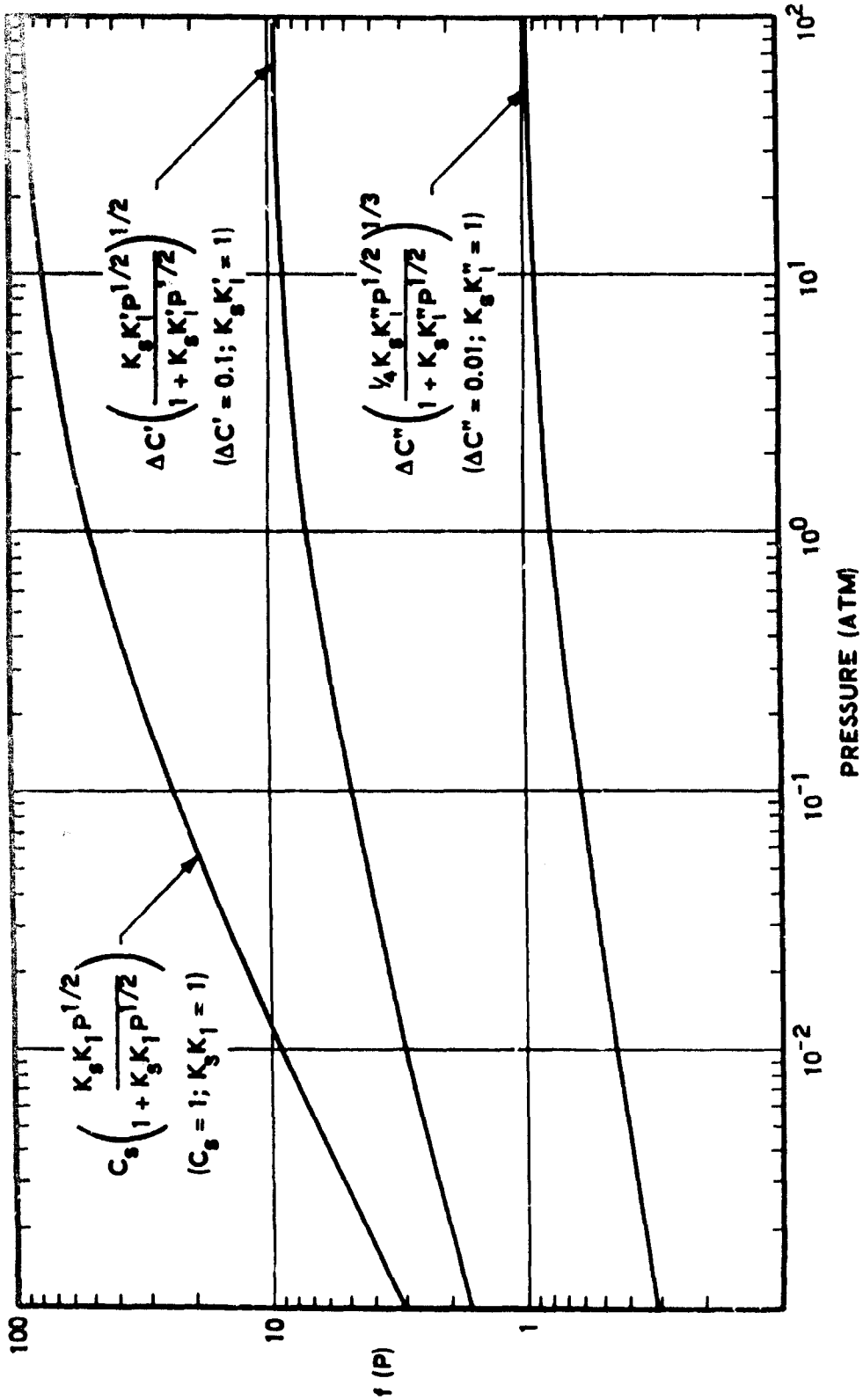

Figure 9. Plot of Pressure Functions. Equations 11, 12, and 13, Versus P, Showing Range of Pressure Insensitivity at High Pressures to P-1/2, P-1/4 and P-1/6 Sensitivity at Low Pressures

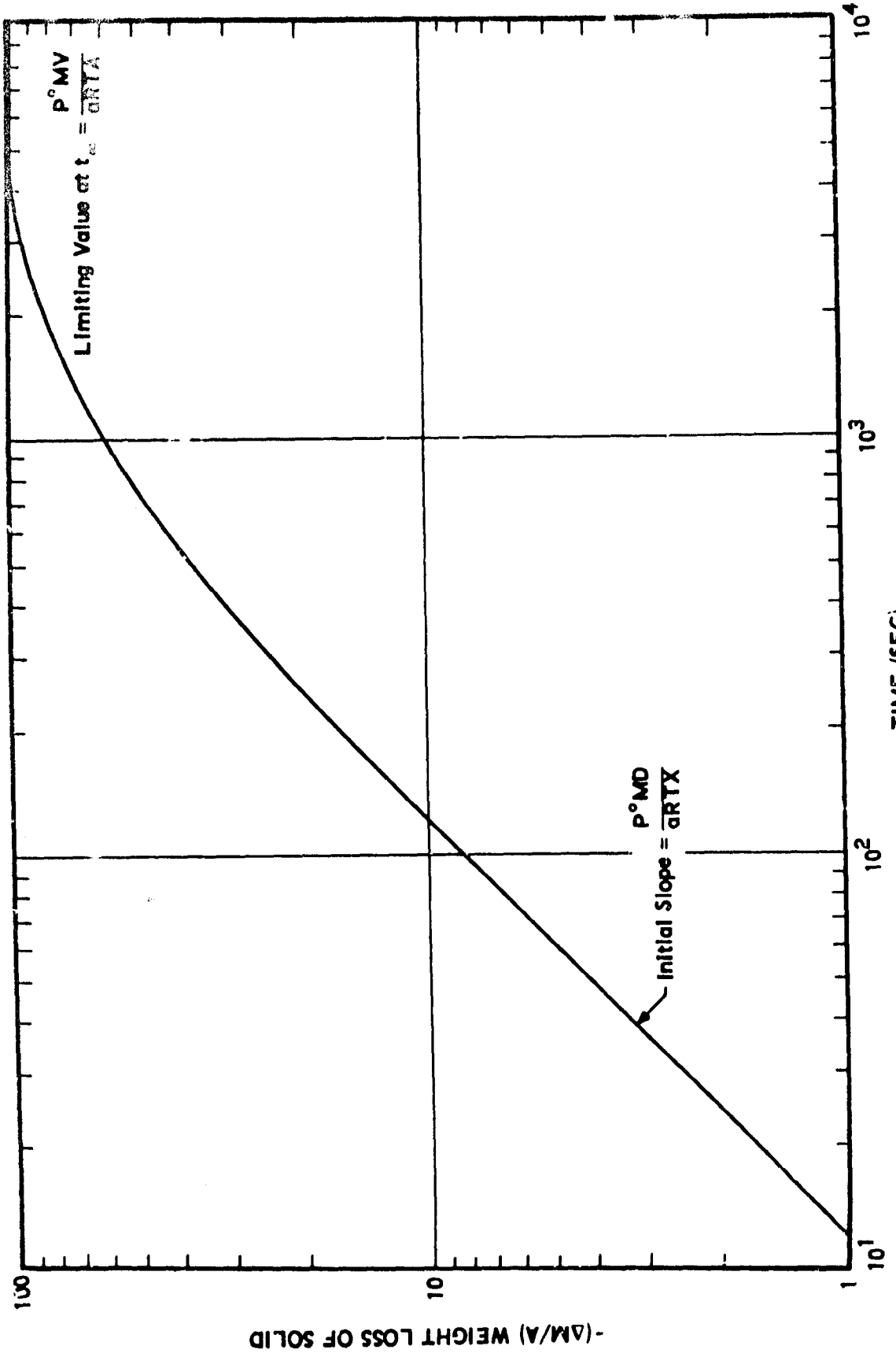

Figure 10. Plot of $-(\Delta M/A)$ Versus t for $\Delta F > 0$ Reactions, with $P_b \rightarrow P^{\circ}$ in a Constant Volume Reactor

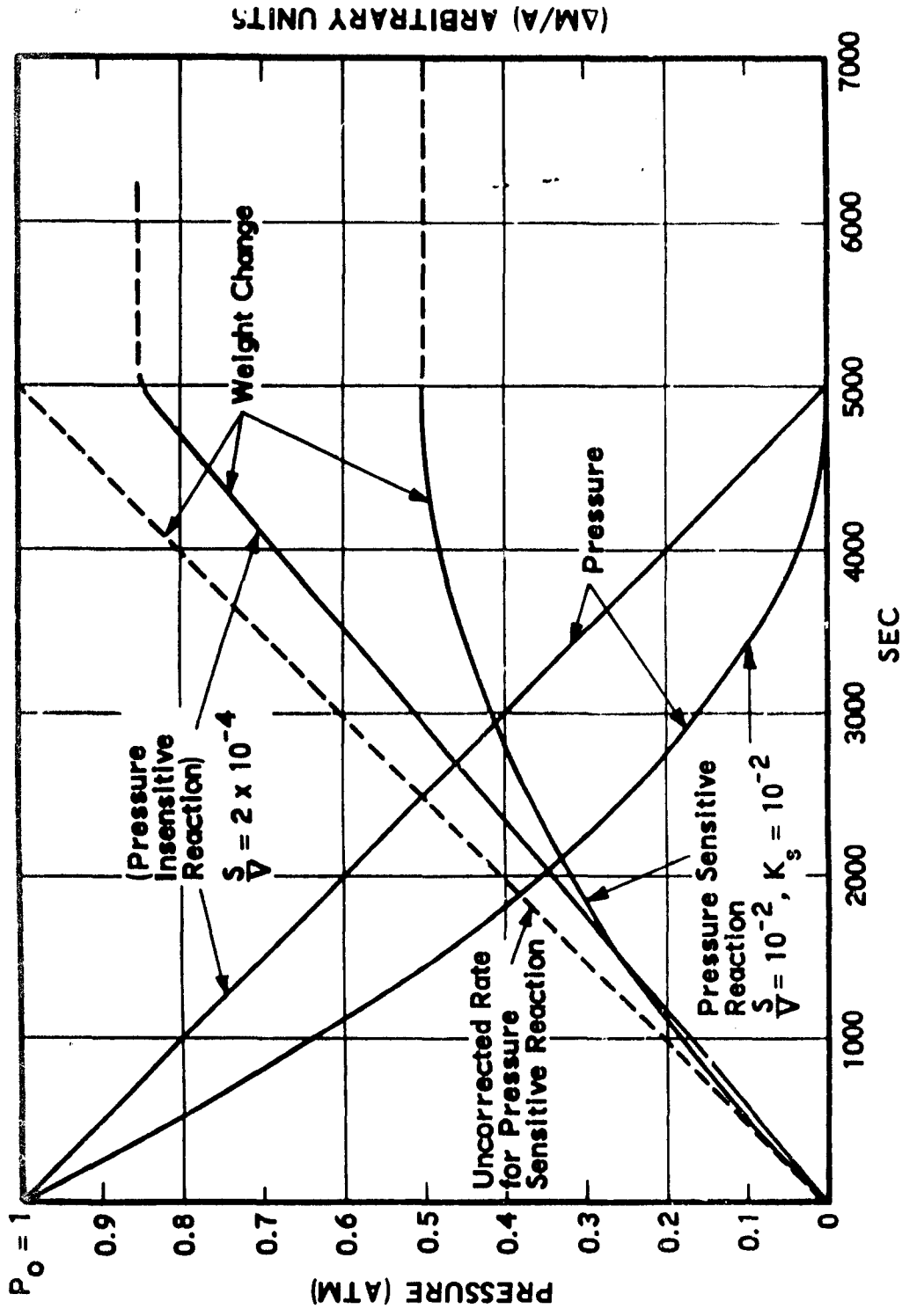

Figure 11. Plot of Constant Volume Reactor Pressure and Specimen Weight Change with Time for Pressure Sensitive and Pressure Insensitive Phase Boundary Reactions

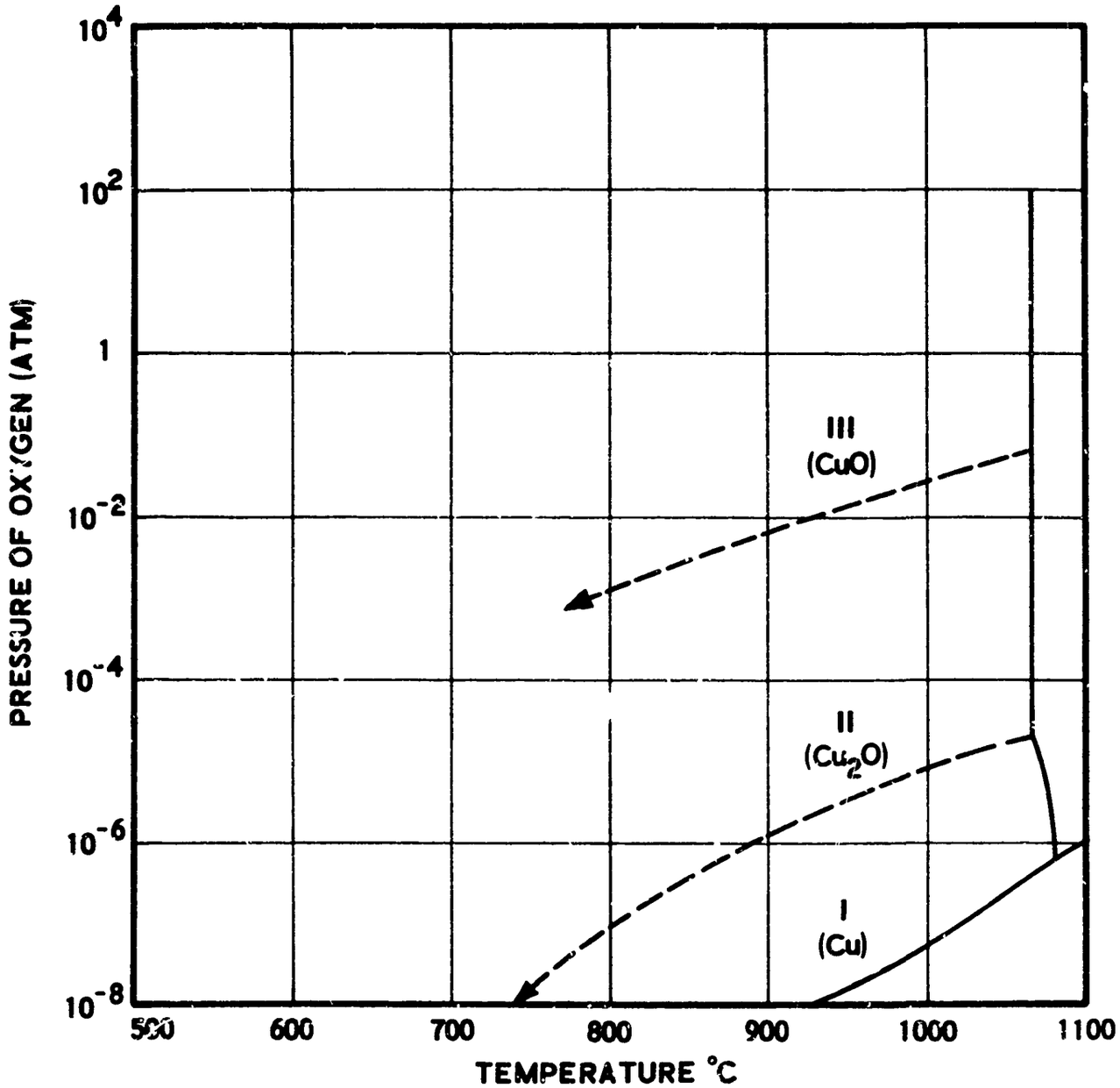

Figure 12. P-T Diagram of Copper-Oxygen System Showing Regions of Phase Stability

INITIAL STAGES OF THE OXIDATION OF TUNGSTEN AND TANTALUM

D. W. Rausch*
K. L. Moazed*

INTRODUCTION

The kinetics of the gaseous oxidation of metals have been studied extensively during the past several decades. Experimental work has been concerned largely with the establishment of rate laws describing gross behavior, while the theoretical work has attempted to rationalize these results in terms of reaction mechanisms (Reference 1). Few theories attempt to describe the mechanism for oxide films thinner than about 100 Å. With the development of the electron microscope came the opportunity to observe and determine surface structure in much finer detail (i.e., to the limit of resolution, about 20 Å). The experimental work which followed greatly extended the knowledge of epitaxy and in a few cases was concerned with the specific problem of initial reaction kinetics (Reference 2). This work demonstrated beyond doubt the critical role of substrate topography (including crystallography and local heterogeneity) and contamination in the initial reaction kinetics and nature of the reaction product. More recently, the development of the field emission microscope and improved vacuum gauges has been responsible for extending the state of knowledge down to atomic dimensions. The use of these instruments has led to a greatly improved, general understanding of adsorption and atomic mobility processes, and a rather detailed understanding of these processes involving oxygen on tungsten.

The purpose of the present work is to study that region of the reaction between the adsorbed state and the thin oxide film state, i.e., the nucleation and growth of oxide in the initial stages.

Previous Work

The gross oxidation behavior of tungsten has been reviewed recently (References 3 and 4) and rate laws for the oxidation of tungsten (References 4 and 5) and tantalum (References 5 and 6) are available. Since detailed and precisely defined experimental results of the oxidation kinetics of tungsten and tantalum in the initial stages of reaction are not available, a brief review of experimental studies dealing with this problem in the oxidation of other metals may be in order.

Much of the experimental work which has been carried out suffers from (1) a lack of positive definition of the initial metallic substrate, (2) a difficulty in observing in fine-enough detail the surface structure and topography, (3) an inability to achieve a sufficiently low reaction rate so that the initial stages can truly be studied (for even at oxygen pressures as low as 10^{-6} mm Hg a monolayer of gas may be adsorbed in a matter of seconds), and (4) the presence of gases other than oxygen. Despite these difficulties and the resulting uncertainty in interpretation, a number of significant observations have been made. The kinetics of the initial reaction on copper has been studied in some detail (Reference 7). The reaction is characterized by three distinct stages: incubation, nucleation, and lateral growth, and after impingement and complete surface coverage, bulk growth perpendicular to the surface. The apparent nuclei exist on a more-or-less undefined "film," and appear simultaneously on a given crystallographic plane. The constancy of nuclei density with increasing reaction time and the decrease in nuclei density with increased substrate temperature (at constant pressure) lead to the concept that each nucleus is surrounded by

* Department of Metallurgical Engineering, The Ohio State University

a "zone of influence" in which another nucleus is not likely to form. The extent of such a zone depends upon the rate of surface diffusion and oxygen pressure. The kinetics are markedly dependent upon crystallography. Other studies on copper, barium, iron, and nickel (References 8, 9, 10, and 11 respectively) are generally consistent with this characterization of the oxidation process.

The role of substrate dislocations in the initial oxidation process is not well understood (Reference 2). However, it appears that certain impurities may be required in the dislocations in order for them to act as preferred nucleation sites.

As opposed to the lack of experimental work on the kinetics of the initial oxidation of tungsten and tantalum, oxygen adsorption and mobility on atomically clean tungsten have been the subject of numerous investigations (References 12, 13, 14, and 15). Since these studies have been reviewed elsewhere (References 4 and 16) only the pertinent experimental details and general results will be mentioned here.

Primarily two experimental methods of approach have been used in the studies of oxygen adsorption on tungsten field emission microscopy (electron and ion), and flash filament techniques. All of these experiments have involved the deposition of oxygen on the substrate at room temperature or below and the subsequent reaction of the contaminated substrate in ultra-high vacuum (10^{-9} mm Hg to several orders of magnitude lower) at temperatures between 4° and ~2000°K. Mobility experiments have generally been carried out below room temperature, while desorption experiments involve higher substrate temperatures. Desorption experiments aim to relate desorption temperature with pressure rise in the vacuum system as the reaction takes place, or with change in the electronic work function of the various crystallographic planes on the substrate.

It has been determined that two chemisorbed monatomic layers are formed below room temperature. About 80 percent of the first layer is formed without activation and is generally immobile. This layer is characterized by a variation in coverage (i.e., surface density of adsorbed species) and binding energy with crystallography. The average binding energy of the first layer is about 160 Kcal per mole (subject to a 20 percent variation). This layer is stable under high vacuum to about 1000°C. Each tungsten atom in the surface is believed to contact only one oxygen atom, with each oxygen atom contacting several tungsten atoms. Such an arrangement permits a second, less-tightly bound, chemisorbed layer on planes other than the most densely packed {110} in body-centered cubic. The second layer is considerably less stable and is desorbed above 300°C in high vacuum.

Additional molecular oxygen may be accommodated in a physisorbed state at low temperatures, but even the complete second chemisorbed layer seems to be formed with difficulty at room temperature (i.e., relatively high oxygen pressures are necessary). Above room temperature undissociated oxygen is believed to be slowly taken up by the chemisorbed layer in a manner resembling "slow oxidation." Mobility within the chemisorbed layer is observed at 130°C and above. Oxidation and desorption apparently take place simultaneously above 300°C in the ultra-high vacuum environment. Neither nucleation in the chemisorbed layers nor nucleation of a second phase has been observed. Arguments have been presented for the existence of oxide microcrystallites (References 15 and 17), probably WO_3, but are not without contradiction (Reference 12). A clear differentiation between the adsorbed state and oxidized state has not been revealed.

The Present Work

As compared to the field emission work described above (namely, oxygen deposition at low temperatures and subsequent heating in the absence of gaseous oxygen), the present work is concerned primarily with the course of reaction on tungsten and tantalum substrates above room temperature with oxygen from the gas phase (i.e., conditions under which appreciable oxidation is expected).

The field electron emission microscope is ideally suited to such a study for the following reasons:

a. Electron emission, a result of quantum-mechanical tunneling of electrons through the field deformed potential barrier at the surface, is dependent upon crystallography and is extremely sensitive to surface contamination.

b. Atomically clean and reproducible surfaces can be achieved on tungsten and tantalum emitter-substrates by heating to temperatures between 2000° and 2600°C.

c. All major crystallographic planes are present on the approximately hemispherical emitter-substrate.

d. High magnification and resolution are readily achieved. The inherent resolution in the depth dimension is one atomic layer and about 20 Å in the lateral dimensions.

e. Observations can easily be made during the course of the reaction since the reaction takes place in the microscope.

The major disadvantage imposed by the use of the microscope is that the size of most crystallographic planes on the substrate is relatively small.

The results and experimental techniques described in this paper represent the initial efforts in an experimental program aimed at elucidating the role of substrate temperature, topography, and oxygen pressure in the kinetics of oxidation in the initial stages.

EXPERIMENTAL PROCEDURE

The field electron emission microscope is essentially an ultra-high vacuum device because the field emitter-tip (i.e., the metallic substrate or specimen) is relatively fragile and it is easily destroyed by ion bombardment. In the presence of relatively high pressure, this destruction may result from the high electric field required for emission. A number of excellent reviews of field emission and ultra-high vacuum techniques are available (References 16, 18, 19, and 20) so a brief description will suffice here.

The vacuum system used in this work is a general-purpose, all Pyrex, ultra-high vacuum system several liters in volume larger than the diffusion pump. It contains in series a mechanical forepump, three-stage oil diffusion pump, zeolite trap, two Bayard-Alpert ionization gauges, two liquid nitrogen traps, and a two-filament gettering bulb containing a tantalum-titanium and a molybdenum getter. For this work the system is operated as a dynamic system (i.e., it is open to the atmosphere through the forepump) in order to rapidly pump out the large amounts of oxygen required for the substrate reaction. Baking, outgassing, gettering, and ionization gauge pumping routinely produce vacua in the low 10^{-9} mm Hg range.

The field emission tube, Figure 1, is constructed of a 250 ml Pyrex flask (F) containing on the inside a transparent electrically conductive coating (C) furnished with an external lead (E). This coating, which serves as the anode, is covered by a calcium tungstate fluorescent screen (S). The emitter-tip (T) is welded to a tungsten loop (L) which serves as the resistive heating circuit for the tip through the two external leads in the four-lead graded glass seal (G). The remaining two leads in this seal are used for potential leads (PL) in measuring the temperature of the tip.

The emitter-tip itself consists of a short length of 5-mil diameter commercial grade tungsten or tantalum wire which is electrolytically polished to a fine smooth point sufficiently small that it cannot be resolved at 500X (i.e., several thousand Å in diameter). After assembling the emission tube, joining it to the vacuum system, and attaining ultra-high vacuum, direct current from storage batteries is passed through the heating circuit in order to out-gas the tip-loop assembly and anneal the tip.

Temperature is measured by continuously recording the potential drop across the section of the heating loop contained between the potential leads. This potential drop is obtained as a function of temperature by potentiometrically measuring the resistance of the section of the heating loop over a range of temperatures measured optically

and by assigning temperatures to additional resistance values measured below the optical pyrometer range on the basis of the well-established variation in the resistance of tungsten with temperature. Temperatures reported in this work are estimated to be accurate within ±20°C.

Two methods of providing oxygen for the reaction are used. For pressures under 10^{-5} mm Hg, a silver bead (B) supersaturated with oxygen and contained on a platinum loop (P) in a side arm (A) is heated resistively to release oxygen. A polyethylene-asbestos jacket is placed around the sidearm and, prior to heating, is filled with liquid nitrogen. Since the silver bead cannot see the tip (i.e., substrate), all oxygen evolved must strike the cold walls of the sidearm prior to entering the emission tube, and is thus purified. For oxygen pressures of 10^{-5} mm Hg and above, commercial grade oxygen is leaked into the vacuum system from a reservoir at about 10^{-1} mm Hg through the diffusion pump, zeolite trap, two liquid nitrogen traps, and gettering region.

Pressures were measured with Bayard-Alpert ionization gauges. Due to the geometry of the system, a correction was applied to such measurements when the silver bead technique was used in order to account for the much greater flux of oxygen at the emitter-tip than at the ionization gauge. The correction factor was determined by observing the length of time required for the emission pattern to change from the clean pattern to some arbitrary state of contamination under two conditions: reaction with a relatively high and stable residual oxygen pressure (achieved by incomplete removal of oxygen admitted from the reservoir), and reaction with oxygen from the silver bead at constant flux. Assuming, then, that the total number of molecules which have impinged on the surface is the same in both cases

$$P\Delta t = KP_s \Delta t_s \qquad (1)$$

where P and t are respectively ionization gauge pressure and time of reaction, with the subscript s referring to the reaction using the silver bead, and K is the correction factor. Such a factor must be determined for each pressure level at which the silver bead is employed. The values of K determined in this work ranged between 10^2 and 10^3. The accuracy of pressures corrected in this manner is estimated at plus or minus a factor of three.

High voltage is supplied by a 0 to 30 kv filtered DC power supply with external line regulation. Applied voltages are measured by a calibrated panel meter estimated to be accurate within ±2 percent full scale. A General Radio Company 1230-A electrometer measures emission currents between the anode lead and ground. The accuracy of this meter is better than ±1 percent.

The experimental sequence is as follows:

a. Clean tip by heating to temperatures above 2000°C,

b. Cool to room temperature and apply field,

c. Repeat "a." and "b." until clean pattern is observed,

d. Photograph emission pattern (a Polaroid camera with close-up lens was used in this work with 3000 speed film),

e. Measure currents and voltages, turn field off, and

f. Heat tip to reaction temperature and activate oxygen flow.

After the desired reaction time, the oxygen flow is stopped, the tip cooled to room temperature, and the above sequence with exception of step "a." is repeated. It is necessary not to apply the high field to a heated emitter-tip during the course of reaction as drastic rearrangement on the surface of the substrate is noted.

The extent of contamination by residual gases may be estimated from the kinetic theory of gases by

$$J = P(2\pi mKT)^{-\frac{1}{2}}, \text{ molecules cm}^{-2}\text{ sec}^{-1} \qquad (2)$$

where J, P, and m are respectively flux, pressure, and mass of the gaseous species, and k and T have the usual meaning. Assuming the residual gases to be oxygen at $P = 10^{-9}$ mm Hg and T = 300°K, a monolayer would be formed in about 15 minutes for a sticking coefficient of 0.1 (independent of coverage) on a step-free, smooth surface. Since about one minute is required at room temperature between consecutive reactions in the experimental sequence outlined above, contamination by residual gases is not very extensive. However, this reaction is checked periodically, independent of the measured pressure of the system, by permitting a cleaned tip to react with the residual gases and observing the rate of reaction as manifested by changes in the emission pattern.

Recovery of ultra-high vacuum is essentially instantaneous after the activation of the silver bead due to the small volume ratio of the emission tube to the entire system, and the large pressure gradient (indicated by the large values of K). After oxygen from the reservoir has been admitted (producing the characteristic large pressure rises throughout the entire system), it is necessary to activate the getters to reduce the oxygen pressure rapidly to the 10^{-8} mm Hg range.

Image magnification is determined either by direct measurement of the emitter-tip radius in the conventional electron microscope or by assuming a value of the average electronic work function of the clean substrate (these values are fairly well established as 4.5 ev and 4.1 ev respectively for tungsten and tantalum) and calculating the radius from the Fowler-Nordheim equation (Reference 21). In either case the magnification is determined after crystallographic poles have been determined in the emission pattern by calculating the ratio of chord lengths between poles on the pattern and on the emitter-tip. In the present work, magnification is given in terms of $\ell_{\{100\}}$ the chord length or distance between the easily identified $\{100\}$ poles which lie on a plane intersecting the points of emergence of these poles on the surface of the tip and parallel to the plane of the photograph (i.e., the central $\{110\}$ plane). These distances are estimated to be accurate within ±20 percent.

RESULTS AND DISCUSSION

Figure 2 (a) and Figure 2 (b) are field electron emission patterns from clean tungsten and tantalum emitter-tips respectively. The shape of these tips is essentially conical with a smooth hemispherical end. Since the radius of this hemisphere is on the order of several thousand A, the tip is usually a single crystal. One of the unique features of such a shape on a single crystal of this size is that all major crystallographic planes are present. The low-index $\{110\}$, $\{211\}$, and $\{100\}$ planes in body-centered cubic crystals are the most densely packed and exist as flat facets on the surface. The regions surrounding these planes as well as other low-index planes are comprised of steplike terraces of low-index plane edges, with each terrace becoming narrower as the distance from the pole of the low-index plane increases. High-index planes on the surface are made up of the edges of low-index plane terraces and are consequently quite rough. Regions of transition from terraces of one plane to terraces of another often consist of rows of atoms protruding above their surroundings and contacting fewer neighbors than other surface atoms.

Since the electronic work function (ϕ) varies from plane to plane as a result of the different coordinations, electron emission is a function of crystallography and permits the indexing of the major crystallographic regions in the emission pattern. Recognition of the twofold and threefold poles in each of the patterns in Figure 2 leads to the indexing of all other positions. These are the usual patterns obtained from drawn tungsten and tantalum wires which exhibit marked $\{110\}$ texture. A stereogram of the low-index poles in the cubic $\{110\}$ projection is given in Figure 2 (c). The central, low-intensity, high ϕ region of the pattern is denoted as the $\{110\}$ region and contains the flat $\{110\}$ plane at its center. The fourfold $\{100\}$ planes are also characterized by low-intensity electron emission, but the $\{100\}$ regions are highly emissive. The less densely packed $\{111\}$ planes manifest their correspondingly lower ϕ by high intensity emission. Three low-intensity $\{211\}$ planes appear around the threefold $\{111\}$ pole in the tungsten pattern but are not

discernible in the tantalum pattern. Since the group VI metals tungsten and molybdenum exhibit identical clean patterns as do the group V metals tantalum and niobium, the differences in the two types of patterns may be rationalized in terms of the effect of the d-electrons (Reference 22).

The adsorption of residual gases at 8×10^{-9} mm Hg on a tungsten substrate at room temperature is shown in the sequence of Figure 3. The applied voltage and accumulative reaction time are given for each photograph in the sequence. Several observations are noteworthy. First, relative emission intensity in the various regions of the pattern is not preserved as adsorption takes place (this corresponds to a disproportionate change in ϕ of the various regions). Second, emission intensity changes gradually or continuously from one region to another. And finally, adsorption takes place quite slowly after initial coverage has been achieved. Based on the flux calculation made for oxygen, Figure 3 (c) represents a coverage of about one layer. In view of the known difficulty with which multiple adsorbed layers are formed on tungsten at room temperature and above and at low pressures, Figure 3 (d) and (e) could not represent more than several layers on the most heavily covered planes. At higher pressures, substantial amounts of adsorbate are observed on tungsten (References 13 and 14) in the undissociated physisorbed state. The existence of preferred sites for such adsorption is apparently responsible for a small degree of highly localized variation of emission intensity over large regions of the pattern. It should be noted that no such variation is apparent in Figure 3.

Tantalum Reactions

The emission patterns obtained in a series of isothermal reactions at ~2600°, 830°, and 1130°C are shown in Figures 4, 5, and 6, respectively.

The patterns of Figure 4 were obtained during an attempt to clean the substrate by heating ~ 2600°C. Patterns (a), (b), and (c) show the emergence and subsequent location of a grain boundary which revealed itself as a result of evaporation of tantalum from the substrate. Since the position of the grain boundary did not change significantly after further evaporation, the surface of the grain boundary is parallel to the axis of the emitter-tip at the emitting end of the wire. The appearance of the clean tantalum pattern is verified by such evaporation patterns. The values given for ℓ_{100} apply to the distance $\{100\}$ poles on the same grain.

Figure 4 (d) demonstrates the effect of residual gas adsorption on the substrate of Figure 4 (c). Figure 4 (d) resulted from an eight-hour exposure to the residual gases at a pressure of 1×10^{-8} mm Hg. There are several similarities between the patterns obtained from tunsten, Figure 3, and tantalum, Figure 4 (d). Gradual changes in emission intensity from region to region on a particular grain are observed in both cases. Likewise an increase in the average ϕ accompanies adsorption in both cases. This is deduced from the higher voltage required by Figure 4 (d) relative to 4 (c) to achieve only a fraction of the emission current of 4 (c). (The emission current of 4 (c) could not be obtained in 4 (d) due to a voltage leak in the emission tube.) In Figure 3 the increase in ϕ is manifested by a decrease in emission at constant voltage.

A dissimilarity between the adsorption patterns of tungsten and tantalum is also noted. Figure 4 (d) exhibits the highly localized changes in emission intensity mentioned before but not present in Figure 3. This is indicative of the physisorbed state.

Since the grain boundary of Figure 4 presented a rather unusual opportunity to study its effect on oxidation, this tip was subsequently reacted with oxygen as shown in Figure 5. The reaction was carried out with oxygen at 10^{-5} mm Hg and the substrate heated to 830°C. Figure 5 (a) represents the clean substrate after cleaning at ~2400°C at the beginning of the reaction. Figure 5 (b) exhibits eight, randomly located, small, more or less circular and highly emissive regions, after two minutes of exposure to oxygen. As opposed to the adsorption

patterns, a discontinuous change in emission intensity is apparent between the bright spots and the adjacent regions on the substrate. Figure 5 (c) and Figure 5 (d) show the subsequent growth of the bright spots upon continued exposure to oxygen. These results may be interpreted in terms of the "field enhancement" effect which is discussed in the following paragraph on the important matter of differentiating between the adsorbed state and a crystalline second phase.

Adsorption from the gas phase onto a clean substrate is envisioned as a process comprised of (chronologically) weak physisorption, diffusion to either desorption or trap sites, and either desorption or chemisorption; the chemisorption step being preceded by dissociation in the case of a polyatomic gas. Trap sites are usually considered to be sites of local heterogeneity such as surface vacancies and ledges. While certain regions on the emitter-substrate do possess a greater density of such sites (e.g., the rough high-index planes and areas of transition from one crystallographic region to another), generally speaking, these sites are distributed more or less randomly over the substrate. Since the resolution of the microscope is normally about 20 Å in the plane of the substrate, the process of chemisorption is characterized in the emission pattern by gradual changes in emission intensity with respect to both time and position on the substrate.

Physically adsorbed molecules, being less tightly bound, often find themselves protruding above the surface to a greater degree than chemisorbed atoms. Such a protrusion on the surface may give rise to local field enhancement (by virtue of its relatively small radius of curvature) and resulting increase in localized emission and magnification. The slight variation in localized emission in Figure 5 (d) is probably the result of this effect.

Transformation from the adsorbed state to a crystalline second phase, however, being a first-order phase transformation, is accompanied by a decrease in the Gibbs free energy of the system as well as discontinuities in the first and higher order derivatives of the free energy (i.e., entropy, enthalpy, volume, etc.). Accordingly, electronic properties generally exhibit a discontinuity accompanying the transformation, and on this basis a discontinuity in electronic work function is expected. Whether or not such a discontinuity can be observed in the emission pattern depends upon the size, the shape, and the position of the volume undergoing transformation. In general, a region of dimensions smaller than the resolution limit will not be defined in the pattern. However, if the shape of the transformed volume is such that protrusion above the surrounding surface exists, increased magnification resulting from field enhancement may permit the observation of such a discontinuity. The net effect, then, is a result of the work function discontinuity and field enhancement, with the latter usually predominating.

On Figure 5 the bright spots exhibiting sharp emission discontinuity at their periphery are interpreted as being the result of the formation of a distinct crystalline second-phase, i.e., oxide nuclei or microcrystallites. One of the interesting features of this sequence is that the variation in emission over the surface of the substrate is rather continuous (except at the periphery of the nuclei). This is indicative of relatively low oxygen coverage in the adsorbed state after nucleation has occurred. The size of the bright spots in Figure 5 (b) corresponds to several hundred Å in diameter, but cannot be interpreted as the size of the nuclei if field enhancement exists. The existence of field enhancement is established in this case by the observation that the relative size of the bright spots on a particular pattern is not independent of applied voltage. (While this effect is not shown in the photographs of Figure 5, it will be shown in a subsequent reaction.) On the other hand, field enhancement does not affect the measurement of distances between nucleating centers. This distance appears to be on the order of several thousand Å.

At higher substrate temperatures the general features of the reaction change only slightly. However, higher pressures are required to achieve nucleation of the oxide in a reasonable period of time. This may imply that a critical degree of surface

coverage is required (Reference 23) and that, as the rate of desorption from the surface increases at higher temperatures, the length of time to reach the critical coverage also increases. Figure 6 shows the reaction at a substrate temperature of 1130°C with oxygen pressure at 10^{-4} mm Hg. Again crystallites are observed to grow and to increase their number with continued exposure. The pattern of 6 (b) is not easily interpreted at this stage of the experimental program, but it strongly resembles desorption patterns obtained by heating a tip, which has been saturated at low temperatures in ultra-high vacuum (i.e., in the absence of an appreciable amount of oxygen in the gas phase) to temperatures above 700°C (Reference 24). With respect to the distinct second phase observed later in the reaction, Figure 6 (b) represents a state of the surface during an incubation period.

Unfortunately, emission currents became dangerously high when the voltage of 6 (c) and 6 (d) was increased in an attempt to increase the emission from the substrate. Further evaluation of the role of the grain boundary was, therefore, not possible. Despite the appearance of Figure 6 (d), it is not certain whether oxide grew across the grain boundary or not. At lower voltages many of the irregularly shaped oxide regions of Figure 6 (d) appeared to divide themselves into approximately circular regions. Such an effect would be obtained if field enhancement (and increased magnification) existed at two protrusions located close together. The apparent absence of preferential oxidation at the grain boundary is most likely the result of a local surface deficiency of oxygen arising from diffusion into the grain boundary.

Another interesting feature of the nucleation and growth process on tantalum is observed in Figures 6 (c) and 6 (d), i.e., an increase in field enhancement with increasing growth. This phenomenon is revealed by the behavior of the second largest bright region in Figure 6 (c) as it grows and becomes the brightest region in Figure 6 (d). The appearance of this region in the photographs of Figures 6 (c), 6 (d), and 6 (e) is a bit misleading in that a sharply defined high-intensity circular spot is observed visually, with other less highly emitting spots in its proximity. Upon decreasing the voltage of Figure 6 (c), the intensity of all spots diminishes until no emission is visible at 15 kv. After further growth (Figure 6 (d)), the spot becomes much more intense at constant voltage and remains correspondingly more intense as the voltage is decreased to 12 kv (Figure 6 (e)).

The sharply defined circular bright spots are most likely the result of emission from a protrusion in the shape of a surface of revolution. For such a protrusion composed of the substrate phase and approximated by a spherical segment, a calculation of the local field shows that enhancement should increase as the radius of the protrusion increases from ~6 to ~40 Å (on a tip of ~1000 Å radius), then decrease upon further growth (Reference 25). Interpretation of the present observations, however, must account for the discontinuity in electronic properties due to the existence of a second phase as well as the size and shape effect. The observation that some regions exhibit continued increase in field enhancement with further exposure to oxygen may be partially explained by a relatively greater growth rate in a direction perpendicular to the substrate than parallel to it (i.e., whiskerlike growth). Such growth could also explain why some nuclei apparently disappear with increasing exposure time (Figure 6 (c) and 6 (d)). The large stresses imposed by the high field might easily tear a fragile microcrystallite from the surface.

While the random occurrence of nuclei is sometimes assumed to be related to the random occurrence of dislocations on the substrate, the presence of dislocations on the substrate surface in the present experiment (Reference 26) is unlikely due to the high annealing temperature employed. If the dislocation density of the annealed single crystal is taken as 10^5 to 10^6 per cm^2 (Reference 27) and the surface area of the observable portion of the emitter-tip is taken as 10^{-8} cm^2 (calculated from the known tip radius), it is apparent that the probability of finding a dislocation on the substrate surface is very low.

Future experimental work utilizing the conventional electron microscope may reveal the true shape of the protrusions, and with the aid of electron diffraction it may be possible to identify the second phase.

The above description of tantalum reactions is characteristic of the high pressure experiments (i.e., pressures above 10^{-5} mm Hg). In the pressure range of 10^{-8} to 10^{-6} mm Hg, the description which follows for tungsten is generally valid for tantalum as well.

Tungsten Reactions

The tungsten-oxygen reaction was been studied over the pressure range of 10^{-5} to 10^{-8} mm Hg with the substrate at temperatures between 30° and 1200°C. Each photographic sequence contains emission patterns obtained at constant current. However, slightly different current levels have been used in the various sequences in order to optimize the appearance of subtle changes in the patterns.

Characteristic of the reaction on substrates below 400°C are the sequences given in Figures 7 and 8 (at room temperature and 400°C respectively). With the exception of Figure 8 (f), the reactions were carried out at an oxygen pressure of 7×10^{-8} mm Hg. Significant differences between the two reactions are not apparent. In both cases the average ϕ of the entire surface increases with time. And in both cases an "end point" in the reaction appears (Figures 7 (e), 7 (f), 8 (d), and 8 (e)), after which changes take place very slowly (if at all) at this pressure. Assuming a constant sticking coefficient of 0.1, five to ten minutes should be required for the tightly bound layer to form at room temperature (Figure 7 (c) and 7 (d). The existence of an "end point" signals the attainment of a saturated state, i.e., a metastable equilibrium between adsorption, desorption, and diffusion into the lattice. The longer time required to reach the stage of Figure 7 (c) and 7 (d) at 400°C is a manifestation of the smaller sticking coefficient and increased rates of the thermally activated processes giving rise to the equilibrium. In view of the difficulty with which the complete second layer is formed at room temperature and low pressure, the saturated state in this case represents between one and two layers. The existence of highly preferred sites for adsorption is manifested by (1) the rapid decrease of intensity in the atomically rough $\{211\}$ regions and (2) the slight variation in emission intensity on a highly localized scale. The latter effect is also noticed in Figure 8 (f), which represents the "end point" of the reaction at 400°C at an oxygen pressure of 10^{-5} mm Hg. This pattern differs only in its clear definition and low intensity of low-index planes from the corresponding pattern (not shown) obtained at room temperature. In these cases, however, the variation in emission intensity on a localized scale is the result of physisorption.

The reaction on substrates at higher temperatures is characterized by a completely different series of events. In the first place, a physically adsorbed state is not apparent. Even the course of chemisorption is changed and is more difficult to analyze due to the increased rate of all thermally activated processes such as diffusion and desorption.

Figures 9 and 10 correspond to the reaction of oxygen at pressures between 10^{-5} and 10^{-7} mm Hg on the tungsten substrate at 750°C. Figure 9, with oxygen at 10^{-7} mm Hg, shows that the reaction begins in a manner similar to the low temperature reactions. This similarity is not long lasting. Figure 9 (f) represents an "end point" under these conditions, as the pattern and voltage-current characteristics do not undergo further change upon continuing the reaction. While the tightly bound layer is known to be stable in this temperature range, the extent and nature of additional adsorption from the gas phase is unknown. Figure 9 (c) can be identified as the pattern corresponding to approximately one layer on the basis of the desorption work described in Reference 15. Assuming a constant sticking coefficient and calculating the flux by Equation 2, a value of 10^{-2} for the average sticking coefficient is obtained. Even if the sticking coefficient remains unchanged after the first

layer is formed, not more than several layers could be present on the tip (Figure 9 (e)). The most outstanding feature of the patterns in Figure 9 is the absence of emission discontinuity on a localized scale.

Figure 10 corresponds to the reaction at the same temperature with the oxygen pressure increased to 10^{-5} mm Hg.

At these higher pressures, the reaction apparently passes through the adsorbed stages of Figure 9 initially, passes through the "end point" of Figure 9 (f), and on to the stages shown in Figure 10(c), 10(d), 10(e), and 10 (f). The localized emission discontinuities in the {111} regions of these patterns must be interpreted as being the result of the field enhancement effect at protrusions which are very closely spaced, i.e., oxide nuclei or microcrystallites. Nucleation apparently takes place simultaneously at many sites: the centers of which seem to be space about 100 Å apart. While growth from or. crystallographic region into another is not in evidence, nucleation in the {110} region is observed after a longer incubation period than in the {111} regions. In Figure 10 (f) most of the current is drawn from the protrusion giving rise to the bright circular spot, thus permitting relatively less current to come from the crystallites in the {111} region. The crystallites in the {110} region exhibit some of the same growth characteristics as were noted in the tantalum oxidation, i.e., an increasing field enhancement effect, an increase in number, and the disappearance of some crystallites; thus indicating that some nuclei apparently prefer to grow away from the surface.

A similar course of events is noticed in Figures 11 and 12 for oxygen pressures of 10^{-7} and 10^{-6} mm Hg respectively and a substrate temperature of 1000°C. Figure 11 is characterized by an "end point" and the absence of highly localized emission discontinuity. The reaction at the higher pressure (Figure 12) apparently passes through these initial stages, reaches a critical coverage, then nucleates oxide at highly preferred sites in the {100} as well as the {111} region.

The oxidized state shown in Figure 12 (d) may also be achieved by heating (in the absence of oxygen in the gas phase) a tip which has been oxidized at lower temperatures. Figure 13, typical of such a transformation, shows a sequence of pattern changes which resulted from the heating of the oxidized tip of Figure 10 (f) at 750°C, then 1000°C in the ultra-high vacuum. Figure 13 (a) is the pattern after heating the tip of Figure 10 (f) for 23 minutes at 750°C. Figure 13 (b), 13 (c), and 13 (d) resulted from additional treatment at 1000°C of a total of 1, 5, and 95 minutes respectively. Figure 13 (c) is quite similar to Figure 12 (d). While Figure 13 (d) could result from desorption and evaporation, the effect of residual gases over such a long period of time is difficult to evaluate and, hence, does not allow an unambiguous interpretation.

To rationalize the occurrence of oxide in different crystallographic regions of the substrate as a function of temperature, further experimental work is required. The interpretation of such work must take cognizance of the variety of oxides which are known to exist in the tungsten-oxygen system (Reference 3) and, particularly, the well-established transformations in WO_3.

At higher oxygen pressures (i.e., above 10^{-6} mm Hg), results such as those shown in Figure 6 for tantalum are also obtained for tungsten. At present it is not possible to fully interpret these results because under the present experimental conditions the reaction is occurring too rapidly to observe the initial stages. These results are probably the consequence of preferential growth of oxide crystallites normal to the surface after the surface is well oxidized.

CONCLUSIONS

This work has demonstrated that the field electron emission microscope is extremely well suited for studies of nucleation and growth in the initial stages of oxidation because of its inherent high resolution, its ability to define atomically the cleanliness of the surface prior to oxidation, its extreme sensitivity to contaminants on the surface, and its definition of all crystallographic planes and regions on the substrate. While the present

work does not permit a complete and detailed description of the intial oxidation kinetics, a number of distinguishing features of the process have been observed, and these features allow the following qualitative description.

The surface product of the reaction of gaseous oxygen on tungsten and tantalum substrates depends critically upon substrate temperature, crystallography, and oxygen coverage. The nucleation of oxide is preceded by adsorption and may require a critical coverage of adsorbate. Growth of these nuclei is characterized by lateral and perpendicular extension. The overall process appears to be a surface reaction which gives rise to rather pronounced protrusions above the surface.

The tungsten-oxygen reaction below 400°C and at oxygen pressures as high as 10^{-5} mm Hg is characterized by stable adsorbed states with no apparent tendency for oxide formation. At temperatures between 400° and 1000°C, an oxide is nucleated after the adsorption of at least a monolayer. Nucleation occurs on preferred regions of the substrate, initially {111} and {100}, depending upon substrate temperature. In these regions, nuclei appear more or less simultaneously at sites which are on the order of 100 Å apart.

The general characteristics of the nucleation of oxide on tantalum are the same as those for tungsten under approximately the same conditions of pressure and temperature.

Under certain conditions (i.e., the higher pressure experiments in which the pressure of the entire vacuum system exceeds 10^{-5} mm Hg) the distribution of oxide crystallites has been observed to be random over a surface exhibiting relatively low coverage. The distance between adjacent crystallites is appreciably larger under these conditions than in the lower pressure experiments. This result is probably due to contamination of possible nucleation sites on the surface by gases other than oxygen which were present in the system as a consequence of the experimental technique utilized to produce high oxygen pressures. The apparent absence of preferential nucleation at a grain boundary is probably the result of a local deficiency of oxygen on the surface caused by diffusion into the grain boundary.

ACKNOWLEDGMENTS

The authors acknowledge the financial support of the Office of Ordnance Research, United States Army, under contract DA-33-019-ORD-3387 and thank Dr. Ralph Klein, Chief, Surface Chemistry Section of the National Bureau of Standards for very helpful discussions of some of his current work. The encouragement of Professor Mars G. Fontana, Chairman, Department of Metallurgical Engineering, The Ohio State University, is greatly appreciated.

REFERENCES

1. O. Kubaschewski and B. E. Hopkins, Oxidation of Metals and Alloys, Academic Press Inc., New York, N. Y., 1962.

2. A. T. Gwathmey and K. R. Lawless, H. C. Gatos Ed. The Surface Chemistry of Metals [illegible]miconductors, 483-521, John Wi[illegible] Sons, Inc., New York, N. Y., 19

3. J. E. Battles, W. T. Ebihara, W. P. Medli, M. J. Pool, R. Speiser, J. W. Spretnak, and G. R. St. Pierre, Research on the Oxidation Behavior of Tungsten, ARL TR 62-324. Aeronautical Research Laboratories, Wright-Patterson AFB, Ohio, 1962.

4. V. D. Barth and G. W. P. Rengstorff, Oxidation of Tungsten, DMIC Report 155, Battelle Memorial Institute, Columbus, Ohio, 1961.

5. O. Kubaschewski and B. E. Hopkins, Oxidation of Metals & Alloys, 219 and 227.

6. J. N. Ong, Jr. Transactions of AIME 1962, Vol 224, 991.

7. J. Bénard, F. Grønlund, J. Oudar, and M. Duret, Z. Elektrochem, 1959, Bd. 63, 799.

REFERENCES (CONT'D)

8. W. W. Harris, F. R. Ball, and A. T. Gwathmey, Acta Met. 1957, Vol 5, 574.

9. R. N. Bloomer, British J. Appl. Phys. 1957, Vol 8, 321.

10. J. Bardolle, Rev. Metall. 1954, Vol 51, 833.

11. U. Martius, Canadian J. Phys. 1955, Vol 33, 466.

12. J. A. Becker and R. G. Brandes, J. Chem. Phys. 1955, Vol 23, 1323.

13. R. Gomer and J. K. Hulm, J. Chem. Phys. 1957, Vol 27, 1363.

14. R. Klein, J. Chem. Phys. 1953, Vol 21, 1177.

15. E. W. Müller, Z. Elektrochem. 1955, Bd. 59, 372.

16. R. Gomer, Field Emission and Field Ionization, Harvard University Press, 1961.

17. R. Gomer, Adv. in Catalysis, 1955, Vol 7, 118.

18. R. H. Good and E. W. Müller, Handbuch der Physik, 1956, Vol 21, 176.

19. E. W. Müller, "Modern Research Techniques in Physical Metallurgy," American Society for Metals, 1953, 33.

20. S. Dushman and J. Lafferty, Scientific Foundations of Vacuum Technique, John Wiley and Sons, Inc., New York, N. Y., 1962.

21. R. Gomer, Field Emission and Field Ionization, 47.

22. E. W. Müller, J. Appl. Phys. 1955, Vol 26, 737.

23. K. L. Moazed and G. M. Pound, "Field Emission Microscopy of Metal Crystal Nucleation," Transactions of Metallurgical Society of AIME, 1964.

24. R. Klein, Private Communication.

25. D. J. Rose, J. Appl. Phys. 1956, Vol 27, 215.

26. E. W. Müller, Newkirk and Wernick, Editors. Direct Observation of Imperfections in Crystals, Interscience Publishers, Inc. 1962, 77.

27. D. McLean, Mechanical Properties of Metals, John Wiley and Sons, Inc., New York, N. Y. 1962, 37.

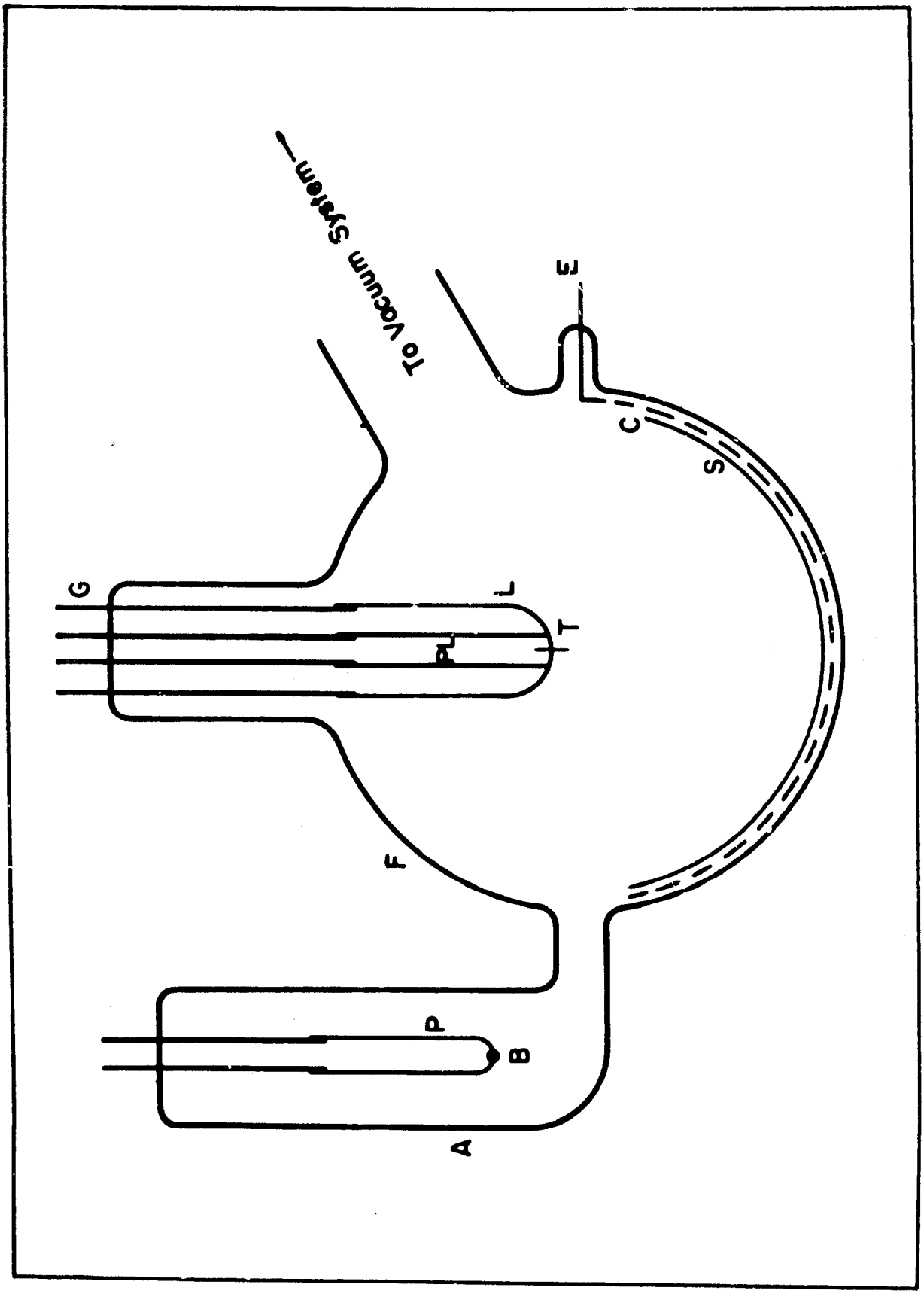

Figure 1. Field Emission Tube and Oxygen-Generating Sidearm (Schematic)

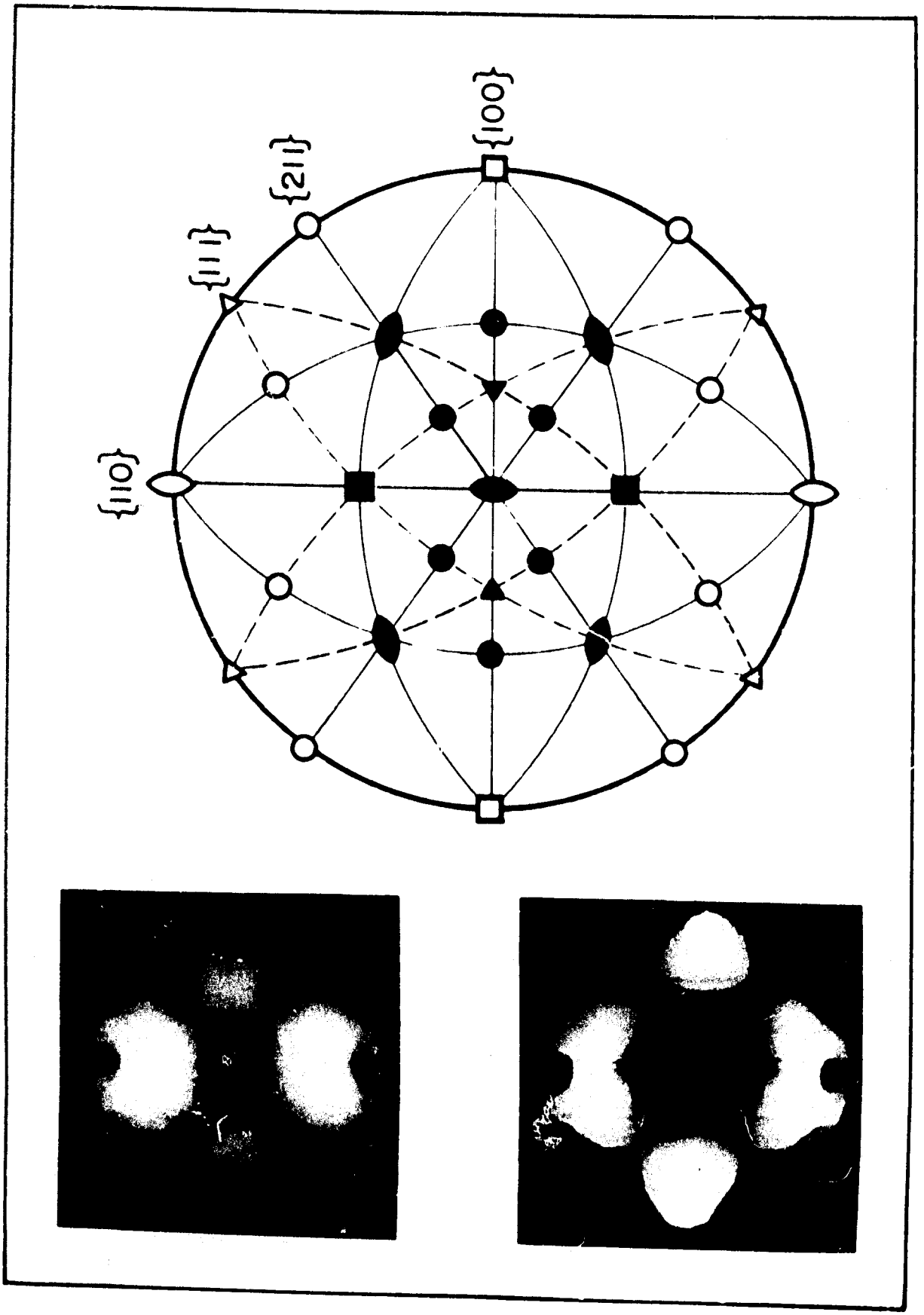

Figure 2. Clean Tungsten and Tantalum Patterns, and Standard Stereographic Projection

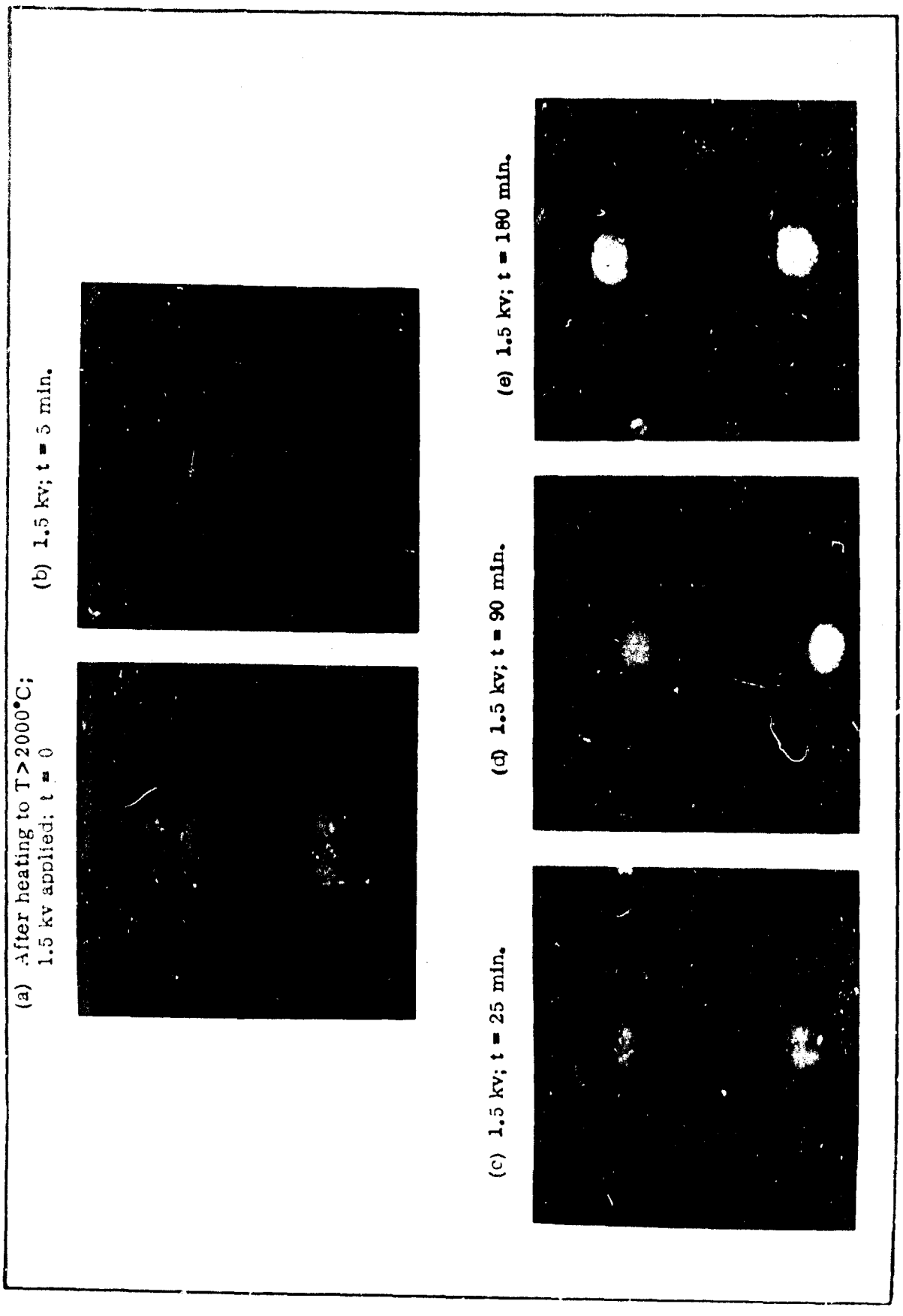

Figure 3. Reactivity Sequence of Residual Gases at 5×10^{-9} m.m. Hg on Tungsten at Room Temperature

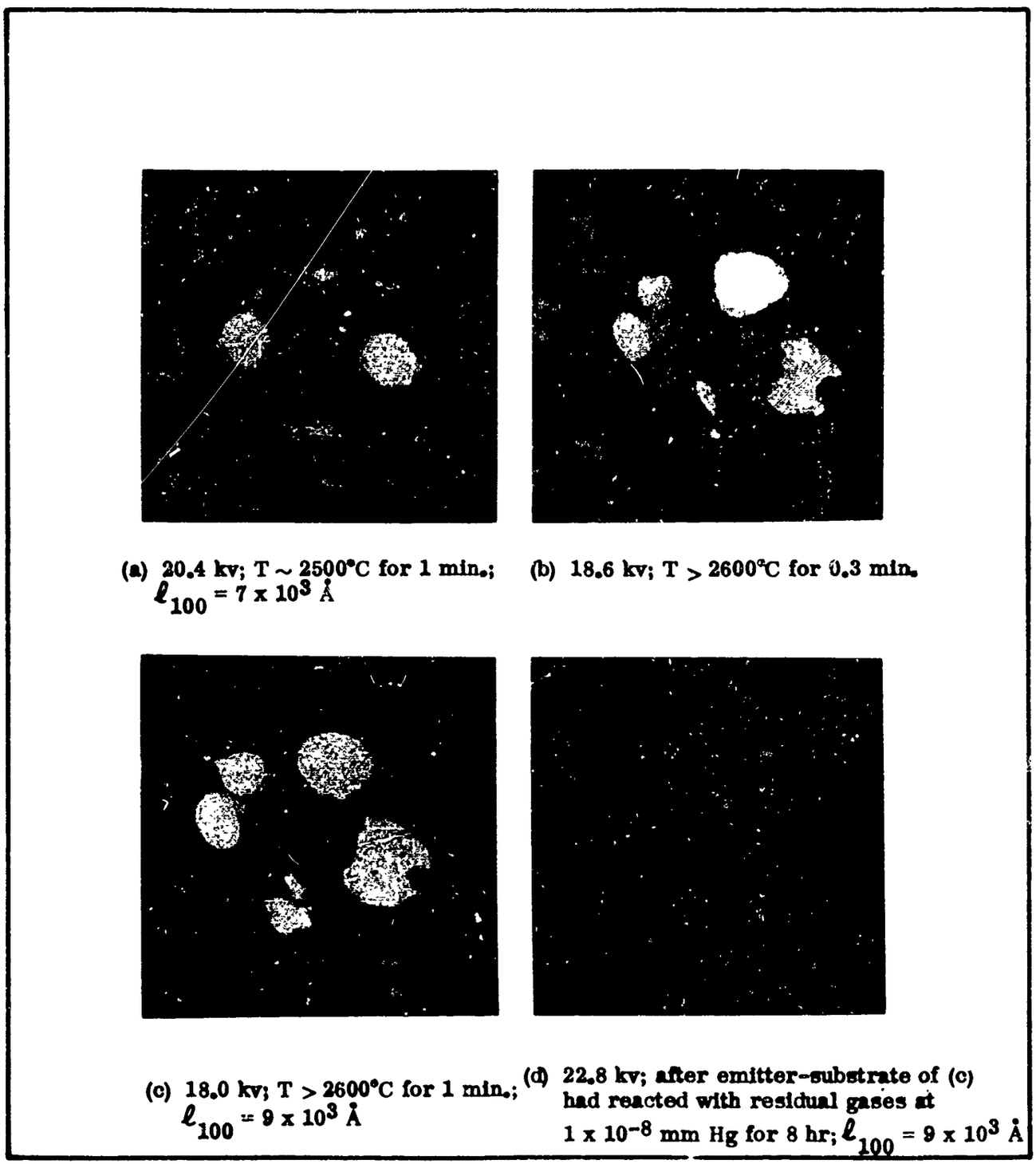

(a) 20.4 kv; T ~ 2500°C for 1 min.; $\ell_{100} = 7 \times 10^3$ Å

(b) 18.6 kv; T > 2600°C for 0.3 min.

(c) 18.0 kv; T > 2600°C for 1 min.; $\ell_{100} = 9 \times 10^3$ Å

(d) 22.8 kv; after emitter-substrate of (c) had reacted with residual gases at 1×10^{-8} mm Hg for 8 hr; $\ell_{100} = 9 \times 10^3$ Å

Figure 4. Tantalum Evaporation at High Temperatures and Reaction With Residual Gases at Room Temperature

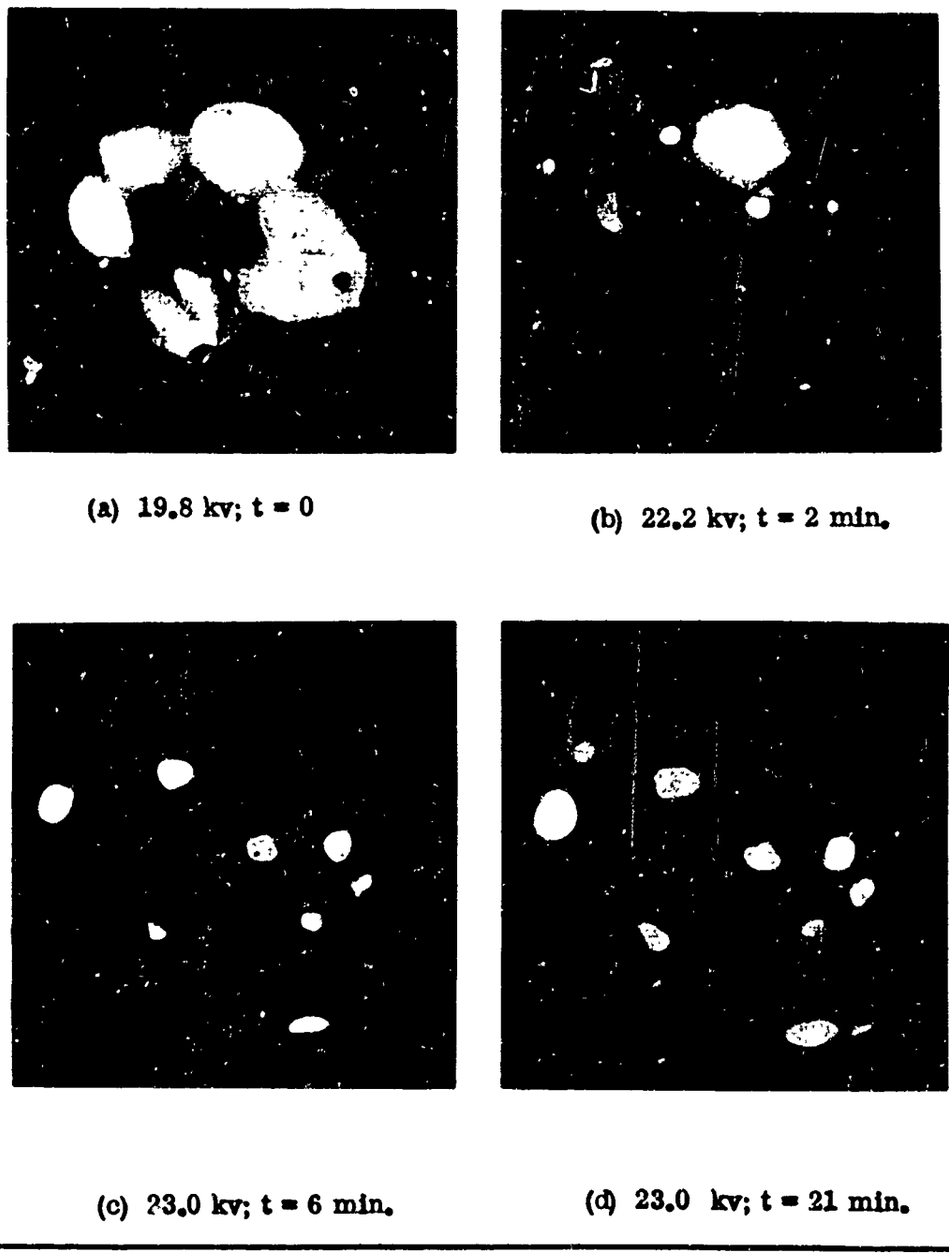

(a) 19.8 kv; t = 0

(b) 22.2 kv; t = 2 min.

(c) 23.0 kv; t = 6 min.

(d) 23.0 kv; t = 21 min.

Figure 5. Isothermal Tantalum-Oxygen Reaction Sequence for Substrate Temperature of 830°C and Oxygen Pressure of 10^{-5} mm Hg ($\ell_{100} = 9 \times 10^3$ Å)

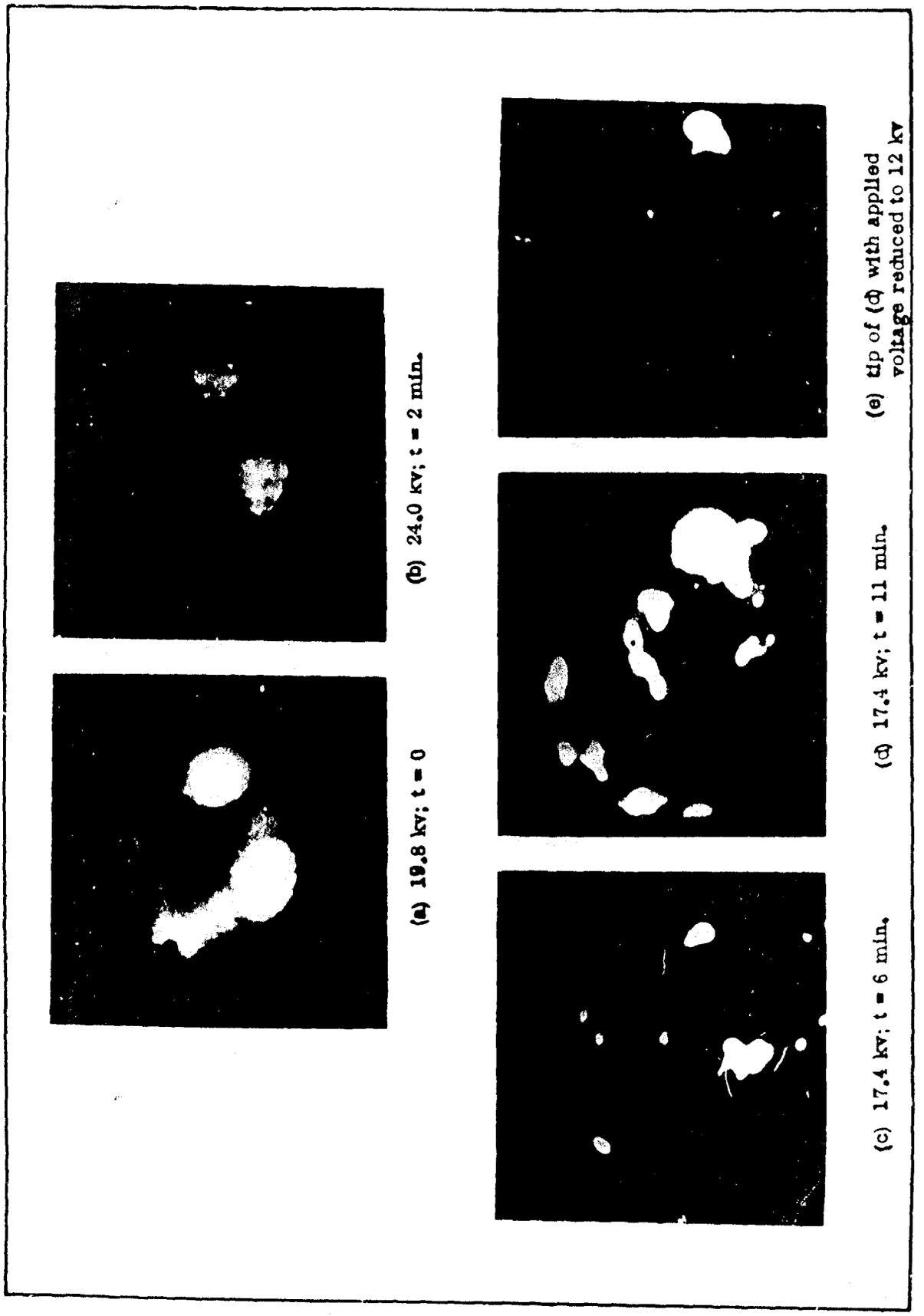

Figure 6. Isothermal Tantalum-Oxygen Reaction for Substrate Temperature of 1130°C and Oxygen Pressure of 10^{-4} mm Hg ($\ell_{100} = 9 \times 10^3$ Å)

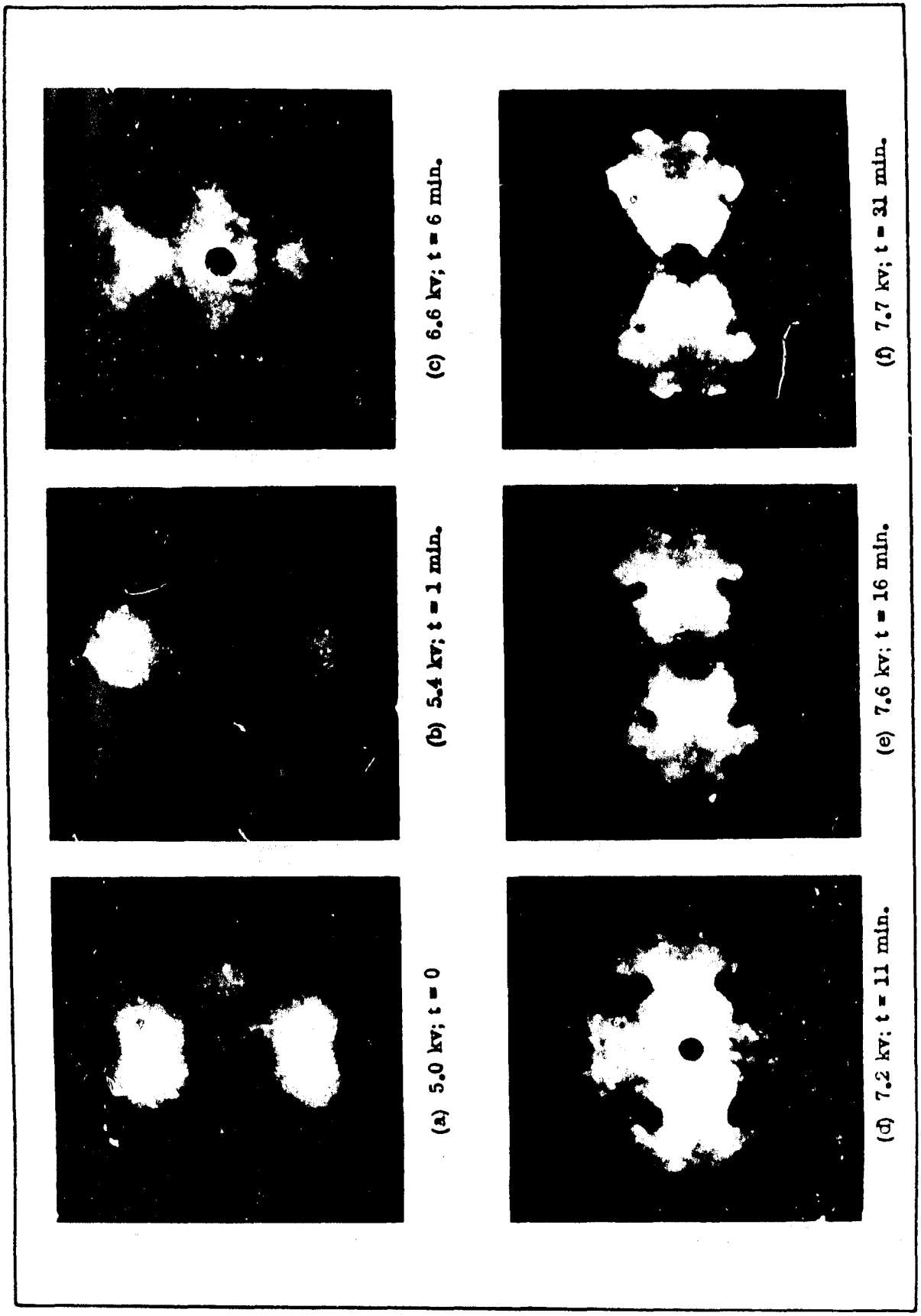

Figure 7. Isothermal Tungsten-Oxygen Reaction for Substrate at Room Temperature and Oxygen Pressure of 6 to 7 x 10^{-8} mm Hg (ℓ_{100} = 4 x 10^{3} Å)

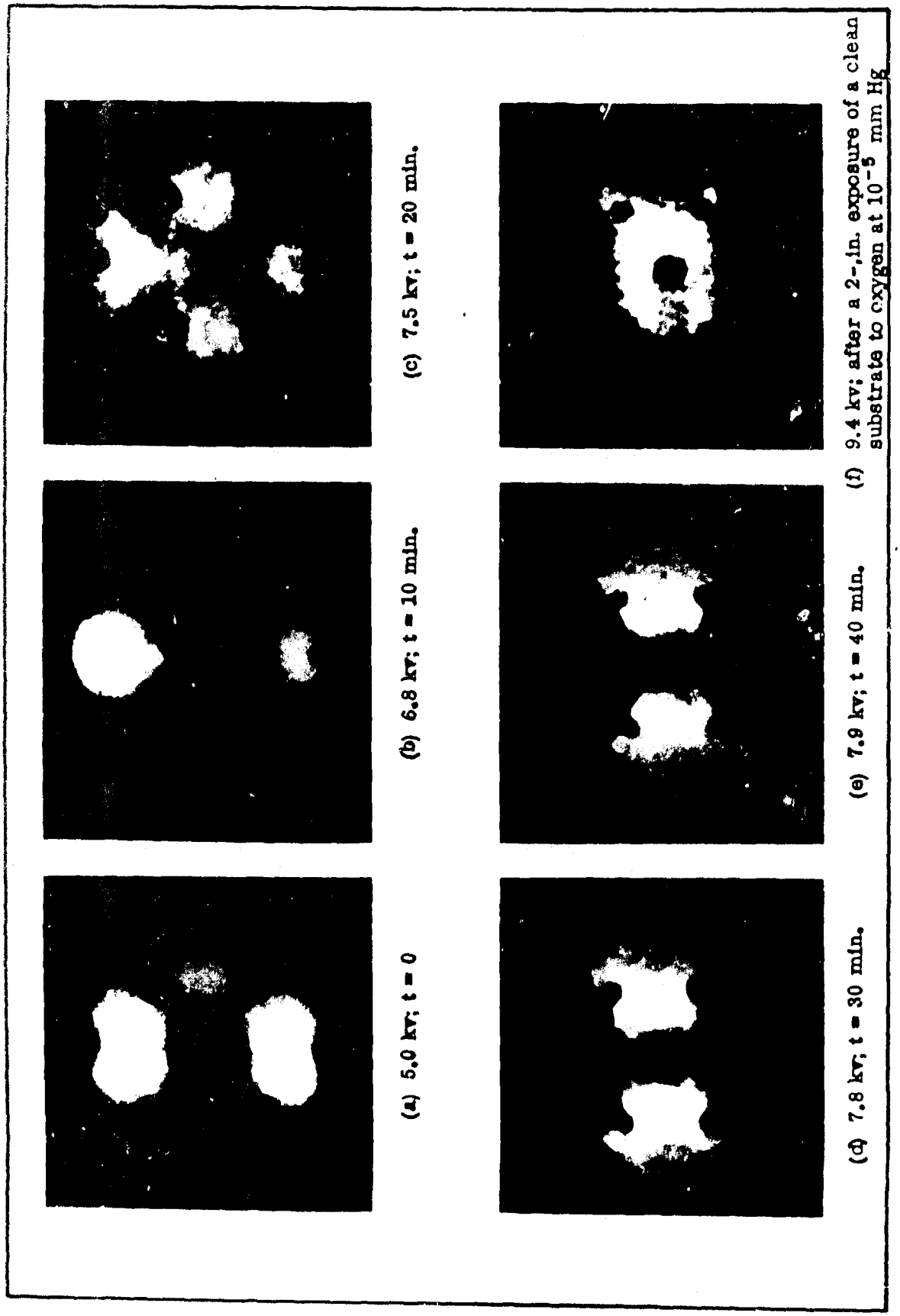

Figure 8. Isothermal Tungsten-Oxygen Reaction for Substrate Temperature of 400°C and Oxygen Pressure: 7×10^{-8} mm Hg ((a) through (e)), 10^{-5} mm Hg (f); ($\ell_{100} = 4 \times 10^3$ Å)

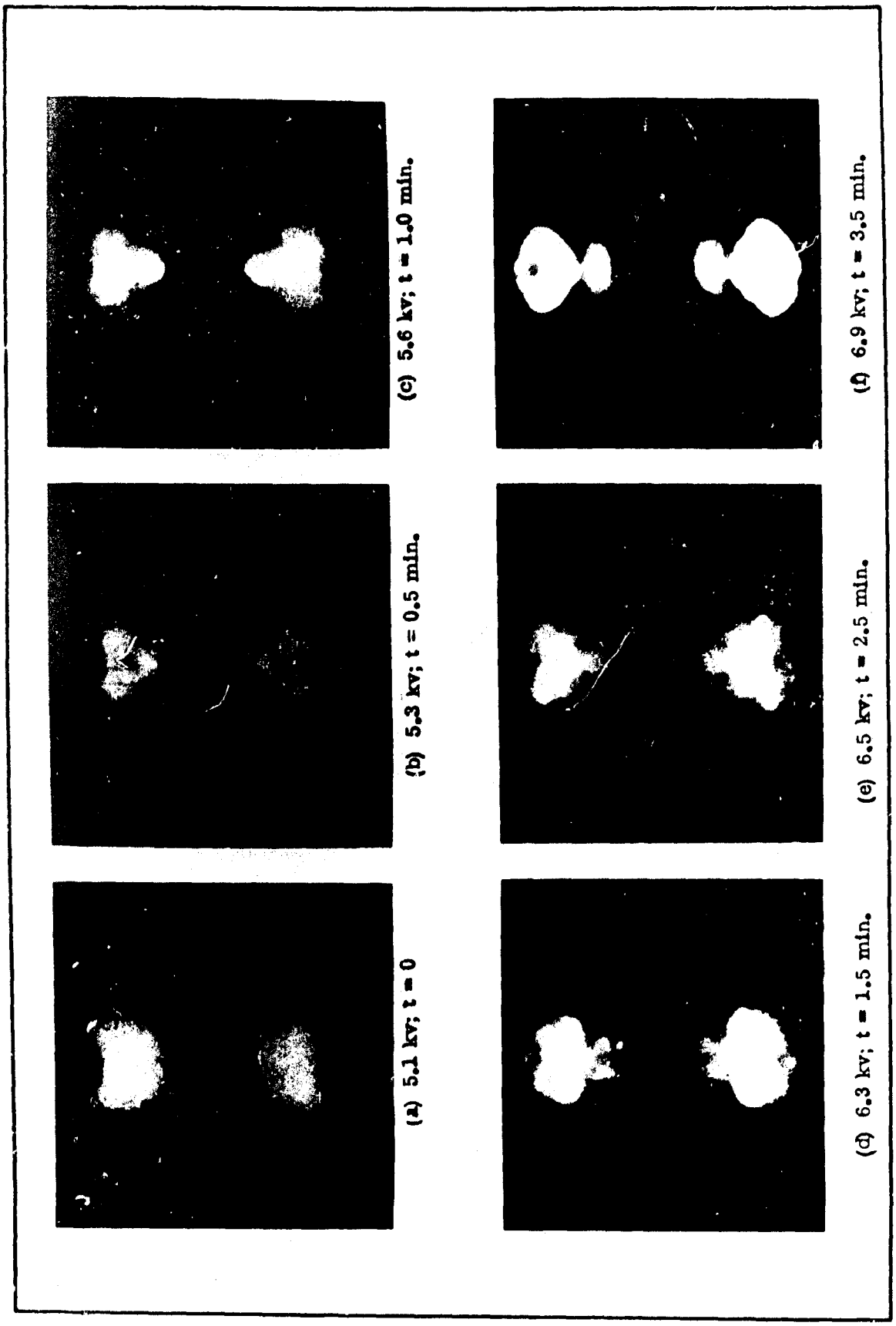

Figure 9. Isothermal Tungsten–Oxygen Reaction for Substrate Temperature of 750°C and Oxygen Pressure of 10^{-7} mm Hg ($\ell_{100} = 4 \times 10^3$ Å)

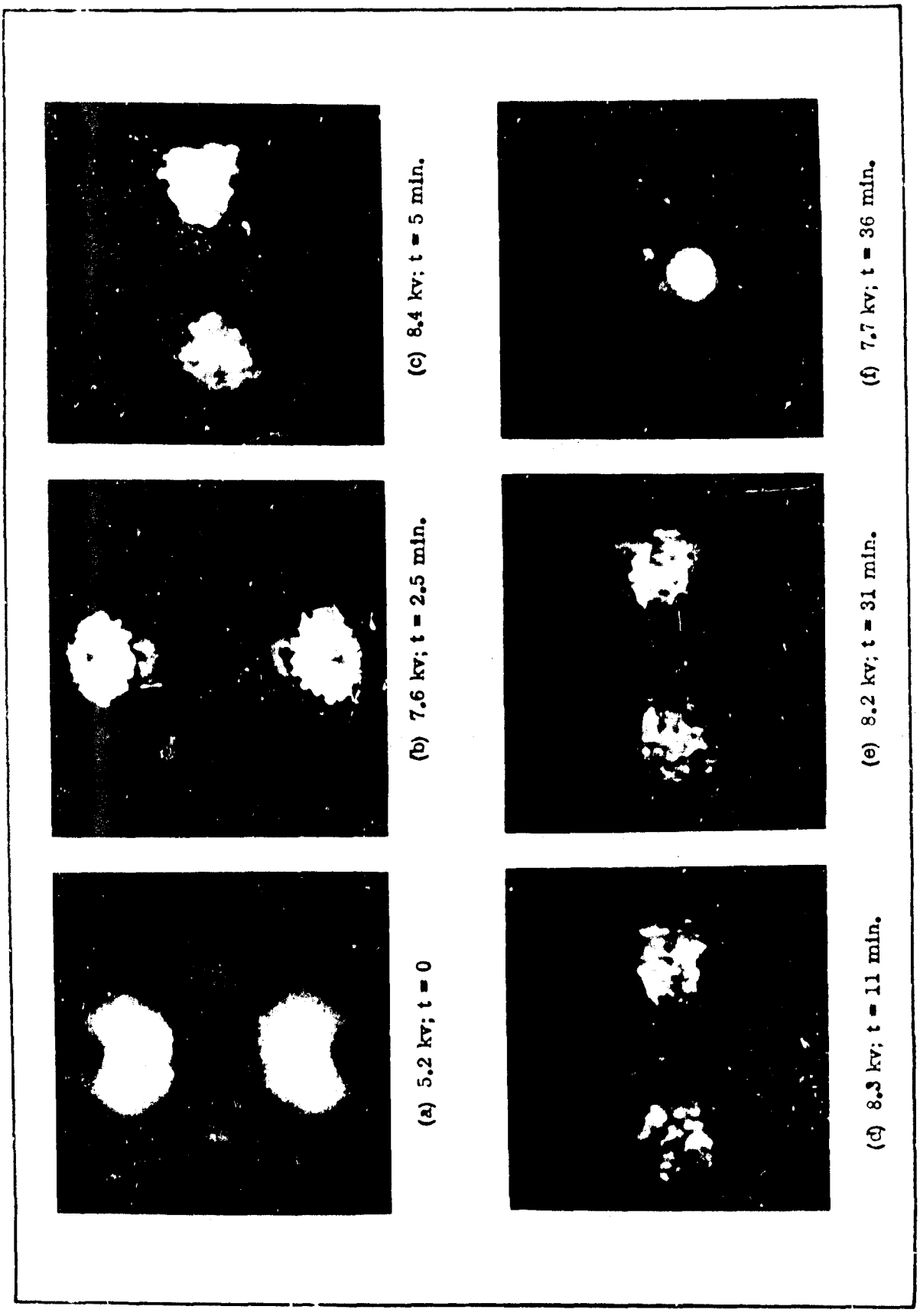

Figure 10. Isothermal Tungsten-Oxygen Reaction for Substrate Temperature of 750°C and Oxygen Pressure of 10^{-5} mm Hg ($\ell_{100} = 4 \times 10^{3}$ Å)

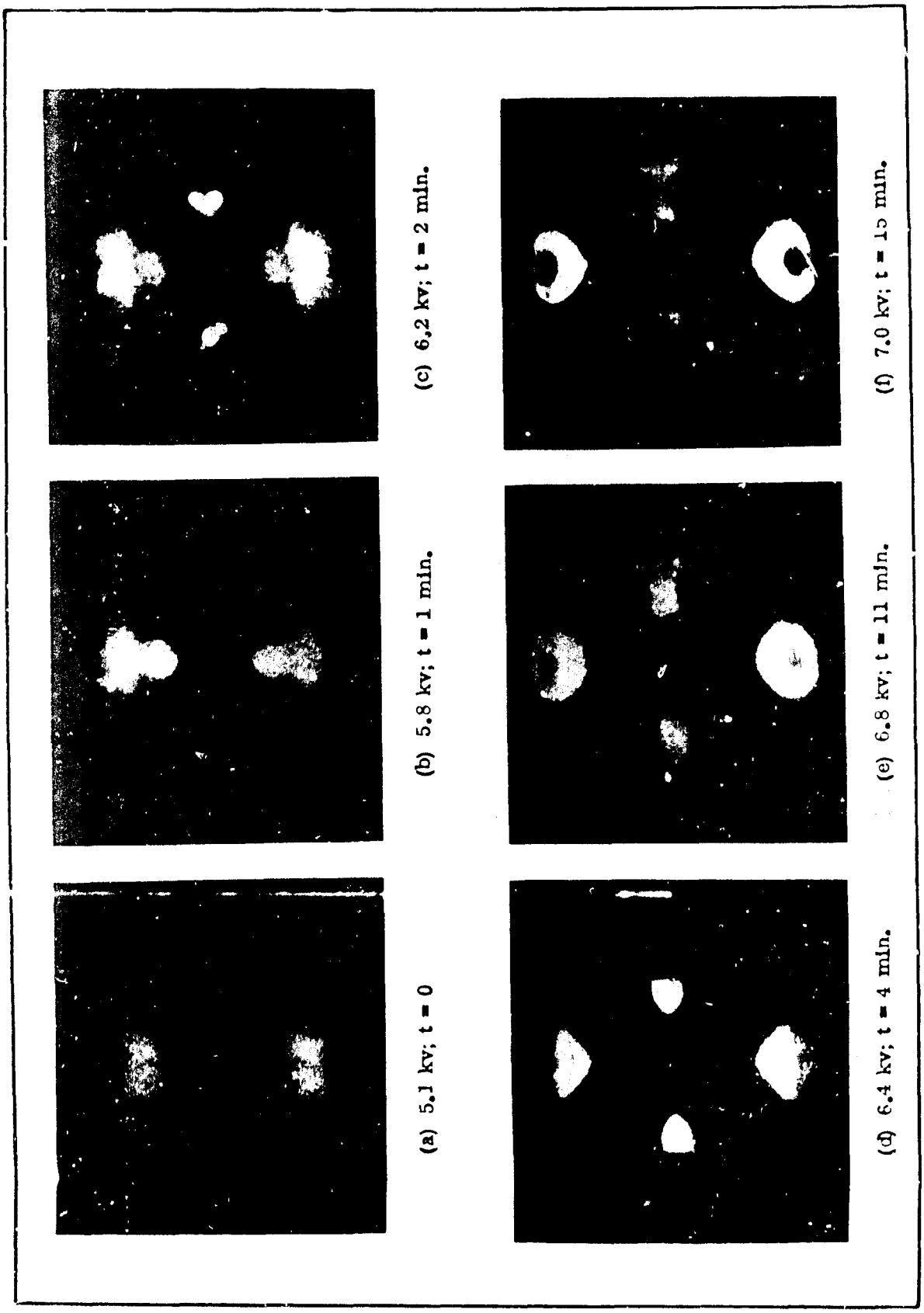

Figure 11. Isothermal Tungsten-Oxygen Reaction for Substrate Temperature of 1000°C and Oxygen Pressure of 10^{-7} mm Hg ($\ell_{100} = 4 \times 10^3$ Å)

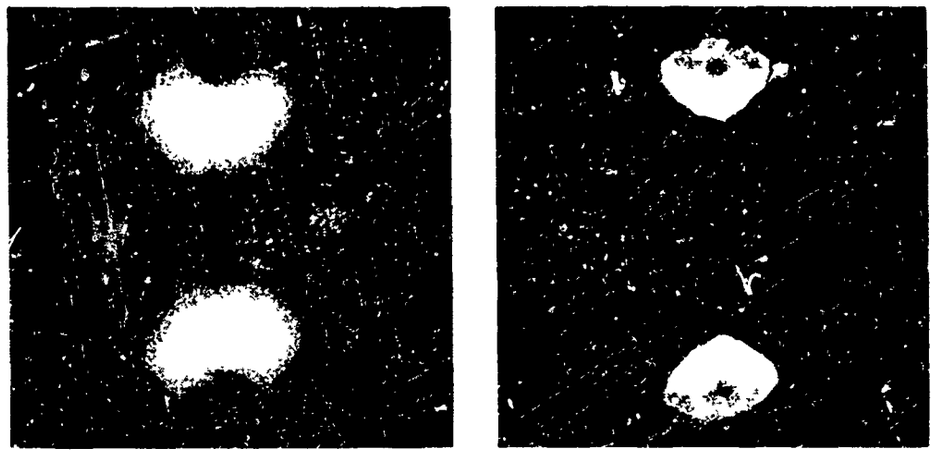

(a) 5.5 kv; t = 0

(b) 7.3 kv; t = 7.5 min.

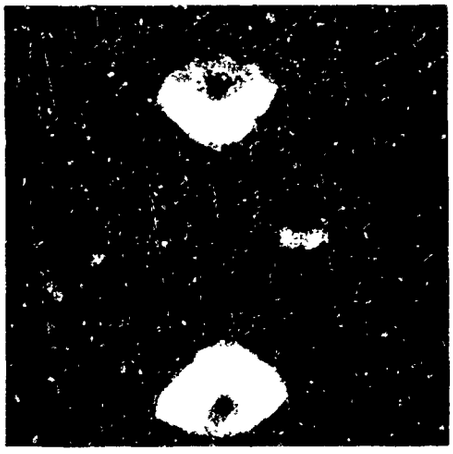

(c) 7.6 kv; t = 10 min.

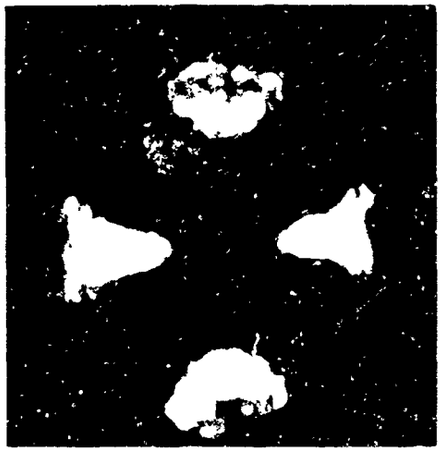

(d) 8.3 kv; t = 15 min.

Figure 12. Isothermal Tungsten-Oxygen Reaction for Substrate Temperature of 1000°C and Oxygen Pressure of 10^{-6} mm Hg ($\ell_{100} = 4 \times 10^3$ Å)

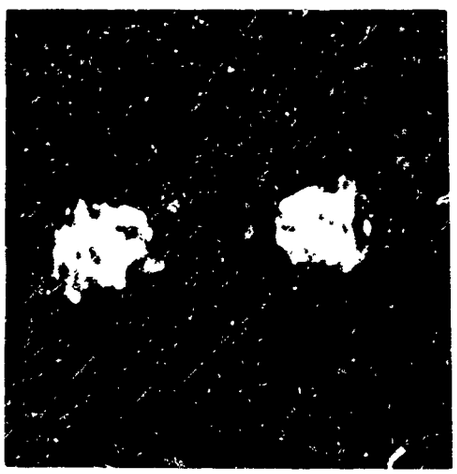

(a) 8.1 kv; after additional 23 min at 750°C

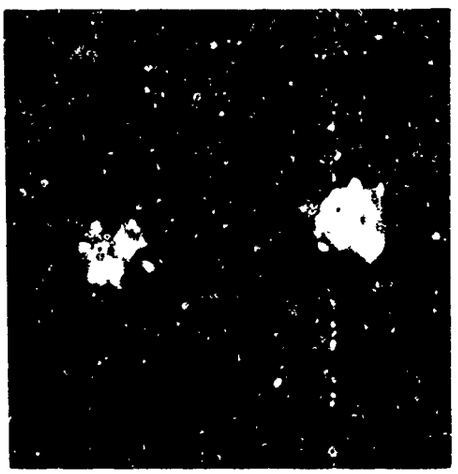

(b) 7.7 kv; after additional 1 min. at 1000°C

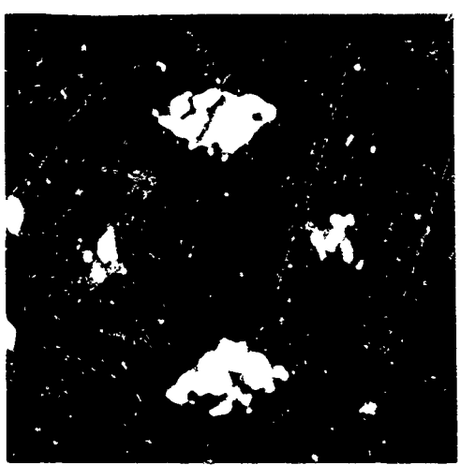

(c) 7.4 kv; after additional 8 min. at 1000°C

(d) 6.4 kv; after additional 165 min. at 1000°C

Figure 13. Substrate of Figure 10 (f) Heated in the Absence of Appreciable Oxygen in the Gas Phase; Residual Gas Pressure = 7×10^{-9} mm Hg ($\ell_{100} = 4 \times 10^{3}$ Å)

INTRODUCTION TO THE AFTERNOON SESSION

I. Perlmutter

This morning Mr. Paul Faust discussed some of the reasons why studies of the oxidation of refractory metals are important to one of mankind's most challenging frontiers, the overall area of Aerospace Technology. This afternoon we will continue to have an opportunity for discussion after each paper. In addition, time has been set aside for an overall discussion period in which I would like us to attempt to turn our attention from the specifics of individual papers to the broader aspects of the implications of this work and what we should be doing in the future. In particular, I don't think it impertinent for me to suggest that we extend our thinking beyond what would constitute additional good science to a consideration of what are the practical implications of our current knowledge and the work now going on, and what additional fundamental work might be most likely to yield practical implications in the future. I ask that we prepare ourselves to consider and discuss questions such as the following:

a. Where do we stand with respect to our overall understanding of the mechanisms of oxidation of these refractory substances? Is intensive further work likely to yield information of practical significance? Are there any major gaps in our knowledge? Is there any need to study oxidation by atomic or ionized species?

b. From our current knowledge of oxidation mechanisms can we draw any inferences of possible routes to follow toward the development of oxidation resistant alloys or is this a forlorn hope pre-doomed to failure? Must we accept high oxidation rates even at moderate fractions of the melting point?

c. Does our developing knowledge about high temperature oxidation of pure metals yield any information of direct value to the problem of developing oxidation resistant coatings?

d. Obviously, we will, at some stage, want to intensify our study of the kinetics and mechanisms of oxidation of typical coating systems relative to work on the pure metals. I take it as self-evident that a background of studies on the pure metals had to be accomplished before we could start to understand these more complex systems. However, can we draw even vague inferences relative to the coating problem from the work on the simple metals? The press of many of our development problems is such that some fundamentally grounded inferences, however speculative, are better than a completely empirical approach.

With this as an introduction, let us proceed with this afternoon's program:

Where should we be going in the future and what inferences might be drawn from this work, or even of work that might be done in the future? I think that a group such as our symposium group is exceptionally well qualified to accept this challenge, and to have the background and imagination to speculate about the reduction to practice possibilities before a relatively complete elucidation of the fundamentals has made them self-evident as well as to speculate about which additional fundamental investigations might prove to have the greatest practical implications. Don't misunderstand me. I well recognize the danger of such speculation, and realize that efforts to explore such ideas should supplement rather than replace a logical, thorough and steady development of the overall underlying science. I submit, though, that progress in science as well as in technology would be slow indeed if it relied only on a methodical approach. What, therefore, should be the work which the Air Force and other agencies support to make the most rapid progress in both a scientific and technological sense.

I should like to offer some ideas of my own, and I do this in the full expectation

that you will consider them as clay pigeons to be shot down, if you will. I will also pose some further questions.

I think some work on the oxidation mechanisms of pure metals should continue with emphasis being placed upon determining the kinetics and mechanisms under temperature, pressure, flow rate, and time conditions such as indicated earlier by Mr. Faust.

I also believe that the time has come to start studying the kinetics and mechanisms of oxidation of alloys of these refractory metals. Such work will, of course, benefit from the knowledge we have gained from the pure metals. Studies of alloys might give us ideas for oxidation resistant alloys or components of coating systems. However, which are the most significant systems to study from either a fundamental or eventually, from a practical viewpoint?

When considering oxidation resistant alloys or coatings we are naturally interested in the formation or deposition of an oxide. It might be well to undertake studies of various types of oxide structures, similar to the molybdates or niobates, which might be of importance here. Whenever we consider the formation of such oxides or their interaction with high temperature oxidizing environments which may include other reactive components such as water, we are brought face-to-face with the general lack of high temperature thermodynamic and kinetic data. This overall lack has been well recognized for some years and large amounts of effort have gone into increasing the background of information here. However, the difficulty of obtaining such data, and the extent of data which might be useful if acquired, presents us with an almost bottomless pit situation, and I ask you to suggest which specific kinetic and thermodynamic data might be of most significance.

ML-TR-64-162

FOUR TYPES OF OXIDATION PROCESSES IN THE OXIDATION OF TUNGSTEN

E. A. Gulbransen*
K. F. Andrew*
F. A. Brassart*

INTRODUCTION

A number of studies have been made on the oxidation of tungsten below 1200°C. A review of these studies was made by personnel of the Westinghouse Research Laboratories and published in 1960 (Reference 1).

Langmuir (Reference 2) was the first to study the reaction of tungsten with oxygen at temperatures above 1200°C. Tungsten filaments were heated electrically in low pressures of oxygen and the reaction followed by observation of the pressure. Filament temperatures between 1070° and 2770°K were used. Langmuir's results showed an increase in reaction rate up to the highest temperature. The rate of reaction was found to be a linear function of pressure below a pressure of 10^{-3} Torr.

Perkins and Crooks (Reference 3) used a modified Langmuir method to study the oxidation of tungsten. Direct electrical heating was used with the rate of oxidation being determined by direct measure of the surface recession. One feature of this work was the finding of a decrease in rate of surface recession above 1900°C. This inversion in the rate of surface recession was related to thermal dissociation of tungsten trioxide.

Our study is directed toward an understanding of the mechanism of oxidation of tungsten from 1150° to 1615°C over a wide pressure range.

EXPERIMENTAL

Kinetic studies of the oxidation of pure tungsten were made using a sensitive weight change method and an oxygen consumption method.

Microbalance

Since large weight changes were occurring during oxidation a gold plated Invar beam balance of low sensitivity was used. The beam of the balance was 14.5 cm long and weighed 46 gm. Calibration of the balance gave a sensitivity of 60 micrograms for a 0.001 cm deflection at 7.25 cm using a weight of 0.83 gm. The specimens were suspended using a 2 mil nickel-chromium alloy wire in the cold zone and an 8 mil section of platinum wire in the hot zone of the furnace tube.

Pressure Measuring System

Oxygen consumed in the reaction is determined by measuring the rate at which the pressure of a calibrated 150 cc reservoir decreases as oxygen is leaked into the reaction system to make up for the oxygen used by the reaction. The leak valve was purchased from the Granville-Phillip Company of Pullman, Washington. The pressure change of a reservoir is measured directly in mm of Hg (Torr) and the weight of oxygen used is calculated from the gas laws.

The major difficulty with this method is that no distinction can be made between oxygen consumed to form an oxide film, oxygen consumed to form the volatile oxide, or oxygen absorbed by the furnace tube. A combination of weight change and oxygen consumption methods enables one to completely describe the reaction.

*Westinghouse Research Laboratories

Furnace Tubes

The furnace tubes, having an outside diameter of one inch, were of high purity vacuum tight alumina and were purchased from McDanel Porcelain Company of Beaver Falls, Pennsylvania. The tubes were closed at one end and attached to the vacuum system by means of a flange and a rubber O-ring. The balance housing and furnace tube details are shown in Figure 1.

One major difficulty was found in using ceramic furnace tubes for tungsten oxidation studies. Alumina was found to react with tungsten trioxide vapor as shown by discoloration of the tube and subsequent cracking. At 1600° the furnace tubes crack after exposure to tungsten trioxide vapors for 10 to 15 minutes. As a result only 1 or 2 experiments can be made on a given ceramic tube. At lower temperatures the tubes have a longer life but cracking occurs at all temperatures used in this work.

Kanthal-Super Furnace for 1600°C

With the development of Kanthal-Super, furnaces can be built to operate at 1600°C for long periods of time. Kanthal-Super is chiefly molybdenum disilicide with a binder and is produced according to powder metallurgical processes in the form of rods of circular cross section. When heated the rods can be formed into suitable hairpin-shaped heating elements.

The specific resistance of Kanthal-Super is low and increases rapidly with temperature. For elements of a 6 mm diameter a current of 125 to 130 amperes is required for an operating temperature of 1600°C. Since the material is brittle and of low impact strength below 1100°C, it is necessary to keep the furnace above 1000°C or at one-half of its operating voltage. The furnace is 10-1/2 inches square and 13 inches high. The hot space is 2 inches square and 6 inches long.

Temperature Measurement

Temperatures were measured using Pt/Pt +10% Rh thermocouples. The thermocouples were calibrated at seven points between 400° and 1200°C. Temperatures above 1200°C were determined by extrapolation of the calibration curve.

When the balance was used, it was impossible to measure the sample temperature directly. The temperature was measured by a thermocouple placed inside the ceramic tube near the sample. When the oxygen consumption method was used, the thermocouple was mounted directly onto the specimen. Comparison was made between the temperatures on the specimen and at a point in the furnace tube near the specimen. All temperatures were corrected to the temperature at the specimen. The thermocouple arrangement is shown in Figure 1.

Specimens and Analyses

Specimens were machined from pure tungsten rod. They weigh about 0.825 gm and have a surface area of 0.680 cm^2. These specimens have a dumbbell shape with hemispherical ends. Sharp edges were avoided. A loop of platinum wire around smaller diameter of the dumbbell-shaped specimens was used to support the specimens.

A spectrographic analysis of the tungsten showed the following in parts per million: Si, 1; Ti, <100; Mn, <4; Sb, <10; Fe, 8; Pb, <4; Mg, <1; Al, 1; Ni, 4; Be, <1; Sn, <4; Cu, 1; Ag, <1; Zn, <10; Co, <10; Cr, <4; Ca, 1; B, <4; Nb, <100; Mo, <100; V, <100; Cd, <4. An unreacted specimen is shown in Figure 2A.

Specimen Preparation and Pretreatment

The pure tungsten samples were machined from rods that had previously been centerless ground. After the samples were machined, they were polished through 4/0 polishing paper and washed in petroleum ether and pure ethyl alcohol. When only pressure device measurements were made, the samples were suspended from a glass hook in the top of the balance chamber.

Between successive experiments it was necessary to bake the ceramic tube for about twenty minutes at or slightly above the temperature of the next planned experiment. This was necessary to avoid reaction between the clean tungsten sample and oxygen

released from the tube during the heat-up of the specimen. Absorbed WO_3 vapor was also expelled from the tube walls during this tube pretreatment.

Performance of Furnace Tubes and Vacuum System

The performance of furnace tubes at temperatures up to 1175°C was discussed earlier by Gulbransen and Andrew (Reference 4). Two criteria were used: (1) the actual pressure achieved at a given temperature after pumping for a definite period of time, (2) the apparent leak rate of gases into the closed reaction system in units of $cm^3\ sec^{-1}$ STP.

Table 1 shows the performance of a typical alumina furnace tube for temperatures between room temperature and 1600°C. If the gas accumulating in the reaction system volume of 2.6 liters was considered to be 20 percent by volume of oxygen, an estimate can be made of the oxygen gas building up in the system. These calculations are shown in Table 1.

Method

Experiments were run using the Invar microbalance in combination with the pressure measuring device. For runs in which the weight changes went beyond the limits of the balance, the pressure apparatus alone was used.

After the specimen was brought to temperature, pure oxygen was admitted to the system from a precharged reservoir to the desired pressure. Weight changes were observed with a micrometer microscope as a function of time. Pressure changes in the reservoir were also noted as a function of time by means of a Wallace and Tiernan pressure gauge. A leak valve was used to maintain the pressure in the reaction system.

RESULTS

Classification of Oxidation Phenomena

The results of this and earlier studies on tungsten may be confusing unless the various phenomena associated with oxidation are systematized. Four basic types of oxidation phenomena occur: (1) Below 500°C oxidation results in the formation of an oxide film or scale which adheres to the metal. There is no evaporation of tungsten trioxide. (2) Between 600° and 900°C oxide scales form. Large cracks appear in the oxide. Edge type of reaction is prevalent. Evaporation of tungsten trioxide is negligible. (3) Between 950° and 1250°C oxide scale is formed with large cracks. Evaporation of tungsten trioxide also occurs which makes an analysis of the oxidation data difficult. (4) Above 1250°C oxidation occurs without formation of an appreciable oxide film or scale. Evaporation of tungsten trioxide occurs as rapidly as it is formed.

This study is concerned largely with Type 4 oxidation. It is essential to first consider the basic facts differentiating types 3 and 4.

Type 3 Oxidation

Figure 3 shows a typical oxidation curve for tungsten at 1150°C and 19 Torr oxygen pressure. Curve A shows the weight gain measurements using the balance while curve B shows the oxygen consumption measurements. Both measurements are plotted in mg/cm^2 versus time in minutes. Using curves A and B the actual oxygen in the oxide scale and the tungsten lost by evaporation can be estimated. Curve C shows the calculated oxygen in the oxide scale; 90 percent of the oxygen reacting remains as oxide scale on the metal.

To relate the weight gain in mgm/cm^2 to oxide thickness in Angstroms, a factor of 67,500 was used. This factor was calculated assuming a density of 7.16 for tungsten trioxide and a surface roughness ratio of unity. These calculations have three limitations: (1) the surface area changes, (2) cracking in the oxide may occur, and (3) lower oxides may form. Calculations on Figure 3 show a thickness of 6.75×10^6 Å or 0.675 mm.

Figure 2B shows a photograph of a specimen oxidized at 1150°C and 5 Torr oxygen pressure. Although rounded cylindrical specimens were used, large cracks developed in the oxide scale.

Curve B of Figure 3 can be used to calculate the weight of tungsten reacting and the surface recession rate. Surface recession is defined as the decrease in the dimension of the metal as reaction proceeds. The weight of tungsten reacting is calculated by multiplying the weight of oxygen used by the factor 3.83. This assumes the oxide is tungsten trioxide. The surface recession in angstroms is related to the oxygen reacted in mg/cm^2 by the factor 19,840.

Another interesting calculation is to compare the actual value of tungsten trioxide evaporating with the theoretical value for a vacuum. Vapor pressure studies of tungsten trioxide (Reference 5) were used to calculate the theoretical value. Table 2 shows a comparison of the actual weight loss to the theoretical value. The result is given as a percentage of the theoretical value. A percentage of 1.8 was calculated.

Type 4 Oxidation

Figure 4 shows both oxygen consumption and tungsten weight loss curves for the reaction at 1250°C and 38 Torr oxygen pressure. Figure 4 also includes the results of the calculated weight losses of tungsten based on the oxygen consumption curves. The agreement of the calculated values with the weight loss measurements supports the direct use of the oxygen consumption measurements to calculate surface recession rates. The type of calculations made for Figure 3 can be applied directly to Figure 4.

Figure 5 shows an oxygen consumption curve for the reaction at 1615°C and 19 Torr oxygen pressure. Figure 5 also includes a weight loss curve calculated from the oxygen consumption curve. Since the surface area of the cylindrical specimen is changing rapidly, calculations on the surface recession are more complicated but they can be made. These are not presented here.

Table 2 shows a comparison of the theoretical weight loss values with the experimental values found for the 1250° and 1615°C experiments. At 1 15°C the percentage of theoretical was 0.0026. This analysis suggests that vaporization of tungsten trioxide was not the rate controlling mechanism for this temperature range.

The agreement of the experimental weight loss curves with values calculated from oxygen consumption measurements establishes the following basic facts about the oxidation mechanism above 1250°C: (1) tungsten trioxide is formed directly in the reaction, and (2) tungsten trioxide evaporates as fast as it is formed.

The transition between Type 3 and Type 4 oxidation was not sharp and was a function of temperature and pressure. The transition conditions must be established before weight loss curves could be calculated from oxygen consumption data.

Effect of Temperature

Figures 6, 7, 8, and 9 show the effect of temperature on the oxidation of tungsten for four pressures, 5, 19, 38, and 100 Torr oxygen pressure. The measurements cover the temperature range of 1150° to 1615°C. Due to the rapid reaction rates observed the longest reaction time was 70 minutes. The curves show the rate of oxidation in terms of weight loss of tungsten. Except for the very fast reactions at the highest temperature, the data were taken with both the Invar beam balance and the oxygen consumption apparatus. For the fast reactions, only oxygen consumption was measured. The tungsten weight loss curves were calculated. All data were calculated on the basis of the original areas of the specimen. The decrease in reaction rate observed with time in curve B of Figure 9 at 1615°C was directly related to the change in surface area of the specimen.

Figure 2A, B, C, and D show photographs of the unreacted and oxidized tungsten specimens. The photographs show the Type 4 oxidation phenomena.

Figure 6 shows the effect of temperature for a pressure of 5 Torr. Linear weight loss curves were found at all temperatures between 1150° and 1615°C. The maximum amount of tungsten lost in these experiments was 19 percent of the original sample weight.

Figures 7, 8, and 9 show the effect of temperature at 19, 38, and 100 Torr oxygen pressures, respectively. Curves A, B, and C of Figure 7 were taken with the balance while curves D and E were calculated from the oxygen consumption measurements. A maximum reaction of 27.6 percent was found for the 1615°C experiment. Curve A shows a different time course for the reaction than curves B, C, D, and E. This behavior was noted for all of the experiments at 1250°C at pressures above 5 Torr. A basic change in the reaction mechanism occurs above 1250°C for oxygen pressures greater than 5 Torr.

In Figure 8 curves A and B were taken using the balance while curves C and D were calculated from oxygen consumption data. Curves C and D show an inversion in the rate of reaction with the 1465°C run being faster than the 1615°C runs. This is ascribed to the small temperature coefficient for the reaction and to the difficulty of obtaining reproducible results. Due to the rapid rate of reaction, only two measurements were made at 100 Torr oxygen pressure as shown in Figure 9. Forty-four percent of the sample reacted with oxygen at 1365°C in 3 minutes.

Table 3 shows a summary of the initial rates of tungsten weight loss taken from large scale plots of the data. Figure 10 shows an Arrhenius plot of the data. The rate data are scattered for the high temperature runs due to the high heat rates associated with the reaction. The inversion seen in Figure 8 does not change the implications of Figure 10 which shows the rate of reaction increases with temperature at all pressures.

The data of Figure 10 were used to estimate a heat of activation of 14,300 cal per mole. Curves B and D were drawn with the same slopes as A and C. It is noted that the data at 1250°C above 5 Torr oxygen pressure are not consistent with the higher temperature data. This suggests a change in the mechanism of oxidation near 1250°C.

An empirical equation similar to that used by Perkins and Crooks (Reference 3) was used to interpret the results:

$$\frac{dW}{dt} = Kp^n e^{-\Delta H/RT}$$

Here $\frac{dw}{dt}$ is the initial rate of tungsten weight loss in units of gm cm^{-2} sec^{-1}; ΔH is the empirical heat of activation in cal per mole; P is the pressure in Torr; T is the absolute temperature; R is the gas constant, and K and n are constants. To determine n it is necessary to consider the effect of pressure on the oxidation reaction.

Effect of Pressure

The effect of pressure on the rate of oxidation is shown in Figures 11 through 15 for temperatures of 1150° to 1615°C. All weight loss values were calculated on the basis of the initial surface area of the sample. Figure 11 shows the results at 1150°C for pressures of 2 to 49 Torr. Pressure has a major influence on the rate of oxidation. For temperatures of 1150°C and higher, pressure is the major factor in determining the kinetics of oxidation. Thus, in Figure 11 a weight gain was observed for the higher oxygen pressures and a weight loss for the lower pressures. Curves D and E are of Type 3 oxidation since tungsten trioxide is evaporating from the oxidized sample. Figure 12 shows the results at 1250°C. All experiments show a weight loss, with the rate of weight loss increasing with oxygen pressure. The oxygen atmosphere was not inhibiting the reaction although the evaporation of WO_3 was probably slowed down. This effect is discussed later.

Figures 13 and 14 show the results at 1365° and 1465°C. Nearly linear weight loss curves were observed. Again, the strong effect of pressure was found. Figure 15 shows the results at 1615°C. The decrease in rate of weight loss with time can be related directly to the surface area of the

specimen. The trend of the curves in Figure 15 shows the 2 and 5 Torr runs out of line with the general trend of the results. This is due to a lack of reproducibility in temperature of the sample or in the flow of gases in the furnace tube. No change in mechanism should be deduced from these two curves.

Figure 16 shows the effect of pressure on the initial reaction rate $\frac{dw}{dt}$ versus log pressure plot. Four temperatures were considered in Figure 16: 1365°, 1465°, 1545°, and 1615°C. The following equation was derived from the data of Figures 10 and 16:

$$\frac{dW}{dt} = 1.9 \times 10^{-3} P^{1.1} e^{-\frac{14,300}{RT}}$$

This equation fits the results for the temperature range of 1365° to 1615°C and for pressures of 5 to 38 Torr to about 10 percent accuracy.

DISCUSSION

Summary of Kinetic Work

In our earlier studies (References 1, 5, and 7) the primary chemical reaction of pure tungsten was studied using thin cylindrical specimens. Above 1250°C and at pressures up to 38 Torr of oxygen the weight change curves showed no evidence of an initial pickup of oxygen to form an oxide film. This does not eliminate the possibility that an adsorbed oxygen layer is formed since the weight change associated with an adsorbed oxygen monolayer would not be measured using our present methods. The observed weight loss curves were nearly linear with time. For a short period of reaction the data could be fitted to the equation $W = Kt$, where W is the weight loss in mgm cm^{-2}, K is a constant, and t is the time. For longer periods of time, surface area changes occurred which decreased the rate of weight loss.

The initial rate constant K could be fitted to an exponential function of temperature, i.e., $K = Ze^{-\Delta H/RT}$. A heat of activation of 14,300 cal per mole was found, while the frequency factor Z has the units of grams of tungsten reacting per square centimeter of area per second.

The effect of pressure on the oxidation of tungsten was studied between 1150° and 1615°C. The results could be fitted to the equation $K = ap^{1.1}$ where K is the rate constant, p is the pressure in Torr, and a is a constant. The value $p^{1.1}$ suggests that the reaction was nearly a linear function of pressure.

Combining the temperature and pressure rate laws, we have the final empirical rate equation

$$\frac{dW}{dt} = 1.9 \times 10^{-3} p^{1.1} e^{-\frac{14,300}{RT}}$$

Here $\frac{dW}{dt}$ is the initial rate of reaction in grams per sec per cm^2. In terms of atoms of tungsten reacting we have the equation

$$\frac{dW}{dt} = 6.2 \times 10^{18} p^{1.1} e^{-\frac{14,300}{RT}}$$

This equation predicts a rate of reaction at 1615°C and 76 Torr of 1.6×10^{19} atoms cm^{-2} sec^{-1}.

Any proposed mechanism must account for the following experimental facts: (1) a nearly linear dependence of the rate of reaction on pressure, (2) a linear time dependence during the initial stages of reaction, (3) a very low temperature dependence above 1250°C, and (4) the very high absolute values for the rate of reaction.

A surface reaction may be separated into at least five distinct processes, the slowest of which determines the rate of reaction: (1) Transport of the reacting gas to the surface, (2) Chemisorption of the gas, (3) Chemical reaction at the surface, (4) Desorption of the reaction products, and (5) Transport of the reaction products into the bulk phase.

In general, processes 1 and 5 are diffusion mechanisms and if these are rate-controlling, the temperature dependence of the reaction rate may be expected to vary with $T^{1/2}$ where T is the absolute temperature. Further, surface reactions usually have activation energies of > 30 Kcal per mole while gas diffusion processes have much lower values (Reference 6).

The low temperature dependence of the rate of oxidation, the linear time dependence, and the pressure dependence suggests that for temperatures above 1250°C the oxidation of tungsten is limited by transport of oxygen gas through the boundary layer of reaction products to the reacting interface.

Temperature Rise of Sample

Because of the rapid oxidation reaction the specimen temperature will increase above the ambient temperature. This can be estimated as follows. Consider a tungsten sample weighing 0.81 gm and having a surface area of 0.68 cm^2 reacting with oxygen at 49 Torr pressure at 1465°C. The experiment shows a weight loss of tungsten of 2.87×10^{-3} gm sec^{-1}. This is equal to 4.22×10^{-3} gm of W cm^{-2} sec^{-1} or 2.30×10^{-5} moles of W cm^{-2} sec^{-1}.

The heat of formation of WO_3, $\Delta H_{f_{WO_3}}$, at 1700°K is -194.75 Kcal per mole of WO_3 (Reference 7). From the same report we note the heat of sublimation, $\Delta H_{s_{WO_3}}$ at 1500°K is 121 Kcal per mole of W_3O_9 or 40.3 Kcal per mole of WO_3. If we make a heat balance of the formation and evaporation processes we have $\Delta H_{g_{WO_3}} + \Delta H_{f_{WO_3}} =$ -154.7 Kcal per mole.

We can now calculate the net heat released at the sample as 2.4 cal per sec. Using the value of heat capacity given by Kubaschewski and Evans (Reference 8) for tungsten as 3.81×10^{-2} cal/°C/gm we calculate a temperature rise of 63°C/sec without radiation losses.

To evaluate the temperature rise we need to know the heat losses. At 1400°C the major heat loss is due to radiation. Estimates from data given by McAdam (Reference 9) shows that natural convection plays a very minor role at 1400°C.

Radiation losses can be evaluated using Planck's equation $h_r = C_r \epsilon (T^4 - Ta^4)$. Here h_r is the heat rate in cal cm^{-2} sec^{-1}, ϵ is the emissivity, $C_r = 1.354 \times 10^{-12}$ cal cm^{-2} deg^{-4} sec^{-1}, T is the sample temperature, and T_a is the furnace tube wall temperature.

Since the emissivity of the sample and walls differ we use the following relation to calculate an average emissivity ϵ.

$$\frac{1}{\epsilon} = \frac{1}{\epsilon_1} + \frac{A_1}{A_2}\left[\frac{1}{\epsilon_2} - 1\right]$$

Here $\frac{A_1}{A_2}$ is the ratio of diameters of specimen and tube, ϵ_2 is the emissivity of the ceramic wall, and ϵ_1 is the emissivity of the sample. If ϵ_2 is nearly 1 and if $\frac{A_1}{A_2}$ is small, the second term becomes small compared to the term $\frac{1}{\epsilon_1}$. For this case $\epsilon \approx \epsilon_1$.

We will calculate the temperature rise for two values of the emissivity, i.e., $\epsilon_1 =$ 1.0 and 0.50. The first case is when the tungsten sample has a thin film of oxide on

the surface, and the second case refers to a brighter surface. Using ϵ_1 of 1.00 and T_a = 1738°K we calculate aΔT of 113°C while using a value of ϵ_1 of 0.50 we calculate aΔT for the sample of 207°C.

Experiments with the thermocouple mounted on the specimen showed temperature increases of 15' to 20°C, much less than those calculated above. The reason for this discrepancy was not clear. Experimentally it was difficult to mount the thermocouple so that the specimen temperature was actually measured. On the other hand, no burnup was observed, which suggests that the temperature coefficient of the reaction was small or that the calculated temperature rises were not taking place. The effect of temperature on the rate of oxidation between 1400° and 1600°C was small which limits the reaction and prevents burnup.

Decrease in Surface Recession Rates Above 1800°C

Perkins and Crooks (Reference 3) have reported that the rate of weight loss of tungsten in air at 1 to 15 Torr oxygen pressure decreases above 1800°C. These experiments utilize observations on the diameter of rods undergoing reaction. Perkins and Crooks relate this inversion to a thermal dissociation of tungsten trioxide. Two facts suggest that these results must be accepted only with reservations. First, thermochemical calculations based on the data of King et al. (Reference 10) show that all the tungsten oxides are stable. Second, Langmuir studied the oxidation reaction for pressures in the micron range where the effect of oxide dissociation would be more readily observed. Using a pressure change method, Langmuir's results show no indication of an inversion in the rate of reaction at 1800°C. It would appear that the direct measurement method should be investigated and the results compared to oxygen consumption or weight loss measurements. One explanation for the decrease in rate of reaction observed by Perkins and Crooks (Reference 3) is that the boundary layer resistance to diffusion changes with temperature. It is possible that the molecular species W_3O_9, WO_3 change with increasing temperature to give more WO_3 which would provide a more effective barrier for oxygen to diffuse to the reacting interface.

SUMMARY AND CONCLUSIONS

The reactions of tungsten with oxygen as a function of temperature and pressure vary greatly. Four types of behavior were noted: (1) formation of a protective oxide film, (2) formation of a nonprotective oxide scale, (3) simultaneous formation of an oxide scale and vaporization of tungsten trioxide, and (4) formation of tungsten trioxide gas without formation of an appreciable oxide film or scale.

Types 3 and 4 oxidation curves were studied in detail by both the weight change method and oxygen consumption measurements. Both measurements are required for type 3 oxidation curves to determine the course of the reaction. Above 1250°C, all of the oxidation rate curves followed Type 4 behavior. Experiments on Type 4 oxidation curves showed that surface recession values could be obtained directly from weight change measurements or by calculation from oxygen consumption measurements.

The effect of temperature on the oxidation of tungsten was studied for four pressures over the temperature range of 1250° to 1615°C. The initial rate of weight loss values followed an exponential function of temperature. A heat of activation of 14,300 cal per mole was estimated.

A study of the effect of pressure also was made. The following rate law was found to fit the data, $K = ap^{1.1}$.

The following empirical rate law equation was determined for the data:

$$\frac{dW}{dt} = 1.9 \times 10^{-3} \, p^{1.1} \, e^{-\frac{14\,300}{RT}}$$

An analysis was made of the kinetic data and the several possible rate limiting processes. It was proposed that for temperatures above 1250°C and for oxygen pressures above 5 Torr that the rate-limiting process is the transport of oxygen through a boundary layer of gaseous reaction products.

An analysis made of the heat effects associated with the high rates of oxidation. For the oxidation at 1465°C and 49 Torr oxygen pressure the experimental value for the tungsten weight loss was 4.22×10^{-3} gm cm^{-3} sec^{-1}. The heat rate for this rate of reaction was 2.4 cal/sec. Assuming the heat was removed by radiation, a temperature rise of 113°C must result if the tungsten surface was assumed to have an emissivity of one. The high heat rates associated with the rapid oxidation reaction may account for the scattering in the experimental results.

ACKNOWLEDGMENT

This research was supported in part by the U. S. Air Force under Contract No. AF33(616)-7888, Aeronautical Systems Division, Wright-Patterson Air Force Base, Ohio.

LIST OF REFERENCES

1. E. A. Gulbransen and K. F. Andrew, "Kinetics of the Oxidation of Pure Tungsten from 500° to 1300°C," J. Electrochem. Soc., Vol. 107, No. 7, July 1960.

2. I. Langmuir, "Chemical Reactions at Very Low Pressures, I. The Clean-up of Oxygen in a Tungsten Lamp," J. Am. Chem. Soc., 35, 105. (1913), and "Chemical Reactions at Low Pressures," ibid. 37, 1139. (1915).

3. R. A. Perkins and D. D. Crooks, "Low-Pressure, High Temperature Oxidation of Tungsten," J. of Metals, 13, 490. (1961).

4. E. A. Gulbransen and K. F. Andrew, "Mullite and Zircon Furnace Tubes for High Temperature and High Vacuum Systems; A New Method for Measuring Pressure," Ind. and Eng. Chem. 4, 2762-7. (1949).

5. E. A. Gulbransen, K. F. Andrew, P. E. Blackburn, T. P. Copan, and A. Merlin, Oxidation of Tungsten and Tungsten Based Alloys, WADC TR 59-575, Part I, Wright Air Development Center, Wright-Patterson Air Force Base, Ohio, February 1960.

6. S. Glasstone, K. J. Laidler, and H. Erying, Theory of Rate Processes, The McGraw-Hill Book Co., Inc., New York. (1941).

7. P. E. Blackburn, K. F. Andrew, E. A. Gulbransen, and F. A. Brassart, Oxidation of Tungsten and Tungsten Based Alloys, WADC TR 59-575, Part II, Wright Air Development Center, Wright-Patterson Air Force Base, Ohio, June 1961.

8. O. Kubaschewski and E. Evans, Metallurgical Thermochemistry, Acad. Press. Inc., New York, N. Y. (1951).

9. W. H. McAdams, Head Transmission, The McGraw-Hill Book Co., Inc., New York. (1954).

10. E. G. King, W. W. Weller, and A. U. Christensen, "Thermodynamics of Some Oxides of Molybdenum and Tungsten," Bureau of Mines Report of Investigations 5664, U. S. Govt Printing Office, Washington, D.C. (1960).

TABLE 1

PERFORMANCE OF ALUMINA FURNACE TUBE AS FUNCTION OF TEMPERATURE

Temp. °C	Initial Press. (Torr)	Apparent Leak Rate $cm^3\ sec^{-1}$ STP	Oxygen Equivalent at 20% of gas gm sec^{-1}
R. T.	1×10^{-6}	1.487×10^{-7}	0.385×10^{-10}
1400	1×10^{-5}	7.18×10^{-7}	1.86×10^{-10}
1500	1×10^{-5}	14.87×10^{-7}	3.85×10^{-10}
1600	8×10^{-5}	9.84×10^{-6}	2.55×10^{-9}

TABLE 2

COMPARISON OF ACTUAL TUNGSTIC OXIDE LOST WITH THEORETICAL VALUE IN VACUUM

Experimental Conditions			Weight Loss of WO_3 in Time t		Percentage of Theoretical
Temp. °C	Pressure Torr	Time t Seconds	Exptl. gm/cm^2	Theor. gm/cm^2	
1150	19	3900	0.044	2.4	1.8
1250	38	720	0.150	6.5	2.1
1615	19	480	0.340	12900	0.00[illegible]

TABLE 3

SUMMARY OF OXIDATION KINETICS

Temp.	$\frac{1}{T} \times 10^4$	Rate ($gm/cm^2/sec \times 10^4$) of Weight Change at Pressure (Torr)							
°C	1/°K	2	5	9.5	15	19	38	49	100
1150	7.027	-0.17	-0.19	---	---	+0.21	+0.39	0.37	---
1250	6.566	-0.54	-0.89	-1.08	---	-1.33	-2.1	-1.1	-3.4
1300	6.357	---	---	-2.2	---	-2.8	---	---	---
1365	6.105	-0.53	-1.3	-2.6	---	-6.1	-10.7	-15.0	-42.5
1400	5.978	---	---	-3.6	---	-5.0	---	---	---
1465	5.753	-0.70	-1.6	-2.7	-3.8	-7.7	-19.0	-27.0	---
1520	5.577	---	---	---	---	---	---	---	---
1545	5.500	---	-2.0	---	---	-9.0	---	---	---
1615	5.296	-4.2	-2.6	-10.0	---	-10.8	-18.9	---	---

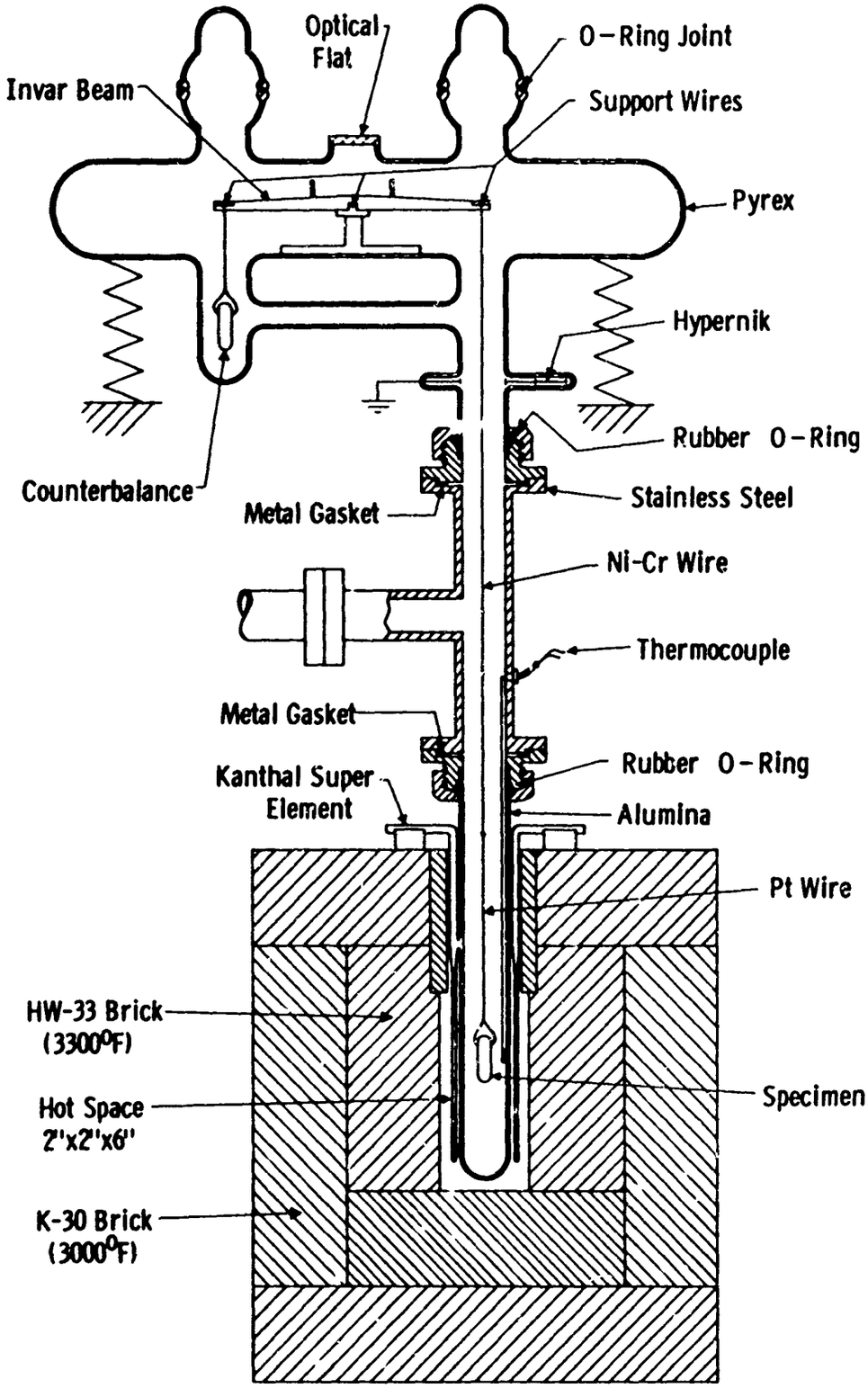

Figure 1. Reaction System Assembly

10X

A. Unreacted W

10X

B. W oxidized at 1150°C
5Torr - 2 hr

10X

C. W oxidized at 1465°C
5Torr - 15 min

10X

D. W oxidized at 1615°C
5Torr - 15 min

Figure 2. Photographs of Tungsten Specimens

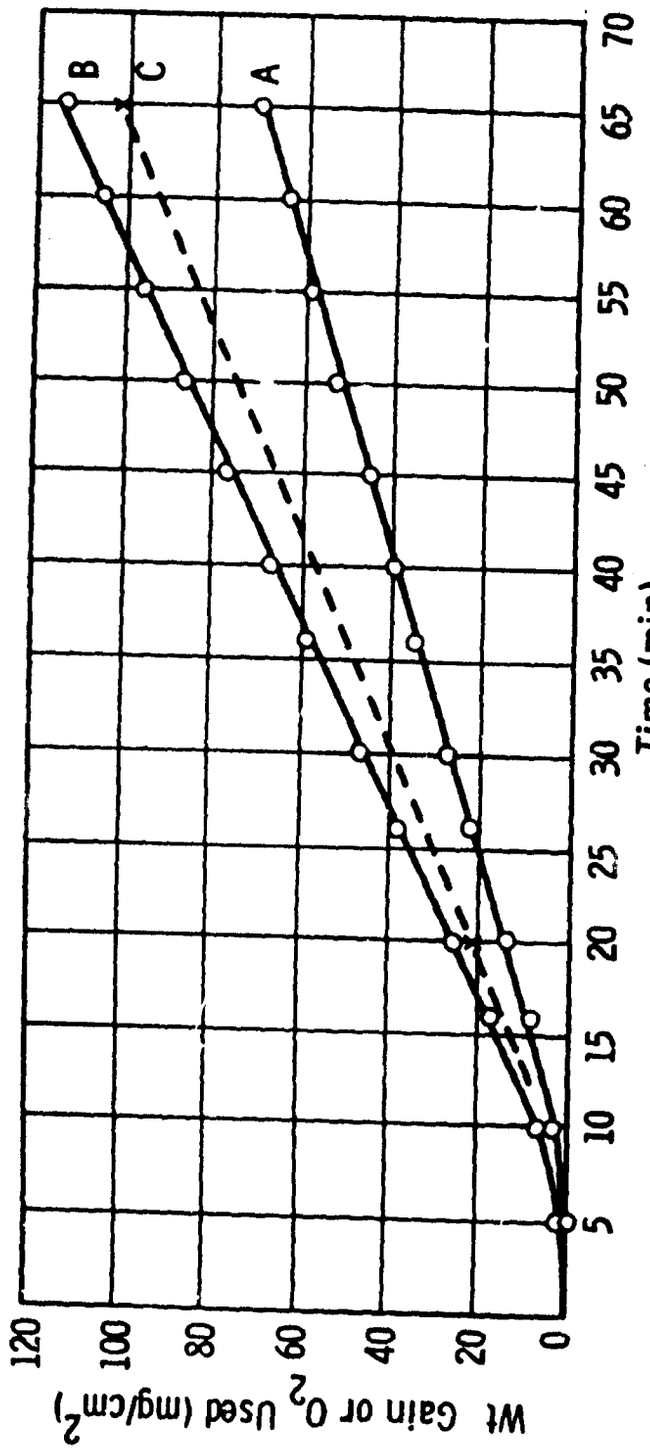

Figure 3. Oxidation of Tungsten, 1150°C, 19 Torr

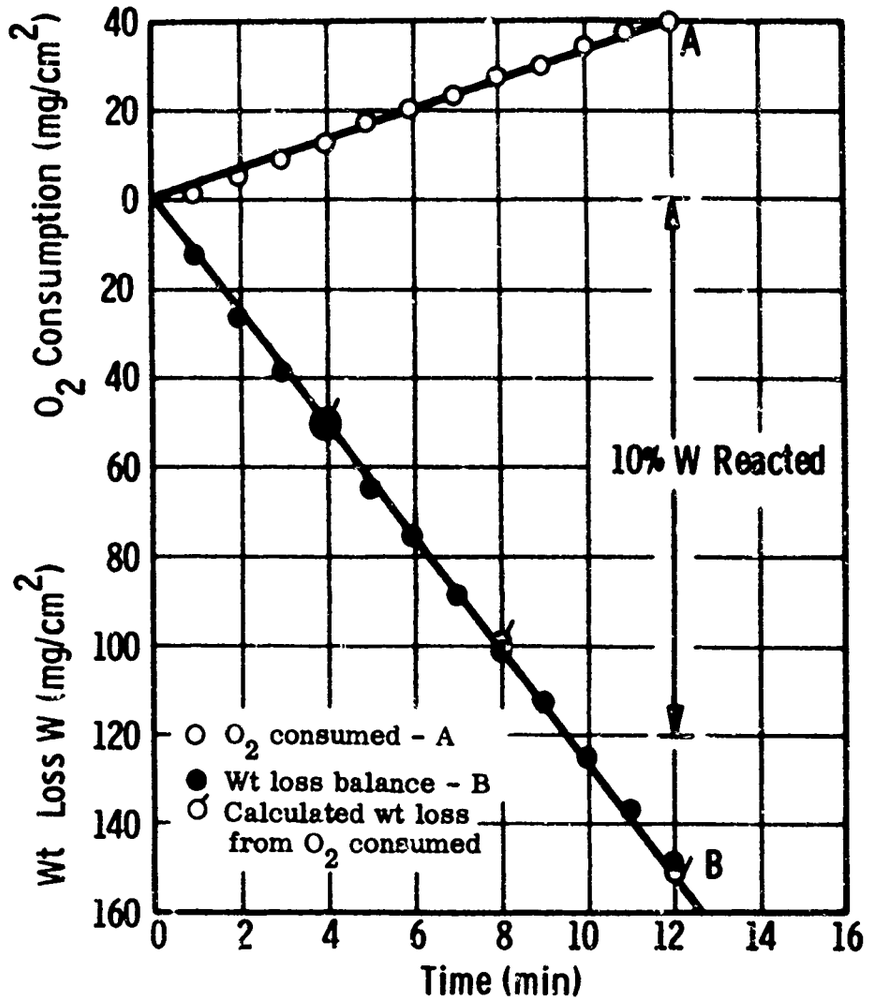

Figure 4. Oxidation of Tungsten, 1250°C, 38 Torr O_2

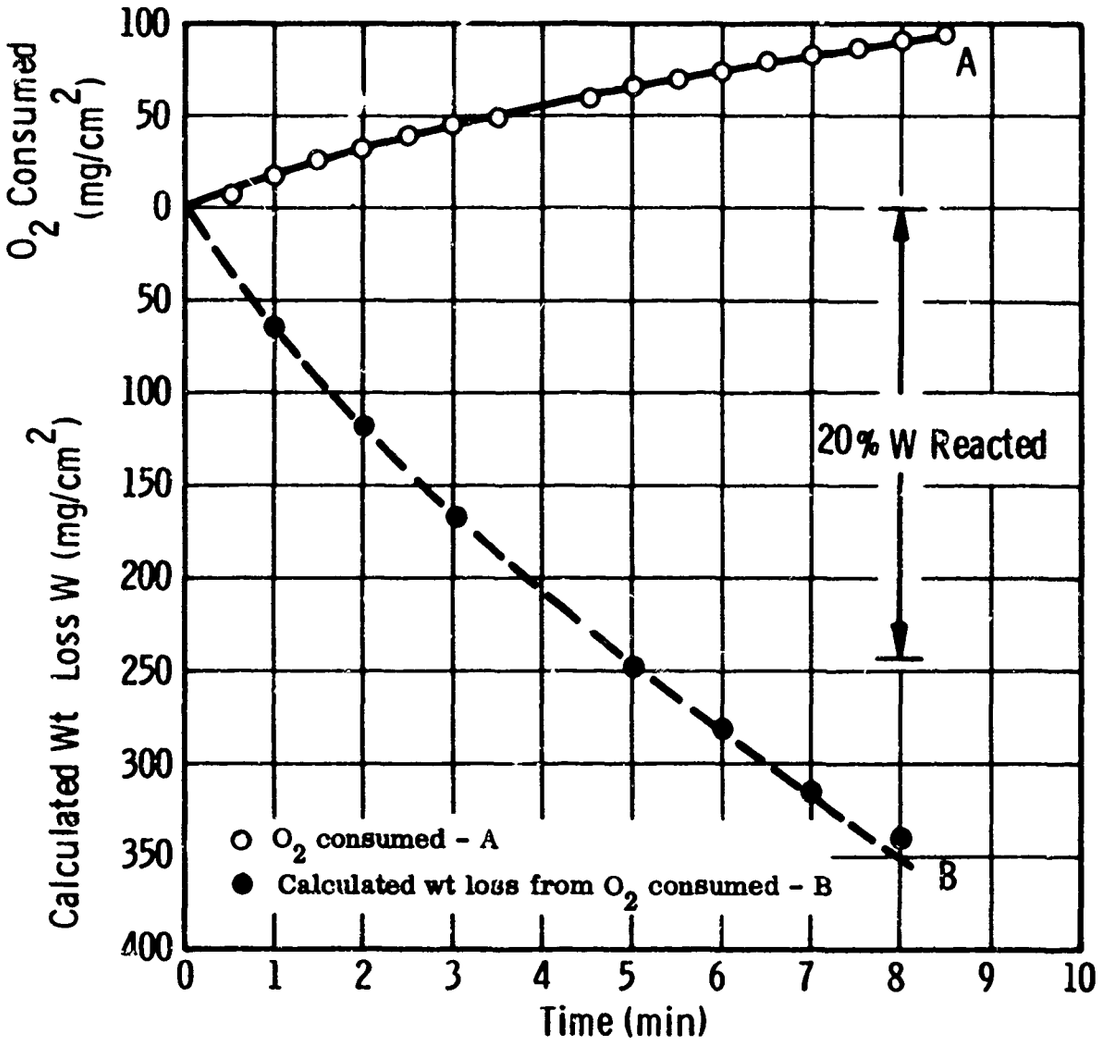

Figure 5. Oxidation of Tungsten, 1615°C, 19 Torr

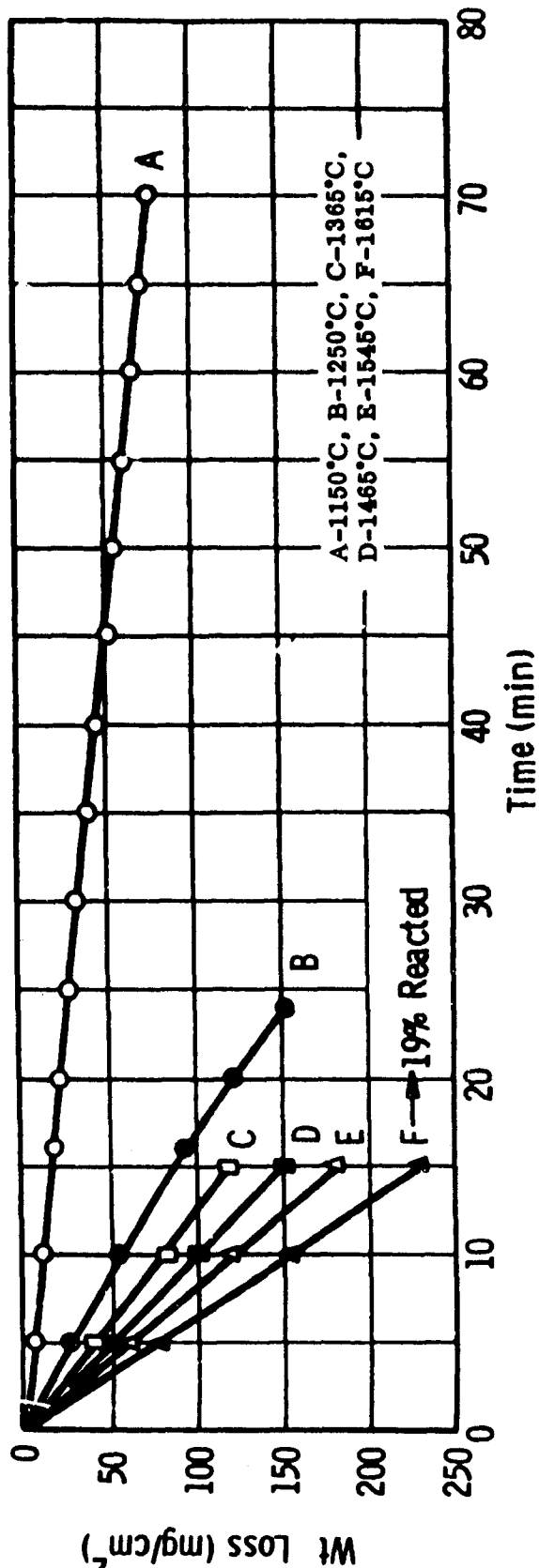

Figure 6. Effect of Temperature on Oxidation of Tungsten, 1150° to 1615°C, 5 Torr O_2

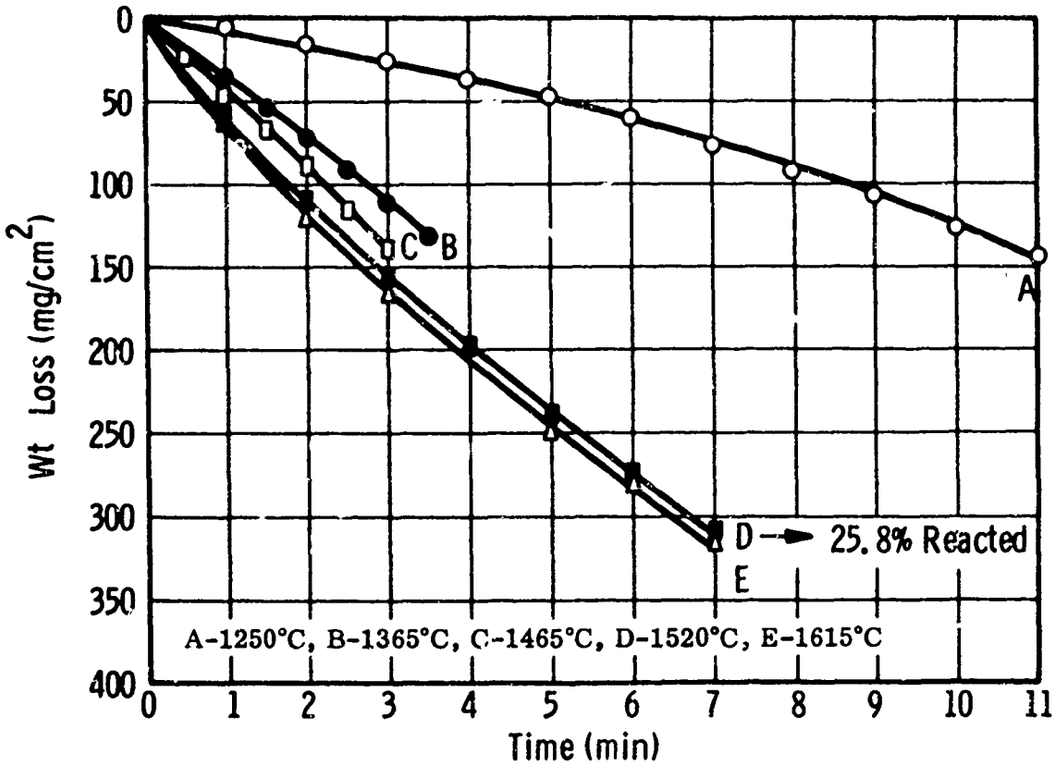

Figure 7. Effect of Temperature on Oxidation of Tungsten, 1250° to 1615°C, 19 Torr 0_2

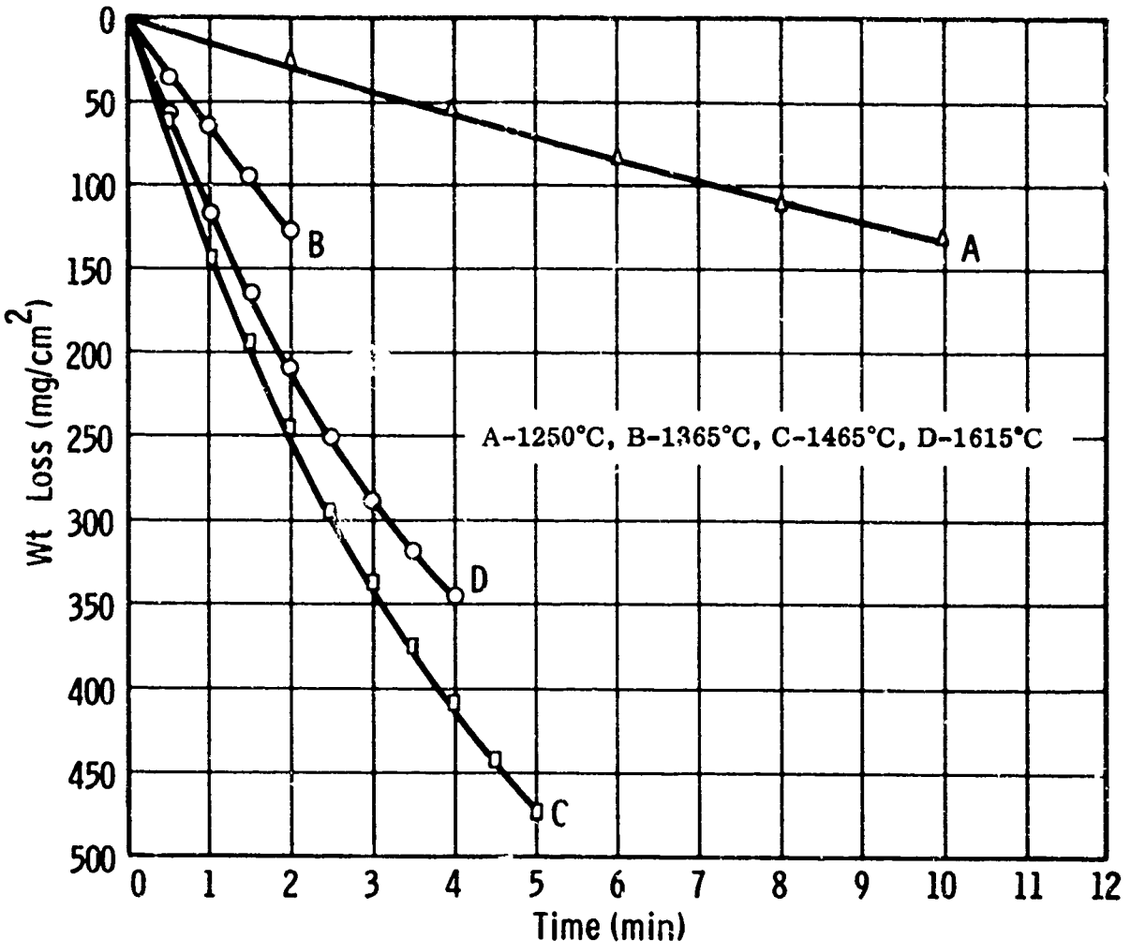

Figure 8. Effect of Temperature on Oxidation of Tungsten, 1250° to 1615°C, 38 Torr 0_2

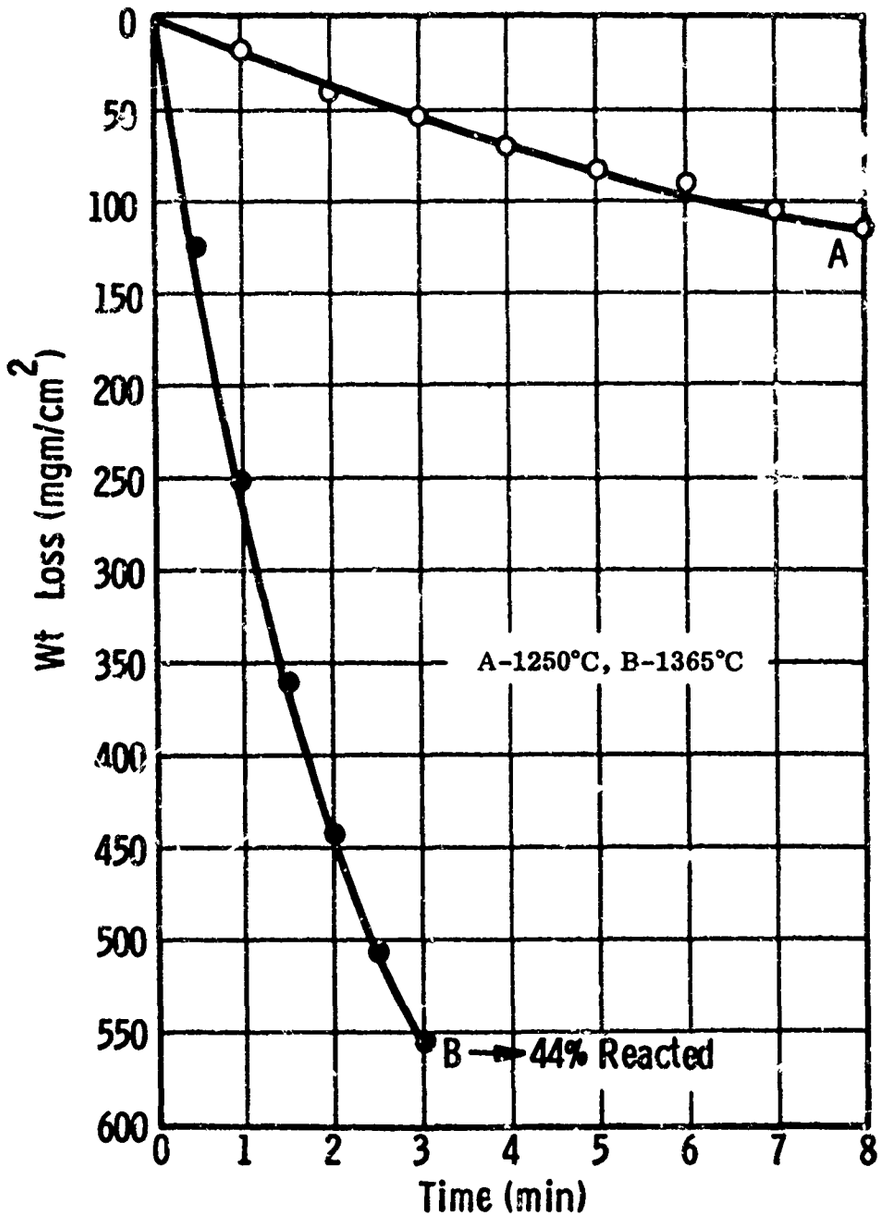

Figure 9. Effect of Temperature on Oxidation of Tungsten, 1250° to 1365°C, 100 Torr O_2

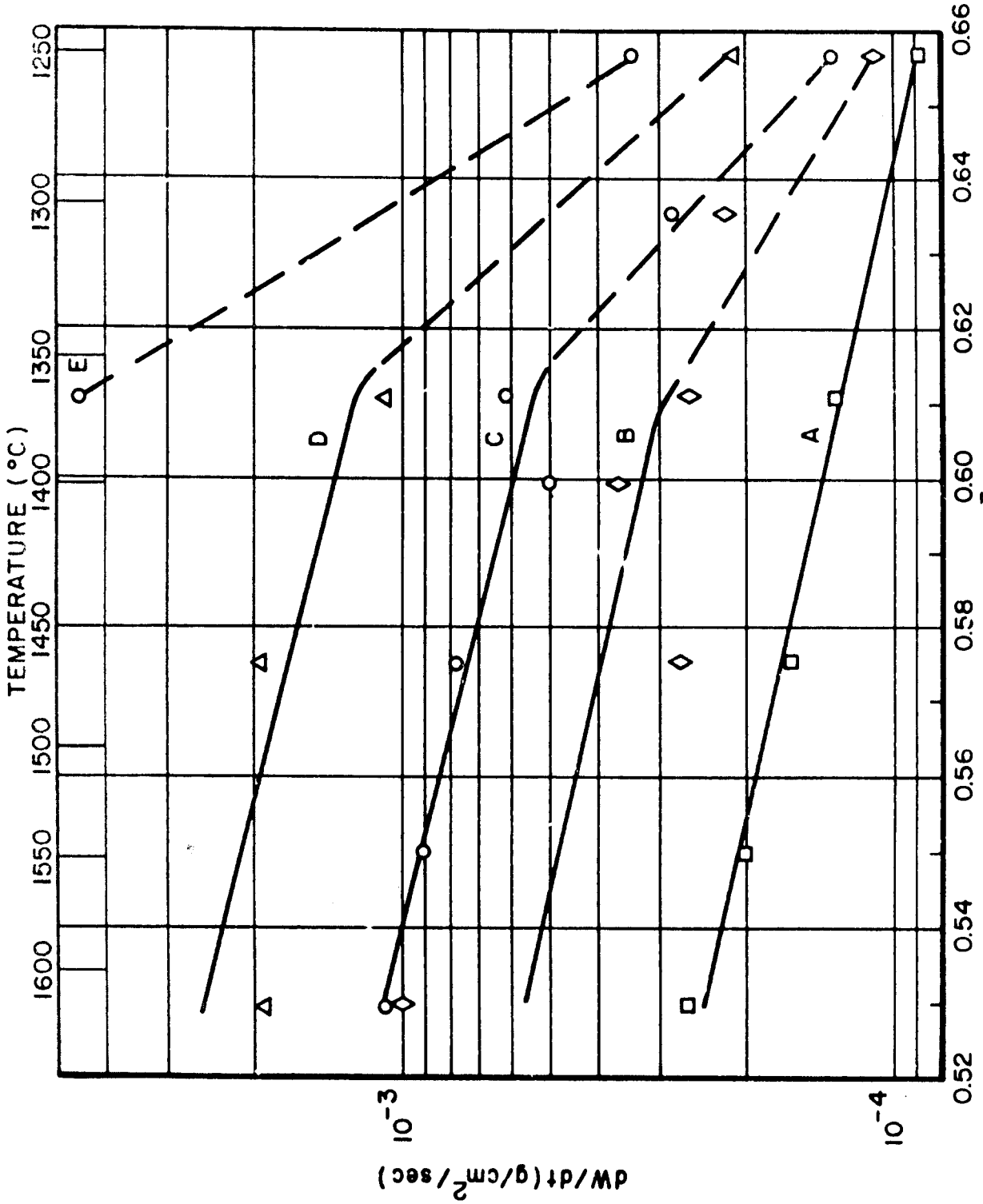

Figure 10. Log dW/dt vs 1/T, 1250° to 1615°C, 5 to 100 Torr of O_2 (A-5 Torr O_2, B-9.5 Torr O_2, C-19 Torr O_2, D-38 Torr O_2, E-100 Torr O_2 ΔH all curves, 14,300 cals/mole)

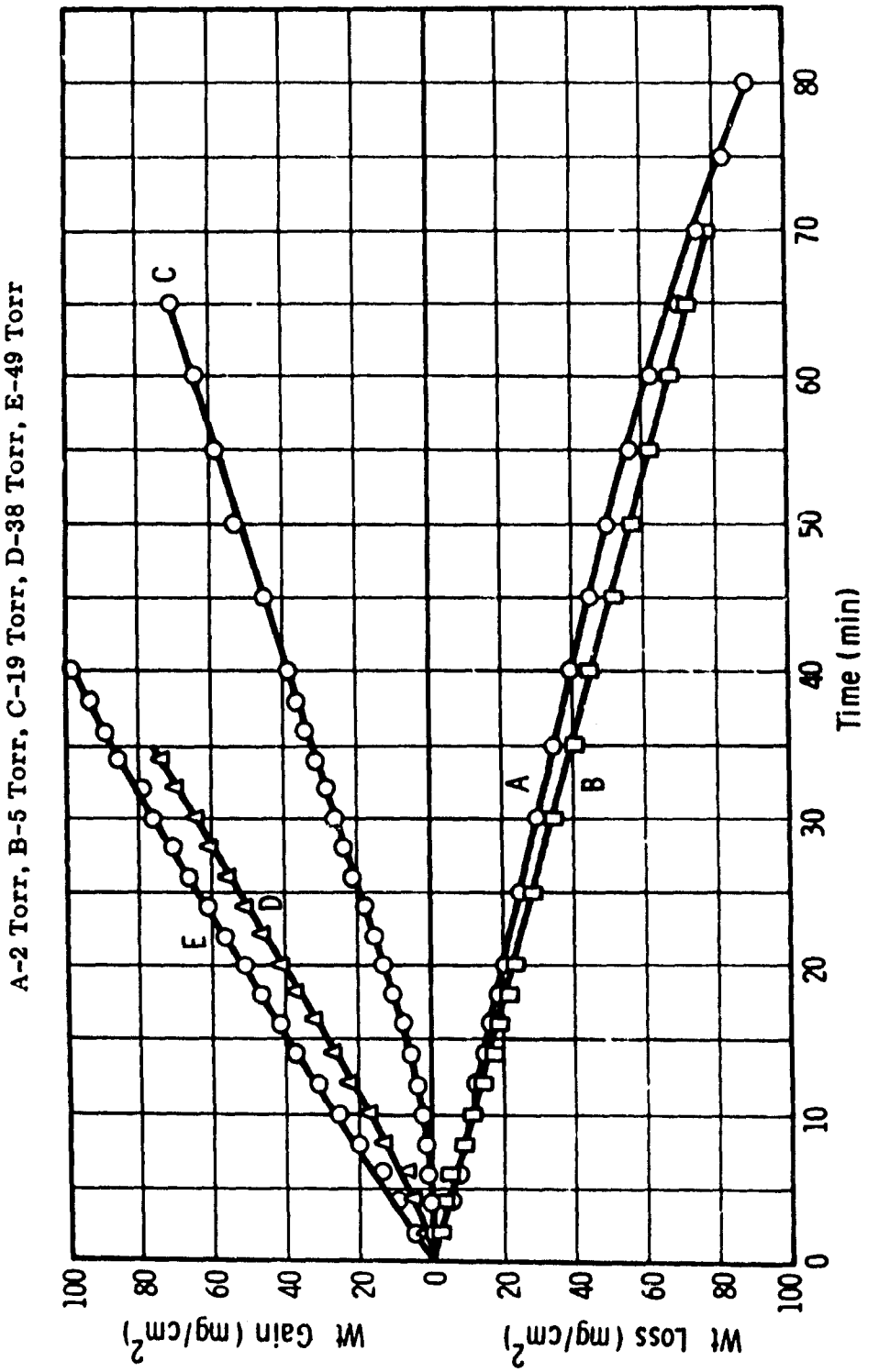

Figure 11. Effect of Pressure on Oxidation of Tungsten, 1150°C, 2 to 49 Torr O_2

A-2 Torr, B-5 Torr, C-9.5 Torr, D-19 Torr, E-38 Torr, F-49 Torr, G-100 Torr

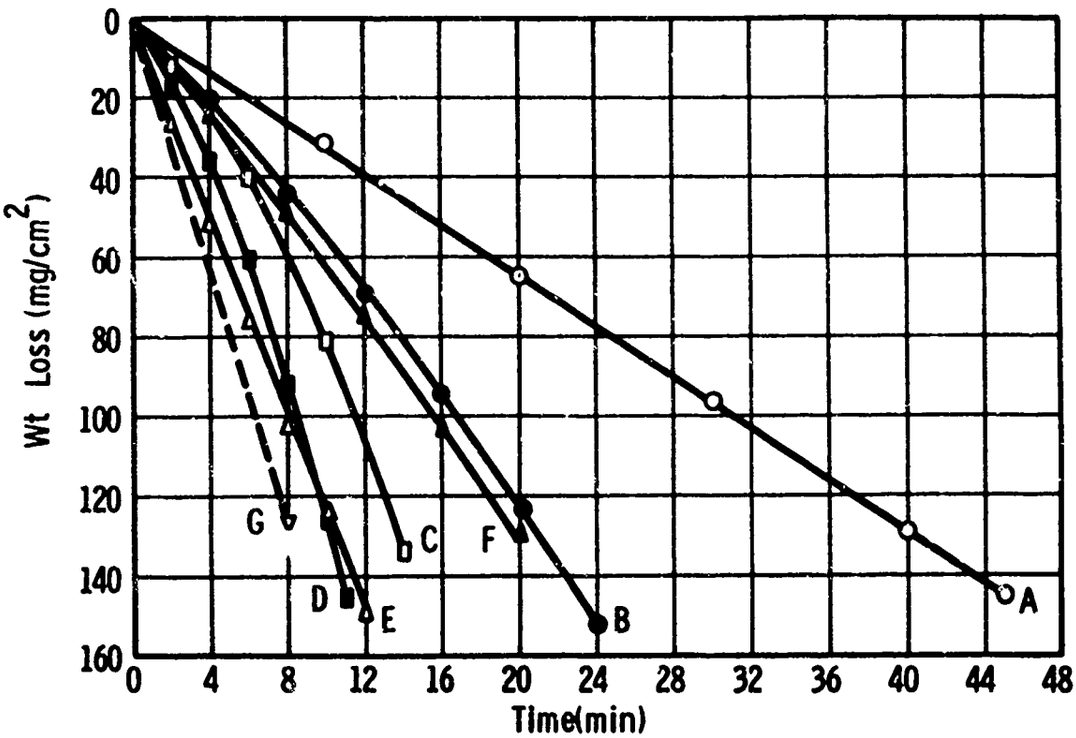

Figure 12. Effect of Pressure on Oxidation of Tungsten, 1250°C, 2 to 100 Torr 0_2

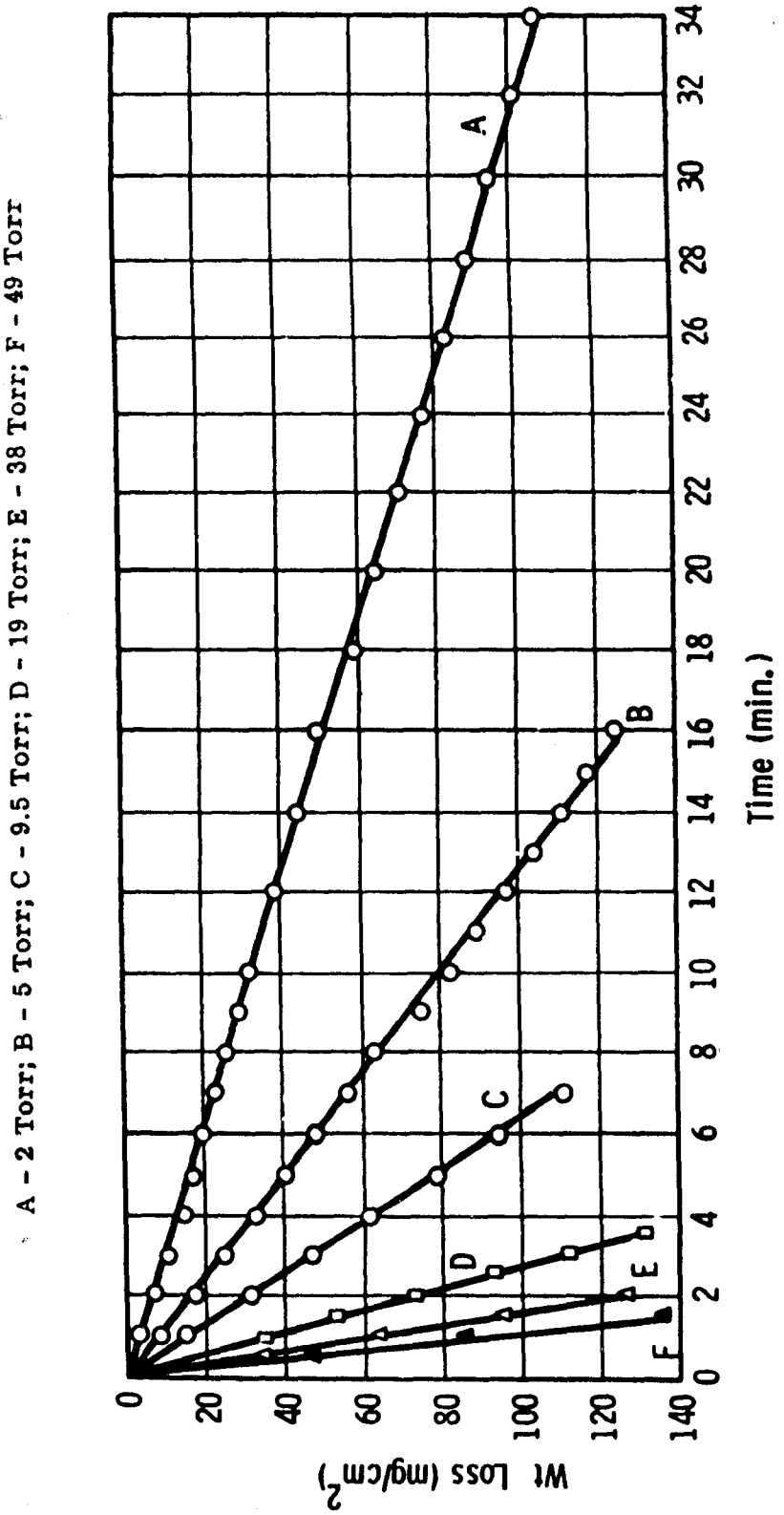

Figure 13. Effect of Pressure on Oxidation of Tungsten, 1365°C, 2 to 49 Torr O_2

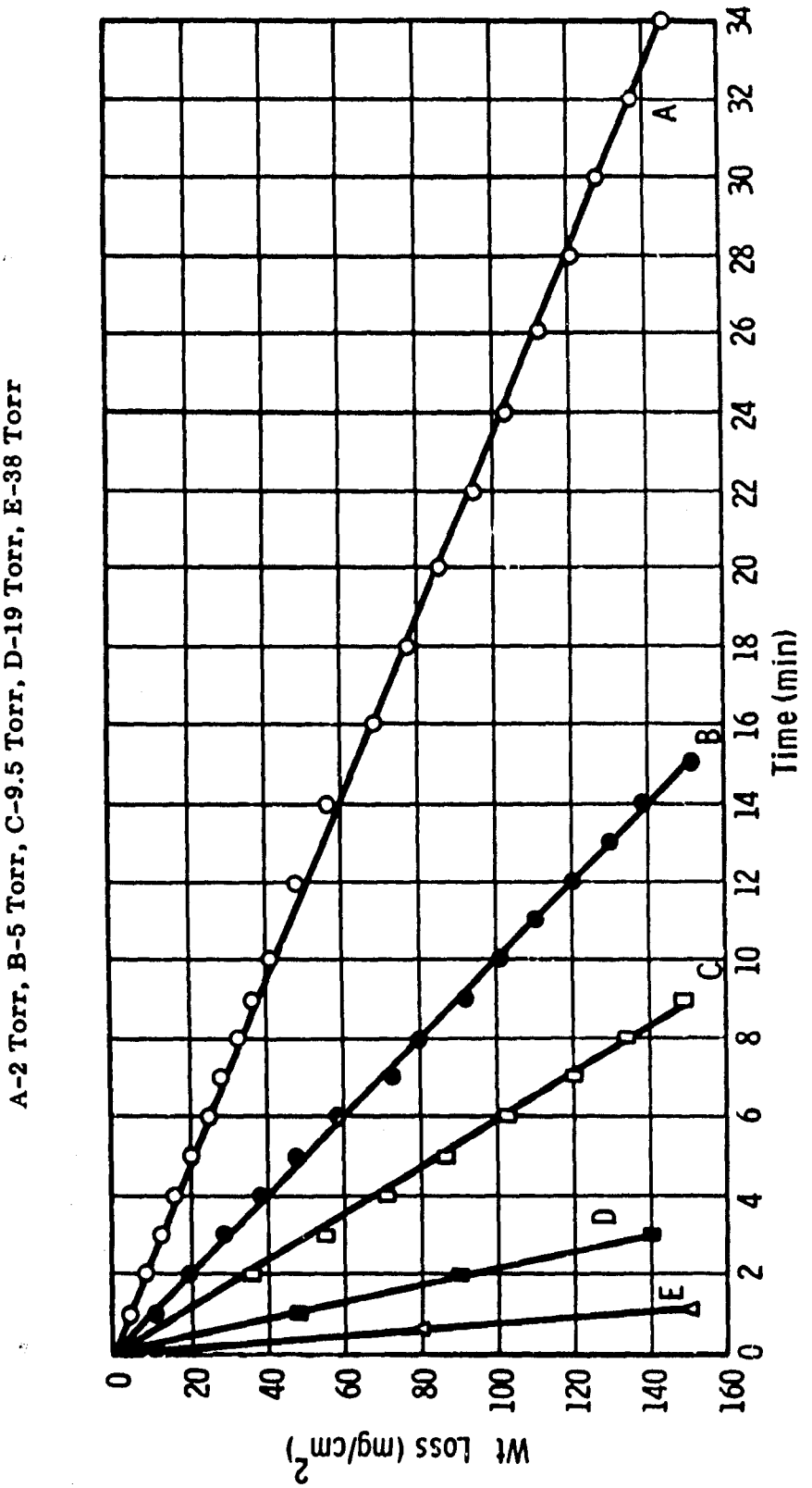

Figure 14. Effect of Pressure on Oxidation of Tungsten, 1465°C, 2 to 38 Torr O_2

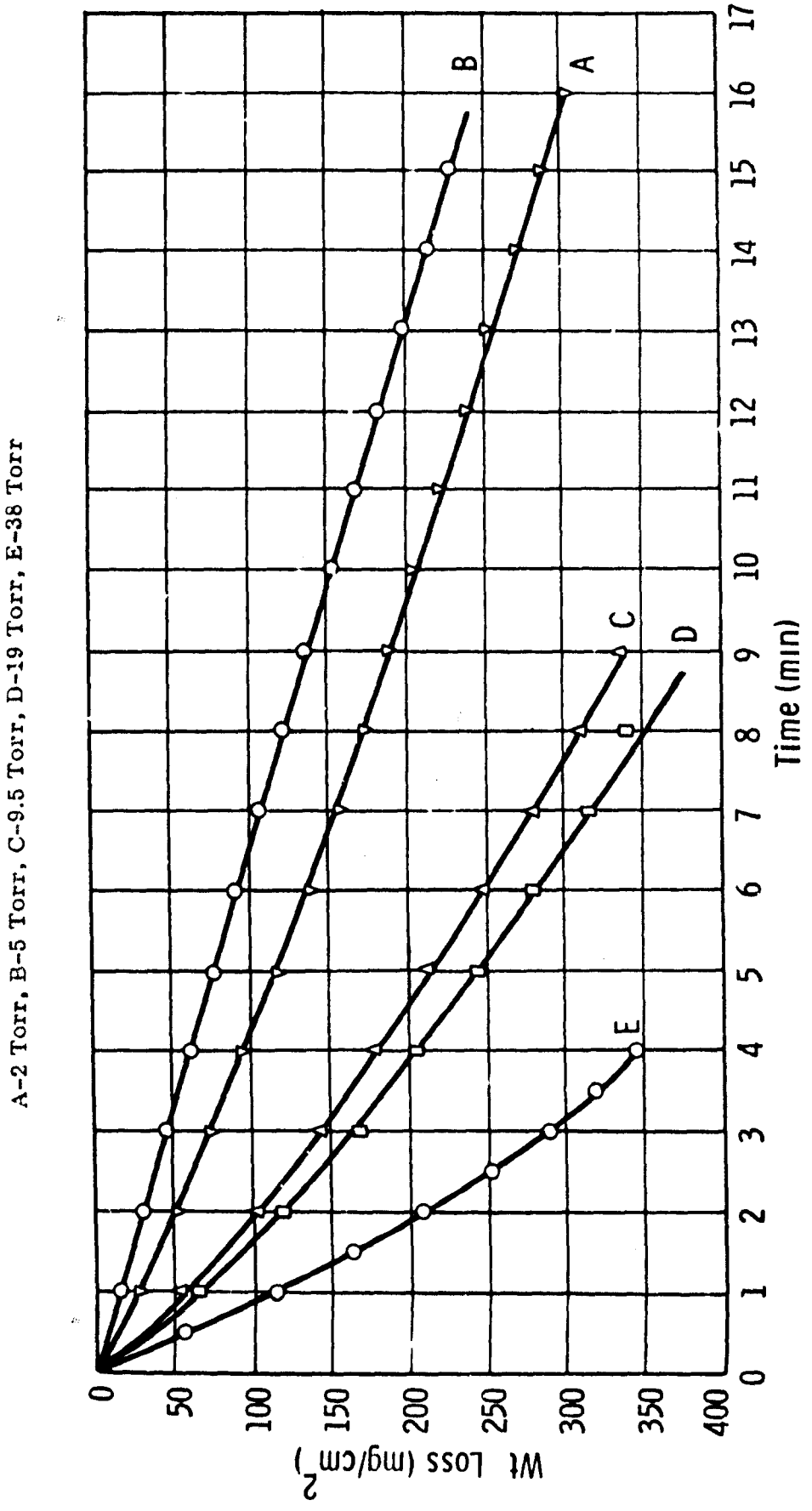

Figure 15. Effect of Pressure on Oxidation of Tungsten, 1615°C, 2 to 38 Torr

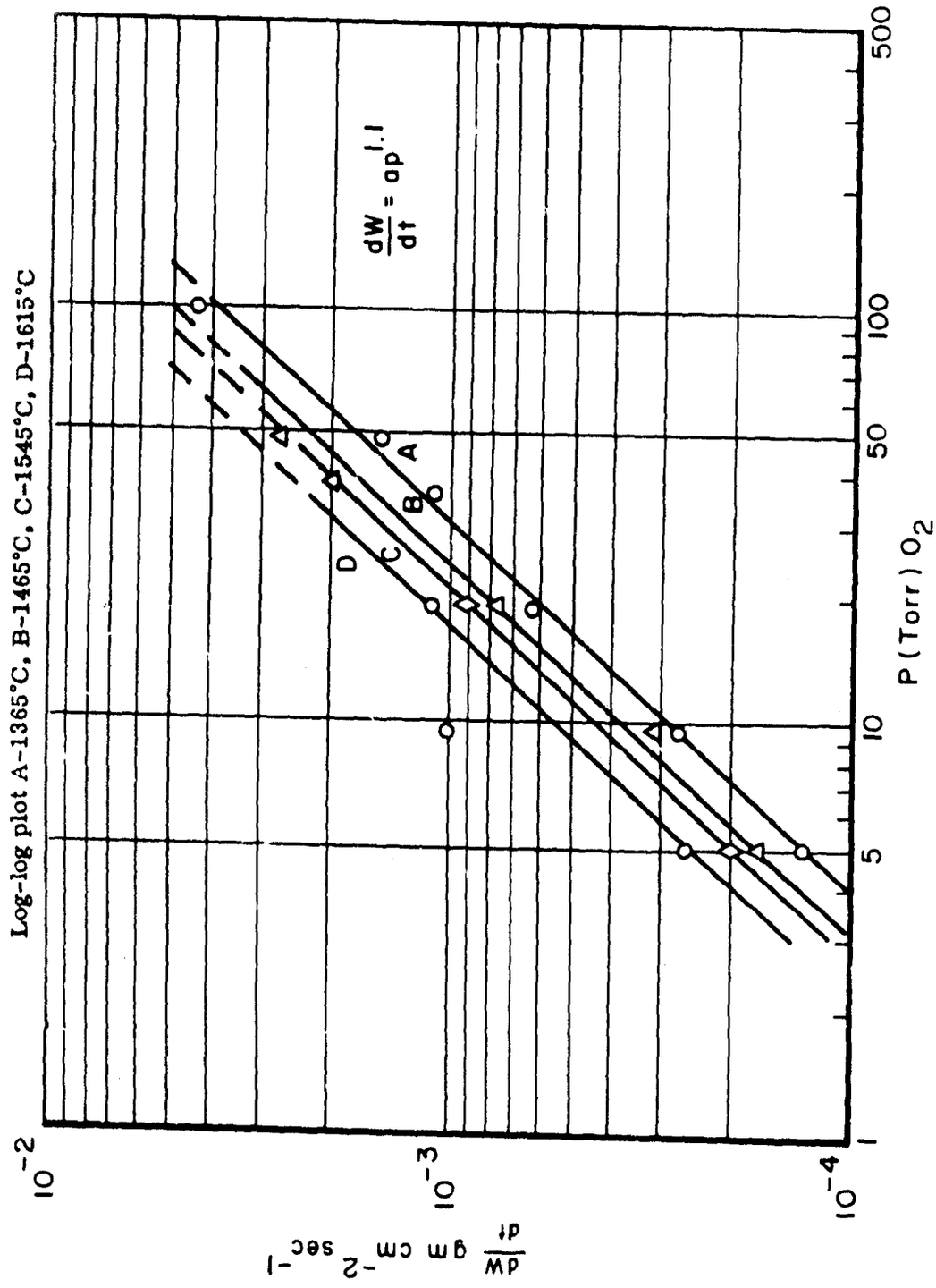

Figure 16. Effect of Pressure on Initial Rate of Oxidation of Tungsten

THE REACTIONS OF GASEOUS SYSTEMS WITH TUNGSTEN AT ELEVATED TEMPERATURE

George R. St. Pierre*
and
Rudolph Speiser*

INTRODUCTION

The destruction of tungsten in gaseous environments at elevated temperature has been studied extensively (Reference 1). In an earlier paper of this report,** the authors review high-temperature techniques useful in studying refractory metal systems. In this paper, experimental data is presented to demonstrate the processes of oxidation and vaporization of tungsten operative in the W-O-H and W-O-C systems.

Fortunately, the thermodynamic properties of the condensed phases of the tungsten-oxygen system are well known (Reference 2). Figure 1 shows the tungsten-oxygen phase equilibria at low temperature. Although "W_3O" has not been isolated as a stable phase at an atmospheric pressure of one (Figure 4), it is shown in another paper in this symposium. On Figure 2 are shown the CO_2-CO ratios for stabilities of the tungsten oxides at higher temperature. The WC field is outlined for comparison. The lines bounding the WC field are calculated from the heat of formation determined by Huff, Squitieri, and Synder (Reference 4). The recent work of Gleiser and Chipman (Reference 5) on the free energy of formation of WC is in agreement with the lines. The line of W-WO_2 coexistence has been determined with CO-CO_2 gas mixtures up to about 1225°C (Reference 2). Above 1225°C, Ebihara (Reference 10) found that it was impossible to equilibrate W and WO_2 with CO-CO_2 gas mixtures. From 1225° to 1450°C, it was found that tungsten metal remained bright in CO_2-CO atmospheres that would be expected to develop oxide scales. Furthermore, tungsten specimens suspended on a balance arrangement exhibited rapid weight loss in this range. Surprisingly, it was found that the tungsten specimens did not lose weight until a sufficiently high CO_2-CO ratio was achieved. At a critical ratio the weight loss became quite large. In every case it was possible to stop the loss of weight by reducing the CO_2-CO ratio to a point below the line shown on Figure 2. The line between W and the gas field should not be interpreted as an equilibrium effect. In all probability the line drawn represents only the condition at which the kinetic rate of formation of a complex W-O-C gas species rapidly increases. Clearer examples of this behavior will be shown for the W-O-H system. Unfortunately, the composition and structure of the W-O-C gas molecule remain undetermined. Certainly it is not the carbonyl, $W(CO)_6$, at such a high temperature. Only careful molecular mass determinations can resolve the uncertainties here.

SCALE FORMATION ON TUNGSTEN

The solubility of oxygen in tungsten is known to be extremely low. In fact it is impossible to detect any changes in the measurable properties of tungsten associated with oxygen saturation. Therefore, the oxidation of tungsten can be considered to begin with condensed oxide scale formation and/or complex gas species formation. The studies of Webb, Norton, and Wagner (Reference 6), Gulbransen and Andrew (Reference 7), Meuli and Spretnak (Reference 8), and Perkins and Crooks (Reference 9) have

*George R. St. Pierre, Junior Member AIME, and Rudolph Speiser, Member AIME, are Associate Professor and Professor, respectively, in the Department of Metallurgical Engineering, The Ohio State University, Columbus, Ohio.

**See "Methods for Studying High Temperature Oxidation Reactions," Figure 4.

demonstrated many of the rate characteristics at moderate to very high temperature and moderate, .001 atmosphere, to high oxygen pressure. Figure 3 presents data at very low effective oxygen pressures obtained at Ohio State University by W. T. Ebihara (Reference 10). The upper four curves are for CO_2-CO ratios in the $W_{18}O_{49}$ range. The lower two curves were obtained under conditions for which only WO_2 can form. The curves shown in Figure 3 and data obtained at other temperatures and pressures establish the protective behavior of WO_2. The rate of growth of the coherent WO_2 layer on tungsten under these conditions can be given in terms of a parabolic rate constant. On the other hand the $W_{18}O_{49}$ which forms on WO_2 in these cases is nonprotective. The $W_{18}O_{49}$ forms whiskers which afford no barrier to continued penetration of oxygen to the WO_2-$W_{18}O_{49}$ interfaces. For the conversion, WO_2-$W_{18}O_{49}$, a linear rate constant can be presented. Long oxidation runs established that the transport of tungsten through the WO_2 lattice is much greater than that of oxygen. Following the classical procedure developed by Wagner, a defect model of the WO_2 lattice is determined. The model is that WO_2 is a tungsten-deficit, cation-hole structure. With each cation vacancy (missing W^{4+} ion) there are associated four single electron holes to maintain electrical neutrality, i.e., the defect structure may be considered to consist of missing W^{4+} ions and W^{5+} ions in the ratio of one to four. With this model, a mass action expression can be derived for the dependence of the cation hole concentration on oxygen pressure. Consider the reaction:

$$5W^{4+} + O_{2(g)} = \square_{W}{}^{4+} + 4\square_{e^-} + 2WO_2 \qquad (1)$$

where $\square_{W}{}^{4+}$ represents a cation vacancy and $\square_{e^-}$ represents a W^{5+} ion. For reaction (1), an equilibrium constant may be written*

$$K = \frac{C_{\square+}{}^{4} \cdot C_{\square e}^{4}}{P_{O_2}} \qquad (2)$$

Equation 2 is based on the following assumptions: (1) the composition of the oxide does not deviate greatly from stoichiometric WO_2; (2) the oxygen pressure is low enough for ideal gas behavior to be assumed; and (3) the activity behavior of $\square+$ and $\square e$ follow Henry's Law within the homogeneity range of interest. All of these assumptions are quite reasonable. Equation 2 may be reduced further by noting that

$$C_{\square e} = 4C_{\square+}.$$

From which,

$$K = 4^{4} C_{\square}^{5} + \propto P_{O_2}.$$

The concentration of cation holes may be given by

$$C_{\square+} = K' P_{O_2}^{1/5} \qquad (3)$$

The unidirectional flux of tungsten through the WO_2 layer may be written as a first order equation in the cation hole concentration in accordance with the representations of Fick's First Law:

$$J_W = -D \frac{\partial C_{\square+}}{\partial x} \qquad (4)$$

In Equation 4, concentration is expressed in number of vacancies per unit volume, x is the distance measured in the direction of the unidirectional flux, D is the phenomenological diffusion coefficient defined by Equation 4, and J_W is the unidirectional flux of tungsten

*The standard states chosen are the following: For W^{4+}, stoichiometric WO_2 at 1 atm total pressure; For O_2, diatomic oxygen at unit fugacity; For $\square+$, the infinitely dilute solution of cation vacancies in stoichiometric WO_2 at 1 atm total pressure; For $\square_e$, the infinitely dilute solution of W^{5+} ions in stoichiometric WO_2 at 1 atm; For WO_2, stoichiometric WO_2 at 1 atm pressure.

through the oxide. If ξ designates the thickness of the WO_2 layer at any time, then

$$C_W \frac{d\xi}{dt} = (J_W)_{x=\xi} = -D \left(\frac{\partial C_{\square+}}{\partial x}\right)_{x=\xi} \quad (5)$$

where C_W is the concentration of tungsten in the oxide expressed in atoms per unit volume. The distance x in Equations 4 and 5 is measured from the metal-metal oxide interface. Equation 5 simplifies when it is recognized that J_W can be taken as constant through the oxide. Furthermore, the variation of D with $C_{\square+}$ can be neglected. From the foregoing statements it follows that

$$\frac{\partial C_{\square+}}{\partial x}$$

is constant within the oxide and

$$\frac{\partial C_{\square+}}{\partial x} = -\frac{J_W}{D} = -\frac{C^{\circ}_{\square+} - C^{i}_{\square+}}{\xi} \quad (6)$$

where $C^{\circ}_{\square+}$ and $C^{i}_{\square+}$ are the vacancy concentrations at the oxidizing interface and at the metal interface, respectively. Equations 5 and 6 can be combined to yield the differential equation for parabolic behavior.

$$C_W \frac{d\xi}{dt} = D \frac{C^{\circ}_{\square+} - C^{i}_{\square+}}{\xi} \quad (7)$$

and

$$\xi d\xi = D \frac{C^{\circ}_{\square+} - C^{i}_{\square+}}{C_W} \cdot dt \quad (8)$$

and for $\xi = 0$ at $t = 0$

$$\xi^2 = \left(2D \frac{C^{\circ}_{\square+} - C^{i}_{\square+}}{C_W}\right) t \quad (9)$$

Equation 9 can be combined with Equation 3 to eliminate vacancy concentrations.

$$\xi^2 = \left(\frac{2K'D}{C_W}\right)\left(P^{\circ 1/5}_{O_2} - P^{i\ 1/5}_{O_2}\right) t \quad (10)$$

$P^{\circ}_{O_2}$ and $P^{i}_{O_2}$ are the oxygen pressure at the WO_2 oxidizing interface and the equilibrium oxygen pressure for coexistence of W and WO_2, respectively. A "parabolic rate constant" can be defined

$$k_p = \frac{\xi^2}{t} = \left(\frac{2K'D}{C_W}\right)\left(P^{\circ 1/5}_{O_2} - P^{i\ 1/5}_{O_2}\right) \quad (11)$$

For a fixed oxidizing atmosphere, oxygen pressure, and temperature, the growth of the oxide scale is predicted to be parabolic. Furthermore, Equation 11 predicts that the defined constant, k_p, increases linearly with the difference, $(P^{\circ 1/5}_{O_2} - P^{i\ 1/5}_{O_2})$.

Because the scale thickness is a linear function of the gain in specimen mass per unit area attributed to the WO_2 layer, a constant in terms of specimen mass, k^1_p, has the same properties as k_p. Figure 4 shows the variation of the parabolic rate constant for WO_2 growth in terms of the oxygen pressure employed. It is clear that the model described is consistent with the observed kinetics. Unfortunately, the oxidation rates at the low oxygen pressures employed are very low and it is impossible to eliminate scatter in the data. Nevertheless, the fit is quite satisfactory. The temperature dependence of the parabolic constant is complicated indeed. An examination of the terms in Equation 11 immediately establishes that the Arrhenius equation could not be expected to describe the variation of k_p with temperature except when $P^{\circ 1/5}_{O_2} >> P^{i\ 1/5}_{O_2}$.

A linear rate constant for the conversion of WO_2 to $W_{18}O_{49}$ has also been calculated from the data and plotted in Figure 5. The relationship of the data obtained in this system to that obtained at much higher

oxygen pressures is indicated. It should be pointed out that the high oxygen pressure studies involved scales of $W_{20}O_{58}$ and WO_3.

VAPOR PHASE REACTIONS

The volatile character of tungsten and its oxides has been recognized for many years (Reference 11). The more recent literature has included operations which suggest a marked effect of water vapor on the stability of the condensed tungsten oxide phases (References 6, 12, and 13). The outstanding efforts of Blackburn et al. (References 14 and 15) and Berkowitz, Chupka, and Inghram (Reference 16) have helped to obtain the species distribution and thermochemical properties of the tungsten-oxygen molecules: W_3O_9; W_4O_{12}; and W_5O_{15}. The thesis research of Bishop, Pool, and Battles (References 17, 18, and 19) has been directed at determining the quantitative nature of the reactions which occur between tungsten and its oxides and water vapor. Figure 6 displays typical reacted tungsten samples observed by Battles. The samples were exposed to H_2O-H_2 atmospheres of oxygen potential just slightly above that required for equilibrium coexistence of W and WO_2. The samples lost mass rapidly because the oxide formed on the surface was converted to vapor species. It is particularly interesting to note the appearance of the macroscopic oxide on the surface. Clearly, preferred regions exist for oxide growth. However, the presence of macroscopic oxide on the tungsten surface is not necessary for tungsten to show marked vapor loss. Figure 7 shows that the vapor loss is very high at oxygen pressures well below those required for stability of condensed WO_2. Figures 7 and 8 display curves of constant temperature and water vapor pressure. In going from left to right on the graphs, hydrogen is replaced with argon to vary the effective oxygen pressure in the gas stream passed over the particular tungsten specimen. The specimens, suspended on a balance arrangement, were weighed semicontinuously to obtain the linear rate constants plotted in the figures. The rate of vapor loss rises rapidly as the effective oxygen pressure is increased toward the equilibrium value for W-WO_2 coexistence. (The arrows at $P_{H_2O}/P_{H_2} = 1.1$ on Figure 7.) Often a distinct change in slope of the vapor loss curve is observed at the equilibrium point; however, the vapor loss rate does not increase greatly above the equilibrium point. The curve for 8.0 inches Hg on Figure 7 does not exhibit a discontinuity at the W-WO_2 equilibrium point but does exhibit an irregularity at the WO_2 – $W_{18}O_{49}$ point. (Again arrows have been added for demarcation.) The effects of temperature and water vapor pressure on the vapor loss are strongly indicated by the curves of Figures 7 and 8. The vapor loss rates of oxide compacts have been studied by Bishop and Battles. These correlate very well with the vapor loss rates of tungsten undergoing simultaneous oxidation and vaporization. The data of Battles shown in Figures 9, 10, and 11 have been marked on Figure 8. The short horizontal dashes by the curves at $P_{H_2O}/P_{H_2} = 1.9$ are the corrected vapor loss rates observed on the oxide compacts. In this range the tungsten is losing mass as rapidly as the WO_2 can be vaporized.

The rationalization of these observations and those of the other contributors mentioned is made difficult because of the lack of information regarding the composition and structure of the vapor species forming. Although the vapor loss rate is observed to vary linearly with the water vapor pressure over the range of conditions studied, it is not valid to infer that a simple first order mechanism can account for the behavior. Many complex reaction sequences can be proposed which approximate to such linearity over narrow ranges of reaction variables. For example, consider that the first step in the vaporization reaction is the adsorption of H_2O on the oxide surface:

$$H_2O_{(v)} = H_2O_{(ads)} \qquad (12)$$

The classical Langmuir treatment for monolayer adsorption can be applied to estimate the fraction of available adsorption sites occupied, f, for a given P_{H_2O}:

$$\frac{dn}{dt} = k_1(1-f)P_{H_2O} - k_2 f \qquad (13)$$

Equation 13 assumes that the adsorbed H_2O reacts slowly with the substrate to form the volatile species. Therefore, the adsorbed H_2O comes to the equilibrium with the vapor and

$$f = \frac{P_{H_2O}}{P_{H_2O}+a} \qquad (14)$$

where $a = K_2 / K_1$

Under conditions for which the surface is far from saturated the occupation concentration is proportional to P_{H_2O} only. If the volatile reaction is first order in the concentration of adsorbed H_2O, the observed vapor loss rates would be expected to vary linearly with P_{H_2O}. The foregoing treatment can account for the observed behavior but can not be relied upon until additional mechanistic studies establish its validity. Furthermore, the nature of the growth of oxide crystals on tungsten must be resolved. In this connection, the research of Moazed and Rausch described in this symposium is very decisive.

SUMMARY

Although much remains to be determined about the interactions of tungsten with oxidizing gas mixtures containing O_2, CO_2, and H_2O, considerable information is accumulating about the W-O-H-C system. In this communication some of the data obtained at Ohio State University have been presented and an attempt has been made to rationalize the observations. The areas of uncertainty have been pointed out to indicate fruitful future investigations.

ACKNOWLEDGMENTS

This paper could not have been written without the patient and careful studies of G.H. Bishop, M.J. Pool, W.T. Ebihara, and J.E. Battles. Their contributions as dedicated graduate research students formed the basis of this effort. Furthermore, the research could not have been undertaken without the major financial assistance of the United States Air Force. The patient guidance of Mr. Paul L. Faust, Project Engineer, AF Materials Laboratory, Wright-Patterson Air Force Base, Ohio, is sincerely appreciated.

REFERENCES

1. For example, see E. A. Gulbransen, K. F. Andrew, F. A. Brassart, and P. E. Blackburn. WADC Technical Report 59-575, Part III. Wright Air Development Center, Wright-Patterson Air Force Base, Ohio, July 1962.

2. G. R. St. Pierre, W. T. Ebihara, M.J. Pool, and R. Speiser. Trans. Met. Soc. AIME, Vol. 224, 1962, p. 259.

3. For discussion of this point see the review paper prepared by the authors for this symposium.

4. G. Huff, E. Squitieri, and P. E. Snyder. J. Am. Chem. Soc., Vol. 70, 1948, p.3380.

5. M. Gleiser and J. Chipman, "Free Energy of Formation of Tungsten Carbide WC," to be published.

6. W. W. Webb, J. T. Norton, and C. Wagner, J. Electrochem. Soc., Vol. 103, 1956, p. 107.

7. E. A. Gulbransen and K. F. Andrews, J. Electrochem. Soc., Vol. 107, 1960, p. 619.

8. J. E. Battles, W. T. Ebihara, R. Speiser, M. J. Pool, G. R. St. Pierre, W. P. Meuli, and J. W. Spretnak. ARL Technical Report 62-324. Aeronautical Research Laboratories, Wright-Patterson Air Force Base, Ohio, 1962.

9. R. A. Perkins and D. D. Crooks, J. of Metals, July 1961, p. 490. See also R. A. Perkins, W. L. Price, and D. D. Crooks, Lockheed Technical Report 6-90-62-98, November, 1962.

10. W. T. Ebihara, M.Sc. Thesis, Department of Metallurgical Engineering, The Ohio State University, 1960.

11. I. Langmuir, J. Am. Chem. Soc., 37, 1915, p. 1139.

12. E. A. Gulbransen and W. S. Wysong, Trans. Met. Soc. of AIME, 175, 1948, p. 175.

13. T. Millner and J. Nengebauer, Nature, 163, 1949, p. 601.

14. P. E. Blackburn, M. Hock, and H. L. Johnston, J. Phys. Chem., 62, 1958, p. 769.

15. P. E. Blackburn, WADC Technical Report 59-575, Part II, June 1961.

16. J. Berkowitz, W. A. Chupka, and M. G. Inghram, J. Chem. Phys. 26, 1957, p. 842. Ibid, 27, 1957, p. 85.

17. G. H. Bishop, M.Sc. Thesis, Department of Metallurgical Engineering, The Ohio State University, 1958.

18. M. J. Pool, M.Sc. Thesis, Department of Metallurgical Engineering, The Ohio State University, 1959.

19. J. E. Battles, M.Sc. Thesis, Department of Metallurgical Engineering, The Ohio State University, 1961.

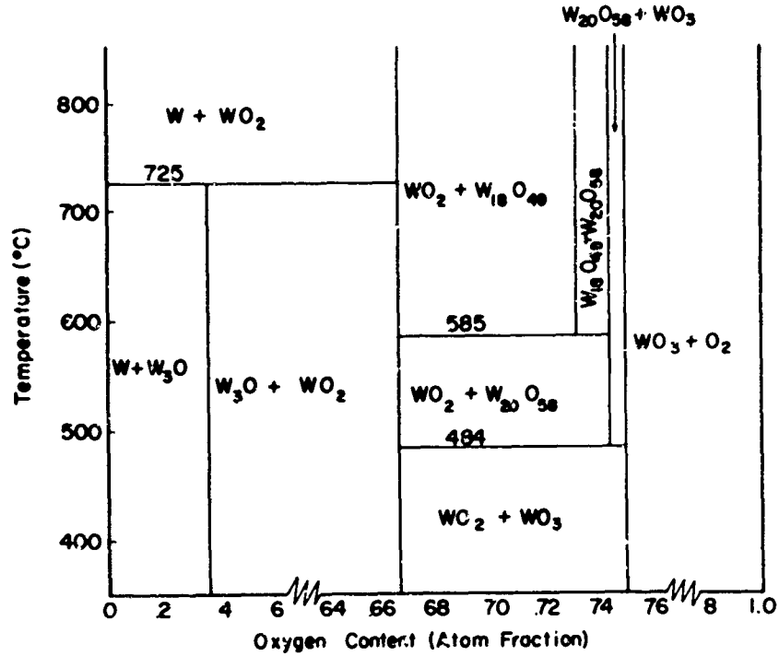

Figure 1. The Tungsten-Oxygen Phase Equilibria at One Atmosphere Total Pressure

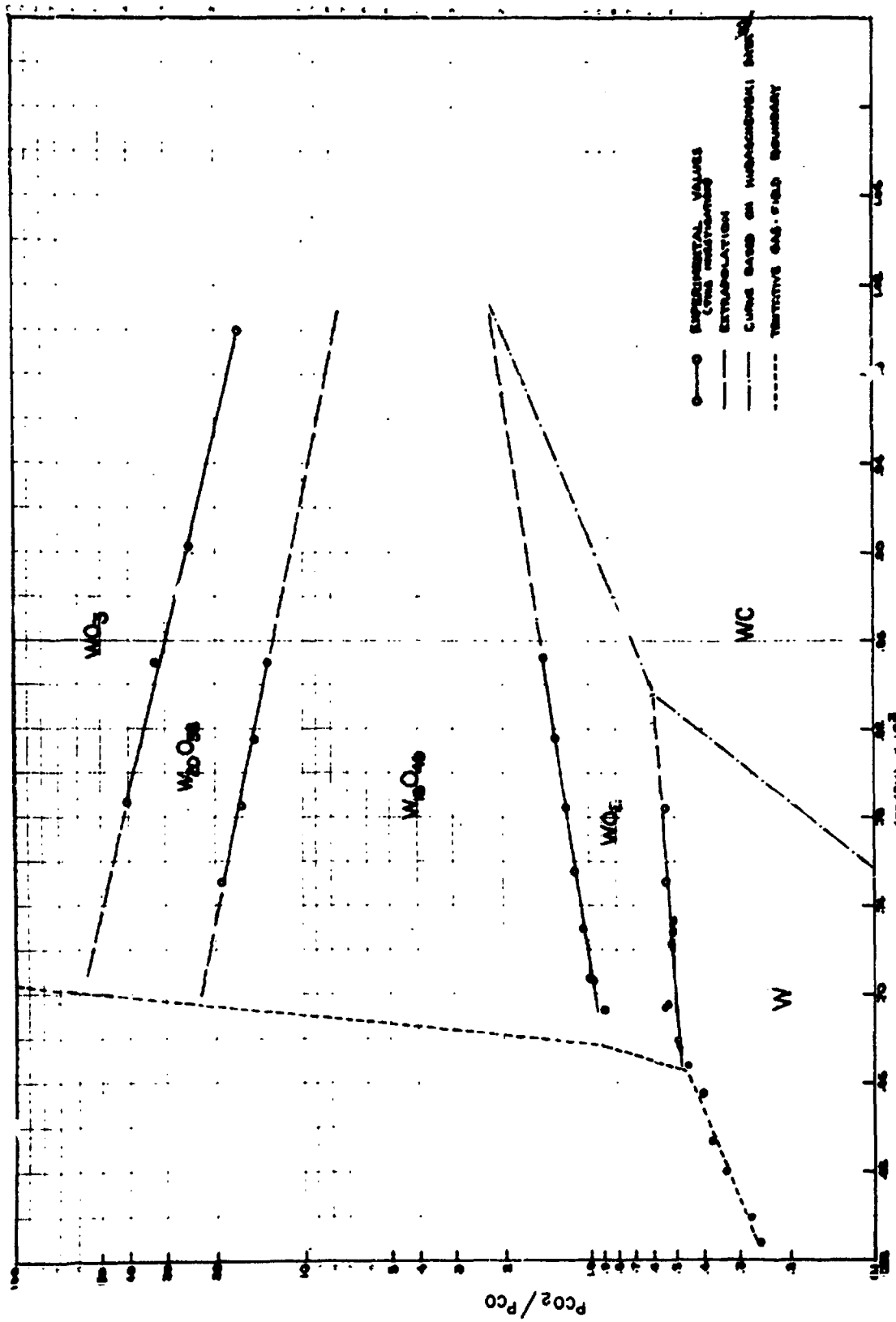

Figure 2. Phase Boundaries in the W-O-C System

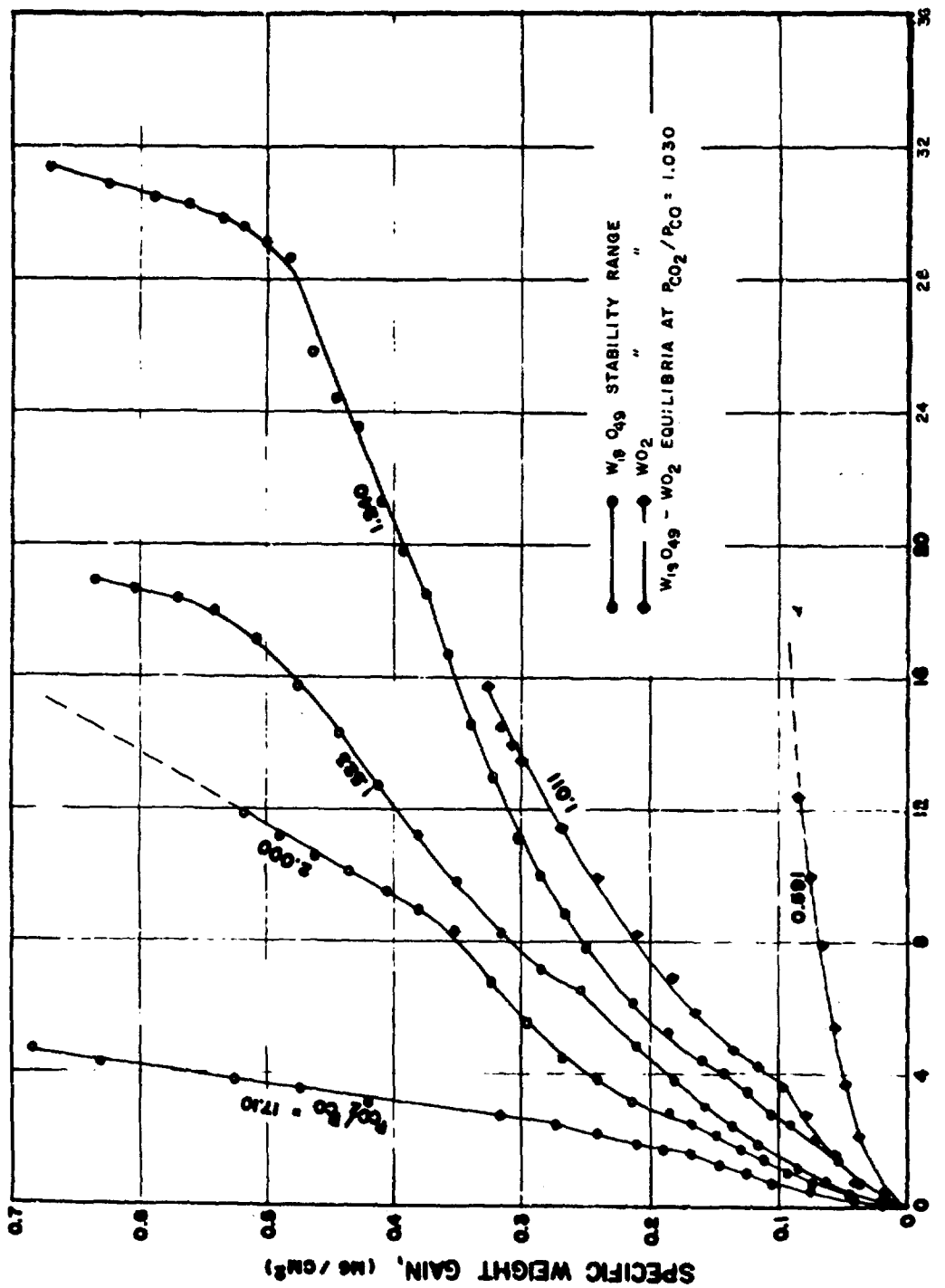

Figure 8. Typical Oxidation Curves of Tungsten at 1100°C

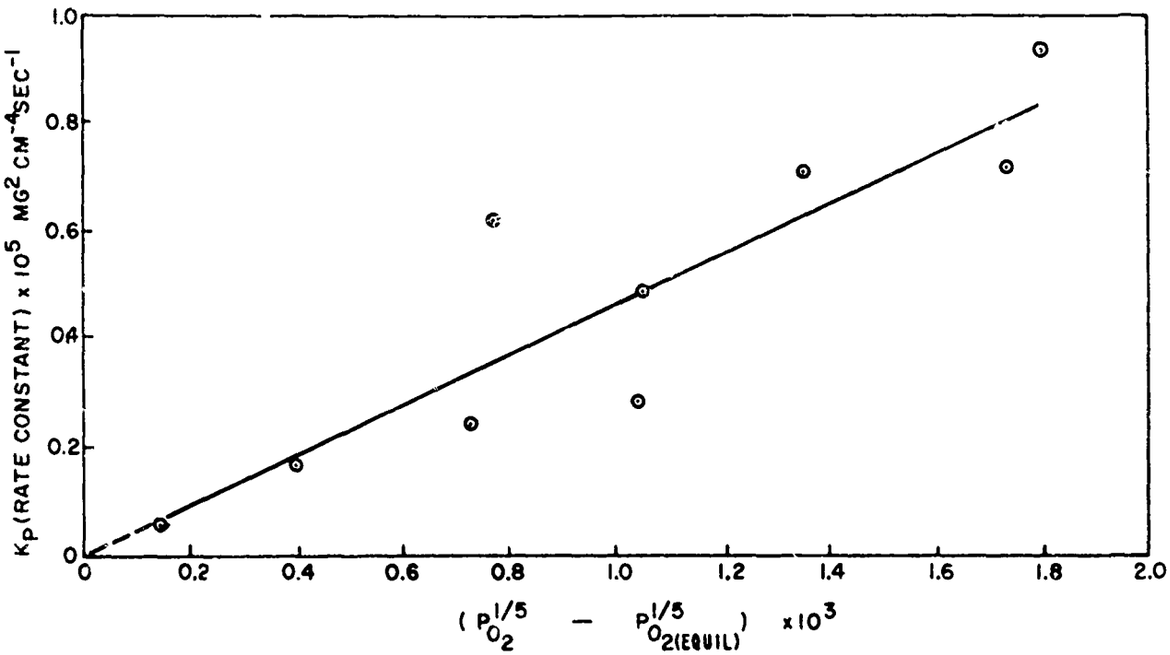

Figure 4. The Oxygen Pressure Dependence of the Parabolic Oxidation Kinetics of Tungsten at 1100°C

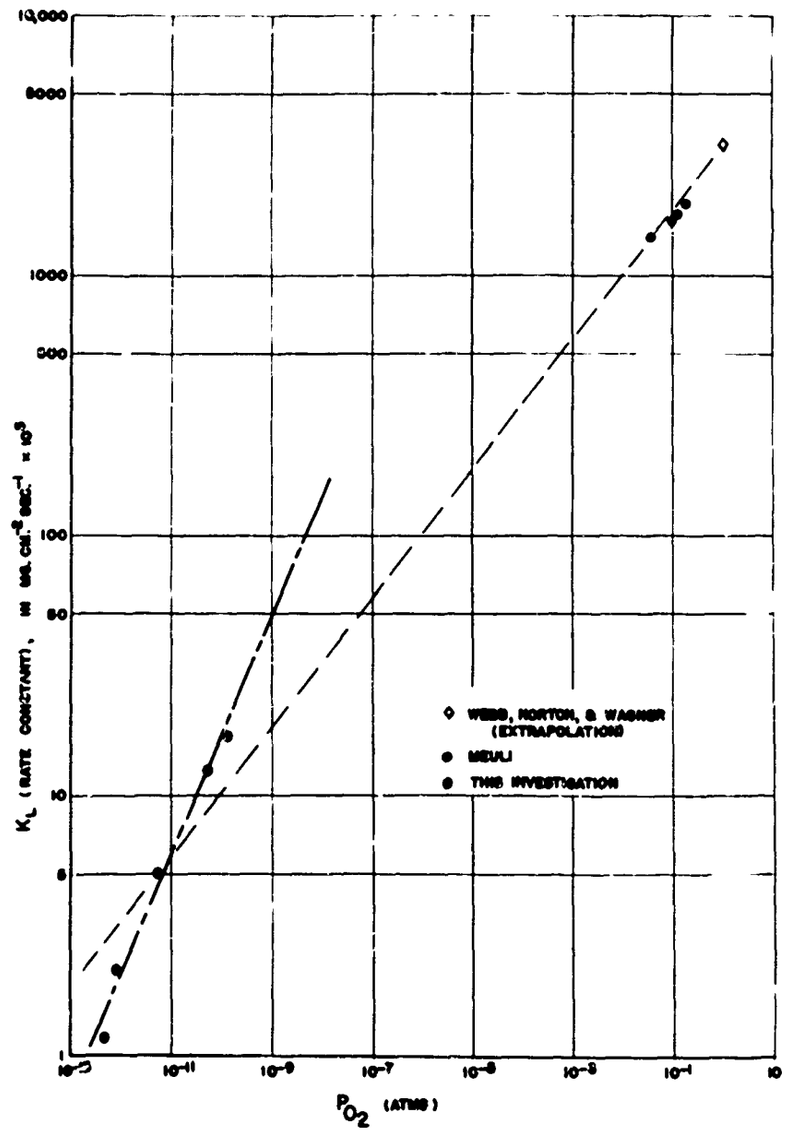

Figure 5. The Oxygen Pressure Dependence of the Linear Oxidation Kinetics of Tungsten at 1100°C

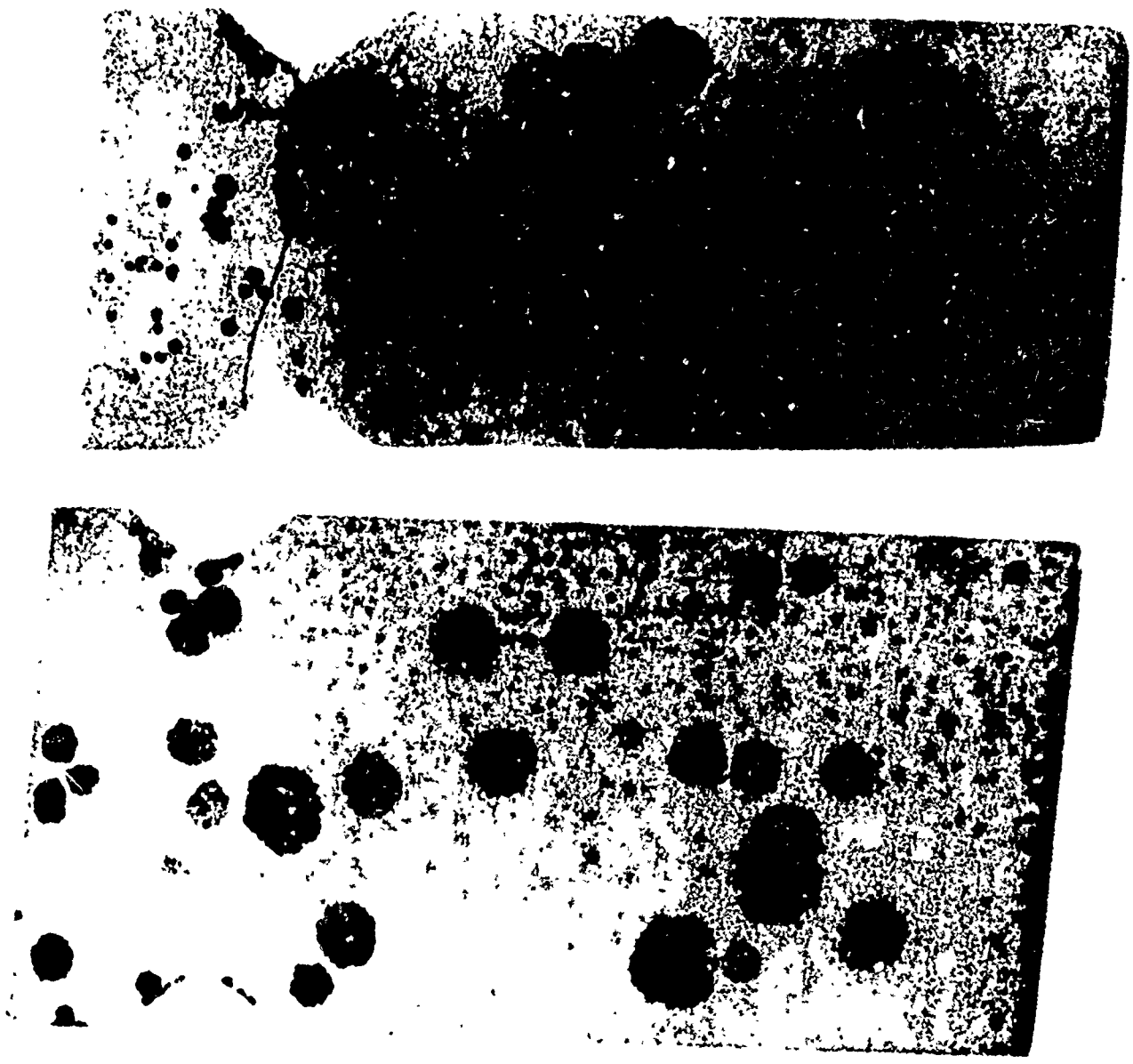

Figure 6. Tungsten Samples Oxidized at 1200°C in H_2O/H_2 Atmospheres Slightly above the W-WO_2 Equilibrium Value

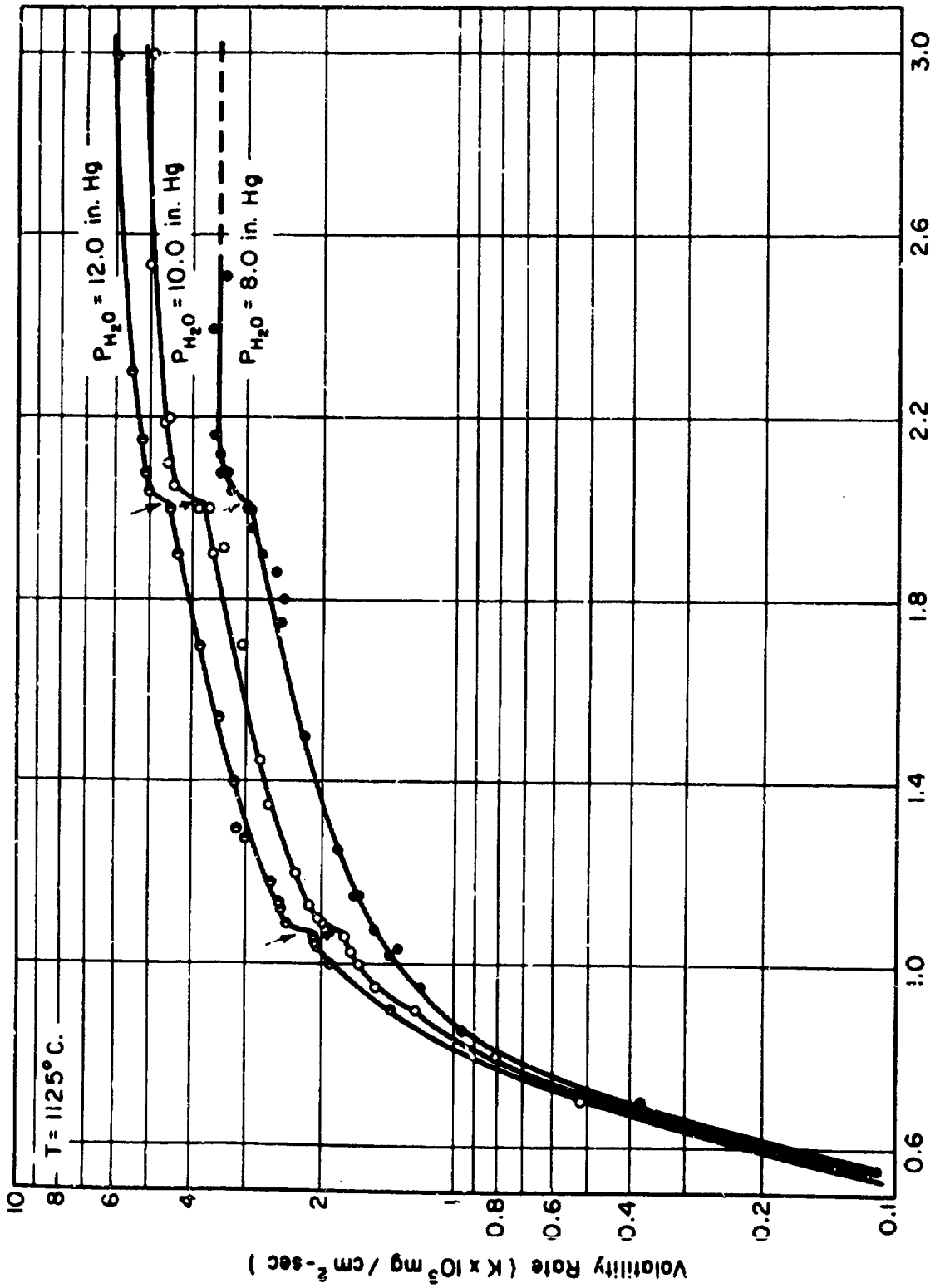

Figure 7. Vapor Loss Curves for Tungsten in Ar-H_2-H_2O Atmospheres – 1125°C

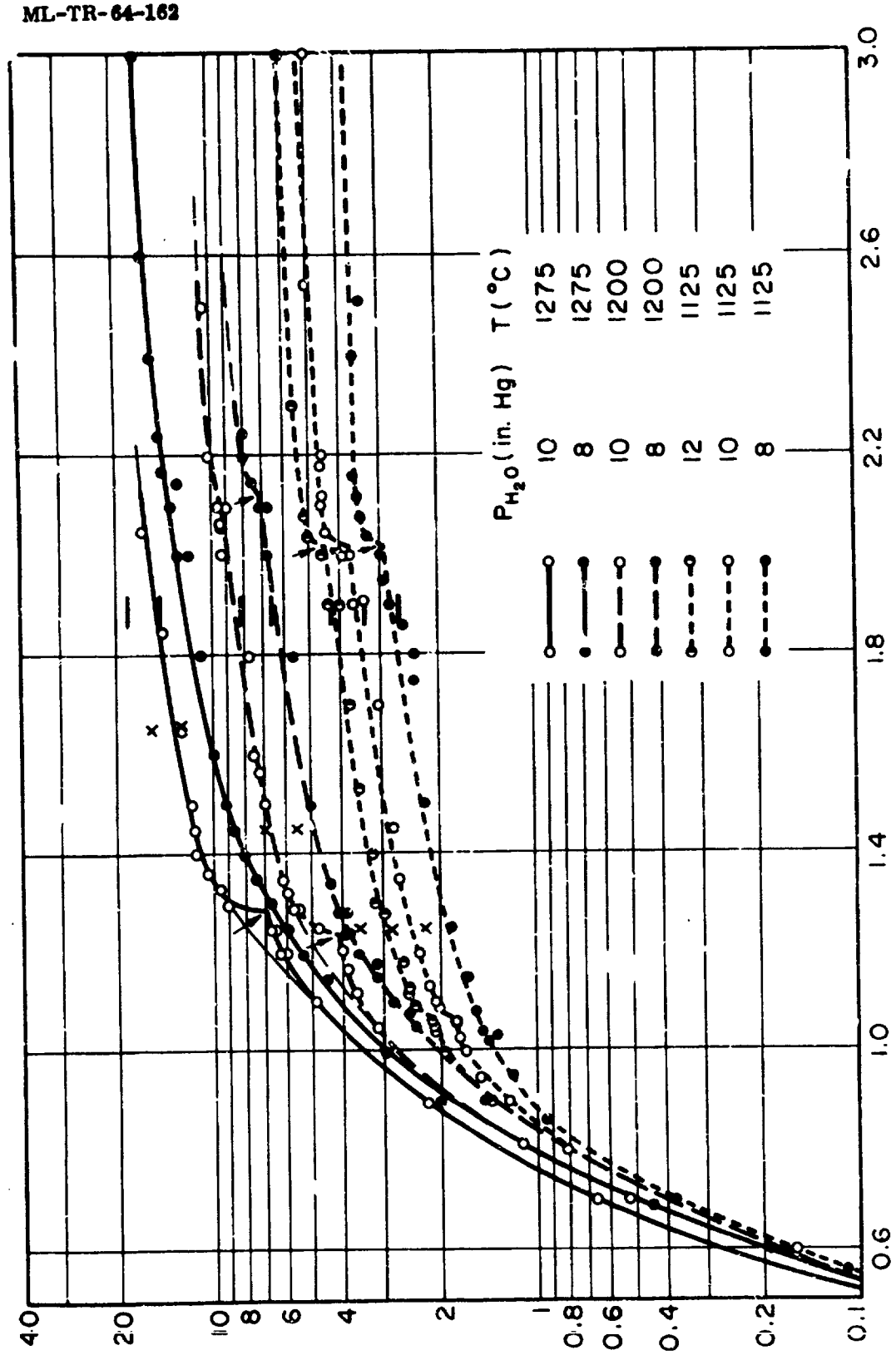

Figure 8. Vapor Loss Curves for Tungsten in Ar-H_2-H_2O Atmospheres

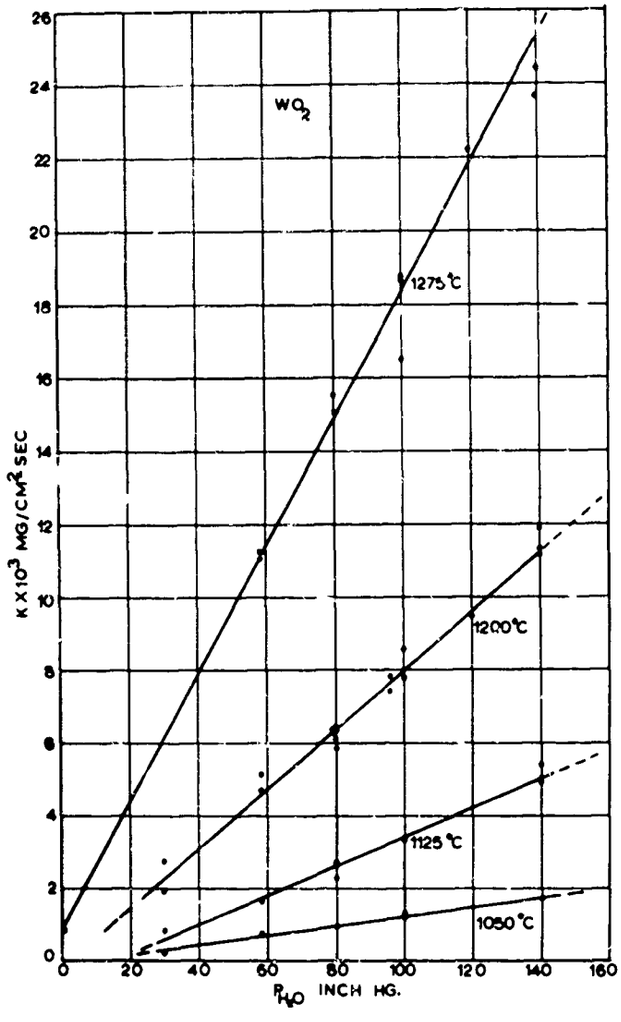

Figure 9. Vapor Loss Curves for WO_2 Compacts

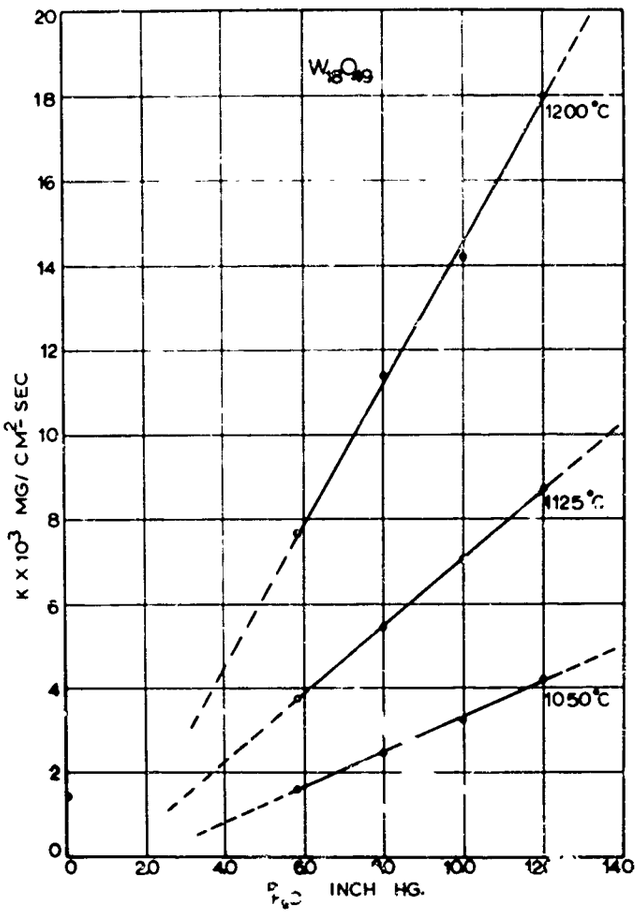

Figure 10. Vapor Loss Curves for $W_{18}O_{49}$ Compacts

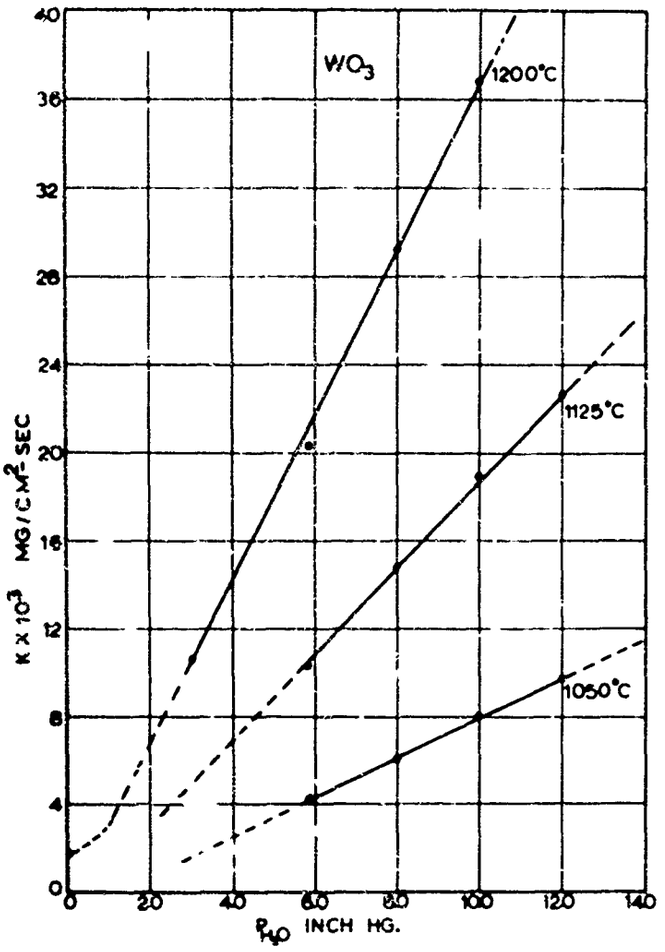

Figure 11. Vapor Loss Curves for WO_3 Compacts

OXIDATION OF TUNGSTEN AT ULTRA-HIGH TEMPERATURES

Roger A. Perkins*
William L. Price*
Donald D. Crooks*

INTRODUCTION

Serious consideration is being given to the use of tungsten in high temperature applications above the limits of available protective coating systems. Components capable of operating at temperatures to 3000°C (5430°F) are being designed, manufactured, and tested today. Although oxidation-resistant coatings are needed for extended use at high temperatures in air, absolute protection from oxidation is not mandatory for a number of applications. Coatings may not be required where high-temperature exposure occurs at a low partial pressure of oxygen for a relatively short time. For example, uncoated tungsten is used successfully at temperatures approaching its melting point in the nozzles of solid propellant rocket engines. Although products of combustion contain oxidizing gases, exposure time is approximately 1 to 2 minutes and loss by oxidation is negligible. Leading edges and heat shields of hypersonic re-entry vehicles will operate at temperatures of 1200° to 3000°C (2190° to 5430°F). Heating occurs in static and high velocity air at pressures of 10^{-4} to 20 mm Hg for periods of 10 to 100 minutes (Reference 1). If surface recession by oxidation under these conditions is small, it can be tolerated by proper design. In some cases, refractory oxide coatings may be used to restrict the access of air and to reduce the oxygen pressure at the metal-oxide interface.

The successful application of this approach to the use of tungsten at ultra-high temperatures demands a precise knowledge of oxidation behavior under the anticipated environmental conditions. The purpose of this investigation (conducted as part of the Lockheed independent research program) was to obtain rate data for the oxidation of tungsten from 1300° to 3400°C (2370° to 6150°F) as a function of oxygen pressure and gas dynamics and to obtain an improved understanding of reaction kinetics that will be of theoretical as well as practical utility.

REACTION KINETICS AT HIGH TEMPERATURE

There have been only a few investigations of the oxidation of tungsten at temperatures above 1300°C (2370°F) and pressures below one atmosphere. Past interest in this subject has been for the use of tungsten as filaments in lamps and electron tubes. Limited data have been obtained for fine-wire and ribbon filaments at temperatures to 2500°C (4530°F) in oxygen at pressures of 10^{-7} to 10^{-2} mm Hg. Oxidation data usually are reported in terms of collision efficiency (E) which is defined as the ratio of the rate of removal of oxygen molecules from the surface as WO_3 to the rate of arrival of oxygen at the surface ($3.5 \times 10^{22} P_{O_2} (32T)^{-1/2}$). Rates are expressed as molecules/cm^2/sec with P_{O_2} in mm Hg. These data can be converted to rates of tungsten loss (R_W) by the following relation:

$$R_W = 4.275\ E\ P_{O_2}\ \text{gm/cm}^2\text{/min} \qquad (1)$$

This assumes that the arrival rate of oxygen is a function of pressure and the temperature of the reaction vessel. (T = 300°K). Langmuir (Reference 2) has shown that at pressures below 10^{-2} mm Hg, the arrival rate of oxygen at the surface is not perceptibly influenced by the filament temperature.

* Materials Sciences Laboratory, Lockheed Missiles and Space Company.

Langmuir (Reference 2) conducted the first high-temperature, low-pressure oxidation study in 1913. The rate of clean-up of oxygen in a sealed bulb was measured by a pressure-drop technique. The rate of oxidation was found to be a linear function of pressure and an exponential function of temperature. The collision efficiency increased with temperature in the manner of an Arrhenius relation as follows:

$$E = 57.54 \times 10^{\frac{-5940}{T}} \qquad (2)$$

This expression in terms of the rate of tungsten loss expressed in the units of the present work is given by

$$R_W = 256\ P_{O_2} \exp(-27200/RT)\ gm/cm^2/min \qquad (3)$$

Above 927°C (1700°F) the oxide volatilized without dissociation, leaving the surface clean and bright. At temperatures above 1500°C (2730°F), the measured rates were less than those predicted by the Arrhenius equation.

In 1959, Eisinger (Reference 3) reported on the oxidation of tungsten from 927° to 2127°C (1700° to 3860°F) in oxygen at pressures of 10^{-5} to 10^{-7} mm Hg. Collision efficiency was determined by measuring the pumping action of high purity single crystal ribbons. Curves of reaction probability vs temperature could be described by the Arrhenius equation at low temperatures but reached a maximum and then decreased with increasing temperature. This behavior was attributed to a decrease in sticking probability of oxygen on tungsten resulting in reduced probability of oxide formation at high temperature. The low-temperature data agree with those of Langmuir, giving an apparent heat of activation of 25,000 cal/mol. Unlike Langmuir's results, collision efficiency was found to be pressure dependent, and the pressure dependency of rate of oxidation was not linear.

Becker, Becker, and Brandes reported on similiar studies in 1961 (Reference 4). Results of tests from 927° to 2227°C (1700° to 4040°F) in oxygen at pressures from 10^{-5} to 10^{-7} mm Hg were similar to those of Langmuir and Eisinger. The collision efficiency was found to increase, pass through a maximum, and then decrease with increasing temperature. This behavior was attributed to changes in the sticking probability and heat of desorption of oxygen on tungsten as a function of temperature. Oxygen was described as adsorbing in two distinct states or layers. For the first layer, the sticking probability (S) was constant at 0.14 with an energy of desorption of 106,000 calories. In the second layer, S = 0.04 with an energy of desorption of 53,000 calories. Two rate equations were derived from theoretical considerations and experimental data. In the range from 927° to 1327°C (1700° to 2420°F), the first layer was filled and the second layer coverage decreased to zero as temperature increased. The collision efficiency is given by

$$E = 60 \times 10^{\frac{-5555}{T}} \qquad (4)$$

which converted to the units of this work becomes

$$R_W = 256\ P_{O_2} \exp(-25400/RT)\ gm/cm^2/min \qquad (5)$$

The rate equation is very close to that of Langmuir's which was obtained by a fit of experimental data to an Arrhenius equation. From 1727° to 2127°C (3140° to 3860°F) the first layer is partially filled and the coverage decreases to zero with increasing temperature. The rate equation becomes

$$E = 0.11\ P^{0.5}\ 10^{\frac{+6060}{T}} \qquad (6)$$

which can be converted to

$$R_W = 0.47\ P^{1.5} \exp(+27700/RT)\ gm/cm^2/min \qquad (7)$$

Thus, at high temperatures rates are predicted to increase with $P^{1.5}$ but to decrease with temperature. Becker et al. also showed that carbon as an impurity in tungsten could accelerate the rate of oxidation by increasing the concentration of adsorbed oxygen on the surface.

The most recent investigation of this phenomenon was conducted by Anderson (Reference 5) in 1962. Oxidation behavior in the region of the rate maximum was studied from 1677° to 2327°C (3050° to 4220°F) in oxygen at pressures of 7.6×10^{-4} to 7.6×10^{-6} mm Hg. The results were similar to those found by previous investigators. In the temperature range from 1877° to 2327°C (3410° to 4220°F), rate of tungsten loss was observed to increase with $P_{O_2}^{1.26}$ and to decrease with increasing temperature. Rates were found to depend on the oxygen atom concentration on the surface and varied with pressure to the 1.0 to 1.5 power depending on surface coverage. Heats of activation were negative and decreased from -14,000 to -20,000 calories as pressure decreased.

Only two direct studies of oxidation behavior above 1300°C (2370°F) at higher pressures have been reported. Perkins and Crooks (Reference 6) studied the oxidation of tungsten from 1300° to 3000°C (2370° to 5430°F) in air at 1 to 15 mm Hg pressure using a surface recession technique. From 1300° to 1700°C (2370° to 3090°F) rates could be described by

$$R_W = 14.5\, P_{O_2}^{0.62} \exp(-31500/RT)\ gm/cm^2/min \qquad (8)$$

Oxidation rates reached a maximum at about 1750°C (3180°F) and then decreased with increasing temperature. Although the curves resemble those obtained at very low pressures, the rates are considerably less than would be predicted from equations that have been cited. As will be shown, oxygen depletion in the reaction chamber is responsible for the observed behavior and the measured rates are characteristic of the system, rather than of the material.

Blackburn et al. (Reference 7) in 1961 reported on the oxidation of tungsten in flowing 21 percent oxygen, 79 percent argon at one atmosphere from 800° to 1700°C (1470° to 3090°F). Rates were determined by oxygen consumption techniques. At temperatures above 1350°C (2460°F) the oxide was found to evaporate as fast as it formed. Oxidation rate was found to increase with temperature according to an Arrhenius relation with activation energy of 21,000 cal/mol. The mechanism was assumed to be that postulated by Langmuir at low pressure; however, the observed rates are considerably less than those which would be predicted by Equations 3 or 5.

By considering the oxidation of tungsten as a series of consecutive reactions, Ong (Reference 8) derived from kinetic theory and experimental data the following rate equation:

$$R_W = 5.89 \times 10^6\, P_{O_{2(ATM)}}^{0.5} \exp(-12170/T)\ mg/cm^2/hr \qquad (9)$$

which in terms of this work becomes

$$R_W = 3.56\, P_{O_{2(MM)}}^{0.5} \exp(-24200/RT)\ gm/cm^2/min \qquad (10)$$

This equation adequately reproduced rate data from three independent investigations at pressures from 1 mm to 15,800 mm Hg and temperatures from 700° to 1300°C (1290° to 2370°F). Although the temperature-dependent term is similar to that of Equations 3 and 5, the pressure-dependent term and constant are significantly different. The rates would be considerably lower than those predicted by other equations. The validity of Equation 9, however, has not been checked at higher temperatures and lower pressures. Similarly, it is not known if Equations 3 and 5 will adequately express rates at pressures above 10^{-2} mm.

One of the objectives of the present work, therefore, is to determine whether a change in mechanism occurs as a function of pressure. The similarity of rate behavior at pressures above 1 mm and below 10^{-2} mm in terms of temperature dependency suggests a common behavior over a wide pressure range. Discrepancies in pressure dependency, however, need to be clarified and resolved. Also, the existence of a maximum in rate vs temperature at pressures above 10^{-2} must be confirmed. A pressure range of 10^{-1} to 5 mm Hg was selected for this study to provide a logical extension of prior work at reduced pressures.

EXPERIMENTAL

Materials

The tungsten used in this investigation was commercial ground seal rod procured from the General Electric Company. This material, designated as Grade MK, is a fine-grained partially doped tungsten which is 99.95+ percent pure. Principal impurities include 0.002, 0.0015, and 0.002 percent, respectively, of carbon, oxygen, and molybdenum. All other impurities are less than 0.001 percent each. The rods were 0.1 inch in diameter by 7 inches long and were centerless ground with a surface finish of 6 to 8. A few tests were made with Grade 218 ground seal rod which is a fully doped material that is, after heating at high temperature, coarse grained compared with Grade MK.

Medical Grade tank oxygen 99.96+ percent pure was used in most of the tests. A number of tests were made with Linde Company Research Grade oxygen which is 99.99+ percent pure. No effects from the impurities in the gas on rates of oxidation were detected. Tests in air were made with normal atmosphere passed through a molecular-sieve column. Changes in relative humidity of the air had no discernible effect on rates.

Equipment

All tests were conducted in a surface recession rate apparatus designed and built by Lockheed Missiles and Space Company (Figure 1). Specimens were heated by direct resistance using alternating current at 100 to 300 amperes and 5 to 15 volts. The rods were positioned vertically in water-cooled electrodes with slip-fit expansion joints to prevent buckling during heating. A water-cooled wrought-copper T-section 6 inches in diameter by 14 inches high was used for the reaction vessel. Total volume of the system including pipes and ballast chamber was about 17 liters. Two sight ports were provided for measurement of temperature and rod diameter. A 1397 B Welch pump and an MCF-300 diffusion pump were used in the vacuum system and an ultimate pressure of 10^{-5} mm Hg with a leak rate of less than 1 micron/min was achieved.

All measurements were made in a plane at the approximate center of the specimen. For most tests, a uniform hot zone 1 to 2 inches long existed in the central section of the rod. Temperature was measured with a micro-optical pyrometer compensated for emissivity and sight glass effects (Figure 2). The pyrometer calibration curve was checked by measuring the apparent melting points of six pure metals fastened to the surface of the rod. Further checks were obtained by measuring evaporation rates of tungsten in vacuum which were compared with published evaporation rate data. The apparent temperature at which the rods melted also was determined for a calibration point. Rod diameters could be measured continuously with a filar micrometer eyepiece attached to a 4X telescope with an accuracy of ±0.0005 inch.

Pressure in the reaction vessel was measured continuously with a Decker Corporation Model 311 Absolute Pressure Meter. The instrument is calibrated from 0.01 to 30 mm in six ranges. Calibration of the gauge was checked weekly against a Wallace and Tiernan Model FA 160 Absolute Pressure Meter. This in turn was calibrated every two months against a secondary standard.

Procedure

Tests were conducted in air and oxygen under three different conditions: static, turbulent, and impinging. For static tests, the gas was admitted through a diffuser located in the main vacuum line. The system was pumped continuously and the gas leak rate was balanced against the pumping rate by micrometer leak valves to achieve any desired chamber pressure. This may be viewed as a quasi-static condition in which no measurable degree of turbulence or flow is created in the reaction chamber. Tests in turbulent atmospheres were conducted by admitting the gas leak directly into the reaction chamber while continuously pumping the system. The gas was introduced from a ring manifold concentric with the upper electrode with jets directed to the chamber walls. In high velocity flow (impinging) tests, gas was admitted from a ring manifold concentric with the specimen near the center

line. Twelve jets arranged like the spokes of a wheel were trained directly on the specimen surface at a distance of about one-half inch. Gas leak and pumping rates were adjusted to provide sonic velocity (1140 fps) at the exit plane of each jet. The dynamic pressure vs static chamber pressure was measured to determine gas velocity at the surface of the specimen. This varied from 200 to 900 fps depending on static chamber pressure. For all impinging tests, the pressure reported is the stagnation (total) pressure of oxygen at the surface.

The normal test procedure was to evacuate the system to less than 10^{-4} mm Hg and heat the rod for 10 minutes at 2000°C (3630°F). This conditioning treatment was used to degas the system and to provide a uniform metallurgical condition from specimen to specimen. A new specimen was used for each test. After conditioning, the temperature was adjusted to the run temperature and the gas admitted. Approximately 15 seconds were required to adjust pressure and temperature to the set values. Zero time was taken at the point when pressure reached about one-half the set value. This usually occurred within five seconds after admitting the gas. At the end of test, the gas leak and power were turned off simultaneously. Final time was taken at the point when pressure had dropped to one-half the set value.

Surface recession at the sight point is one-half the difference between initial and final diameters as measured by micrometers. Rates were calculated by the following relation:

$$R_W = \frac{49\left(\frac{D_o - D_f}{2}\right)}{t} \text{ gm/cm}^2\text{/min} \qquad (11)$$

where D_o and D_f are initial and final diameters in inches and t is total time in minutes. This relation also assumes a plane surface and does not take surface roughness into account. All rates are expressed as gm/cm^2/min and can be converted to surface recession in inches/min by dividing by 49. Initially, diameter was measured continuously by optical telescope and plotted as rate curves to obtain a mean or average rate. However, it was found that surface recession was perfectly linear with time so that the measurement of initial and final diameter was sufficient to establish an accurate rate. Total time of testing varied from 2 to 60 minutes depending on temperature and pressure.

RESULTS

Rate Reproducibility

Early in the experimental program it was discovered that oxidation rates varied markedly with crystallographic orientation (Figure 3). Originally smooth surfaces developed well-defined crystal facets after a few minutes exposure to air or oxygen at high temperature. The extent of faceting was temperature dependent and tended to become less pronounced on a macro scale at higher temperatures. At temperatures above 2800°C (5070°F) surfaces having a mirror finish were often produced. However, at high magnification even these surfaces were found to be far from smooth (Figure 3). Cylindrical single-crystal rods formed square cross sections and developed well-defined pyramids on the surface during oxidation at low pressure.

As shown in Figure 4, this behavior had an effect on the ability to measure rates in an accurate and reproducible manner. The rate of surface recession in gm/cm^2/min is indicated on the figure. For single-crystal rods, rates varied from 0.0235 across the "square" faces to 0.0310 across the "diagonal." For polycrystalline material the results were a roughened surface and uneven recession. It became particularly difficult to measure recession in coarse-grained tungsten due to the orientation effect. The rate for Grade 218 tungsten as shown in Figure 3 varied from 0.0302 to 0.0326 depending on the point of diameter measurement. In fine-grained material, Grade MK, the effect was averaged and specimens retained a fairly cylindrical cross section with minimum surface roughness. It is for this reason that the type MK fine-grained rod was selected for all test work.

The reproducibility of rate measurements in three different ranges of temperature and pressure for tungsten in turbulent oxygen is shown in Table 1. The two major sources of error were in control of specimen temperature and in measurement of pressure. The temperature can be measured to within ±5°C but is difficult to control due to changes in cross section of the rod with time. It is controlled by adjusting the current and tends to drift in an unpredictable manner. This will cause rate variations in consecutive tests as well as in tests conducted at later dates. The effect will be most pronounced in regions where rates are very sensitive to temperature changes. Thus, at 1627°C (2960°F) and 0.22 mm, most of the variation was due to errors in temperature. Pressure on the other hand is easy to control within close limits but the absolute value for any gauge reading may vary due to drift in gauge calibration. Experience revealed that significant drifts in calibration could occur within the course of several days. At least weekly calibration checks were required togive reproducible data. Consecutive tests proved quite reproducible and errors appeared mostly on a day to day basis. At 1960°C (3560°F) and 0.92 mm, five consecutive runs were reproducible to within ±1.4 percent. The day to day variation, most likely due to pressure shifts, resulted in a ±5 percent reproducibility. On the average, most rate data were reproducible to ±10 percent and were within calculated 2-sigma limits. The greatest variability was found at low temperatures where rates had a high temperature dependency.

Reactions in Air

In order to obtain rate data that could be applied directly to oxidation problems in aerospace structures, initial tests were conducted in static and moving air at low pressure. The preliminary results of this work which were published in 1961 (Reference 6) indicated that rates in static air reached a maximum at about 1750°C (3180°F) and then decreased with increasing temperature. This behavior has been studied in more detail at a pressure of 5 mm Hg and found to be the result of oxygen depletion which occurs under static or mildly turbulent conditions.

At the start of oxidation, the tungsten rapidly consumes oxygen which must be replenished by diffusion or mass transport from the air inlet port. If the system volume is small and the inlet port is remote from the chamber, rates of oxidation can be limited by transport of oxygen to the reaction chamber. Evidence that this, in effect, does occur under quasi-static conditions was provided by noting that rate curves were not linear with time for tests beyond 20 to 30 minutes. As shown in Figure 5, the slope of the rate curve in static air increased with time. The rate after 60 minutes of test was almost double that for the initial 10 minutes of test.

Samples of the atmosphere in the reaction vessel were taken at various time intervals to determine if changing concentration of oxygen was responsible for changes in rate. A gas sample of about 100 ml was drawn into an evacuated bulb and analyzed on a mass spectrometer to determine the ratio of oxygen to nitrogen. These ratios are expressed as percent 0_2 in the mixture. Samples were taken from near the surface of the specimen and near the wall of the chamber during test. Analysis of the air before test gave 0_2 values of 19 to 21percent. As shown in Figure 5, the "air" near the surface of the rod after five minutes of test contained 11.9 percent 0_2. Oxygen concentration at the chamber wall was slightly greater but still below normal, indicating that a general depletion of oxygen in the system had occurred. After 30 minutes, the concentration increased to 14.9 percent and at the end of one hour it had reached 16.3 percent. Thus, the increase of rate with time is shown to be due to an increase in oxygen concentration with time.

The oxygen content of the atmosphere is governed by a balance between the rate at which the specimen will consume oxygen and the rate at which oxygen can be supplied. If the rate of consumption at a given temperature exceeds the rate of transport in the system, the gas in the chamber is rapidly depleted of oxygen. The rate of consumption then drops until a balance is achieved. Normally, a steady-state condition where consumption rate equals transport rate should be reached at some reduced oxygen pressure. However, in this type of test the total surface

area and the average temperature of the specimen decrease with time. Constant temperature is maintained only at one point on the surface. The total rate of oxygen consumption at any pressure, therefore, will decrease with time, causing a shift in the balance point to higher oxygen pressures. The net effect is an increase in the rate of oxidation at the point of measurement where temperature is held constant.

If this analysis is correct, then the oxygen concentration in the gas should decrease with increasing specimen temperature. To verify this, samples of the atmosphere were taken for analysis after four minutes of testing at temperatures from 1350° to 3000°C (2460° to 5430°F). As shown in Figure 6, oxygen concentration decreased from a high of 19 percent at 1377°C (2510°F) to a low of 2.4 percent at 2590°C (4690°F).

These data are semi-quantitative and are not an absolute measure of oxygen concentration at the surface. They clearly show, however, that the rate maximum and the decrease in rate with increasing temperature in static air is due to oxygen depletion of the atmosphere. Such rate data are characteristic only of the system and do not reflect the true oxidation behavior of tungsten. For tests in air, it is necessary to increase the rate of transport of oxygen in the system until it is not rate-limiting over the temperature range of interest.

Increased rates of gas transport were achieved by admitting air directly to the reaction chamber to create turbulence, and by impinging air on the sample. The results of tests at 5 mm Hg are given in Figures 5 and 6. The rate of oxidation is significantly increased when turbulence is created; however, depletion of oxygen near the surface still occurs. This is shown by nonlinearity of the rate curve and by comparison with impinging air data. Rates in impinging air were linear with time and were higher than those in turbulent air. At 2400°C (4350°F), the impinging air rate was 20 times the static rate and 3 times the turbulent rate.

The rate data in impinging air at 5 mm Hg reveal three different regimes of oxidation behavior with increasing temperature:

1. From 1300° to 1760°C (2370° to 3200°F), rate increased with temperature by an Arrhenius relation with an apparent activation energy of 43,900 cal/mol.

2. From 1760° to 2630°C (3200° to 4770°F), rate increased with temperature by an Arrhenius relation with an apparent activation energy of 24,500 cal/mol.

3. Above 2630°C (4470°F), rate increased to a maximum at 2710°C (4910°F) and then decreased with increasing temperature. The apparent heat of activation decreased to zero and became negative with increasing temperature.

Reactions in Oxygen

To further explore the role of gas transport on oxidation behavior and to establish the validity of rates in impinging air, tests were made in static, turbulent, and impinging oxygen at a pressure of 1.1 mm Hg. These data are compared with those from tests in impinging air at 5 mm Hg (P_{O_2}=1.05 mm) in Figure 6. At an oxygen pressure of 1.05 to 1.1 mm Hg, the rates of oxidation from 1300° to 2350°C (2370° to 4260°F) as measured under four different conditions, static, turbulent, impinging oxygen, and impinging air, are identical. Gas velocity up to 900 fps had no measurable effect on kinetics. The data show that under these conditions gaseous transport of reactants and products is not rate-limiting. Data obtained in oxygen can be used directly to predict rates in moving air at velocities approaching Mach 1. Oxygen pressure under dynamic conditions must be taken as the total or stagnation pressure of oxygen at the surface. Although it is believed that no effect of velocity will be found at the higher flow rates characteristic of atmospheric re-entry, extrapolations of the data should be used with a degree of caution.

At oxygen pressure of 1.05 to 1.1 mm Hg and temperatures above 2300°C (4170°F), a marked dependency of rates on gas velocity was indicated. In static oxygen, the rate reached a maximum at 2465°C (4470°F) and

then decreased with rising temperature. In impinging oxygen at 230 fps, the rate maximum was reached at 2710°C (4910°F) followed by a similar drop with temperature. Although it is possible that the position of the rate maximum will be shifted to still higher temperatures with increased flow, the data suggest that a limiting condition is being approached. The rate maximum for impinging air (v = 900 fps) occurred at the same temperature as that for impinging oxygen (v = 230 fps) at equivalent oxygen pressures (Figure 6). The fourfold increase in velocity had little effect and actually resulted in lowered values of oxidation rate.

Pressure Dependency

The pressure dependency of the reaction of tungsten and oxygen was studied from 0.11 to 3.0 mm Hg at 130[illegible] 3350°C (2370° to 6060°F), and from 0.[illegible] 21 mm Hg at two selected temperatures. As shown in Figure 7, the curves of log rate vs 1/T have identical form at pressures from 0.11 to 3.0 mm Hg. The curves as drawn represent an average fit of all the data, and good agreement of data points with lines of uniform slope at each pressure is shown. The apparent heats of activation are the same as those reported for tests in impinging air: 43,900 cal/mol below the rate transition and 24,500 above. The apparent heats of activation at temperatures above the maximum rate range form -21,100 to -13,800 cal/mol, the slope decreasing with reduced pressure.

Since the slopes in the linear region are parallel for all pressures, the pressure dependency of reaction rate is constant over the temperature range of constant slope. The position of the curves shows that the pressure dependency is higher at temperatures above the rate transition point than at those below. Similarly, pressure dependency beyond the point of maximum rate is higher than that below.

Pressure dependency has been measured for each of these three regions as shown in Figure 8. A plot of log rate vs log pressure should be linear with a slope, N, equal to the pressure dependency of the reaction. In the low temperature (high activation energy) region, oxidation rate was proportional to oxygen pressure to the 0.59 power. At 1627°C (2960°F) in turbulent oxygen, pressure dependency deviated from 0.59 at about 2 to 3 mm Hg and became smaller with increasing pressure. Under impinging conditions, it was constant at 0.59 with increasing pressure to 10 mm Hg. This behavior suggests that transport of reactants or products can be a problem in oxygen atmospheres at pressures above 2 to 3 mm Hg. At 1627°C (2960°F) and a pressure of 0.2 mm Hg, the rate transition point is crossed and pressure dependency at lower pressures increased to the value corresponding to that of the second region.

In the second (low activation energy) region, pressure dependency at 1960°C (3560°F) was constant at 0.82 from 0.1 to 10 mm Hg. The same value was found in turbulent and impinging oxygen. At about 8 mm Hg pressure, the rate transition point is crossed and pressure dependency at higher pressures will drop to a value of 0.59 which is characteristic of the first region. Thus, it can be seen that at constant temperature the dependency of rate on pressure will change whenever the point of rate transition is crossed. This must be taken into account when data are to be extrapolated to higher or lower pressures from any given point.

The pressure dependency at a temperature beyond that of the rate maximum was not constant with pressure under turbulent conditions. At 2984°C (5400°F), the value of N approached 1 at pressures below 0.10 mm and approached 0.8 at a pressure of 1 mm Hg. In impinging oxygen, the value of N was close to 1.0, indicating a linear dependency on pressure in this region.

DISCUSSION

There are many similarities between the results of this investigation and those of others conducted at much lower pressures. We used Eisinger's and Anderson's data to compare the effect of temperature on oxidation rate at oxygen pressures from 10^{-6} to 3.0 mm Hg (Figure 9). The low-temperature portion of Eisinger's data fit an Arrhenius rate equation with an apparent activation

energy of about 25,000 cal/mol. The slope of the second region from our work (24,500 cal/mol) is in excellent agreement with that value. Similar values were reported by Langmuir and Becker. None of the other investigations at low pressure detected the rate transition to a high activation energy region at lower temperatures. However, if the temperature for rate transition as determined in this investigation is extrapolated to lower pressures, it can be seen that the other investigations were not conducted at sufficiently low temperatures to detect the break.

One possible exception is the work of Langmuir which was conducted at low enough temperatures but in which no break was found. Direct comparison with Langmuir's data may not be valid, however, since the pressure was changing from 5×10^{-2} to 2×10^{-4} mm Hg during his test. All the other studies were made at pressures which were constant or varied over a small range. In order to develop a complete picture of oxidation behavior it will be necessary to study reactions at pressures below 10^{-1} mm Hg in the temperature range where a rate transition would be expected. The existence or absence of such a break will have an important bearing on any mechanistic interpretation of results.

The position and shape of the curves in Figure 9 suggests a common behavior pattern over the entire range of pressures. If this is true, then it should be possible to correlate the rates and the position of the maximum rate with pressure and temperature. The rate of oxidation at the point of maximum rate for these three independent investigations is correlated with oxygen pressure in Figure 10. The agreement is surprisingly good, considering the very wide range of pressures and rates and the differences in experimental procedure. This correlation shows that the maximum rate of oxidation is close to a linear function of oxygen pressure from 10^{-6} to 1 mm Hg. The maximum rate can be predicted by the following simple relation:

$$R_{max} = 0.295\ P_{O_2}^{1.08}\ gm/cm^2/min \qquad (12)$$

The temperature at which the rate maximum will occur is plotted vs the oxygen pressure in Figure 11. It can be seen again that an excellent correlation exists between the results of three different investigations. The values from this investigation in turbulent oxygen deviate from the linear relationship at pressures above 0.11 mm Hg. With impingement of oxygen, the point of maximum rate shifted to higher temperature and approached the linear relation. The relation between temperature and pressure for the point of maximum rate can be expressed as follows:

$$P_{O_2} = 2.537 \times 10^{7} \exp(-104{,}000/RT) \qquad (13)$$

Further correlation of the results of the three investigations was obtained by the comparison of calculated and experimental rates. By using an empirical equation fitted to the experimental results of this investigation (P_{O_2} = 0.11 to 3.0 mm Hg), the rate of oxidation was calculated for a point on the linear portion of the log rate vs 1/T curves for five different pressures from 1.2×10^{-6} to 3.0 mm Hg. The results together with values calculated from the equation derived by Becker from theoretical considerations are presented in Table 2. An excellent correlation between measured rates and those calculated from the equation derived from our data is shown. Calculated and experimental rates agree with ±20 percent over a three million-fold range of pressure and a 950°C range of temperature. The magnitude of rates which are accurately predicted varies by a factor of almost ten million. Values calculated from Becker's equation give fair agreement at low pressure but deviate from measured rates at higher pressure. They are too high by a factor of 10 at pressures of 0.1 to 3.0 mm Hg although this is reasonable agreement considering the range of values. Langmuir's equation similarly yields increasingly poor fit with measured rates at increased pressure.

The foregoing comparisons clearly suggest that a common mechanism exists in oxidation of tungsten over an extremely wide range of temperature and pressure. Becker has proposed a mechanism based on the fractional

coverage of adsorbed oxygen atoms. Atoms are envisioned as chemisorbing in two distinct layers with the energies of adsorption or desorption being lower in the second layer than in the first. Similarly, the energy of formation and desorption of the oxide is estimated to be lower in the second layer. The transition from two layers to one layer is postulated to occur in the region of the rate maximum. The theory predicts that the rate should decrease with increasing temperature (energy of -27500 cal/mol) at low coverage ($\theta < 1$) and increase with pressure to the 1.5 power. At high coverage ($\theta \sim 1$), the rate should increase with temperature (energy of +25300 cal/mol) and be a linear function of pressure. The relation of pressure and temperature for a monolayer coverage ($\theta = 1$) as derived by Becker is shown in Figure 11. Good agreement with the curve for the points of maximum rate is indicated. The slope of 106,000 cal/mol is defined by Becker as the heat of adsorption of oxygen on tungsten when the oxygen atom coverage is a monolayer or less.

Although Becker's theory predicts the correct dependence of rate on temperature in the vicinity of the rate maximum, it cannot be accepted as a valid description of reaction mechanism without additional proof. Any mechanistic explanation of the experimental data must be consistent with all aspects of the observed behavior over the entire range of pressure. Specifically, theory must account for the following observations:

1. The rate of oxidation is a fractional rather than linear order of oxygen pressure. This fact most likely accounts for the inability of previously derived rate equations to accurately predict rates over a wide range of pressure.

2. The temperature and pressure dependency of rate at temperatures below the maximum point change as the temperature is decreased.

3. The maximum rate occurs at anomalously low temperatures at high pressures and its position is influenced by gas velocity. (In this case, velocity per se may not be the factor responsible for the change since increased velocity is accompanied by decreased gas temperature.)

4. The rate is dependent on crystal orientation; however, the magnitude of dependence decreases with increased temperature.

The overall problem of developing an adequate mechanistic explanation of observed rate data is complicated by micro and macro faceting of the surface due to orientation effects. Three sources of error result in a significant difference between measured and true rates of the reaction. The surface after a few-minutes test resembles a mountain range (Figure 3). Peaks and valleys are formed as each crystal orientation exposed to the gas assumes its own characteristic rate of recession. On close inspection, it can be seen that the surface consists of a multitude of small plane areas that intersect at well-defined crystallographic angles. Since the amount of metal removed is measured at the peaks, the weight loss is less than the true value by the amount of material which has been removed from the valleys. If the grain size is small and the surface recession large, this difference becomes negligible. A more serious error results from the fact that the measured rate is based on recession of the peaks rather than on recession of the plane faces where the reaction occurs. A geometrical analysis will show that the peak of a pyramid which is growing shorter by recession of its four plane faces will be receding at a faster rate than each face. Thus the measured rate of recession is higher than the true rate of the reaction. The major error results, however, when the rate per unit area is based on an assumed plane surface area which is much smaller than the true surface area exposed to the gas.

The considerations given above imply that when marked faceting of the surface occurs, the measured rate of reaction is significantly larger than the true rate of reaction. Since the degree of faceting decreases with increasing temperature, significant changes in slope and measured values of activation energy and pressure dependency can occur. This problem has no bearing on the value of the data for engineering purposes. However, if the data are to be used in developing a mechanistic explanation, a serious question as to the validity of calculations can be raised. A study of rate as a function of

orientation and true surface area would be helpful in resolving the questions that have been raised. In addition, continuing work on adsorption and desorption, effects of gas temperature and velocity, and identification of oxide vapor species is needed to develop a completely adequate theory.

The results of this investigation are presented in summary form in Figure 12 and fill a primary need for engineering data for many potential uses of tungsten. They are expressed as equations which define (1) the boundaries where changes in rate behavior occur and (2) the rates of oxidation within each region of uniform behavior as a function of pressure and temperature. A low temperature boundary that describes the limits for formation of a visible oxide film on tungsten also is presented. Due to a large change in emissivity, it was possible to determine the maximum temperature for any pressure at which solid oxide exists as a visible film or scale on tungsten. The oxide has been tentatively identified as $W_{18}O_{49}$ by its characteristic red-violet color. This is an important boundary for applications in radiatively cooled structures since a major change in emissivity occurs. The defining equation is in terms of oxygen pressure; however, in air, the boundary is a function of the total pressure. It is not known whether a change in temperature dependency of rate will occur on crossing this boundary.

The applicability of laboratory test data to performance in operational environments is always an important consideration where marked differences are apparent. The data presented encompass the effects of pressure, temperature, and flow. The range of applicability and limitations of the data have been cited. Two important factors in atmospheric re-entry applications, however, have not been incorporated in this work. These are the gas temperature and molecular dissociation. The gas which strikes the surface of a re-entry structure has been heated to very high temperatures in passing through the shock wave, and the oxygen probably is dissociated. The laboratory studies are based on the reaction of a heated surface with a molecular gas that is close to room temperature at low pressure. Practically all other oxidation data are from tests where the gas and metal are at the same temperature. If the rate is determined by a reaction on the surface rather than by the impact of gas molecules with the surface, then the effect of gas temperature usually will be negligible. Langmuir found that reaction rate was determined by the temperature of the metal and was not affected by variations in gas temperature over a 300°K range. Additional work is needed, however, to prove conclusively the independence of rate on gas temperature.

The effect of dissociation of the gas before striking the surface is unknown and is a factor that should be investigated. If the heat of adsorption of oxygen is a factor in determining rates as proposed by Becker, then dissociation would have a significant effect.

CONCLUSIONS

1. The rate of oxidation of tungsten from 1300° to 3350°C (2370° to 6060°F) in air or oxygen at pressures below 5 mm Hg is equal for the same partial pressure of oxygen. Rate is a function of metal temperature, oxygen pressure, and crystal orientation.

2. In static or slowly moving air at all pressures and in oxygen at pressures above 3.0 mm Hg, rates may be limited by transport of oxygen to the surface. High velocity flow is needed to provide a known and constant pressure of oxygen. When a constant oxygen pressure is maintained at the metal surface, gas velocity up to Mach 1 has no effect on the rate of reaction.

3. At temperatures above a boundary defined by

$$P_{O_2} = 1.161 \times 10^{14} \exp(-93500/RT)$$

a visible oxide scale does not form on tungsten in oxygen at low pressure. In air, the boundary is defined by the total pressure.

4. At temperatures above the oxide-scale boundary, rate of metal loss is described by the relation

$$R_w = 2385\ P_{O_2}^{0.59} \exp(-43800/RT)\ gm/cm^2/min$$

5. A transition in rate behavior occurs at a boundary defined by

$$P_{O_2} = 1.082 \times 10^{10} \exp(-93500/RT)$$

At temperatures above this transition, the rate of tungsten loss is described by

$$R_W = 20\ P^{0.82} \exp(-24500/RT)\ gm/cm^2/min$$

6. The rate of oxidation reaches a maximum at a temperature defined by

$$P_{O_2} = 2.537 \times 10^{7} \exp(-104000/RT)$$

The maximum rate of metal loss at any pressure is given by the relation

$$R_W = 0.295\ P_{O_2}^{1.08}\ gm/cm^2/min$$

At pressure above 10^{-1} mm Hg, behavior near the temperature of maximum rate is influenced by gas velocity.

7. At temperatures above the rate maximum, the rate of metal loss increases as a linear function of oxygen pressure and decreases with temperature.

8. A commom mechanism appears to exist in the oxidation behavior of tungsten at high temperatures in oxygen at pressures from 10^{-6} to at least 10 mm Hg. The empirical rate quations in conclusions 5 and 6 above will accurately predict rates which vary by a factor of up to 10 million in this pressure range.

REFFRENCES

1. R. A. Perkins, L. A. Riedinger, and S. Sokolsky. Seventh Symposium on Ballistic Missile and Space Technology. August 1962.

2. I. Langmuir. J. Am. Chem. Soc. Vol. 35, 2. (1913). p. 105

3. J. Eisinger, J. Chem. Phys. Vol. 30. (1959). p. 412.

4. J. Becker, E. Becker, and R. Brandes. J. App. Phys. Vol. 32, 3. (1961). p. 411.

5. H. Anderson. Ph.D. Thesis, Univ. of Calif. Lawrence Radiation Laboratory, Contract No. W-7405-eng-48. April 1962.

6. R. Perkins and D. Crooks, J. of Metals. July 1961, p. 490.

7. P. Blackburn, K. Andrew, E. Gulbransen, and F. Brassart. WADC TR 59-575, Part II. Wright Air Development Center, Wright-Patterson Air Force Base, Ohio. June 1961.

8. J. N. Ong. Research Laboratory Report, Aeronutronic Division, Ford Motor Co. October 1961.

9. C. J. Smithells. Metals Reference Book. Butterworths, Washington, 1962.

TABLE 1

REPRODUCIBILITY OF OXIDATION RATES

TURBULENT OXYGEN

1627°C - 0.22 MM HG

DATE - 5/17/62	5/21/62	7/31/62
0.00717	0.00882	0.00874
	0.00980	0.00923

AVG. - 0.00875 ± 18% 2σ = 20%

1960°C - 0.92 MM HG

DATE - 7/30/62	9/14/62	9/18/62
0.0756	0.0716	0.0737
0.0777		0.0733
0.0763		
0.0767		
0.0765		

AVG. - 0.0752 ± 5% 2σ = 5.2%

2755°C - 3.0 MM HG

DATE - 6/20/62	9/11/62	9/18/62
0.465	0.402	0.420
	0.409	

AVG. - 0.424 ± 9.7% 2σ = 11.6%

TABLE 2

CALCULATED VS EXPERIMENTAL RATES AT LOW OXYGEN PRESSURE

EXPERIMENTAL				CALCULATED	
SOURCE	PRESSURE MM HG	TEMPERATURE °C	RATE $GM/CM^2/MIN$	A THIS WORK	B BECKER (4)
THIS WORK	3.0	2077	2.57×10^{-1}	2.63×10^{-1}	33.2×10^{-1}
THIS WORK	1.1×10^{-1}	2077	1.73×10^{-2}	1.72×10^{-2}	12.2×10^{-2}
ANDERSON(5)	7.6×10^{-4}	1677	1.10×10^{-4}	0.99×10^{-4}	2.76×10^{-4}
EISINGER(3)	1.2×10^{-5}	1127	2.31×10^{-7}	2.81×10^{-7}	3.31×10^{-7}
EISINGER(3)	1.2×10^{-6}	1127	4.87×10^{-8}	4.18×10^{-8}	3.31×10^{-8}

A) $R_w = 20 P^{0.82} EXP. \frac{-24800}{RT}$ B) $R_w = 256 P^{1.0} EXP. \frac{-25400}{RT}$

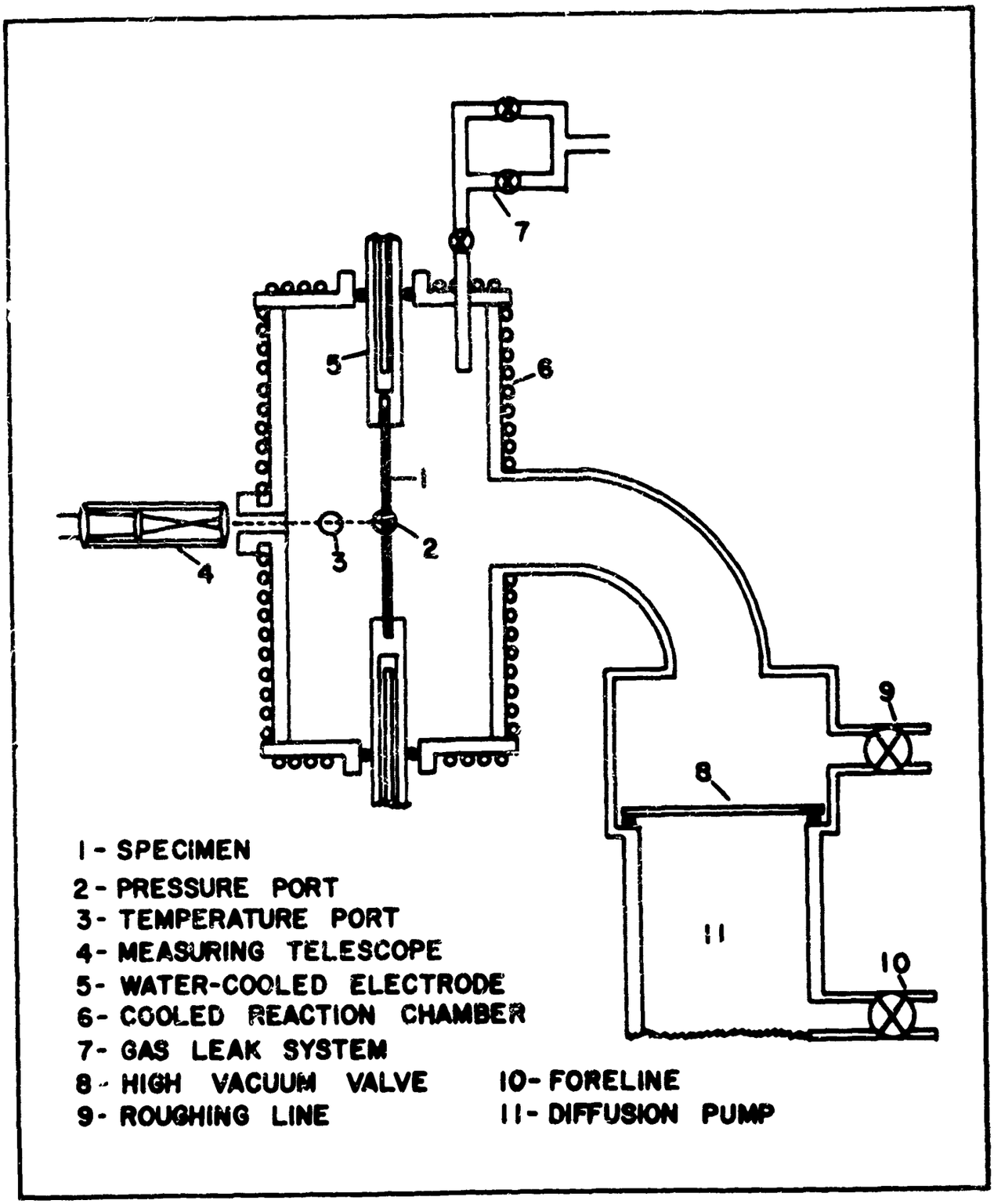

FIGURE 1. Oxidation Rate Apparatus

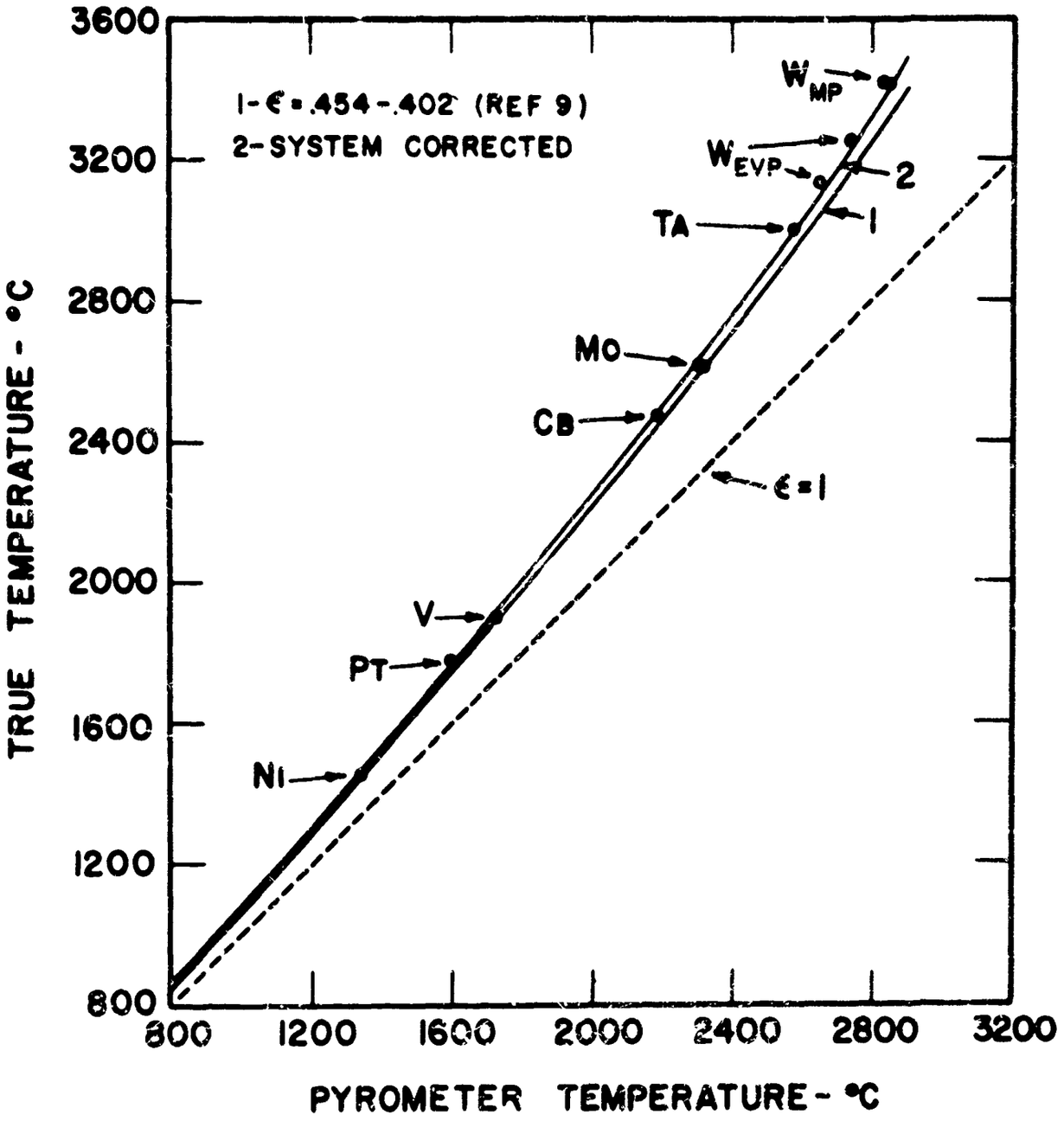

FIGURE 2. Pyrometer vs True Temperature Calibration

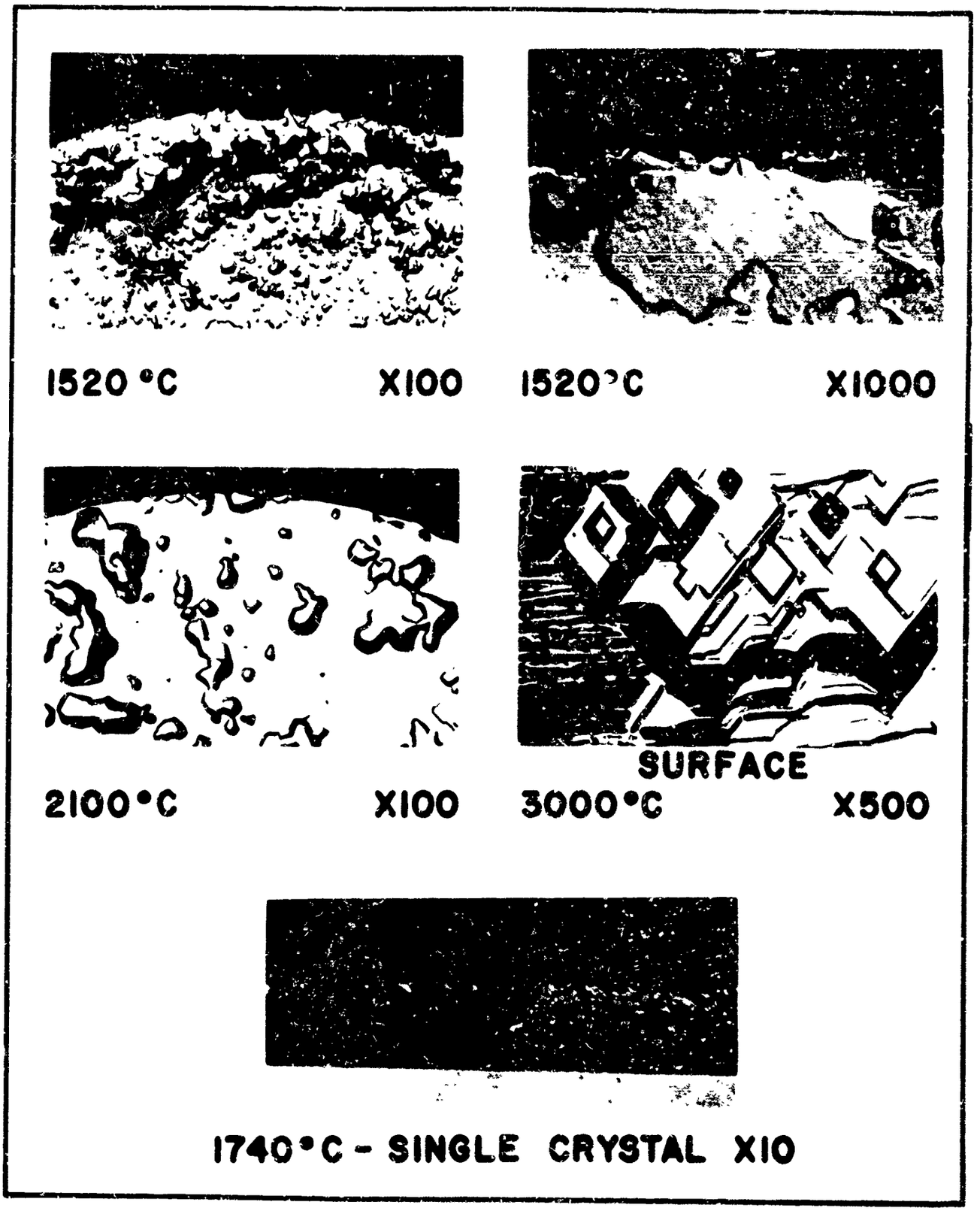

FIGURE 3. Orientation Dependence of Rate at Low Pressure

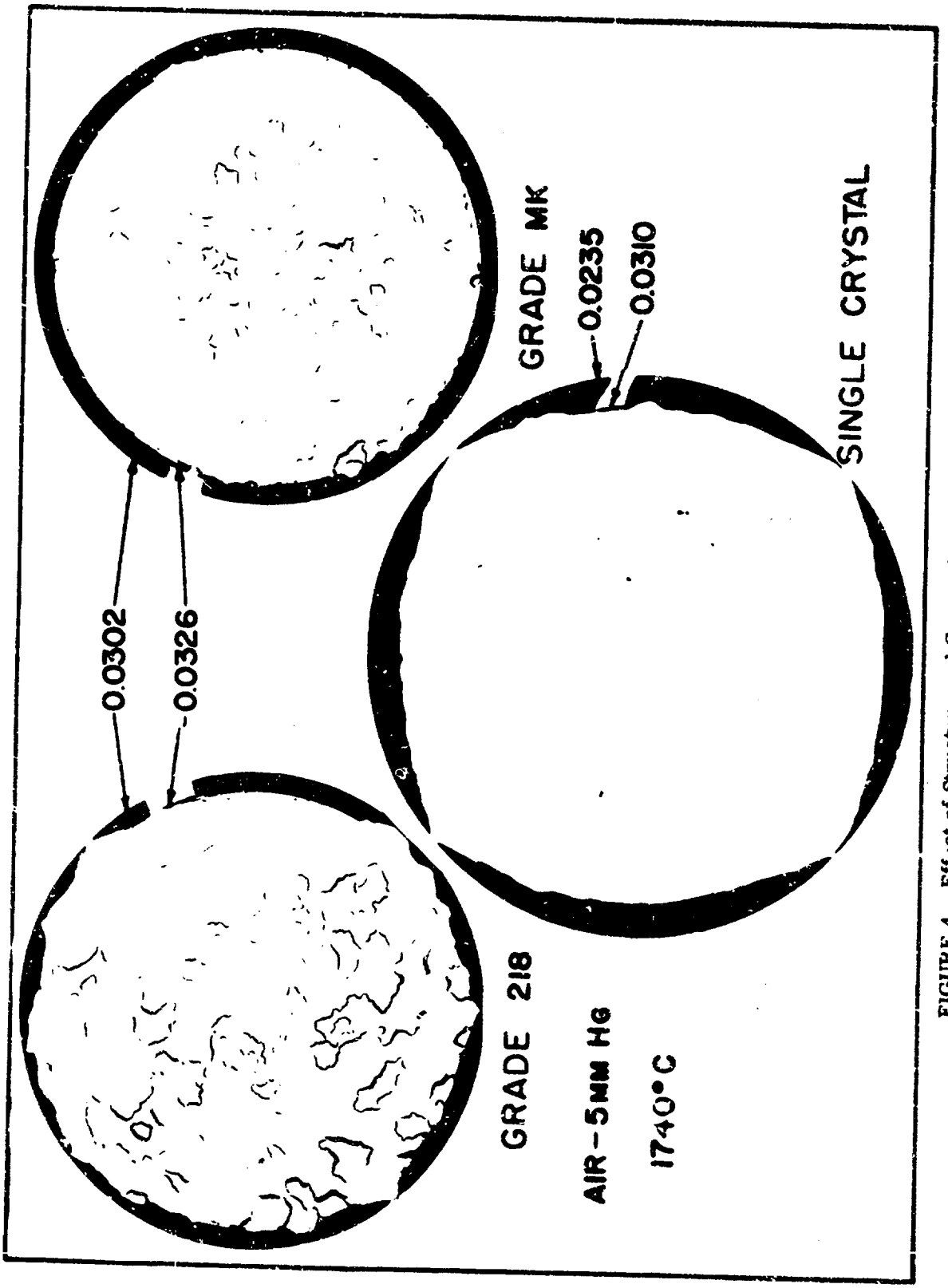

FIGURE 4. Effect of Structure and Composition on Rate Measurements

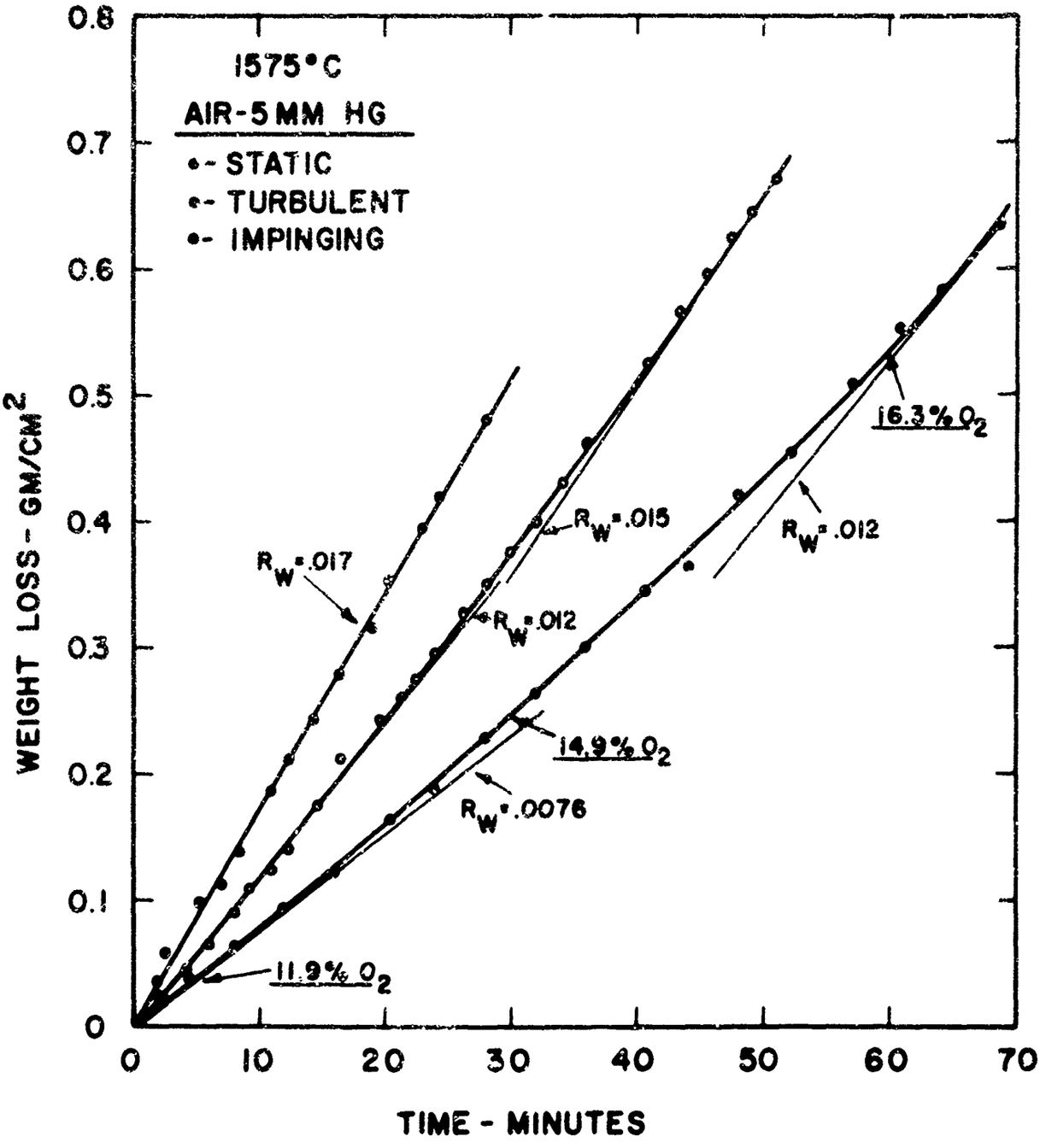

FIGURE 5. Effect of Gas Dynamics on Oxidation Rates in Air

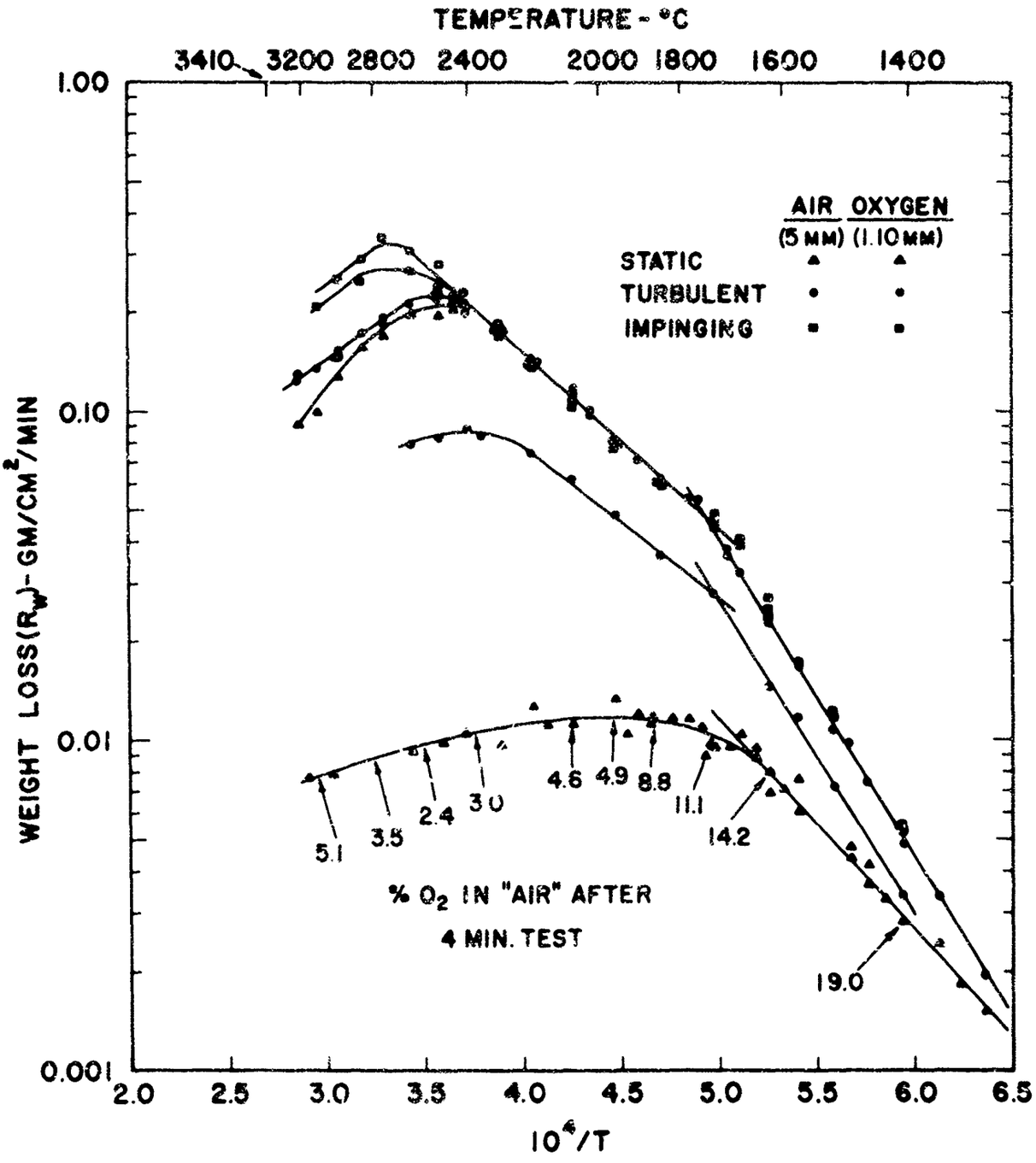

FIGURE 6. Comparison of Oxidation Behavior in Air and Oxygen

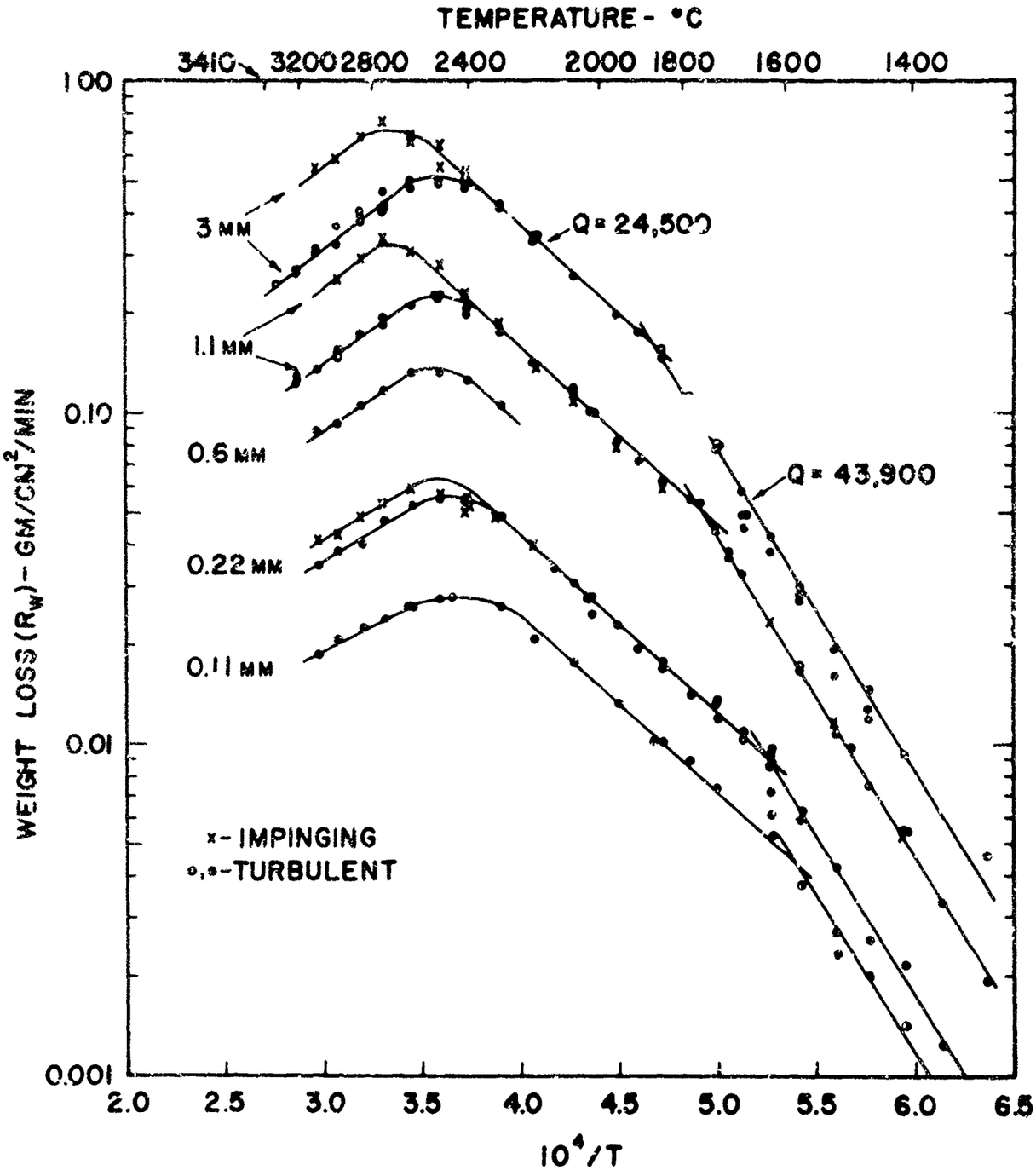

FIGURE 7. Results of Tests from 1300° to 3350°C in Oxygen at 0.11 to 3.0 mm Hg

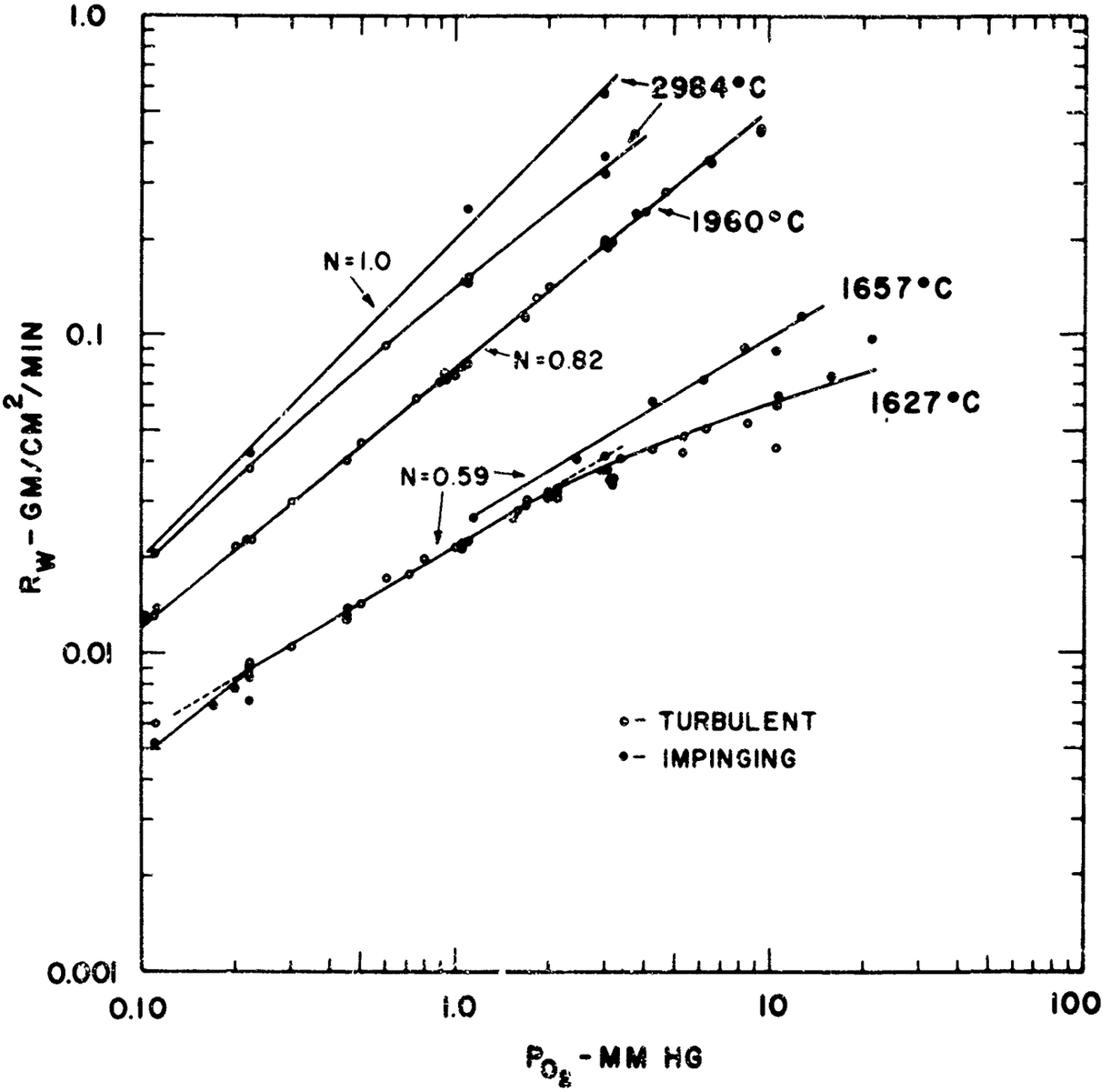

FIGURE 8. Pressure Dependency of Rate in Oxygen

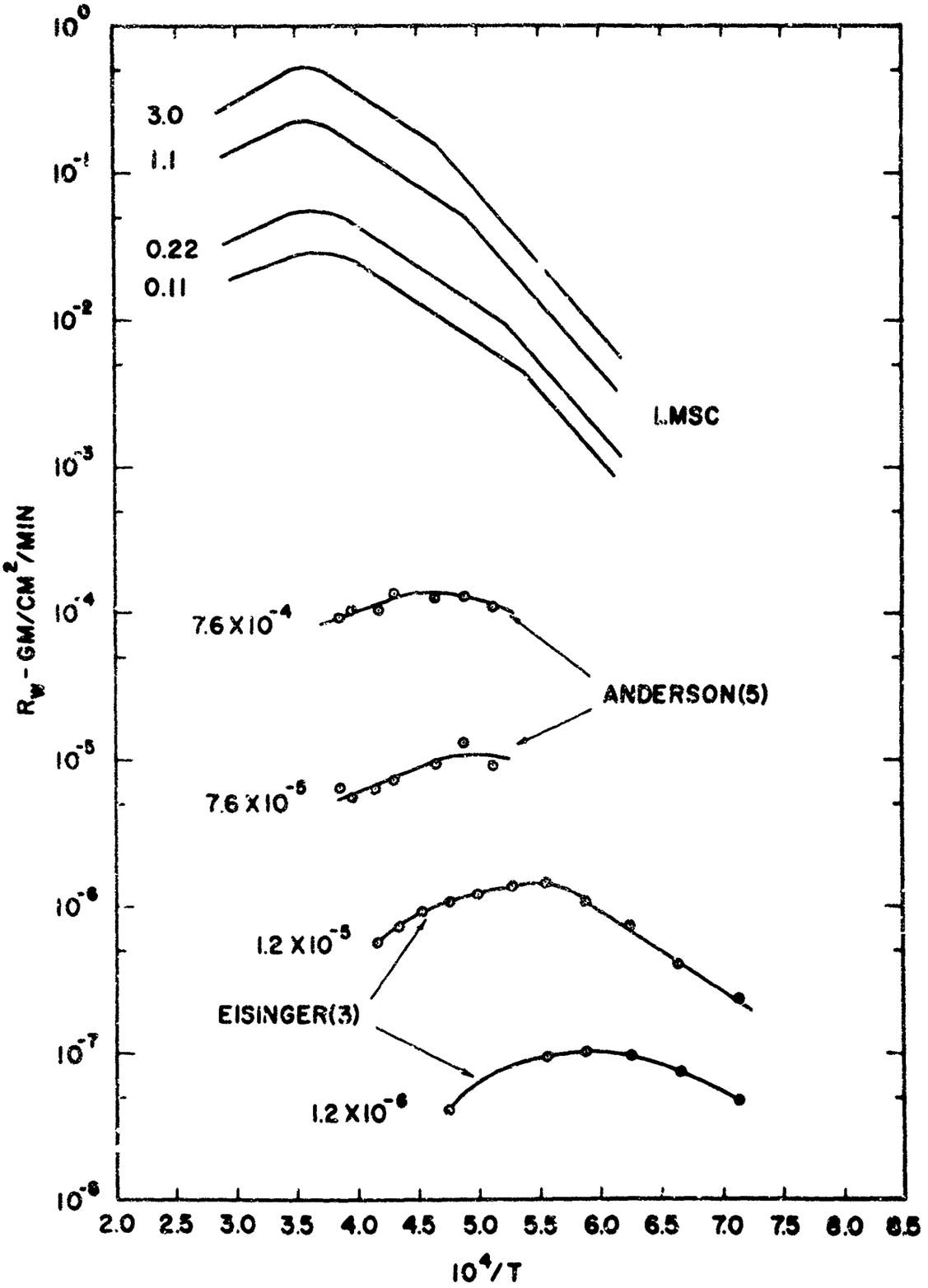

FIGURE 9. Comparison of Low Pressure Oxidation Rate Data

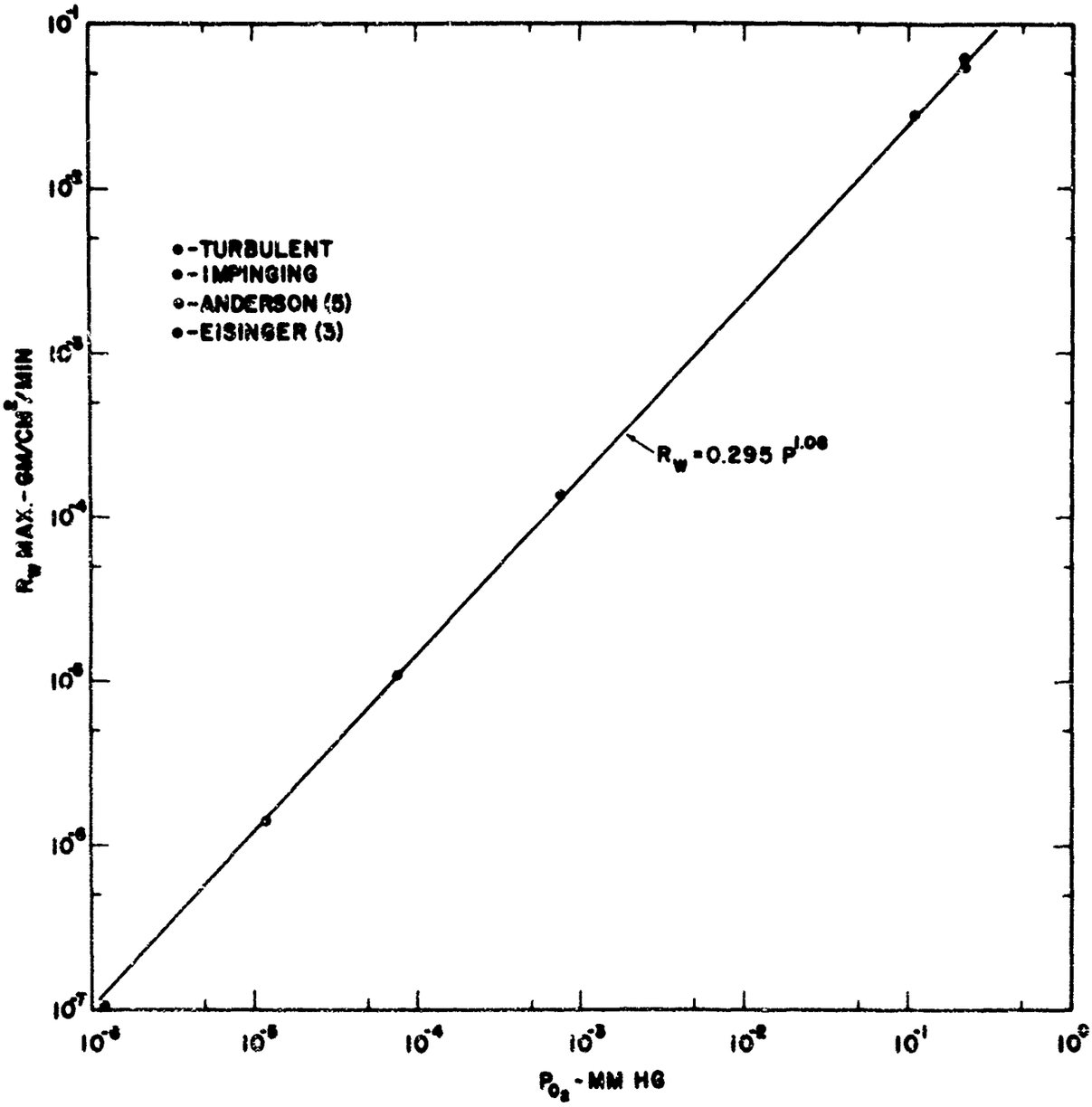

FIGURE 10. Pressure Dependency of Maximum Rate of Oxidation

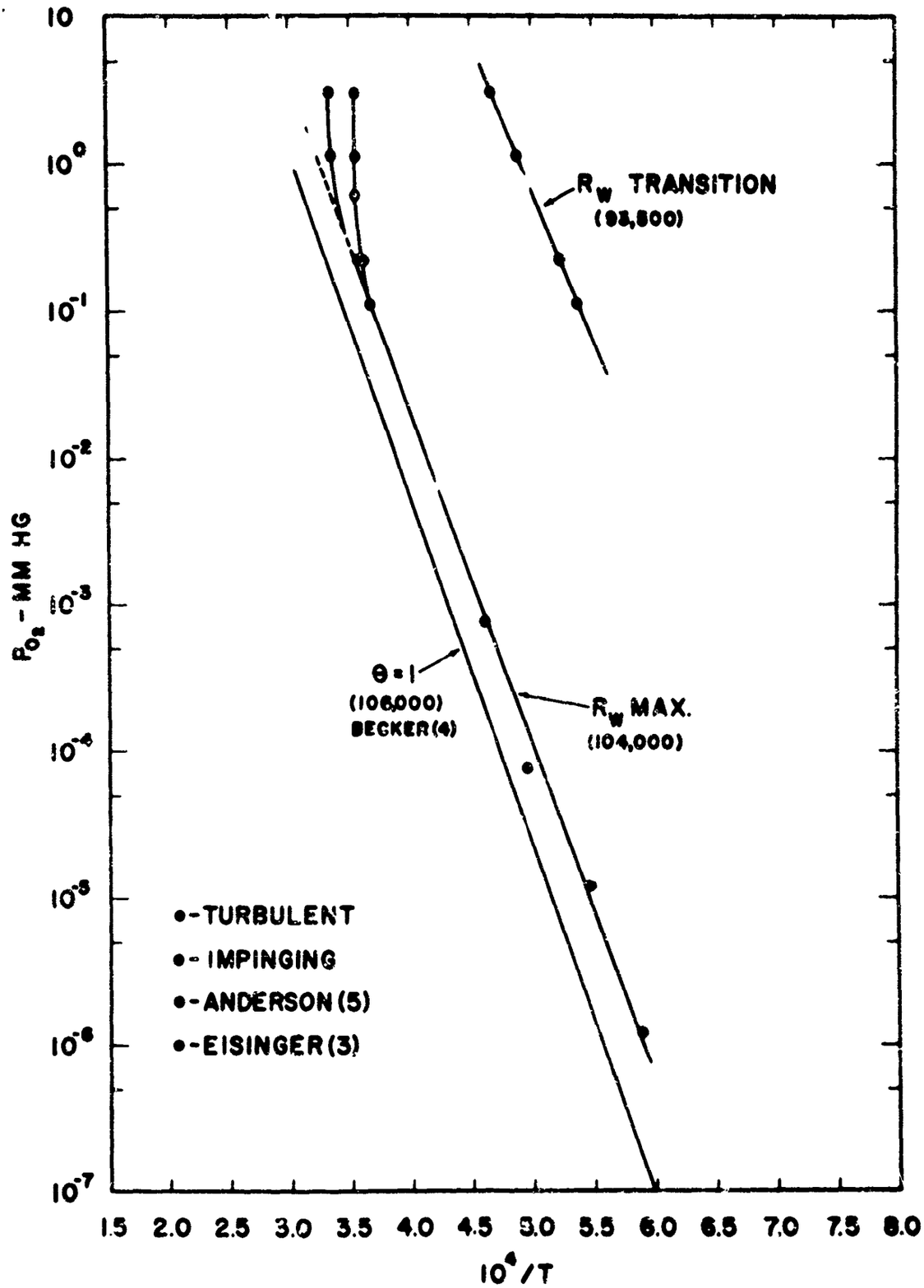

FIGURE 11. Temperature-Pressure Relation for Rate Maximum and Transition Points

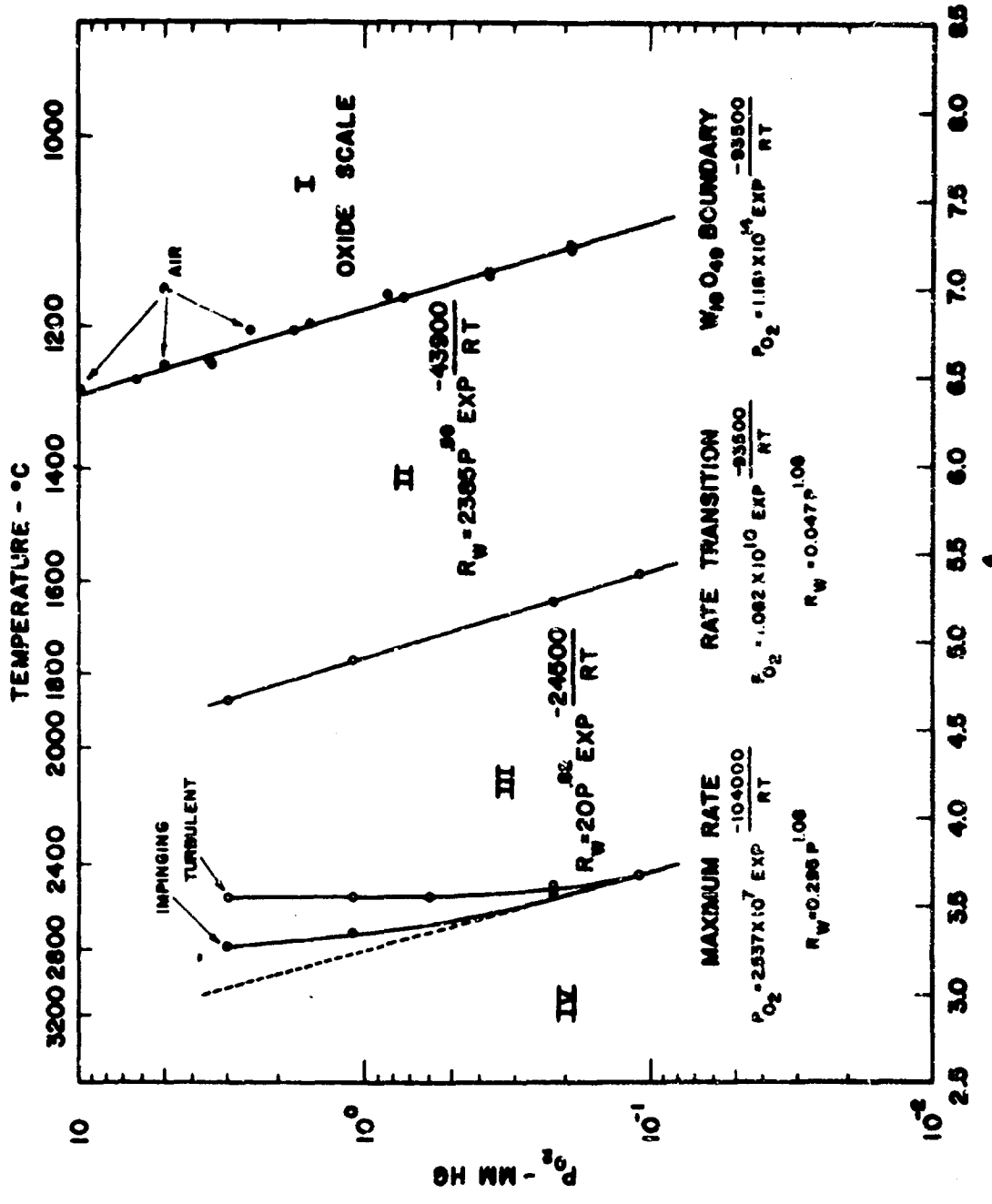

FIGURE 12. Summary of Oxidation Behavior at Low Pressure and High Temperature

OXIDATION BEHAVIOR OF TANTALUM AND NIOBIUM AT HIGH TEMPERATURES

Per Kofstad*

INTRODUCTION

A major shortcoming of tantalum and niobium as high-temperature materials is their pronounced reactivity with oxygen and other gases at elevated temperatures. In considering applications of tantalum and niobium and their alloys as constructional materials at high temperatures a detailed knowledge and understanding of the oxidation behavior of these metals is required.

The oxidation behavior of niobium and tantalum have many features in common. Both exhibit a complex oxidation behavior which involves oxygen dissolution in the metal and formation of various oxide phases which include those of metallic and higher oxides. The relative importance of the various part-processes which constitute the total oxidation reaction is dependent on temperature, oxygen pressure, and time of oxidation.

Studies at this laboratory on the oxidation of tantalum and niobium are described and discussed in this paper. Tantalum is considered first because in the author's opinion the oxidation behavior of this metal is somewhat better understood at present. Niobium is considered in less detail since many of the more general conclusions and interpretations for tantalum also apply to niobium. More detailed reports on various aspects of the oxidation behavior of these metals have been published elsewhere (References 1 to 8).

OXIDATION OF TANTALUM

Oxidation of Tantalum at 500° to 600°C

Oxidation of tantalum below 600°C initially approximates a parabolic stage. This is followed by a breakaway oxidation which becomes linear. These features are shown in Figure 1 which gives results of gravimetric oxidation rate measurements in 1 atm of O_2 at 500° to 575°C (Reference 4). The parabolic "incubation" period for the breakaway oxidation becomes shorter with increasing temperature. At and above 600°C the incubation period becomes too short to be observed in the gravimetric measurements.

Oxidation during Incubation

During the incubation period oxidation involves oxygen dissolution in the metal and formation of the metallic oxide phases of tantalum (suboxides) TaO_y and TaO_z (References 4 and 5). TaO_y has only been observed after oxidation at and below 500°C. During the early stages of the incubation period no Ta_2O_5 has been detected on the metal surface. The initial oxidation of tantalum may thus be described by the following equations:

$$1/2\,O_2^{(g)} \xrightarrow{\text{chemisorption}} O_{\text{chemisorbed}} \qquad (1)$$

$$O_{chem} + Ta \xrightarrow{\text{diffusion}} Ta\text{-}O \text{ solid sol'n} \qquad (2)$$

and

$$Ta\text{-}O \text{ sol. sol'n} \longrightarrow TaO_y \longrightarrow TaO_z \qquad (3)$$

The metallic oxide phases grow as oxide platelets and wedges extending into the metal from the surface. TaO_z grows as platelets parallel to the 320 sets of planes of the metal (References 7 and 9). An example of TaO_z formation is shown in Figure 2, which

* Central Institute for Industrial Research (Blindern, Oslo, Norway).

refers to a tantalum specimen oxidized for 1300 minutes at 600°C and 0.01 Torr O_2 (Reference 7).

Microhardness traverses on oxidized specimens have shown that the oxygen penetration into the metal agrees with calculated values (Reference 10) using the diffusion coefficient of oxygen in tantalum, $D = 0.01 \exp(-27{,}700/RT)$, as determined from internal friction measurements. Furthermore, lattice parameter measurements directly on oxidized surfaces (References 4 and 5) have indicated that during the incubation period the oxygen concentration at the metal surface reaches 5 to 7 atomic weight percent.

In terms of the above mechanism it is of interest to compare theoretically estimated weight gains due to oxygen dissolution alone with the experimentally measured values. The amount of dissolved oxygen may be estimated from the equation (Reference 11)

$$n = 1.1284\sqrt{Dt}\,(c_s - c_0) \qquad (4)$$

where c_s represents the oxygen concentration at the metal surface and c_0 the oxygen impurity content in the metal. By using a value of 6 atomic weight percent for the oxygen concentration at the metal surface, the calculated weight gain due to oxygen dissolution at 500°C is given by the broken line in Figure 1. The estimated and measured weight gains show agreement, thus confirming the proposed mechanism. The weight gain above that of the oxygen dissolution is furthermore concluded to reflect the formation of TaO_y and TaO_z.

It should be noted that oxygen concentration of 5 to 7 atomic weight percent exceeds the equilibrium solubility of oxygen in tantalum at these temperatures. Vaughan et al. (Reference 12) found an oxygen solubility of 2.5 atomic weight percent at 500°C. However, this latter solubility refers to tantalum-oxygen solid solutions in equilibrium with Ta_2O_5. The presently observed concentration (5 to 7) has been found either when only traces of or when no Ta_2O_5 at all has been detected on the surface. Thus the high oxygen concentrations probably pertain to an equilibrium of Ta-O solid solutions with TaO_z. This again infers that TaO_z is metastable. It should also be noted that supersaturations of oxygen in tantalum are necessary to initiate oxide nucleation. During later stages of the reaction and as large amounts of Ta_2O_5 are formed on the surface, the oxygen concentration at the metal surface decreases and probably approaches the solubility characteristic of Ta-O solid solutions in equilibrium with Ta_2O_5 (References 4 and 5).

Breakaway Oxidation

The first traces of Ta_2O_5 are formed during the later stages of the incubation period and occur in spots and local areas on the surface. Breakaway oxidation is associated with heavy Ta_2O_5 formation. Furthermore, electron micrographs and optical examination have revealed numerous cracks and blisters indicating that the oxide has little or no protective properties (Reference 4). If the surface oxide is removed the characteristic pattern of TaO_z is revealed, as shown in Figure 2. These studies also indicate that Ta_2O_5 is formed on the TaO_z platelets (Reference 7). This oxide growth results in separate Ta_2O_5 nuclei and it is concluded that this is the cause of the discontinuous and porous Ta_2O_5 scale under these conditions.

Oxidation at 800° to 1000°C

Above 800°C a change in the kinetics takes place; initial oxidation again becomes parabolic, and is followed by an approximately linear oxidation (Reference 8). The initial parabolic oxidation at various oxygen pressures at 900°C is shown in Figure 3.

Concurrently with the change to a parabolic-linear oxidation above 800°C there is a change in the reaction scheme. Although

TaO_z is the intermediate reaction product below 800°C, X-ray diffraction measurements indicate that TaO gradually becomes the intermediate reaction product above this temperature. However, TaO is only present in trace or small amounts at the metal-oxide interface (Reference 8).

At these temperatures (above 800°C) X-ray diffraction measurements of the tantalum lattice parameter indicate that the oxygen concentration at the metal surface is approximately equal to the solubility limit for Ta-O solid solutions in equilibrium with Ta_2O_5. On this basis calculated weight gains due to oxygen dissolution alone have been estimated by the use of Equation 4. The values are indicated by the broken line in Figure 3. The weight gain due to oxygen dissolution is of minor importance compared to the total weight gain except at the very initial stage of the reaction. However, the importance of oxygen dissolution increases with decreasing oxygen pressure.

Initial Parabolic Oxidation Above 800°C

During the parabolic stage above 800°C Ta_2O_5 is the main reaction product, and it is concluded that the initial parabolic oxidation above 800°C is governed by a rate-determining transport of oxygen ions through the Ta_2O_5 scale according to a Wagner-type mechanism.

The parabolic rate constants for Ta_2O_5 formation at 900° and 1000°C are dependent on oxygen pressure, as shown in Figure 4. At 900°C the parabolic rate constant is proportional to $p_{O_2}^{1/3.8}$ at and above 1 Torr O_2. From 1 to 0.1 Torr O_2 there is a relatively large drop in the value of the parabolic rate constant, and at 0.1 to 0.01 Torr O_2 the parabolic rate constant is essentially independent of oxygen pressure. At 1000°C a similar change in oxygen pressure dependence takes place between 10 and 1 Torr O_2.

The change in oxygen pressure dependence is probably related to the defect structure of Ta_2O_5 (Reference 13). This oxide has been found to be a p-conductor at oxygen pressures close to 1 atm O_2 and an n-conductor at lower oxygen pressures. It has been proposed that Ta_2O_5 has an anti-Frenkel defect structure involving oxygen interstitials (p-type) and oxygen vacancies (n-type). At 900° and 1000°C the p-n transitions take place at 0.8 and 3.5 Torr O_2, respectively, and the transition pressures are indicated by the stippled vertical lines in Figure 4. The results suggest that the change in oxygen pressure dependence of the parabolic rate constant occurs at oxygen pressures corresponding to those of the p-n transitions, and the results are thus in general agreement with Wagner's oxidation theory. On the basis of this model, the defect structure of the Ta_2O_5 in the scale predominantly involves oxygen vacancies at pressures lower than those of the p-n transition, while above this pressure an outer layer of the scale also consists of Ta_2O_5 predominantly involving interstitial oxygen.

The parabolic rate constants both above and below the p-n transitions have an activation energy of 45 kcal/mole (Reference 8). It is concluded that this activation energy corresponds to that of oxygen vacancy diffusion.

Breakaway Oxidation Above 800°C

The transition from parabolic to linear oxidation above 800°C exhibits a breakaway type of behavior at the higher oxygen pressures. This may be seen in Figure 5 which shows the results of the gravimetric oxidation rate measurements at various oxygen pressures at 1000°C. On the basis of these measurements it is concluded that the transition is a result of a breakdown of the protective scale through cracking due to stresses in the oxide scales. Metallographic examinations of oxide scales on specimens oxidized well into the linear region also suggest a porous scale. At the metal-oxide interface traces of an oxide apparently different from the bulk oxide

were also observed, and by comparison with the X-ray diffraction measurements it is concluded that these reflect the presence of TaO.

Oxygen Pressure Dependence and Mechanism of Linear Oxidation at 500° to 1000°C

An Arrhenius plot of the linear rate constant in the temperature range 500° to 1000°C is shown in Figure 6. At one atm O_2 a reversal in the temperature dependence takes place at about 700° to 750°C. At 100 Torr O_2 the oxidation rate is approximately independent of temperature, and at 10 Torr O_2 and below, no reversal occurs. At all pressures the linear rate constant increases rapidly with temperature above 800°C.

A plot of the linear rate constant at 500° to 1000°C as a function of oxygen pressure is shown in Figure 7. The linear rate shows a varying dependence on the oxygen pressure and a comparison of Figures 6 and 7 shows that the reversal in temperature dependence may be considered to arise from differences in the oxygen pressure dependence above 10 Torr O_2.

A consideration of temperatures below 800°C, where TaO_z is the intermediate reaction product, reveals that the linear rate constant tends to become independent of oxygen pressure at low temperatures (e.g., 500°C) and high oxygen pressures, but is proportional to the square root of the oxygen pressure at high temperatures (700°C) and low oxygen pressures. This oxidation behavior is interpreted in terms of an oxygen chemisorption equilibrium prior to the rate-determining formation of Ta_2O_5 from TaO_z. This may be written

$$\text{site} + 1/2\,O_2^{(g)} \underset{}{\overset{K}{\rightleftharpoons}} \text{O-site} \qquad (5)$$

or

$$\text{O-site} + TaO_z \xrightarrow{k} Ta_2O_5 \qquad (6)$$

Equation 5 involves chemisorption of oxygen on TaO_z and Equation 6 denotes the rate-determining formation of Ta_2O_5 which is proposed to be governed by nucleation and growth of Ta_2O_5 nuclei. The duration of the incubation period discussed above is concluded to be the result of the time lag associated with the nucleation and growth of Ta_2O_5 nuclei (Reference 4).

According to Equations 5 and 6 the linear rate of oxidation is given by

$$k_{lin} = \frac{ak\,Kp_{O_2}^{1/2}}{(RT)^{1/2} + Kp_{O_2}^{1/2}} \qquad (7)$$

where a is the number of available chemisorption sites.

In the limiting cases Equation 7 reduces to

$$k_{lin} = \frac{ak\,Kp_{O_2}^{1/2}}{(RT)^{1/2}} \quad \text{when } (RT)^{1/2} \gg Kp_{O_2}^{1/2} \qquad (8)$$

and to

$$k_{lin} = ak \quad \text{when } Kp_{O_2}^{1/2} \gg (RT)^{1/2} \qquad (9)$$

Thus at high temperatures and low oxygen pressures the rate of Ta_2O_5 formation will become approximately proportional to $p_{O_2}^{1/2}$, but at low temperatures and high oxygen pressures Ta_2O_5 formation will be approximately independent of oxygen pressure.

The experimental results below 800°C give the values (Reference 4) for K and ak as follows:

$$K = 1.2 \cdot 10^{-5} \exp\left(\frac{64{,}000}{RT}\right) \text{ and } ak = 1.7 \times 10^{17} \exp\left(-\frac{71{,}100}{RT}\right)$$

(when expressing p_{O_2} in atmospheres and R in liter-atm/°C/mole °C). Calculated values of k_{lin} (Equation 7) are given by the dotted lines in Figure 7. A good agreement is

obtained between the experimental results and the assumed model.

The above value of K gives a heat of chemisorption of oxygen of

$$\Delta H_{chem} = 128.8 \text{ kcal/mole}$$

From Equations 7-9 we see that the linear oxidation has an activation energy of 71.1 kcal/mole when k_{lin} is independent of oxygen pressure (Equation 9) and an apparent activation energy of 6.7 kcal/mole when $k_{lin} \propto p_{O_2}^{1/2}$ (Equation 8). Between these limiting conditions the activation energy continually changes from 71.1 to 6.7 kcal/mole (Figure 6).

At and above 800°C the oxygen pressure dependence of the linear rate constant is interpreted in terms of a similar model. The only difference from the above treatment is that TaO is the intermediate reaction product above 800°C. The oxygen pressure dependence may thus be described by an equation which is equal to Equation 7 but which contains different values for a, k, and K.

For the results at 800° to 1000°C it is not equally easy to estimate values of the parameters in Equation 7. Furthermore, Figure 10 shows that the apparent activation energy increases from 800° to 1000°C. This is interpreted as reflecting a gradual transition in the oxidation mechanism from TaO_z to TaO as an intermediate reaction product. In terms of Equation 7 this means that the number of chemisorption sites (TaO sites) also gradually increases with temperature at 800° to 900°C.

The Reversal in Temperature Dependence

In the above discussion the reversal in temperature dependence at 1 atm O_2 and 750°C has already been interpreted as a result of the change in the oxygen pressure dependence associated with the transition in reaction mechanism. An additional interpretation may also be made in terms of a decreased thermal stability of TaO_z with increasing temperature.

When Ta_2O_5 is formed via TaO_z according to Equation 7 it has been assumed that the rate of formation of TaO_z is much faster than that of Ta_2O_5, i.e., that the surface under all conditions is "saturated" with TaO_z. However, if the thermal stability of TaO_z decreases with increasing temperature, the situation may arise when the concentration of TaO_z begins to affect and limit the oxidation. TaO_z is formed from Ta-O solid solutions and is also simultaneously consumed through Ta_2O_5 formation. The concentration of TaO_z may thus be described by

$$\frac{d(TaO_z)}{dt} = k_n - k_o p_{O_2}^{1/2} \qquad (10)$$

in which k_n denotes the rate of formation, i.e., the rate of nucleation and growth of TaO_z nuclei from Ta-O solid solution, and k_o denotes the rate of depletion of TaO_z through Ta_2O_5 formation; at 700°C k_o is proportional to $p_{O_2}^{1/2}$.

If the thermal stability of TaO_z decreases with increasing temperature, k_n will, according to the general theory of nucleation and growth of nuclei, have an activation energy which decreases with temperature. Thus as temperature is increased, k_n will become of the same order of magnitude as that of k_o. The occurrence of a reversal will be dependent on the oxygen pressure because of the term $k_o p_{O_2}^{1/2}$. At high oxygen pressures, the value of $k_o p_{O_2}^{1/2}$ is relatively large and may therefore cause a reversal; at low oxygen pressures the term $k_o p_{O_2}^{1/2}$ will be of minor importance, will not appreciably affect the concentration of TaO_z, and will cause no reversal in the temperature dependence as observed in the kinetic studies.

Comparison with Previous Investigations

Oxidation of tantalum under conditions similar to those of the present study has previously been studied by other investigators (References 14 to 16).

Peterson, Fassel, and Wadsworth (Reference 14) found tantalum to oxidize linearly at 500° to 1000°C at oxygen pressures from 1/2 to 40.8 atm. The oxidation was interpreted as involving an equilibrium adsorption process prior to the rate-determining step. The oxygen pressure dependence was fitted to a Langmuir Type I adsorption isotherm.

Albrecht, Klopp, Koehl, and Jaffee (Reference 15) found that the reaction in one atm O_2 follows a linear rate in the temperature range 500° to 1250°C. At 1000°C the reaction followed a square root of pressure dependence.

A comparison between the present results and those of Peterson et al. and Albrecht et al. is shown in Figure 8. There is fair agreement between the results of the three studies. The results of Peterson et al. and Albrecht et al. also suggest reversals in the temperature dependence.

Ong (Reference 17) has presented a theoretical discussion of the oxidation behavior of tantalum. In this treatment the oxide scale is considered nonprotective and the intermediate species involved in the rate-determining step is assumed to be interstitial atomic oxygen in the metal in the immediate region of the metal-oxide interface. It is furthermore assumed that the concentration of interstitial oxygen is related to the oxygen pressure through an adsorption equilibrium on the surface. Dilute solution of oxygen in tantalum are also considered non-ideal by assuming that attractive interactions exist between interstitial oxygen atoms.

By estimating and assuming values for the enthalpy of adsorption of oxygen, the entropy and enthalpy of solution of oxygen in tantalum, and the interaction energy between interstitial oxygen atoms, Ong has calculated values for the linear rate constant as a function of temperature and oxygen pressure. The value at 0.5 atm O_2 is shown as a stippled curve in Figure 8. Ong's treatment predicts a cusp or a reversal in the temperature dependence at all oxygen pressures and maintains that the reversal takes place at decreasing temperature as the oxygen pressure decreases.

Ong's treatment does not give a satisfactory description of the present experimental results. In the author's opinion one of Ong's fundamental assumptions also appears questionable. This refers to the assumption that the concentration of interstitial oxygen in the metal is related to the oxygen pressure through an oxygen adsorption equilibrium at oxygen pressures around one atm. Thus by extrapolating Pemsler's results (Reference 18) on the thermodynamics of the interaction of tantalum with oxygen, the partial pressure of oxygen over tantalum containing 2 atomic weight percent of oxygen is approximately 10^{-22} to 10^{-24} atm at 700°C. Thermodynamically, tantalum should thus be saturated with oxygen at any oxygen pressure above 10^{-22} at 700°C. Although kinetic considerations are very important in this connection, there appears to be no reason why the tantalum metal at the metal-oxide interface should be anything but saturated with oxygen at pressures of about one atm O_2.

OXIDATION OF NIOBIUM

Oxidation at 400° to 600°C

The oxidation behavior of niobium in many ways closely resembles that of tantalum. Thus oxidation of niobium below 500°C involves an initial incubation period followed by a breakaway approximating linear oxidation. Hurlen has shown by continuous X-ray diffraction measurements directly on reacting specimens (Refrences 1 and 2) that the oxidation during the initial stage constitutes oxygen dissolution in the metal. In addition the formation of two metallic oxide phases (suboxides) of niobium, NbO_x and NbO_2, also occurs (References 1, 2, and 7).

The latter phase is isomorphous with TaO_z (Reference 6). The oxidation during the initial incubation period may thus be written

$$1/2\,O_2^{(g)} \longrightarrow O_{chemisorbed} \quad (11)$$

and

$$O_{chem} + Nb \xrightarrow{diffusion} Nb\text{-}O\ sol.sol'n \rightarrow NbO_x \rightarrow NbO_z \quad (12)$$

Hurlen reports that NbO_x could only be found on specimens oxidized at temperatures up to 400°C. NbO_z is easily observed on specimens oxidized at reduced oxygen pressures at 400° to 500°C and is formed as oxide platelets extending into the metal from the metal's surface. One example of the NbO_z formation is shown in Figure 9 (Reference 7). Both the metallographic examination and X-ray diffraction measurements suggest that the (100) plane of NbO_z is parallel to one of the (100) planes of the metal lattice (Reference 6). This is different from the metal-suboxide platelet oxidation relationship for the corresponding tantalum system. NbO_z has not been found on specimens oxidized above 600°C.

Lattice parameter determinations on specimens oxidized during the incubation period indicate that the cubic lattice parameter of niobium at the surface may reach values as high as 3.328 to 3.340 Å (References 1 and 3). These results compared with Seybolt's (Reference 19) values of the lattice parameter as a function of oxygen concentration indicate that large apparent supersaturations of oxygen in niobium occur during the incubation period. It is proposed that these large oxygen solubilities reflect niobium-oxygen solid solutions in "equilibrium" with NbO_x and NbO_z rather than with NbO.

The transition to breakaway oxidation is associated with Nb_2O_5 formation in spots on the surface, while the breakaway oxidation involves the formation of a heavy and porous Nb_2O_5 scale. It is probable that NbO and NbO_2 also are formed as intermediate reaction products. Electron micrographs and optical examination show that the scale contains large numbers of cracks and volcanolike blisters (References 1 to 3) which suggests that the scale has little or no protective properties. At 550°-600°C the oxide also spalled during oxidation (Reference 3).

Oxidation at 600° to 800°C

At temperatures above 600°C there is a change in the kinetics and under these conditions the initial oxidation exhibits (as described before) a protective paraboliclike behavior, which is followed by an almost linear oxidation. This is shown in Figure 10 which gives results of oxidation rate measurements on niobium at 700°C (Reference 3). NbO_z is no longer observed at the metal-oxide interface at these temperatures (References 1 to 3); rather, on specimens oxidized at reduced oxygen pressures we find NbO and NbO_2 as intermediate reaction products (References 1 to 3). Thus it is concluded that at these temperatures the reaction scheme changes from

$$Nb\text{-}O\ sol.sol'n \rightarrow NbO_z \rightarrow NbO \rightarrow NbO_2 \rightarrow Nb_2O_5 \quad (13)$$

to

$$Nb\text{-}O\ sol.sol'n \rightarrow NbO \rightarrow NbO_2 \rightarrow Nb_2O_5 \quad (14)$$

Lattice parameter measurements on the metal surface of specimens oxidized at reduced oxygen pressures at 700°C have given a lattice parameter value of about 3.314 Å (Reference 3). Thus the oxygen concentration at the metal surface is smaller compared to lower temperatures. Behavior equivalent to that discussed above was also observed for tantalum. This decrease in the oxygen concentration is due to an absence of NbO_z under these conditions and, as a result, the oxygen concentration at the metal surface now approaches the value characteristic of Nb-O solid solution in equilibrium with NbO. An estimate of the relative importance of the

oxygen dissolution is shown as a broken curve in Figure 10. The values have been estimated assuming $D = 2{,}12.10^{-2} \exp(-26{,}900/RT)$ (Reference 27) and $c_s = 0.7$ atomic weight percent of oxygen (Reference 21). The estimates indicate that oxygen dissolution is of minor importance compared to the total weight gain under these conditions.

At the higher oxygen pressures Nb_2O_5 is the main reaction product under these conditions and it is believed that the protective oxidation reflects a rate-determining transport of oxygen through the γ-Nb_2O_5 scale. Unfortunately the defect structure of γ-Nb_2O_5 is not known, but this oxide is isomorphous with β-Ta_2O_5 and it would not be unreasonable to assume that the two oxides also have the same defect structure. The same interpretation would thus apply to the initial parabolic oxidation of niobium at 600° to 800°C as it would for tantalum at 800° to 1000°C.

The linear oxidation following the initial parabolic stage exhibits at the higher oxygen pressures a breakaway type of behavior. This is also evident from Figure 10. It is thus concluded, as in the case of tantalum, that the parabolic-linear transition reflects a breakdown of the protective scale. The resulting linear oxidation is furthermore interpreted to be governed by the rate of nucleation and growth of Nb_2O_5 at the metal-oxide interface beneath the cracks in the oxide scale.

Oxygen Pressure Dependence and Mechanism of Linear Oxidation at 600° to 800°C

As shown by many investigators the linear oxidation of niobium at one atm O_2 exhibits a reversal in the temperature dependence at about 600°C (References 3, 22 to 24). An Arrhenius plot of the linear rate constant at 500° to 800°C at 1 atm O_2 is shown in Figure 11 (Reference 3). At 76 Torr Gulbransen and Andrew (Reference 25) found the oxidation to be approximately independent of temperature at about 600°C, and at lower oxygen pressures such reversals are absent (Reference 3).

A plot of the linear rate constant as a function of oxygen pressure is shown in Figure 12 (Reference 3). The reversal may, as in the case of tantalum, be considered to be due to a change in the oxygen pressure dependence at the higher oxygen pressures.

Below 600°C the oxygen pressure dependence of the linear oxidation also closely resembles that of the oxidation of tantalum. As suggested by the results in Figure 12 and as demonstrated by Hurlen (Reference 1 and 2) the linear rate constant becomes approximately independent of oxygen pressure at low temperatures and high oxygen pressures and is proportional to $p_{O_2}^{1/2}$ at low oxygen pressures. Thus the oxygen pressure dependence and the oxidation mechanism may be described by an equation equivalent to Equation 7. The only difference between niobium and tantalum is that the oxygen pressure dependence is higher than $p_{O_2}^{1/2}$ above 100 Torr O_2 at 600°C in the case of niobium. This unexpectedly large oxygen pressure dependence is not fully understood, but it is believed to be associated with the change in reaction scheme and mechanism (from Equation 13 to 14) at this temperature.

At 700° to 800°C the same gradual change occurred in oxygen pressure dependence as it did for tantalum at 800° to 1000°C. The oxidation mechanism is interpreted in equivalent terms. The reversal in temperature dependence is furthermore concluded to be a result of the change in oxygen pressure dependence associated with the change in the reaction scheme at about 600°C. As for tantalum, an additional interpretation may be made in terms of described thermal stability of NbO_2 and, on oxidation, reaction governed by nucleation and growth of oxide nuclei. A more detailed discussion of such a mechanism has been given elsewhere (Reference 26).

SUMMARY AND CONCLUSIONS

The oxidation behavior of niobium and tantalum below 1000°C are closely similar.

The initial oxidation at low temperatures (<500° to 600°C) involves oxygen dissolution in the metal and the formation of metallic oxide phases. The initial stage is followed by a breakaway oxidation which is associated with pentoxide formation on the metallic oxide phases.

At about 600° and 800°C for niobium and tantalum, respectively, there is a change in the reaction mechanism. Above these temperatures the metallic oxide phases are no longer found at the metal-oxide interface. Concurrently, the initial oxidation, which primarily involves pentoxide formation, is approximately parabolic, and we conclude that during this stage the reaction is governed by a rate-determining diffusion of oxygen through the pentoxide scale. The parabolic stage is followed by a near linear oxidation, which is a result of a breakdown of the protective properties of the scale.

Arrhenius plots of the linear oxidation rate constants show reversals in the temperature dependence at one atm O_2 at about 600°C and 700° Å to 750°C for niobium and tantalum, respectively. At lower oxygen pressures corresponding reversals are absent. The reversals are concluded to be a result of the change in oxygen pressure dependence associated with the changes in the reaction schemes at corresponding temperatures. An additional cause of the reversal may be a decreased thermal stability of the metallic oxide phases which are intermediate reaction products at lower temperatures.

At temperatures above 700° to 700°C and at oxygen pressures above about 0.01 Torr, oxygen dissolution is of minor importance compared to the total weight gain during oxidation. However, the oxygen dissolution, which is governed by the rate oxygen diffusion into the metal as long as oxide is present on the surface, is relatively rapid. Because dissolved oxygen has adverse effects on the mechanical properties of niobium and tantalum, the oxygen dissolution is an important part-process in considering constructional applications of these metals.

In attempting to alloy niobium and tantalum for better oxidation resistance, a primary aim must be to reduce oxygen dissolution and the rate oxygen diffusion in the metals. Only after achieving this should such alloying additions be considered as will favor the formation of protective films on the surface.

ACKNOWLEDGMENT

The work has been sponsored, wholly, or in part, by the Research and Technology Division, AFSC, through the European Office, Office of Aerospace Research, United States Air Force.

REFERENCES

1. T. Hurlen, H. Kjøllesdal, J. Markali, and N. Norman, TN No. 1, AF 61(052)-90, Oxidation of Niobium. Central Institute for Industrial Research, Blindern, Oslo, Norway. April 1959.

2. T. Hurlen, J. Inst. Metals, Vol. 89 (1961) p. 273.

3. P. Kofstad and H. Kjøllesdal, Trans. AIME, Vol. 221 (1961) p. 285.

4. P. Kofstad, J. Inst. of Metals, Vol. 90 (1961-2) p. 253.

5. P. Kofstad, TN No. 3, AF EOAR 61-42, Oxidation of Tantalum at 300-550°C. November 1961. J. Inst. of Metals, Vol. 91 (1962-63) p. 209.

6. N. Norman, J. Less-Common Metals, Vol. 4 (1962) p. 52.

7. N. Norman, P. Kofstad, and O. J. Krudtaa, J. Less-Common Metals, Vol. 4 (1962) p. 124.

8. P. Kofstad, TN No. 8, AF 61(052)-466, The Oxidation Behavior of Tantalum at 700°-1000°C, November 1962. J. Electrochem. Soc., Vol. 110 (1963) p. 491.

9. J. V. Cathcart and R. E. Pawel, Acta Met., Vol. 10 (1962) p. 149.

10. R. W. Powers and M. V. Doyle, Trans. AIME, Vol. 215 (1959) p. 655.

REFERENCES (CONT'D)

11. L. S. Darken and R. W. Gurry, Physical Chemistry of Metals, New York and London (The McGraw-Hill Book Co.) 1953, p. 445.

12. D. A. Vaughan, O. M. Stewart, and C. M. Schwartz, Trans. AIME, Vol. 221 (1961) p. 937.

13. P. Kofstad, J. Electrochem. Soc., Vol. 109 (1962) p. 776.

14. R. C. Peterson, W. M. Fassel, and M. E. Wadsworth, J. Metals, Vol. 200 (1954) p. 1038.

15. W. M. Albrecht, W. D. Klopp, B. G. Koehl, and R. I. Jaffee, Trans. AIME, Vol. 221 (1961) p. 110.

16. M. G. Cowgill and J. Stringer, J. Less-Common Metals, Vol. 2 (1960) p. 233.

17. J. N. Ong, Jr. Paper presented at the AIME, St. Louis, February 1961

18. J. P. Pemsler, J. Electrochem. Soc., Vol. 108 (1961) p. 744.

19. A. U. Seybolt, J. Metals, Vol. 6 (1954) p. 774.

20. R. P. Elliott, Trans. ABM, Vol. 52 (1960) p. 990.

21. R. T. Bryant, J. Less-Common Metals, Vol. 4 (1962) p. 62.

22. D. W. Bridges and W. M. Fassel, J. Electrochem. Soc, Vol. 103 (1965) p. 326.

23. B. B. Argent and B. Phelps, J. Inst. Metals, Vol. 88 (1959) p. 301.

24. D. W. Aylmore, S. J. Gregg, and W. B. Jepson, J. Electrochem. Soc., Vol. 107 (1960) p. 495.

25. E. A. Gulbransen and K. F. Andrew, Ibid, Vol. 105 (1958) p. 4.

26. P. Kofstad, "On the Role of Oxide Nucleation and Growth of Oxide Nuclei in Oxidation of Niobium." Paper presented at the 1st. International Congress on Metallic Corrosion, London, April 1961.

27. R. W. Powers and M. V. Doyle, J. Appl. Phys. Vol. 30 (1959) p. 514.

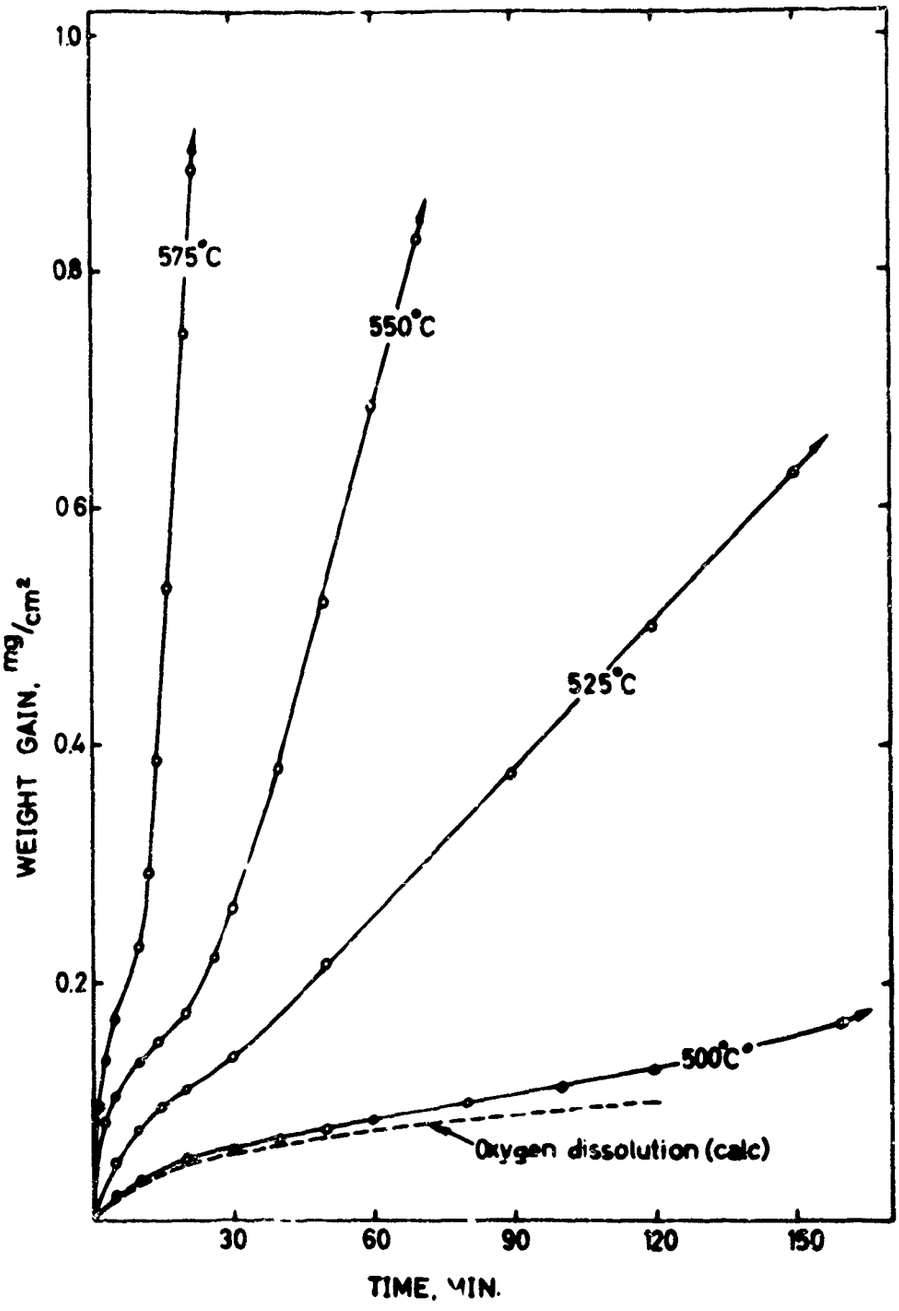

Figure 1. Tantalum Oxidized at 1 Atm O_2 and 500° to 575°C (Reference 4)

Figure 2. High-Vacuum Annealed Tantalum Oxidized at 0.01 Torr O_2 and 600°C for 1300 Min. (250X) (Surface polished and etched after oxidation. Platelets of TaO_2 with surface oxide of Ta_2O_5. (Reference 7)

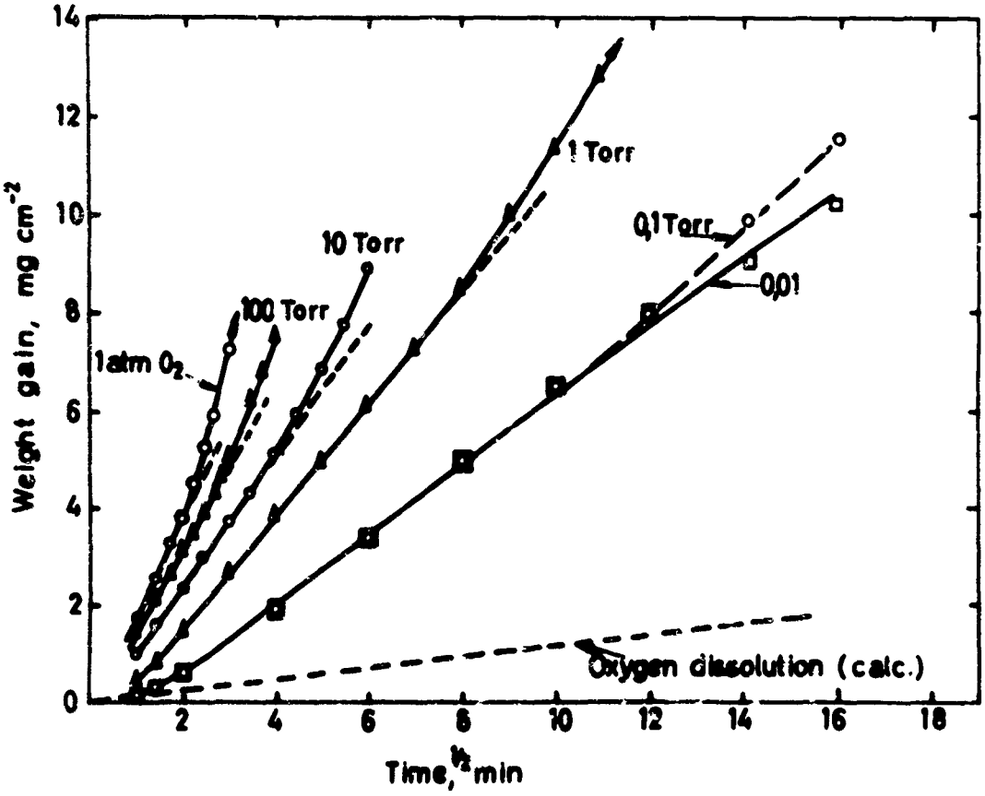

Figure 3. Parabolic Plot of Initial Oxidation of Tantalum at 900°C (Reference 8)

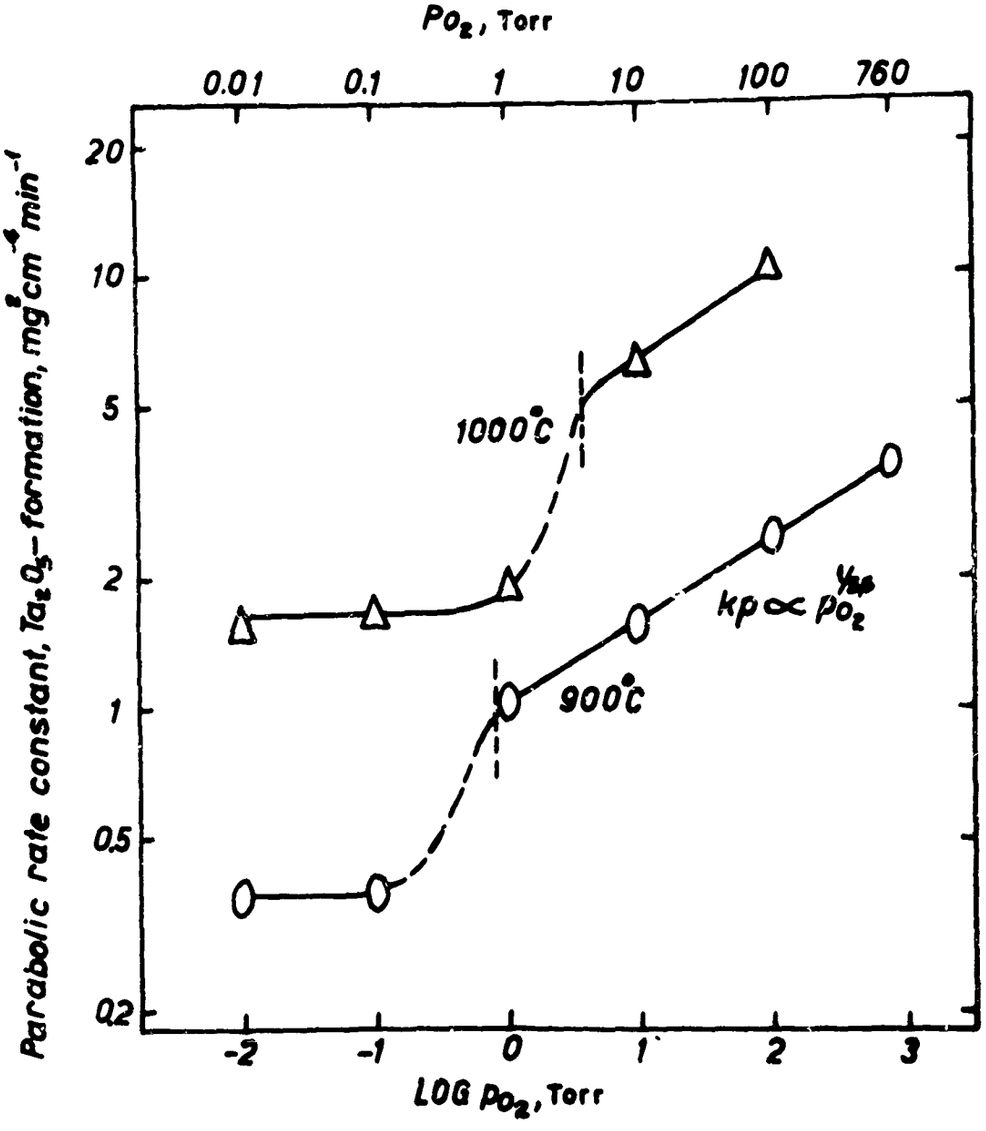

Figure 4. Parabolic Rate Constant for Ta_2O_5 Formation at 900° to 1000°C as a Function of Oxygen Pressure (Reference 5)

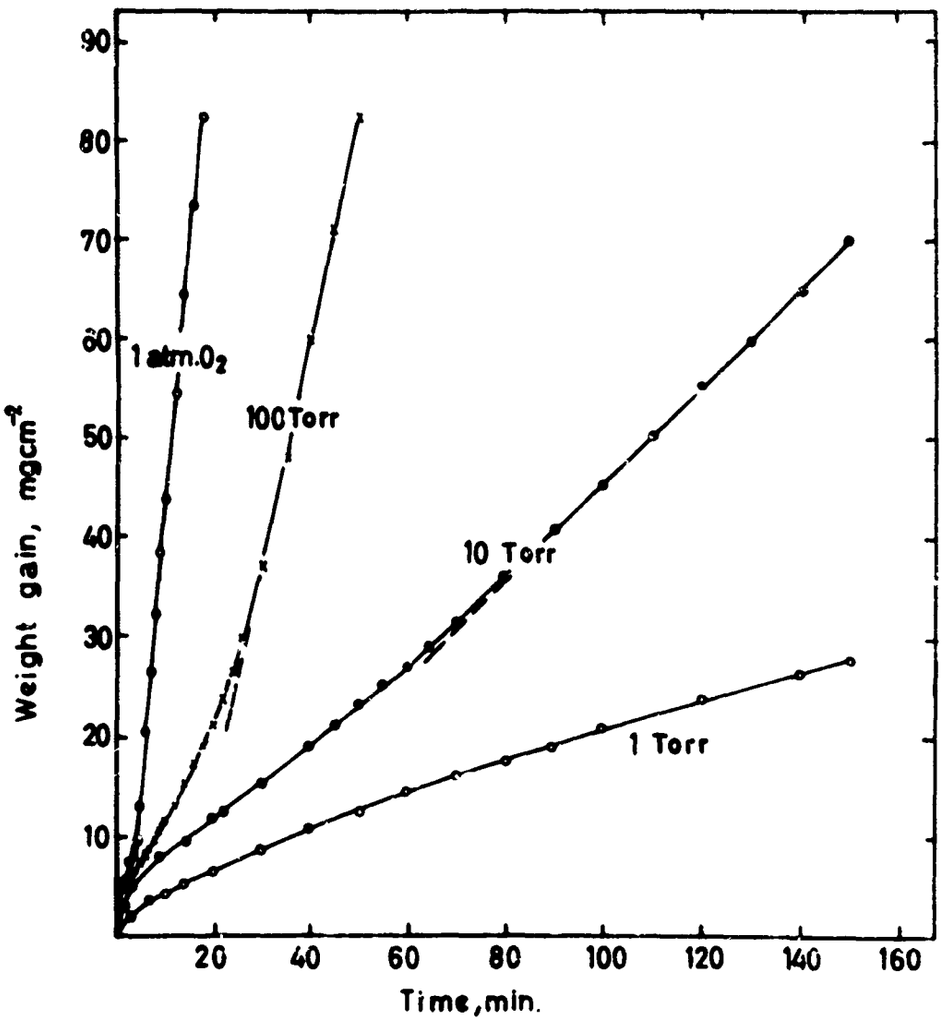

Figure 5. Linear Plot of Oxidation of Tantalum at 1000°C as a Function of Oxygen Pressure (Reference 8)

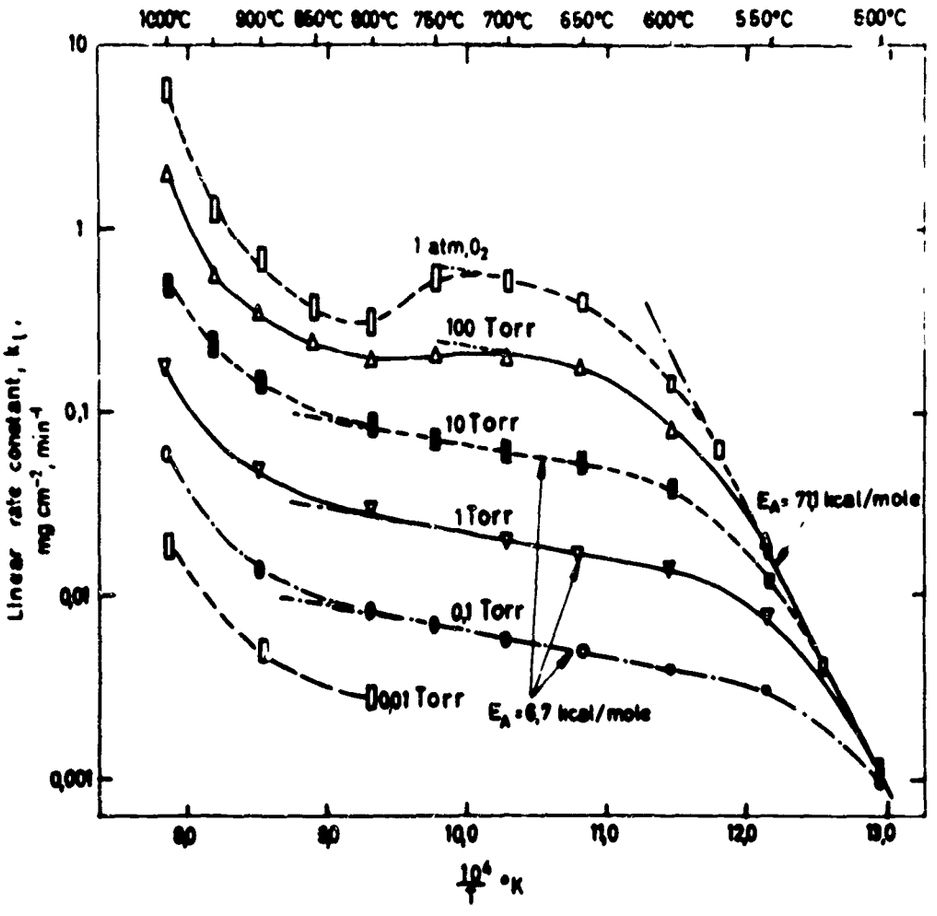

Figure 6. Arrhenius Plot of the Linear Rate Constant of Oxidation of Tantalum at 1 Atm, 100, 10, 1, 0.1, and 0.01 Torr O_2 (Reference 8)

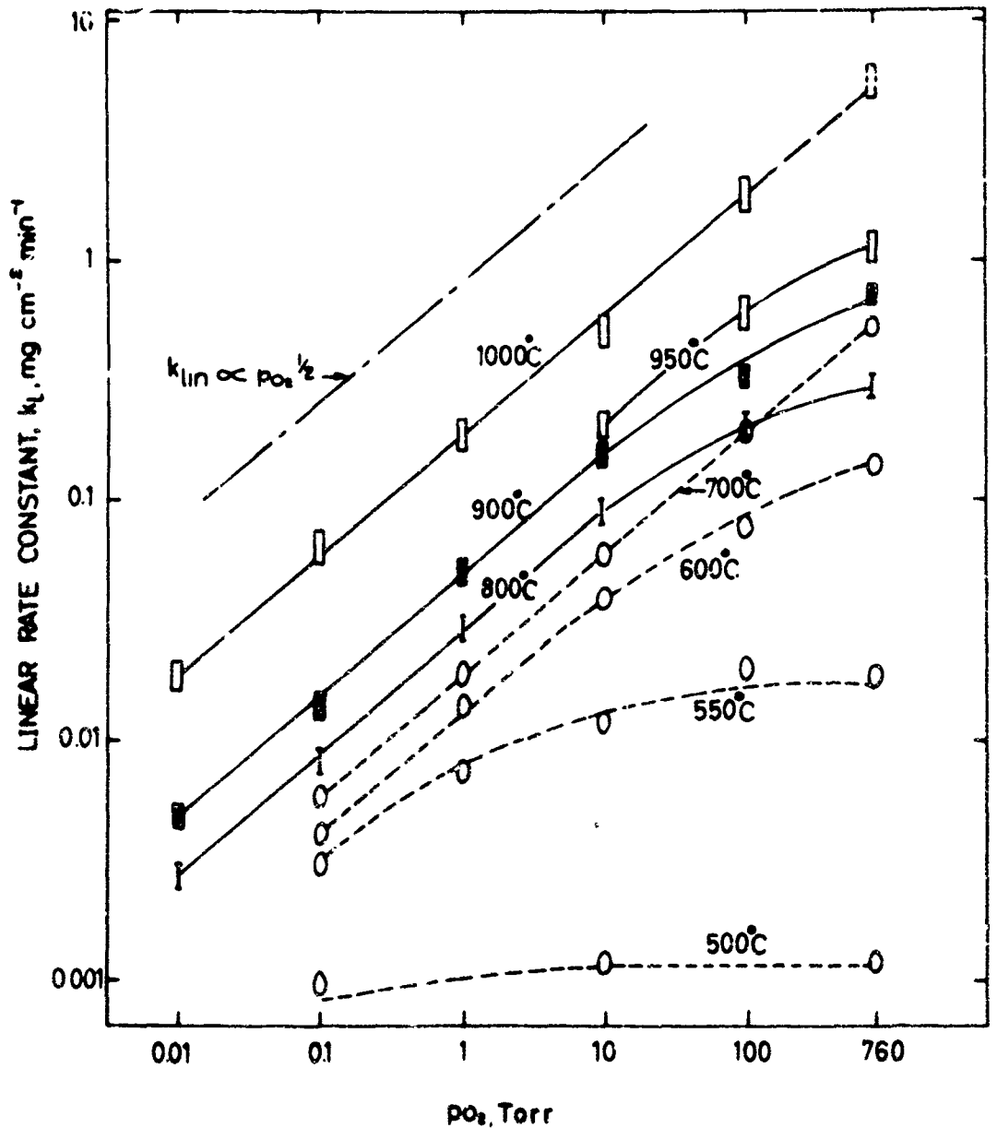

Figure 7. Linear Rate Constant of Oxidation of Tantalum at 500° to 1000°C as a Function of Oxygen Pressure (References 4 and 8)

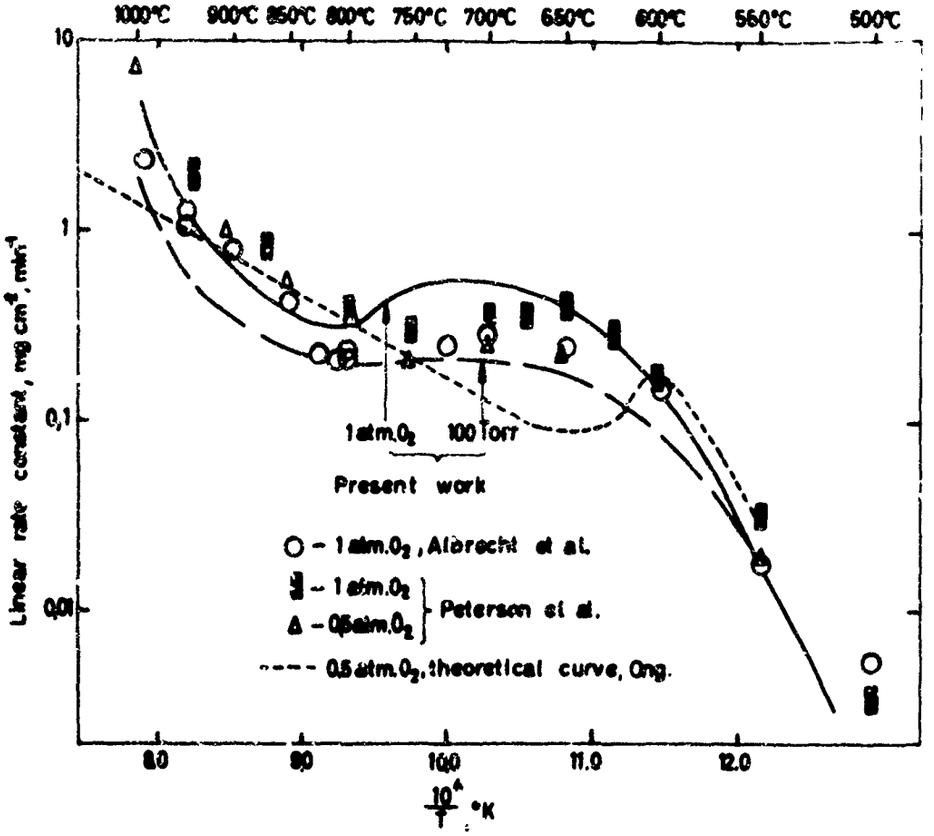

Figure 8. Arrhenius Plot of Linear Oxidation of Tantalum at 500° to 1000°C (Reference 8)

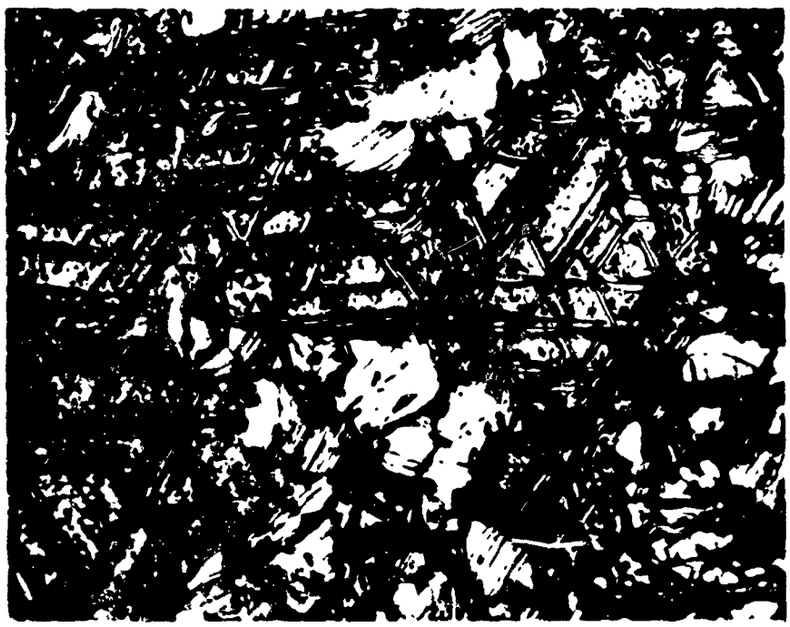

Figure 9. High-Vacuum Annealed Niobium Oxidized at 0.01 Torr 0_2 and 500°C for 1440 Min. (400X) (Surface polished and strongly etched after oxidation. (Reference 7)

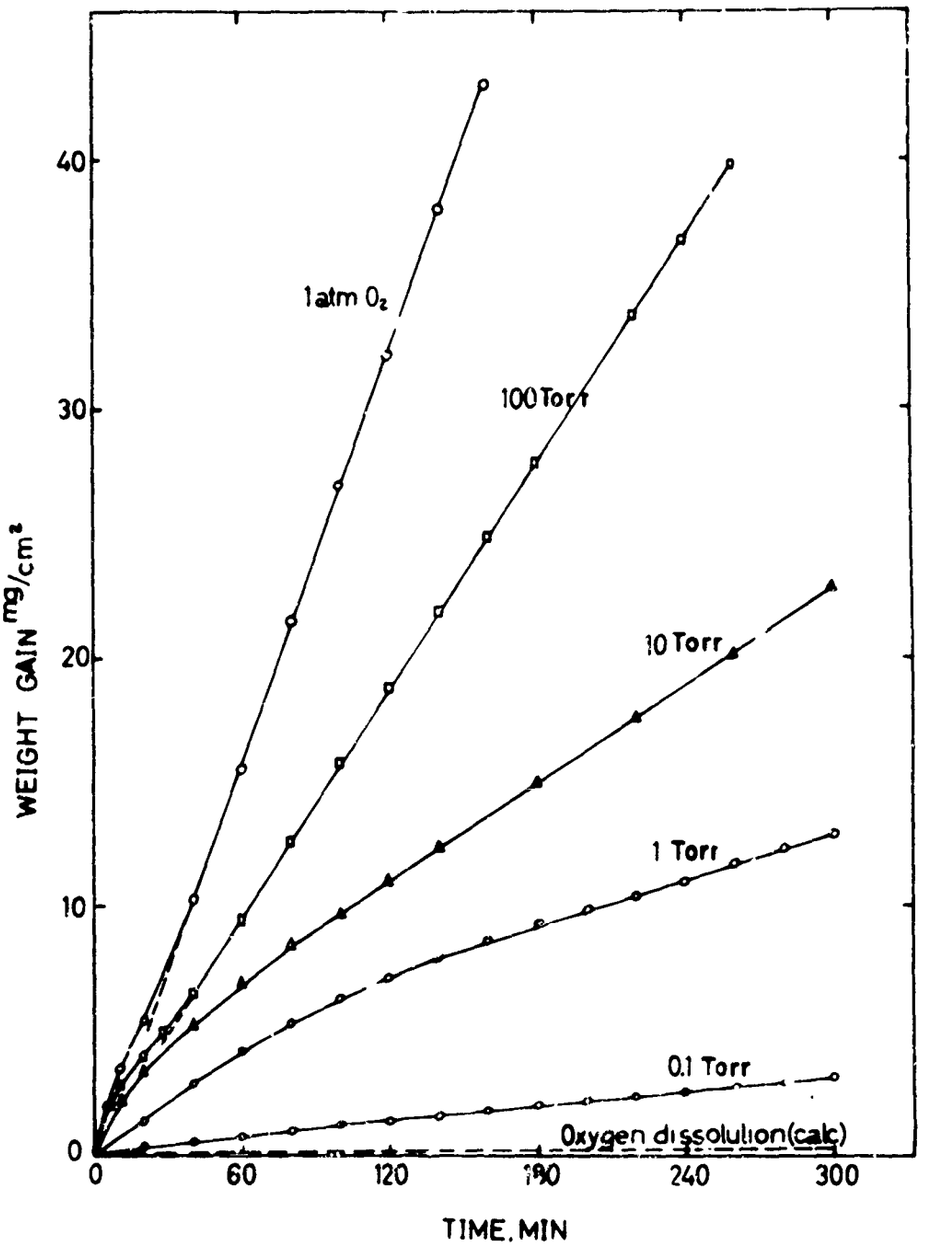

Figure 10. Niobium Oxidized at 700°C as a Function of Oxygen Pressure

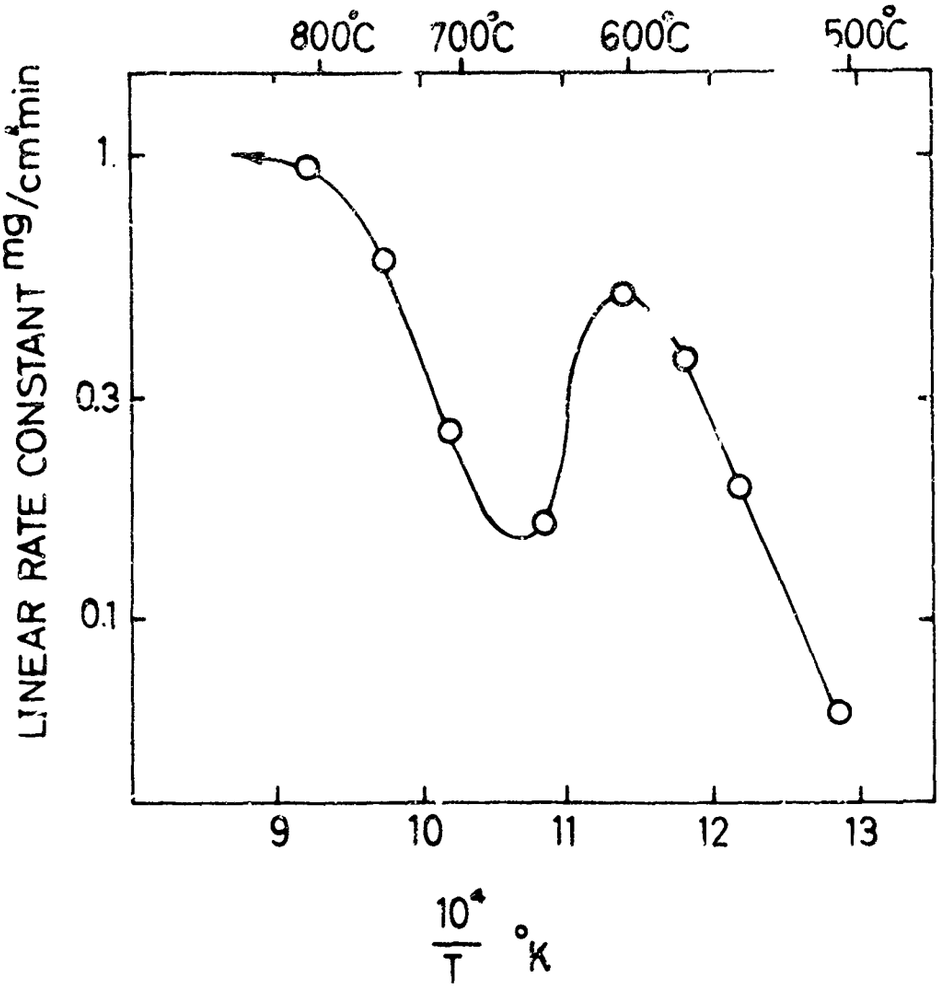

Figure 11. Arrhenius Plot of the Linear Rate Constant of Oxidation of Niobium

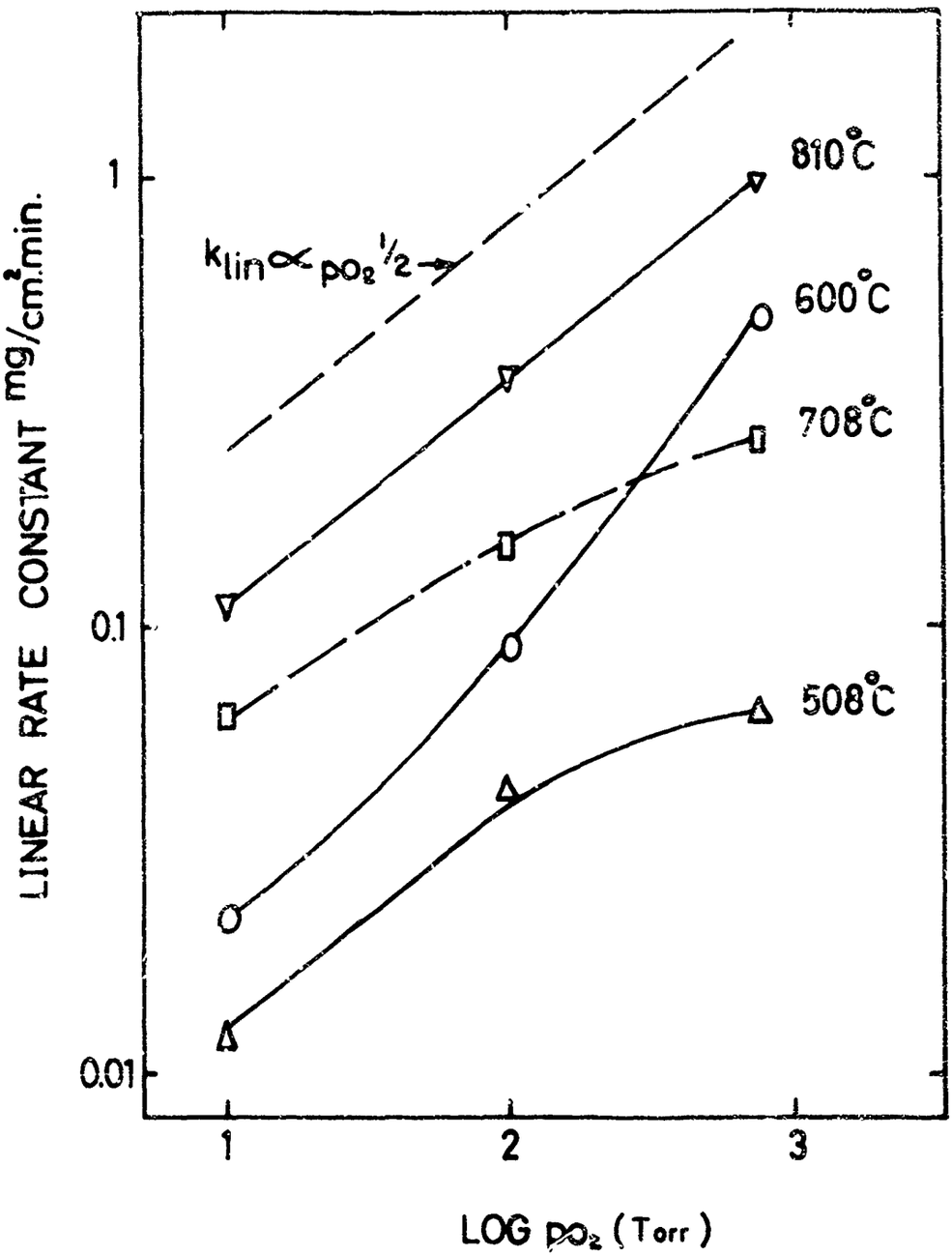

Figure 12. Linear Rate Constant of Oxidation of Niobium at 500° to 800°C as a Function of Oxygen Pressure

BASIC FACTORS IN THE DESIGN OF PROTECTIVE COATINGS FOR TUNGSTEN

M. G. Nicholas*
C. D. Dickinson*
A. L. Pranatis**
C. I. Whitman***

INTRODUCTION

A number of formidable problems have to be overcome before the full potential of tungsten and tungsten-base alloys as structural materials can be realized. On a strength-to-weight basis, they look particularly promising at temperatures above 1500°C and are possibly the only metallic materials which have reasonable strength at 2000°C and above. However, many potential applications call for long service lives in oxidizing environments (Reference 1) and therefore their poor high-temperature oxidation resistance is a severe limitation.

Although a number of studies of the influence of alloying on the oxidation resistance of tungsten have been made, the volatility of the tungsten oxides negates the possibility of producing a satisfactory dilute alloy with good high-temperature oxidation resistance by the application of Wagner-Hauffe principles in order to modify the defect structure of the tungsten oxides (Reference 3). Considerable attention is being paid at present, therefore, to the development of protective coatings for very high temperature use. Some of those already developed by basically empirical programs can confer protection for considerable periods at temperatures of up to 1800°C (Reference 2), but so far none are able to withstand temperatures in excess of 2000°C for reasonable times (Reference 1).

In addition to the technological difficulties, such as the development of techniques for the application of adherent, pore-free coatings, some of the present lack of success may be the poor definition of the phenomena that are of primary importance in determining the behavior of coatings at high temperatures. An analysis of the performance of high-temperature coating systems being conducted for the Aeronautical Systems Division (Reference 4) suggests that this is the case, and an attempt has been made to define the relevant phenomena. From a practical viewpoint, however, it is not sufficient merely to identify the phenomena; their relative importance must also be considered. An attempt will be made to do this, and the potential of some existing coating systems will be evaluated and the types of coatings which might be developed in the future will be discussed.

REQUIREMENTS FOR HIGH-TEMPERATURE COATINGS

An ideal coating is one that forms a solid (or extremely viscous) inert and impermeable barrier between the oxidizing environment and the protected substrate. Although this is easy to state, the combination of properties needed to achieve this ideal are exceedingly complex. Many types of coatings have been investigated (Reference 1), but one class has been found to be more successful

*General Telephone & Electronics Laboratories, Inc.

**Lawrence Radiation Laboratories, University of California.

***Copper Products Development Association.

than the others for most environmental conditions, metal coatings, particularly intermetallic compounds, diffusion-bonded to the protected substrate. These compounds are usually composed of metals of widely differing reactivities, protection being conferred through the oxidation characteristic of the most reactive metal. This will be the only type to be considered.

The success of this type of coating has been achieved even though it is not inert. Upon exposure to air, any metal surface is covered by oxide, and possibly nitride, layers; furthermore, reactions occur between the coating and the substrate and, indeed, are a necessity if good adherence is to be obtained. It is highly desirable, therefore, that the products of these reactions as well as the initial coating should be solids or extremely viscous liquids at operational temperatures.

As well as chemical reactions, purely physical processes may proceed at significantly rapid rates at high temperatures and therefore must be considered, the most important of these being diffusion and vaporization. One factor which controls the rate of oxidation through a protective oxide film is diffusion either of cations or anions through the oxide. At low or intermediate temperatures, the rate becomes small after a film of reasonable thickness is formed, but at high temperature (and the temperatures for protection of tungsten certainly fall in this category), the rate of diffusion can be the factor which controls time to failure. In principle, the rate of gaseous permeation is also of importance, but, except in a few special cases, this may be ignored in practice provided the coatings are several mils thick and lives of many thousands of hours are not expected. These departures from the ideal rule out the possibility of developing an infinitely durable simple coating consisting of an inert layer.

The structures of actual protective coating systems are far more complex than those of the ideal system discussed. Multilayer coating systems have often proved to be the most successful and, in practice, even coatings applied as a single layer become multilayer during service, due to reactions with the environment and the substrate. A WSi_2 coating on tungsten, for example, degenerates from a two-layer to a five-layer system. Moving in from the external surface, these are:

1. An outer layer of oxide which, if formed at high temperature, is mainly SiO_2.

2. A layer of W_5Si_3 formed from the original WSi_2 coating by the preferential oxidation of silicon.

3. The residue of the original WSi_2 coating.

4. A layer of W_5Si_3 formed from the original WSi_2 coating, due to the diffusion of silicon into the tungsten substrate.

5. The tungsten substrate which is now alloyed with silicon.

Both the oxide scale and the zones adjacent to the scale and the protected substrate thicken with time and, eventually, the initial coating reservoir will be consumed entirely. In effect, a coating is protective no longer once this occurs, since oxygen diffusing through the external oxide will come into contact with either the protected substrate or a layer which is leaner in the reactive element than the original coating material, W_5Si_3 in the case of WSi_2 coatings. By definition, the substrate has a poor oxidation resistance and, in practice, the compounds or alloys forming the zones adjacent to the outer oxide scale and the protected substrate are seldom as oxidation-resistant as the initial coating. Therefore, knowledge of the rates of consumption of the original layer by oxidation and reaction with the substrate is of importance. The rate of vaporization may be significant, and this too must be taken into consideration along with any physiological effects that may be produced by the coating system.

The lack of ultra-high temperature kinetic data means that reaction and vaporization rates have to be estimated by extrapolation of whatever data is available for lower

temperatures. For meaningful extrapolations, the mechanisms controlling the processes at operational temperatures must be known and must be identical to those operative at the temperatures for which data is available. Assumptions that the mechanisms are the same at high and low temperatures are particularly hazardous with respect to oxidation reactions. Provided that these reservations are borne in mind, however, it is possible to deduce some of the factors determining the protectiveness of coating systems at 2000°C and above from the known behavior of metallic coatings at lower temperatures. The foregoing arguments have indicated that the main groups of factors are those controlling coating environment reactions, coating-substrate reactions, and material loss by vapor transport.

FACTORS DETERMINING THE EFFICACY OF COATING SYSTEMS

It is not always a simple task to determine the relative importance of the phenomena mentioned, even in demonstrated protective coating systems, and therefore all of them must be considered as potential causes of failure in an attempt to predict the behavior of untested systems. At temperatures above 1900°C, where no protective systems now exist, it is necessary to extrapolate that which is known on each of the phenomena, in an attempt to arrive at some judgment as to which factors are more important. Through knowledge of what these facts are and of their temperature dependence, it should be possible to estimate if a specific coating system will be useful at temperatures above 2000°C. For the sake of clarity, each of the phenomena will be considered separately.

Reactions with Environment

The reaction of most metals with air at low temperatures produces a compact, adherent oxide film forming a barrier between the reactants. The rate of reaction and film growth is then governed by the rate of diffusion of the reactants and, at very low temperatures, by the rate of interfacial reaction. Under these circumstances, oxidation proceeds slowly, sometimes almost infinitesimally slowly. At high temperatures, however, many materials react rapidly to produce crumbly, porous, or even volatile oxides. A change from one type of reaction to the other can occur quite suddenly during an isothermal oxidation run, or as a result of a slight temperature increase, and give rise to a marked increase in the rate of oxidation and a change in the type of oxide film growth law obeyed.

This change in oxidation behavior, breakaway, is highly undesirable if the oxide is to form part of a coating system. The mechanistic and phenomenological details of breakaway have been studied for a few materials only, and while factors such as vaporization of the metal substrate, phase changes, oxide solution and re-precipitation, and lattice mismatch of the oxide and metal, have been suggested as causes, no general pattern has yet emerged. No matter what the cause, however, it is generally found that the processes resulting in a change to a linear oxide growth law involve rupture of the protective oxide scale, due to the growth of stresses at the oxide-metal interface or within the oxide itself. Even though the mechanics of breakaway are not understood completely, the conditions under which it occurs have been defined for many oxides growing from their parent metals in terms of time, temperature, oxide thickness, gas composition, and pressure. Unfortunately, many of the very refractory oxides which could be employed in coating systems for use above 2000°C undergo breakaway during formation and growth from their parent metals at quite low temperatures (References 5-17)*. If these oxides are to be employed in actual coating systems, means will have to be developed for the prevention of breakaway. The achievement of this objective is of major importance to the development of future coating systems.

*(Figure 1.) Although straight lines are drawn in the figure, this may be an oversimplification of the data; kinks, and even temporary reversals, in plots of temperature versus the logarithm of the time at which a linear oxide growth law is obeyed, being known to occur for some materials.

Even if breakaway could be prevented or delayed and the films grown by diffusion-controlled processes at high temperatures, oxidation of the protected substrate would occur ultimately when all the coating material had been converted into its oxide or oxides, since inward diffusing oxygen ions would then come into direct contact with the substrate. Although the onset of this could be delayed by the use of thicker coatings, indefinite delay is impossible. The rates of coating destruction due to diffusion-controlled reactions with the environment can be estimated by extrapolation of low temperature data, if it is assumed that the controlling diffusion mechanism is not temperature-dependent. Data is presented in Figure 2 (References 5-20) for a few metals forming refractory oxides, and it can be seen that oxidation will consume 10^{-3} to 10^{-2} gram atoms/cm^{-2} of all the metals chosen during a one-hour exposure at 2000°C. Thus, a coating of zirconium or beryllium with a typical thickness of 0.1 mm will be entirely consumed in just about one hour at 2000°C, even if reactions with the substrate do not occur. If reasonably thin coatings capable of conferring protection for considerable periods at 2000°C are to be developed, therefore, this diffusion-controlled rate must be decreased either by reducing the defect concentration of the lattice, or by changing the lattice itself. At the very high temperatures involved, the abundance of thermal vacancies is probably such that impurity doping will have a negligible effect and therefore it may be necessary to alter the lattice structure. One of the most promising ways of changing the structure would be to attempt to form some of the complex refractory oxides which have been ignored so far in this discussion. It is far from simple, however, to suggest what complex oxides should be formed; although many are known to be refractory, few, if any, of those presently identified are as refractory as thoria and hafnia. Furthermore, relatively little is known about diffusion processes in, or the growth kinetics of, complex oxide films.

For the sake of simplicity and completeness, the data presented in Figures 1 and 2 refer to the oxidation of pure metals. However, except for the platinum-group, it is unusual for pure metals to be used as coatings, intermetallic compounds such as silicides and aluminides being far more typical. In the selection of compounds as coating materials, it is usually assumed that thermodynamic factors determine which oxide will be formed. It is not always easy, however, to define which oxide has the greatest thermodynamic stability when the substrate is an alloy or compound. The formation of a given oxide automatically depletes the binary metal substrate of the more reactive specie and hence alters the relative thermodynamic stabilities of the components in the system. The depletion of the reactive specie will be particularly severe at the oxide-metal interface, but diffusion of the depleted element from the richer interior will tend to homogenize the material. Ultimately, a state of dynamic equlibrium will be attained and the concentration of the reactive specie at the interface, and hence the relative thermodynamic stabilities of the various possible oxidation products, will be determined in part by the relative rates of depletion by formation of oxide and diffusion from the richer regions of the substrate (Reference 21). The influence that depletion can have is well illustrated by the effects of stoichiometry on the oxidation of intermetallic compounds: at 1000° to 1400°C, WSi_2 produces a protective film of silica when the compound is stoichiometric, but a nonprotective film of silica and tungsten oxides when the compound is silicon-lean (Reference 2).

Layer growth during the oxidation of a compound is a complex process, since it is a special case of diffusion in a ternary system in which one component is a gas. While the sequence of layers in a binary system is determined solely by the relative thermodynamic stabilities of the phases and can be predicted simply by drawing an isothermal line across the appropriate phase diagram, this is not necessarily true of layer growth in ternary systems (References 22-24). The present state of our knowledge of ternary diffusion processes is far from adequate and, in fact, for a detailed understanding of layer growth in a ternary system, we are almost completely dependent upon the work of Clark and Rhines (Reference 24) in the Al-Mg-Zn system. While these workers formulated a number of rules and conclusions on the basis of their experimental data, no other experimental work

is known which can confirm or contradict their validity. If the Al-Mg-Zn system is typical, however, the relative rates of diffusion of the components affect not only the kinetics of layer growth, but also the composition and phase sequence of the layers. A quantitative evaluation of the importance of this effect is, regrettably, virtually impossible for actual coating systems, at the moment.

Vaporization

Three vaporization processes can affect the behavior of a coating system; vaporization of the protective external oxide film, reaction with the environment to produce volatile products, and vaporization from an internal layer. Even the commonest form of vapor phase loss from coating systems (evaporation of the external oxide layer) is undesirable, since thinning of this layer leads to an increased oxidation rate. It is important, therefore, to be able to predict the rates under actual service conditions.

Estimates of vaporization rates into a perfect vacuum can be made through use of the Langmuir equation (Reference 25) if the equilibrium pressures and molecular weights of the vaporizing specie are known. For most refractory oxides these are low, since their vapor pressures at 2000°C are 10^{-5} to 10^{-3} mm (Reference 26). The rates are even lower if the environment is not a perfect vacuum, since many of the vaporizing molecules are reflected back onto the material surface. Under these circumstances, the actual rate is controlled by the speed of diffusion of the vaporizing molecules through the blanketing layer of the environmental gas above the vaporizing surface. This will depend in part upon the temperature and the molecular density, and hence the pressure is of great importance in practice. This dependence is well illustrated by Gulbransen's (Reference 27) recent measurements of the vaporization of WO_3; the vaporization rate into an environment at one-atmosphere pressure is two to three orders of magnitude less than that predicted by the Langmuir equation for the temperature range employed, 1000° to 1200°C. The actual rates also decrease if the molecular weight of the environmental species is increased. Conversely, a high environmental gas velocity reduces the depth of the blanketing layers and results in an increased rate of vaporization. As well as simple evaporation, vaporization may be promoted by chemical reactions between the coating and the environment. A previously formed protective oxide layer may dissociate when the environmental temperature is raised or pressure decreased or, for example, the product of the oxidation process may be volatile. In both of these cases, the effect of increasing environmental pressure often is to suppress the harmful reaction due to either a change in the thermodynamic stabilities of the reactants or, simply, to an increased environmental blanketing effect. Thus, the rate of vaporization due to dissociation alone can be expected to decrease steadily with increasing environmental pressure. On the other hand, vaporization due to a chemical reaction producing volatile compounds will increase initially with increasing oxygen pressure, since the rate of reaction depends on the rate of oxygen arrival, but ultimately the rate should decrease with increasing pressure, since oxygen arrival will be impeded by a blanket of the volatile species. Thus, a maximum in the rate of vaporization can occur at a certain pressure, increases or decreases in which both reduce the rate of vaporization.

Vaporization at an internal interface is extremely harmful to coating stability, since it may cause disruption of the protective external oxide layers or modify the oxide growth mechanism. Two types of vaporization can occur internally, simple evaporation of one component or the vaporization of the products of the reaction between two layers. Examples of these two processes are the evaporation of the chromium substrate, which has been suggested to be responsible for the breakdown of protective oxide film growth on that metal at 800° to 900°C (Reference 28), and the interaction of silica and the substrate to produce volatile silicon monoxide which is thought to cause the bubbling of silica films at high temperatures (References 2 and 29).

In any one coating system, more than one vaporization process can be of importance.

For silicide coatings, a reaction between the silica layer and the substrate can occur, as we have commented already, but simple evaporation of silica, dissociation into silicon monoxide, and the preferential formation of silicon monoxide are also of importance. The relative importance of each of these processes depend not only on temperature, but also on the blanketing effects of environmental pressure. It is difficult to predict the actual rates when blanketing effects can be significant, but a qualitative idea can be gained by use of the Langmuir equation. Figure 3 presents these calculated rates for silica evaporation and dissociation as a function of temperature. The rates for the silica-silicide reaction are difficult to calculate because the thermodynamics of the reaction are unknown and will depend on the particular silicide involved. Furthermore, the calculated rate for that vaporization process will deviate from the actual rates even more than usual because material loss can occur only when the monoxide has passed through the outer viscous silica layer, and the rate of bubbling through this layer will be the controlling factor even when the environment is a vacuum.

Coating-Substrate Reactions

Except insofar as they promote adherence, coating-substrate reactions are not desirable, since they may result in the formation of volatile or liquid phases at the coating-substrate interface, or a change in the composition of the oxide film formed on the external surface. Even if the reactions will not have these harmful effects, they will deplete the effective coating thickness. While experimental data and mechanistic studies of low temperature solid-solid reactions are plentiful, little quantitative high-temperature data are available for reactions between tungsten and possible coating materials. An exception of direct pertinence which might be mentioned is the recent work of Passmore, et al. (Reference 30), who have been studying the inter-diffusion of tungsten and a number of metals (Table 1). Nevertheless, some conclusions as to the controlling factors can be drawn, the foremost of which is that reaction and diffusion kinetics are so fast at 2000°C and above that any thermodynamically favored reaction will occur to an appreciable extent in a reasonably short time.

Unfortunately, high-temperature thermodynamic data for many reactions of interest are unknown and can be found only by hazardous extrapolations. Due to the possible existence of unidentified compounds which may be produced during intermediate stages of the reaction and the sometimes marked effects of minor variations in the reaction environment, it is often difficult to specify the exact nature of reactions. The literature contains many reports of the existence of new, complex compounds, and it is reasonable to assume that more will be found, some of which may be involved in vital intermediate reactions. Furthermore, some reactions, such as that between alumina and tungsten, are rendered possible by slight, almost negligible, changes in the environmental atmosphere; the standard free energy for the reaction

$$W + Al_2O_3 \longrightarrow 2\,Al + WO_3$$

is about + 100,000 cal/gram mole at 2700°K, but Steinitz and Resnick (Reference 31) noted a vigorous reaction in argon which had been passed over ice at -40°C and no reaction in completely dry argon.

Even when the chemical reaction involved can be written with precision, thermodynamic calculations can still lead to erroneous conclusions if it is assumed automatically that the reactants are stoichiometric. This fact has been emphasized recently by Kubaschewski (Reference 32) in a review in which he pointed out as an example that the standard free energy of formation of TiO_2 was lowered by 140,000 cal/gram mole by a 0.5 atomic percent deviation in the oxygen content.

Our ability to estimate the likelihood of reactions in actual systems at high temperatures is far from being satisfactory. So many unknown factors may influence the progress of a reaction that it is most difficult to predict its course. As Margrave said recently, "When the totally unexpected

occurs in a high-temperature process, calculations are meaningless — there is no substitute for experimental studies" (Reference 33).

HIGH-TEMPERATURE POTENTIAL OF PLATINUM-GROUP METAL AND SILICIDE COATINGS

Having discussed the requirements of coatings and defined some of the factors which determine their usefulness at high temperatures, it is now possible to attempt to predict the high-temperature capabilities of actual systems. Two such systems of particular interest are platinum-group metal coatings, because of their seeming approach to the ideal of an inert barrier, and intermetallic silicides, because these are by far the most successful type of high-temperature coatings developed so far.

Platinum-Group Metal Coatings

The reported low-temperature behavior of these coatings suggests that their high-temperature usefulness will depend upon four factors; the minimum solidus temperature of the noble metal-tungsten system, the rate of coating-substrate reaction, the rate of coating erosion in oxygen, and the rate of permeation of oxygen through the coating.

Although the tungsten-noble metal phase diagrams are not well known, the melting points of the noble metals are. On this basis, platinum and rhodium are of marginal interest only because their melting temperatures are below 2000°C. The probability of harmful coating-substrate reactions can be estimated from data on the high-temperature reaction kinetics of noble metal-tungsten couples. The available data (Table 1) suggest that the extent of reaction decreases with increasing refractoriness of the noble metal. Therefore, as far as coating stability in non-oxidizing environments is concerned, it is desirable to use the more refractory noble metals such as iridium.

It is unfortunate that the susceptibility of platinum-group metals to erosion in oxidizing environments increases with increasing refractoriness over certain temperature ranges. At the temperatures of interest, all the platinum-group oxides are volatile, and therefore the maximum possible rates of erosion can be calculated from the vapor pressure data of the oxides by use of the Langmuir equation. Although the data are somewhat limited, they indicate that the erosion rates of noble metals at 2000°C will be substantial and may be as high as several grams/cm /hr (Figure 4) (Reference 34).

Although normally of minor significance, the permeability of noble metals to oxygen cannot be ignored, since they are known to offer very little resistance to the passage of inert gases. Only one paper (Reference 35) is known which deals with the permeation of oxygen through a noble metal, and even this is qualitative in nature, since it reported that no permeation through platinum could be detected at 1425°C when a mass spectrometer was used. It was estimated that the rate must have been less than 2×10^{-11} $cm^3/sec/cm^2$ area/mm thickness/atmospheric pressure difference. Studies of platinum-group metal coatings provide qualitative confirmation that oxygen permeation is not a significant factor (Reference 36).

On the basis of this information, although admittedly somewhat skimpy, it seems unlikely that platinum metals, as such, can be developed as successful coatings for tungsten at 2000°C and above. The use of noble metal alloys still remains a possibility, but there is not sufficient requisite data to attempt an evaluation at this time.

Silicide Coatings

Silicide coatings, probably the most successful developed so far, are normally produced by diffusing silicon into the refractory metal substrate, thus forming molybdenum silicide layers on molybdenum, tungsten silicide layers on tungsten, and so on. Since there is no reason, in principle, why $MoSi_2$, for example, could not be used as a coating for tungsten provided that modified application techniques were adopted, silicides in general will be considered and not merely those of tungsten.

All silicide coatings suffer from one major limitation, an anomalously rapid rate of oxidation over well defined low-temperature ranges. Because of similarity in appearance of failed silicide coatings to the low-temperature tin transformation, this is often called "pest." Although the onset of pest can sometimes be [illegible] by modifying the coating by the [illegible] other materials (Reference 2), [illegible] not be prevented. The high-temperature capabilities of silicide, however, are excellent. An 8-mil coating of WSi_2, for instance, can protect tungsten for as long as 30 hours at 1800°C (Reference 2). The factors which logically, and in practice, set the useful upper temperature limit of silicide coatings, are refractoriness of the coating components, the rate of conversion to oxide, the necessity that this oxide is silica, the rate and location of vapor phase material loss, and the rate of reactions within the coating and between the coating and the substrate.

The refractoriness of silicide coatings depends on the melting points of the initial coating material and all the products of the reactions with the substrate and environment. The unoxidized coating is generally composed of thin layers of the silicon-lean silicide, a wide layer of the most silicon-rich intermetallic in the binary system. This silicon-rich intermetallic is converted into lower silicides and silica during oxidation (Figure 5) (Reference 2). Since the phase diagrams of the binary silicon systems are fairly well known, the refractoriness of the silicide layers in the coating system can be estimated. The refractoriness of the oxide formed, however, is a more complex quantity to estimate, even if it is assumed that it is pure silica. The viscosity of liquid silica rather than the melting point of the solid oxide is the important parameter in practice because silicide coatings often are used at temperatures above the melting point of silica. Data on the high-temperature viscosity of silica are not plentiful, but what there is (Reference 37) indicates that silica is relatively fluid in the temperature range 2000° to 2500°C (Figure 6).

Unfortunately, it cannot be assumed with certainty that the oxide formed on the silicide coating surfaces is pure silica, since the oxidation of such a coating is a special case of layer growth in a ternary system. In practice, however, it is not unreasonable to assume that the oxide is basically silica, since the free energy of formation of that oxide is far greater than that of the common oxides of the refractory metals, and a glassy appearance of the very high-temperature oxidation products of silicides has been reported. These glassy films are not prone to breakaway, possibly due to their excellent ductility, but virtually no high-temperature kinetic growth data is available, although it is known that the films do not grow to great thicknesses. These observations, however, are in seeming disagreement with the results of permeation studies of silica and silica-base glasses using inert gases, and a recent study of the permeation of oxygen through vitreous silica (Reference 38), which suggest that the glassy oxide films formed at high temperatures will be poor diffusion barriers.

The reason why the glassy films on silicides are found not to be very thick in practice may be that vapor phase loss of silica is appreciable. This could occur by two processes: simple evaporation, or through decomposition into volatile silicon monoxide. The thermodynamics of these processes have been studied fairly extensively (References 39 and 40) and therefore it is a simple matter to gain an idea of the maximum, Langmuir, evaporation rates (Figure 3). Silicon monoxide may be formed also by reaction of silica with the metallic silicide, a possibility to which particular attention must be paid since this reaction occurs at an internal interface and may lead to early coating failure due to the disruption of the outer protective layer of silica when bubbles of silicon monoxide pass through it. The thermodynamics of silica-silicide reactions are unknown, but it is interesting to note that the standard free energy of the reaction between silica and pure silicon is zero, and the silicon monoxide pressure is one atmosphere, at 1925 ± 50°C, a temperature at which bubbling of tungsten silicide coatings has been noted (Reference 2).

Although the data is far from being complete, it is possible to conclude that the upper temperature limit of silicide coatings is probably about 2000°C or even below. The basis for this is the calculated rates of silica vaporization, about 2 gram/cm^2/hr at 2000°C in vacuum, reactions between silica and the silicide coating at 1900° to 2000°C, the melting points of the silicides, and the decreasing viscosity of silica.

FUTURE COATING SYSTEMS

Neither the seemingly ideal platinum-group metal nor the very successful silicide coatings are likely to be of more than limited use at 3000°C and above. It will be necessary, therefore, to develop entirely new types of coatings. On the basis of the previous considerations, it should be possible to predict the general nature of these new systems and to indicate some of the factors that will determine their high-temperature potential.

The prime requirement of any coating system is that all the components, including the oxide layer, should be refractory. This in itself limits severely the number of available materials from which a selection can be made. If a minimum oxide melting point of 2500°C is adopted as a criterion of refractoriness and it is assumed that simple oxides will be formed by the reaction with the environment, the only available materials are those forming ThO_2, HfO_2, UO_2, MgO, ZrO_2, CeO_2, CaO, and BeO. Unfortunately, at least one of these oxides, MgO, is of doubtful refractoriness due to its vaporization at high temperatures (Reference 41). The refractoriness of BeO and CaO at high temperatures may also be something of an illusion under many conditions, due to the readiness with which they hydrate (Reference 41).

Most successful coating systems as mentioned before are essentially intermetallic compounds of two metals with widely different activities, the most reactive being the parent of the desired protective oxide. Thus, thorides, etc., are logically the most promising types of materials for ultra-high temperature coatings. It cannot be assumed, however, that the oxidation of any thoride will result in the production of ThO_2, even though thoria and the other refractory oxides are thermodynamically very stable. A certain amount of experimentation may be necessary before it is possible to select suitable compounds. A better understanding of the mechanism of ternary diffusion would, of course, greatly ease the selection difficulties.

Even if the desired refractory oxides are produced, protection may not be conferred, since they fail to grow from their parent metals by diffusion-controlled processes at quite low temperatures (Figure 1), and it is reasonable to expect that this will also be true of their growth from intermetallic substrates. Before actual coating can be developed, means must be found of circumventing or delaying breakaway, but lack of understanding of the basic mechanisms involved makes the prediction of these means somewhat hazardous. It may be significant, however, that a number of liquid and semi-liquid coatings have been reported recently, their success being derived, possibly, from a decreased stress at the oxide-substrate interface (References 42 and 43). It may be necessary, therefore, to employ non-refractory materials in future, if it is wished to form oxide films which grow by a refractory diffusion-controlled mechanism.

Data on the diffusion-controlled growth of oxides at 2000°C and above is lacking, but extrapolation of low-temperature data suggests that it will be rapid (Figure 2). It will probably be necessary, therefore, to decrease the rate of diffusion through the oxide films if protection is to be obtained for long times. Due to the large concentration of thermal vacancies at high temperatures, this modification may have to be a change in the structure of the oxide, or perhaps even conversion to a complex oxide, rather than merely a decrease in the structure-sensitive defect concentration produced by doping.

Data on the nature and rate of high-temperature oxide-substrate and tungsten

coating reactions are sparse, even for the coatings composed of pure metals rather than intermetallics (Table 1). In fact, any discussion as to the most suitable materials based on these factors would be speculative. Two other factors, however, must be considered even before attempting to produce a coating which will form the oxides mentioned previously: toxicity and radioactivity. ThO_2 and UO_2 are both radioactive and, to an extent, toxic; BeO is markedly toxic.

On the basis of the types of information briefly indicated so far, the most preferable type of new coating system would be one which oxidized to form a protective film of HfO_2 or ZrO_2. These systems are the most promising because of the refractoriness of the oxides, their relative lack of proneness to breakaway, the low rates of vaporization of the oxides, their resistance to hydration, and their lack of toxicity and radioactivity. Before these systems can be defined in terms of metal composition, certain minimum requirements must be met. It must be shown either by experimentation or by theoretical calculation that the metal coating will react to form the desired oxide, and the incidence of breakaway must be delayed or circumvented. These requirements cannot be achieved easily at present, and future development programs will be considerably hampered unless a better understanding of diffusion processes, internary systems, and breakaway can be gained. The other processes, vaporization, coating-substrate reactions, etc., are of importance only if the desired oxide can be grown by a diffusion-controlled process. It seems, therefore, that workers involved in coating development programs will have to pay particular attention to the progress of basic research on these two processes if avoidable delays are not to be encountered.

REFERENCES

1. Report of the Subpanel on Coating (Draft), Refractory Metals Sheet Rolling Panel of the Materials Advisory Board, February 1962.
2. Nicholas, M. and Dickinson, C. D., "High-Temperature Protective Coatings for Refractory Metals," Part II, Sixth meeting of the Refractory Composites Work Group, Dayton, Ohio, 1962.
3. Kubaschewski, O., and Hopkins, B. E., Jnl. of Less Common Metals, 2, 172, 1960.
4. Air Force Contract AF 33(616)-8175
5. J. Loriers, Compt. Rendus 234, 91, 1952.
6. Leibowitz, L., Schrizlein, J. G., Bingle, J. D., and Vogel, R. C., Jnl. Electrochem. Soc., 108, 1155, 1961.
7. Cubicciotti, D., Jnl. Amer. Chem. Soc., 74, 1079, 1952.
8. Levesque, P., and Cubicciotti, D., Jnl. Amer. Chem. Soc., 73, 2028, 1951.
9. Probst, H. P., Ph. D. Thesis, Case Institute of Technology, 1959.
10. Kendall, L. F., Wheeler, R. B., and Bush, S. H., Nucl. Sci. Eng., 3, 171, 1958.
11. Hayes, E. T., and Robeson, A. H., Trans. Electrochem. Soc., 96, 142, 1949.
12. Phalnikar, C. A., and Baldwin, W. M., Proc. ASTM, 51, 1038, 1951.
13. Belle, J., and Mallett, M. W., Jnl. Electrochem. Soc., 101, 339, 1954.
14. Cubicciotti, D., Jnl. Amer. Chem. Soc., 72, 41[illegible], 1950.
15. Gulbransen, E. A., and Andrew, K. F., Trans. AIME, 209, 394, 1957.
16. Gadd, J. D., and Evans, E. B., Corrosion, 17, 109, 1961.
17. Sinnad, M. T., and Smeltzer, W. W., Acta Met, 5, 328, 1957.
18. Gerds, A. F., and Mallett, M. W., Jnl. Electrochem. Soc., 101, 171, 1954.

19. Porte, H. A., Vogel, R. C., Fischer, D.A., and Schnizlein, L.G., Jnl. Electrochem. Soc., 107, 506, 1960.

20. Gulbransen, E. A., and Andrews, K. F., Jnl. Electrochem. Soc., 97, pg. 383, 1951.

21. Wagner, C., Jnl. Electrochem. Soc., 99, 369, 1952.

22. Kirkaldy, J. S., Can. Jnl. Phys., 36, 907, 1958.

23. Guy, A. G., and Smith, C. B., Trans. Quarterly, ASM, 55, 7, 1962.

24. Clark, J. B., and Rhines, F. N., Trans. ASM, 51, 199, 1959.

25. Langmuir, I., Phys. Rev., 2, 329, 1913.

26. Brewer, L., Chem. Rev., 51, 1, 1953.

27. Blackburn, P. E., Andrew, K. F., Gulbransen, E. A., Brassart, F. A., WADC TR 59-575, Part II.

28. Gulbransen, E. A., and Andrew, K. F., Jnl. Electrochem. Soc., 104, 334, 1957.

29. R. Perkins, "Evaluation of Silicide Coating," Electrochem. Soc. Conference, May 1962.

30. Passmore, E. M., Boyd, J. E., Neal, L. P., Anderson, C. A., and Lement, B. S., WADD TR 60-343, and Progress Report No. 6, April 1961, AF 33(616)-6354.

31. Steinitz, R., and Resnick, R., "High-Temperature Reactions Between Tungsten and Several Refractory Compounds," Fifth Meeting of the Refractory Composites Work Group, Dallas, Texas, 1961.

32. Kubaschewski, O., Trans. Brit. Ceramic Soc., 60, 67, 1961.

33. Margrave, J. L., Symposium on "High Temperatures — A Tool for the Future," Stanford Research Institute, 1956.

34. Calculated from the data of C. B. Alcock and G. W. Hooper, Proc. Royal Soc., A., 254, 551, 1960.

35. Norton, F. J., J. Appl Phys. 29, 1122, 1958.

36. Withers, J. C., "Protective Coatings for Refractory Metals," Fifth Meeting of the Refractory Composites Work Group, Dallas, Texas, 1961.

37. McKenzie, J. D., Jnl. Amer. Ceramic Soc., December, 1961.

38. Norton, F. J., Nature, to be published.

39. Shick, H. L., Chem. Rev., 60, 331, 1960.

40. Ramsted, H. F., and Richardson, F. D., Trans. AIME, 221, 1021, 1961.

41. Rumck, R. J., "High Temperature Technology," John Wiley & Sons, New York, 1956.

42. Lawthers, D. D., and Sama, L., ASD TR 61-232.

43. Ozx, G. E., and Coffin, L. E., Trans. AIME, 218, 541, 1960.

TABLE 1 (Reference 30)

SUMMARY OF INTERDIFFUSION MEASUREMENTS ON COMBINATIONS ANNEALED AT 1700° C

Combination	Intermediate Phase Width (in Microns) After 1 Hr	4 Hrs	Total Diffusion 1 Hr	Zone Width (in Microns) After 4 Hrs
W-Re	2	6	60	60
W-Os	2	6	30	50
W-Ir	8	12	50	60
W-Rh	14-20	--	60-90	--
W-Pt	8	--	110-200	--
W-Hf	6	--	25	--
W-V	--	--	60	--
W-Zr	15	--	120	--
W-Cb	0	0	15-40	50
W-Cr	0	0	150	7320

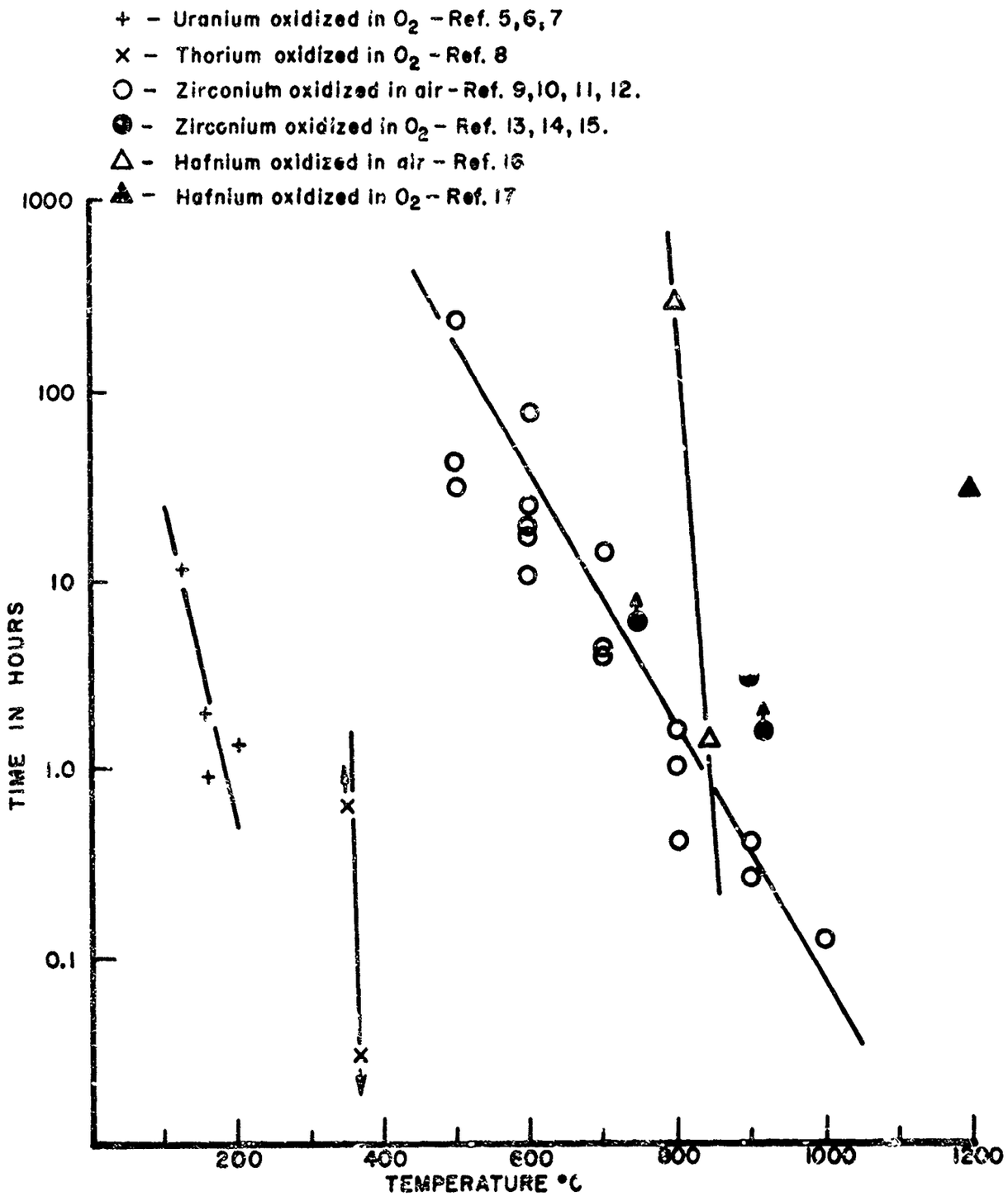

Figure 1. The Conditions Under Which the First Deviations from Parabolic Growth Occur for a Number of Refractory Oxides

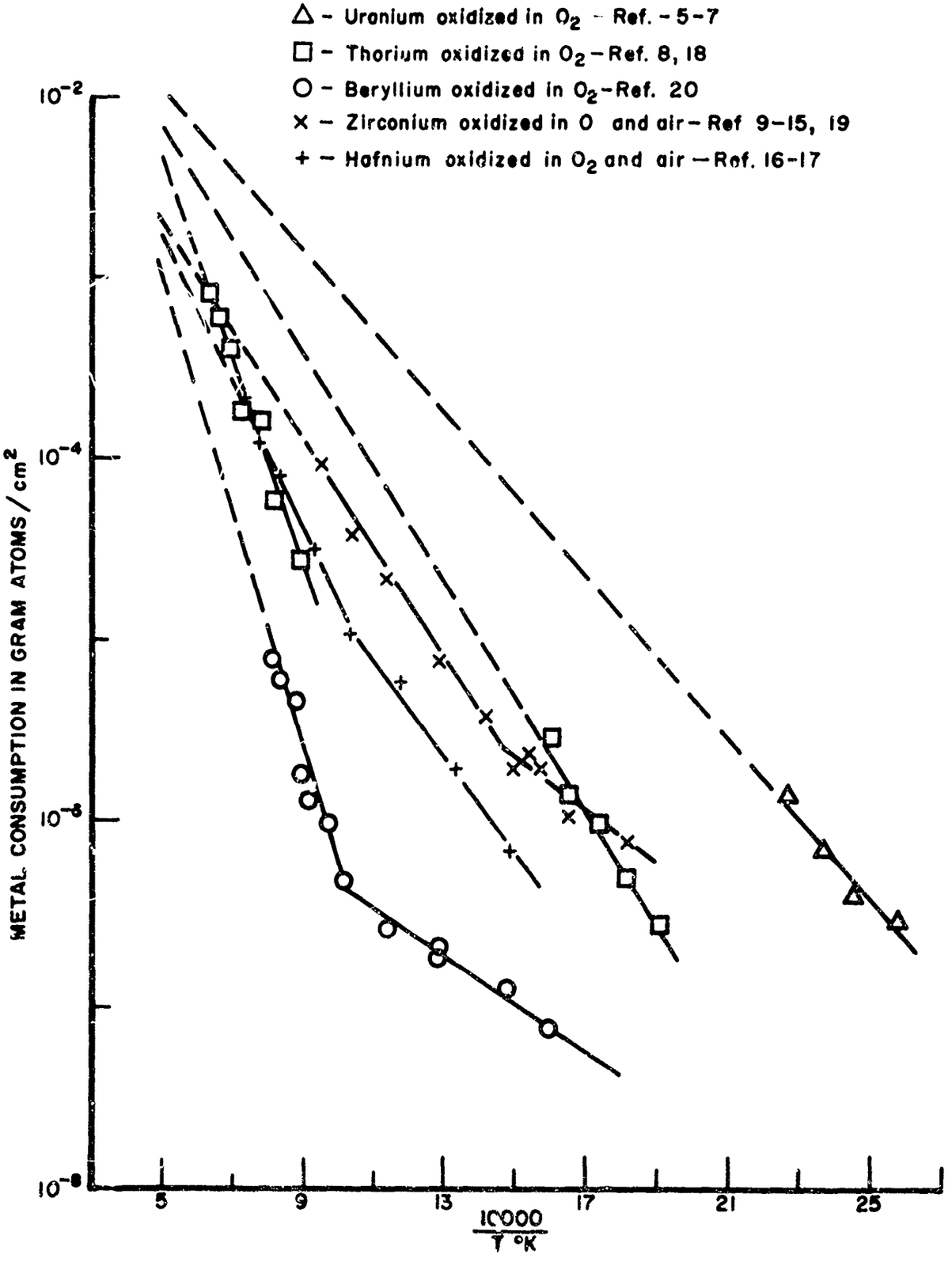

Figure 2. The Consumption of Several Metals, During the First Hour of Diffusion Controlled Oxide Growth, as a Function of Temperature

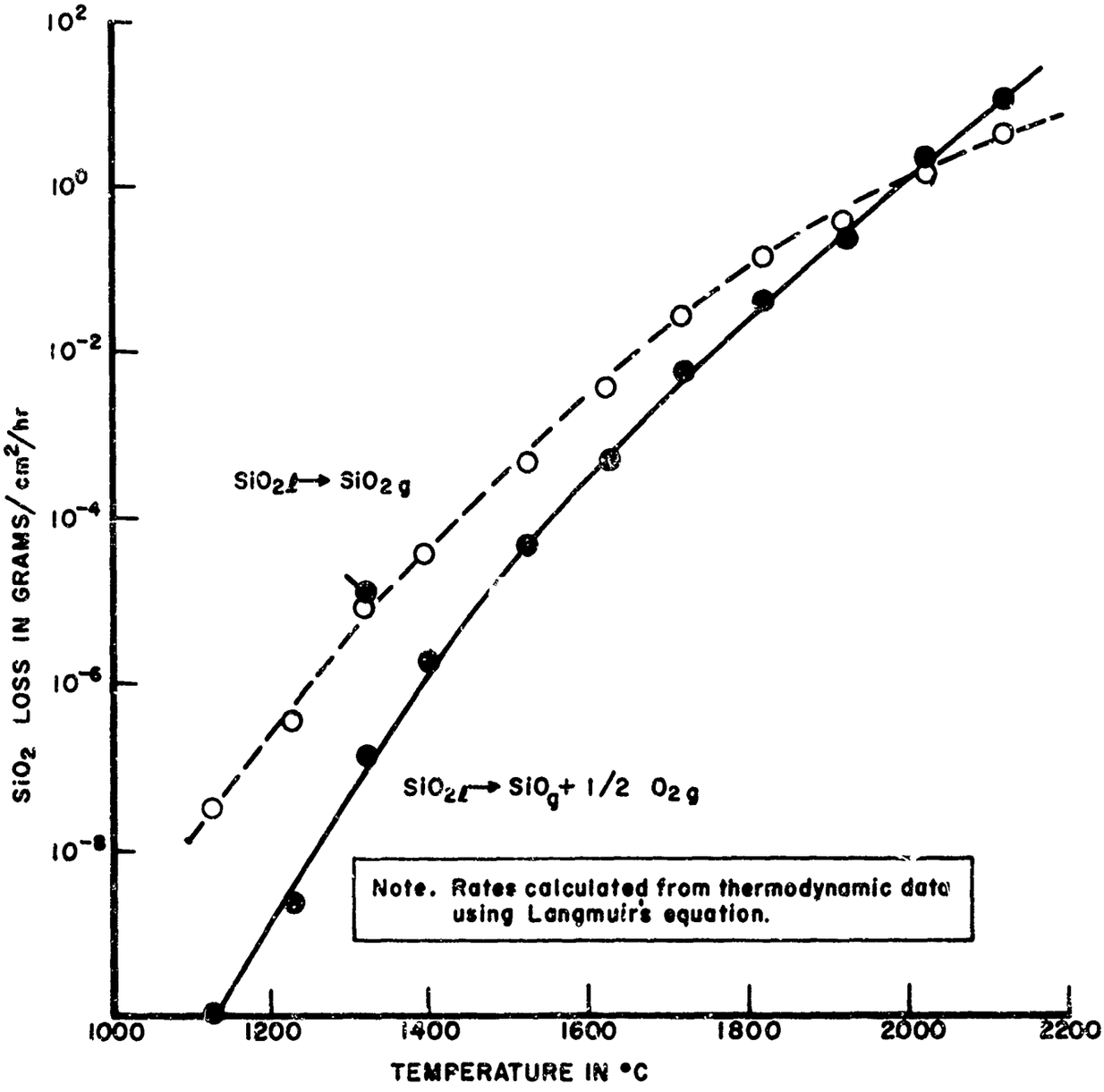

Figure 3. The Rate of Vapor Phase Loss of SiO_2 into a Perfect Vacuum Due to The Reactions

(1) $SiO_{2\ell} \rightarrow SiO_{2g}$
(2) $SiO_{2\ell} \rightarrow SiO\ g + 1/2\ O_{2g}$

Note: Solid lines show the range of temperatures over which experimental data is available, dotted lines are extrapolations. Calculated from the data in Reference 34.

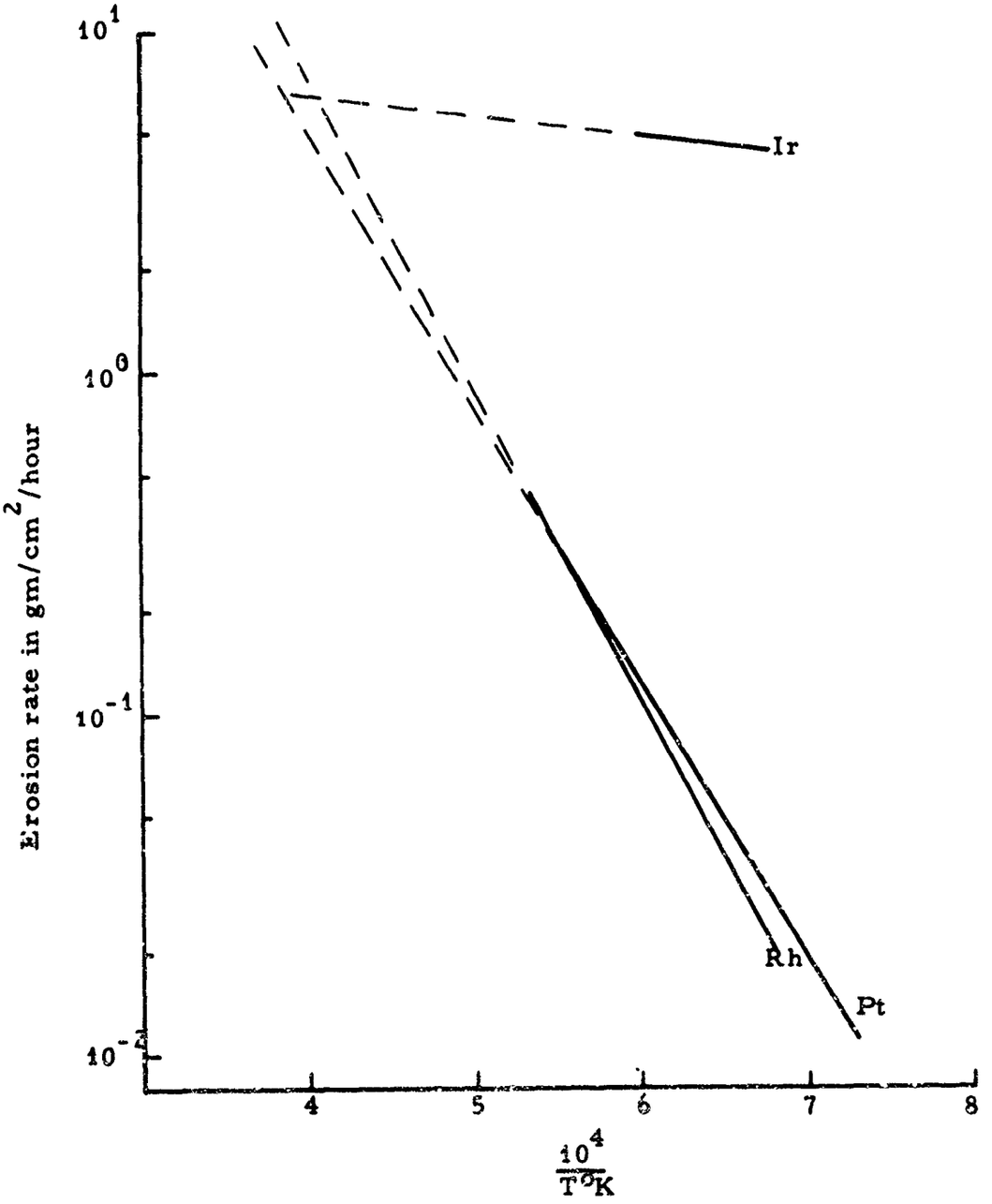

Figure 4. The Maximum Theoretical Errosion Rates in Air of Platinum, Rhodium, and Iridium

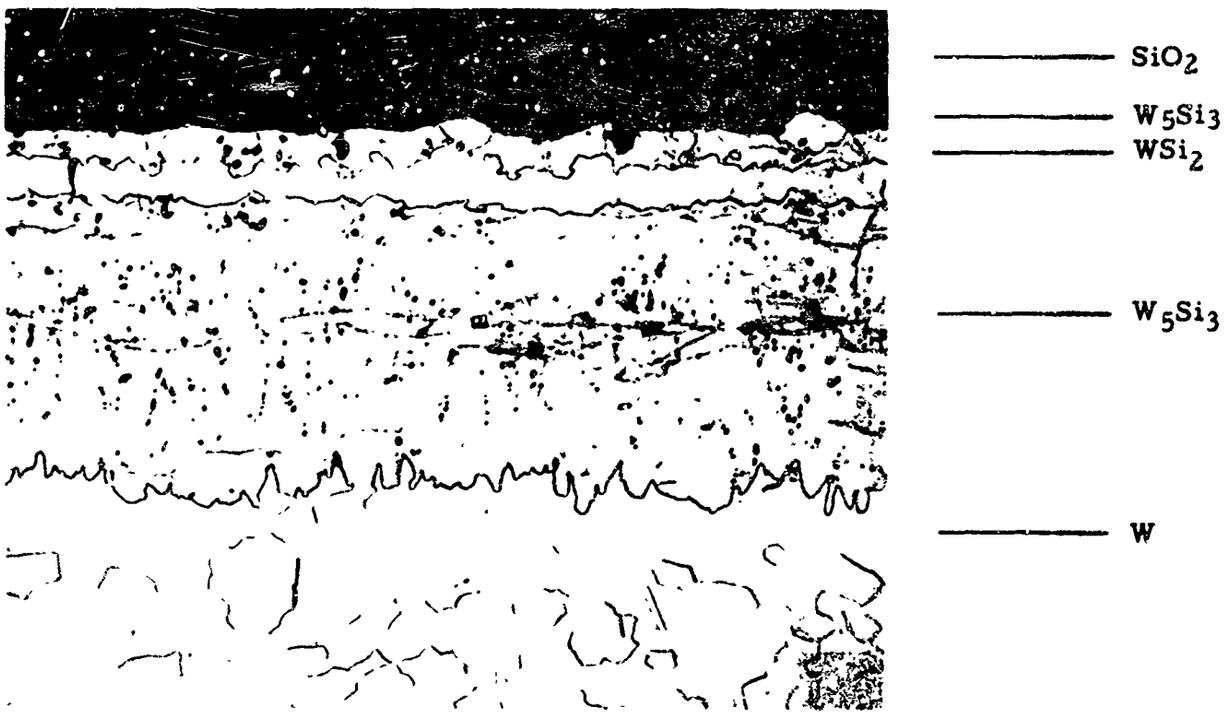

Structure of W Si_2 Coating on Tungsten After 13 hours at 1650°C. (250X)

Figure 5. The Appearance of Oxidized W Si_2 Coatings

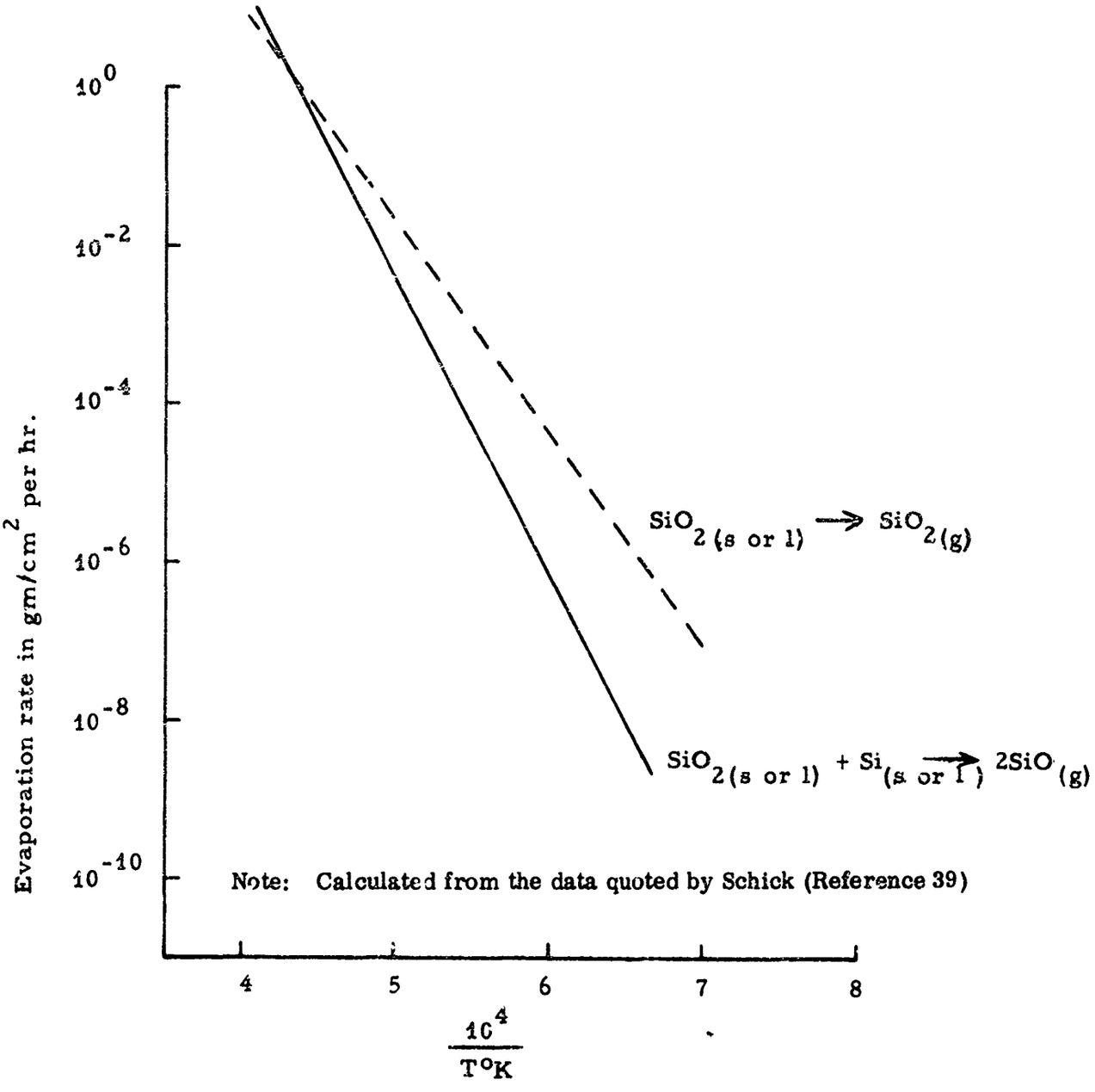

Figure 6. Rate of Vapor Phase Loss of Silica Due to Simple Evaporation and Decomposition

UNCLASSIFIED

Security Classification

DOCUMENT CONTROL DATA - R&D

(Security classification of title, body of abstract and indexing annotation must be entered when the overall report is classified)

1 ORIGINATING ACTIVITY (Corporate author) American Institute of Mining, Metallurgical and Petroleum Engineers (AIME) and Air Force Materials Laboratory	2a REPORT SECURITY CLASSIFICATION Unclassified 2b GROUP N/A

3 REPORT TITLE

Oxidation of Tungsten And Other Refractory Metals

4. DESCRIPTIVE NOTES (Type of report and inclusive dates)

Summary of Symporium Proceedings - 31 October 1962

5. AUTHOR(S) (Last name, first name, initial)

Faust, Paul L. (AF Project Monitor)

6. REPORT DATE	7a TOTAL NO OF PAGES	7b. NO OF REFS
April 1965	190	245

8a. CONTRACT OR GRANT NO. N/A b. PROJECT NO. 7312 c. d. 731202	9a. ORIGINATOR'S REPORT NUMBER(S) N/A 9b. OTHER REPORT NO(S) (Any other numbers that may be assigned this report) N/A

10 AVAILABILITY/LIMITATION NOTICES

None

11. SUPPLEMENTARY NOTES	12. SPONSORING MILITARY ACTIVITY
None	Air Force Materials Laboratory (Co-sponsor)

13. ABSTRACT

This report consists of eight papers presented at a symposium conducted by the AIME and the AF Materials Laboratory, Research and Technology Division, Wright-Patterson Air Force Base, Ohio, on the Oxidation of Tungsten and Other Refractory Metals. The symposium, consisting of two sessions, was held 31 October 1962 in New York City. Topics discussed included progress in research and in experimental methods in the investigation of the kinetics and mechanisms of oxidation of tungsten, tantalum, and columbium.

DD FORM 1 JAN 64 1473

UNCLASSIFIED

Security Classification

14. KEY WORDS	LINK A		LINK B		LINK C	
	ROLE	WT	ROLE	WT	ROLE	WT
Oxidation, Tungsten, Refractory Metals, AIME - AFML Symposium Proceedings.						

INSTRUCTIONS

1. ORIGINATING ACTIVITY: Enter the name and address of the contractor, subcontractor, grantee, Department of Defense activity or other organization *(corporate author)* issuing the report.

2a. REPORT SECURITY CLASSIFICATION: Enter the overall security classification of the report. Indicate whether "Restricted Data" is included. Marking is to be in accordance with appropriate security regulations.

2b. GROUP: Automatic downgrading is specified in DoD Directive 5200.10 and Armed Forces Industrial Manual. Enter the group number. Also, when applicable, show that optional markings have been used for Group 3 and Group 4 as authorized.

3. REPORT TITLE: Enter the complete report title in all capital letters. Titles in all cases should be unclassified. If a meaningful title cannot be selected without classification, show title classification in all capitals in parenthesis immediately following the title.

4. DESCRIPTIVE NOTES: If appropriate, enter the type of report, e.g., interim, progress, summary, annual, or final. Give the inclusive dates when a specific reporting period is covered.

5. AUTHOR(S): Enter the name(s) of author(s) as shown on or in the report. Enter last name, first name, middle initial. If military, show rank and branch of service. The name of the principal author is an absolute minimum requirement.

6. REPORT DATE: Enter the date of the report as day, month, year, or month, year. If more than one date appears on the report, use date of publication.

7a. TOTAL NUMBER OF PAGES: The total page count should follow normal pagination procedures, i.e., enter the number of pages containing information.

7b. NUMBER OF REFERENCES: Enter the total number of references cited in the report.

8a. CONTRACT OR GRANT NUMBER: If appropriate, enter the applicable number of the contract or grant under which the report was written.

8b, 8c, & 8d. PROJECT NUMBER: Enter the appropriate military department identification, such as project number, subproject number, system numbers, task number, etc.

9a. ORIGINATOR'S REPORT NUMBER(S): Enter the official report number by which the document will be identified and controlled by the originating activity. This number must be unique to this report.

9b. OTHER REPORT NUMBER(S): If the report has been assigned any other report numbers *(either by the originator or by the sponsor)*, also enter this number(s).

10. AVAILABILITY/LIMITATION NOTICES: Enter any limitations on further dissemination of the report, other than those imposed by security classification, using standard statements such as:

(1) "Qualified requesters may obtain copies of this report from DDC."

(2) "Foreign announcement and dissemination of this report by DDC is not authorized."

(3) "U. S. Government agencies may obtain copies of this report directly from DDC. Other qualified DDC users shall request through _____."

(4) "U. S. military agencies may obtain copies of this report directly from DDC. Other qualified users shall request through _____."

(5) "All distribution of this report is controlled. Qualified DDC users shall request through _____."

If the report has been furnished to the Office of Technical Services, Department of Commerce, for sale to the public, indicate this fact and enter the price, if known.

11. SUPPLEMENTARY NOTES: Use for additional explanatory notes.

12. SPONSORING MILITARY ACTIVITY: Enter the name of the departmental project office or laboratory sponsoring *(paying for)* the research and development. Include address.

13. ABSTRACT: Enter an abstract giving a brief and factual summary of the document indicative of the report, even though it may also appear elsewhere in the body of the technical report. If additional space is required, a continuation sheet shall be attached.

It is highly desirable that the abstract of classified reports be unclassified. Each paragraph of the abstract shall end with an indication of the military security classification of the information in the paragraph, represented as *(TS), (S), (C), or (U)*

There is no limitation on the length of the abstract. However, the suggested length is from 150 to 225 words.

14. KEY WORDS: Key words are technically meaningful terms or short phrases that characterize a report and may be used as index entries for cataloging the report. Key words must be selected so that no security classification is required. Identifiers, such as equipment model designation, trade name, military project code name, geographic location, may be used as key words but will be followed by an indication of technical context. The assignment of links, roles, and weights is optional.